Petrography and mineral chemistry of lamproite-hosted xenoliths from Kjakebeinet, western Dronning Maud Land, Antarctica.

24.10.2006
MSc. thesis
Ilona Romu
Department of Geology
Geology and Mineralogy
University of Helsinki

HELSINGIN YLIOPISTO
HELSINGFORS UNIVERSITET
UNIVERSITY OF HELSINKI

Tiedekunta/Osasto - Fakultet/Sektion – Faculty	Laitos - Institution – Department
Matemaattis – luonnontieteellinen	Geologia

Tekijä - Författare – Author
Ilona Romu

Työn nimi - Arbetets titel – Title

Petrography and mineral chemistry of lamproite-hosted xenoliths from Kjakebeinet, western Dronning Maud Land, Antarctica.

Oppiaine - Läroämne – Subject
Geologia ja mineralogia

Työn laji - Arbetets art – Level	Aika - Datum – Month and year	Sivumäärä - Sidoantal – Number of pages
Pro gradu tutkielma	27.10.2006	104

Tiivistelmä - Referat – Abstract

Jurassic (159 Ma), ultrapotassic, mica-rich dykes of Kjakebeinet represent the youngest magmatic rock type observed in western Dronning Maud Land, Antarctica; abundant xenoliths are enclosed by the dykes.

A petrographical description of the xenoliths and one of the dykes was made to distinguish the rock types and to gain information of the unknown basement below Kjakebeinet, situated on the southern edge of Vestfjella mountainrange. The mineral chemistry and petrography of the xenoliths and one of the lamproite dykes were studied using petrographic microscope and electron microprobe (EDS-mode). Rb-Sr and Sm-Nd isotopic determinations were made on metagabbroic and carbonatite xenoliths.

Most of the xenoliths record evidence of granulite facies metamorphosis and they represent several crustal rock types. Tonalite, alkali feldspar granite, and augen gneisses, metagabbros and metasedimentary xenoliths were observed. Two of the xenoliths, carbonatite, and phlogopite rock, are cognate.

This thesis shows that the crust below the southern Vestfjella is heterogenic, and contains differentiated metaigneous rock types. The xenoliths include Proterozoic basement gneisses, and possibly also Permian sedimentary rocks and Mesozoic igneous rocks. The studied lamproite dyke is phlogopite-sanidine-diopside-olivine lamproite which shows affinity to madupitic lamproites and group II kimberlites.

Avainsanat – Nyckelord – Keywords
xenolith, lamproite, mineral chemistry, petrology, basement, Kjakebeinet, western Dronning Maud Land, Antarctica

Säilytyspaikka – Förvaringställe – Where deposited
Helsingin yliopisto

Muita tietoja – Övriga uppgifter – Additional information
447 mikroanalyysiä, 9 taulukkoa, 53 kuvaa, 3 liitettä.

Contents

1 INTRODUCTION

A minor suite of ultrapotassic dykes was discovered during the Finnish Antarctic Research Program (FINNARP) 1997-1998 expedition. These dykes were subsequently dated at 159 Ma (Luttinen et al. 2002); and they represent the youngest magmatic event identified on western Dronning Maud Land. The dykes contain abundant xenoliths which were sampled during the expedition of summer 2001. The mineralogy and petrography of xenoliths recovered from the lamproite dyke 1 and from boulders are described in this study.

1.1 Study area and previous studies

The dykes and xenoliths studied in this thesis are from the Kjakebeinet nunatak (73º47`02``N, 14º52`40``W), western Dronning Maud Land (WDML), East-Antarctica (fig. 1). Kjakebeinet is situated on the southern edge of Vestfjella, which is c. 130 km

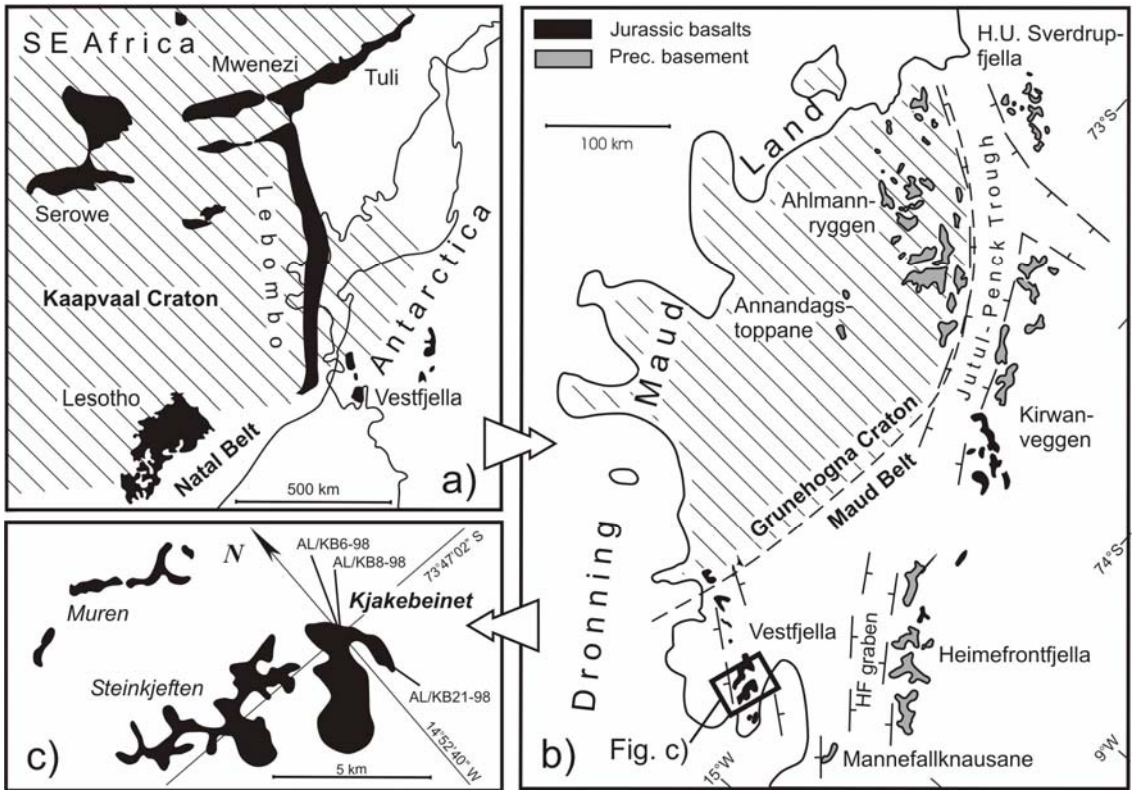

Figure 1. The western Dronning Maud Land, Antarctica. The Archean cratons are hatched, black colour refers to Jurassic basalts and grey is the Proterozoic basement. A) Prior to breakup of the Gondwana WDML and south eastern Africa were adjacent to each other. B) The main lithological units of the WDML. C) Lamproite sample localities, AL/KB6-98 is from dyke 1, AL/KB8-98 from dyke 2, and AL/KB21-98 from dyke 3. Reconstruction after Gondwana is after Lawver, Gacahan & Coffin (1992) (Luttinen et al. 2002).

long, NNE-SSE trending mountain range on the westernmost part of WDML. The outcrops (isolated ridges and nunataks) are dominated by Jurassic flood basalts intruded by Mesozoic mafic dykes and gabbroic intrusions. Sedimentary rocks are also present as minor intercalations. The geology project of FINNARP started in 1989 and has focused on the flood basalts (e.g. Luttinen and Siivola 1997, Luttinen et al. 1998, Luttinen 2000, Luttinen et al. 2000) and gabbroic intrusives (e.g. Vuori 2004). A brief study on the lamproite dykes of Kjakebeinet was presented by Luttinen et al. (2002). Studies on Mesozoic plutonic intrusives of the WDML (Harris & Grantham 1993, Vuori 2004), the Proterozoic metamorphic basement (e.g. Juckes 1972, Groenewald et al. 1995, Jacobs et al. 1998, Jacobs et al. 1996), and the geophysics of the ice covered sutured area (Corner 1994) are also relevant to this thesis. For more complete references to previous studies of western Dronning Maud Land and Vestfjella see Tingey 1991 and Luttinen 2000, respectively.

1.2 The aims of the study

On the basis of preliminary study the dykes of Kjakebeinet are alkaline ultramafic rocks called lamproites (Luttinen et al. 2002). A detailed mineralogical study, however, is required to classify this type of rocks. The nearest locality of comparable alkaline rocks is at Pensacola Mountains, Ferrar magmatic province, more than 1000 km southwest of Vestfjella (Boyd 1987, Leat et al. 2000). The age and paleogeographical location adjacent to southern Africa connects the dykes to South African mica-rich kimberlites (Luttinen et al. 2002). The rapid ascent of these rocks from upper-mantle source regions (Mitchell and Bergman 1991, p. 396) facilitates the preservation of xenoliths eroded from the walls of magma conduit. In Vestfjella, the xenoliths offer a unique opportunity to collect data on the ice-covered Proterozoic basement and thick supracrustal sequences; mantle-derived nodules and diamonds have also been observed in these rock types (Mitchell and Bergman 1991, p. 371). Basaltic magmatism consists often of different stages which are identified from each other on the basis of magma composition: gabbroic xenoliths in lamproite might give further information on the crustal evolution of WDML. This study describes the mineralogy and petrography of lamproite-hosted xenoliths and one of the lamproite dykes. Their origin is discussed on the basis of the mineral chemical data. A petrographical comparison to the other dykes of Kjakebeinet was made to observe possible compositional diversity.

2. GEOLOGICAL BACKGROUND

2.1 Geology of the western Dronning Maud Land

2.1.1. Precambrian basement

The Precambrian shield of East Antarctica comprises of Archean cratons that are surrounded by Proterozoic and younger orogenic belts. In western Dronning Maud Land the Grunehogna province, which consists of 3000 Ma granitic basement and overlying 1000 Ma sedimentary and volcanic rocks, is juxtaposed with the Mesoproterozoic 1600-900 Ma orogenic Maud belt (fig. 1b). The Precambrian bedrock shows similarity to south eastern Africa and has been interpreted as a part of the Kalahari craton that was detached during the Gondwana break-up. The Proterozoic sedimentary and volcanic succession of the Grunehogna province is called the Ritscherflya supergroup (fig. 1b) and it has been intruded by the mafic Borgmassivet sills 800-1000 Ma ago (Groenewald et al. 1995). The supergroup has been cut by steep shear zones c. 520 Ma ago (Peters et al. 1989 according to Groenewald et al. 1995), which are probably related to the Pan-African collisional orogeny recorded in central Dronning Maud Land between 560 and 490 Ma (Jacobs et al. 2003). The Maud belt consists of relatively juvenile volcanic arc material accreted to the Grunehogna craton (Thomas 1989 according to Groenewald et al. 1995) and is characterized by granulite to amphibolite facies gneisses (Groenewald et al. 1995). Mesoproterozoic rocks, mainly strongly foliated gneisses, schists and amphibolites (Ardus 1964 and Worsfold 1967 according to Tingey 1991) are exposed on Heimefrontfjella, c. 100 km east from Kjakebeinet. H.U. Sverdrupfjella in the north eastern part of WDML (fig. 1b) has been studied more in detail and structures there indicate overthrusting of the eastern, high-grade metamorphosed rock types onto the western, lower-grade rocks (Groenewald et al. 1995). Aeromagnetic studies imply that the Proterozoic basement extends under the Mesozoic supracrustal sequence (Corner 1994) and the Cambrian-Ordovician suture is close to the Maud belt, probably in northern Vestfjella (Groenewald et al. 1995).

2.1.2 Phanerozoic bedrock

The Jurassic tholeiitic flood basalts exposed in Vestfjella, the westernmost mountain range, represent a part of the South African Karroo Province volcanic rocks that were erupted during the Gondwanaland break-up (Luttinen & Furnes 2000). This event is recorded by gabbroic intrusions in southern Vestfjella; the intrusions show affinity to both low-Ti continental flood basalts and transitional-Ti mid-ocean ridge basalts (Vuori 2004). A suite of dolerite dykes in Ahlmannryggen, comprising of low- and high-Ti magma types, were studied by Riley et al. (2005). Picrites and ferropicrites, interpreted as high temperature magmas, are also present there. The dykes intruded between 190 and 178 Ma ($^{40}Ar/^{39}Ar$ determination). The rifting episode is remarkable for its short duration: both South African volcanic rocks as well as their counterparts on Antarctica extruded between 184 and 179 Ma ($^{40}Ar/^{39}Ar$ and U-Pb determinations) according to Duncan et al. (1997). The MORB compositions of Karroo province and the voluminous magma production provide evidence on the plume-induced character of the flood basalt magmatism (cf. White 1997). The latest stage of magmatism was recorded by rhyolites in the Lebombo area (Allsop et al. 1984 according to White 1997). In Straumsvola, on the eastern side of Jutul-Penck through, WDML (fig. 1b) Harris and Grantham (1993) reported a 170 Ma nepheline syenite complex. They stated that it probably implies local rifting. A schematic model for the break-up event on WDML is represented in the PhD thesis of Vuori (2004); the final stage of rifting is recorded by the 160 Ma Kjakebeinet lamproites (Luttinen et al. 2002). A variety of Permian-Carboniferous sedimentary rocks (sandstones, graywackes, limestones, conglomerates, and coal layers) are described in north-eastern Heimefrontfjella (Juckes 1972).

2.1.3 Jurassic ultrapotassic dykes

The Kjakebeinet lamproites comprise a minor suite of N-S trending mica-rich dykes that cross-cut Jurassic basalt lavas and dolerites. Such rock type has not earlier been found from WDML. The dykes are c. 1 m wide, sub-vertical, and contain abundant xenoliths. Two of the dykes are located at the summit of Kjakebeinet (73º47`02``N, 14º52`40``W) the third one is c. 2 km southwards from the summit (fig. 1). Preliminary research described these dykes as lamproites that are geochemically quite similar to Leucite Hills lamproites

(Luttinen et al. 2002). Their SiO_2-content is low and CaO- and P_2O_5- content high relative to other lamproites. Based on $^{40}Ar/^{39}Ar$ dating of phlogopite, the 158.7±1.6 Ma dykes represent the youngest magmatic event so far identified in western Dronning Maud Land (Luttinen et al. 2002). Their age and paleogeographical location adjacent to southern Africa connect them to South African mica-rich kimberlites. Diamonds have not been observed, but systematic prospecting has not been done (Dr. Arto Luttinen pers. comm. 2004).

2.2 Lamproites and related rocks

Lamproites, kimberlites, and lamprophyres are mesocratic to melanocratic, usually hypabyssal igneous rocks (Woolley et al. 1996). The texture is often panidiomorfic and the rocks contain abundant mafic phenocrysts of dark mica and/or amphibole. Pyroxene and olivine may also be present. Feldspar is restricted to the groundmass. There seem to be no genetic connections between these three rock types. Earlier, however, these rocks were classified as lamprophyres (Mitchell 1994). Chemical composition of lamproites and kimberlites is alkaline. There are several ways introduced by a number of authors to classify a rock type as an alkaline one. The majority of these are based on the whole-rock chemical composition; Sørensen (1974) also uses the modal compositions. Shand (1922), according to Sørensen (1974), defines a rock as alkaline one if molar (Na_2O+K_2O), Al_2O_3 and SiO_2 in relation to each other is >1:1:6, respectively, and it is also Al_2O_3 or SiO_2 deficient. A silica saturated rock is considered alkaline, if it contains sodium pyroxene, sodium-calcium amphibole and/or alkaline amphiboles. Enrichment in certain incompatible and compatible trace elements is characteristic. The whole-rock chemistry of lamproites, kimberlites and some ultramafic lamprophyres is often so similar that mineralogical data is required to distinguish them (Mitchell and Bergman 1991). Lamproites and kimberlites are often associated with old major fault zones found in continental areas where lithospheric units with different ages are juxtaposed (White et al. 1995). Lamprophyre locations, instead, are diverse (Mitchell and Bergman 1991). White & McKenzie (1989) stated that potassic magmatism is often related to lithospheric thinning in extensive continental areas. According to Mitchell and Bergman (1991), lamproites and kimberlites do not emplace during the main episode of rifting which is dominated by basaltic magmatism.

2.2.1 Lamprophyres

Lamprophyres, in general, are quite incoherent group (Woolley et al. 1996). Some ultramafic lamprophyres and peralkaline minettes are distinquished from lamproites on the basis of mineralogy. Ultramafic lamprophyres, such as alnöite, aillikite, and alvikite contain melilite, monticellite, nepheline, melanite-grossular-andradite garnet and carbonates, but are sanidine and leucite free (Mitchell and Bergman 1991). Minette is usually a slightly alkaline rock comprised of biotite or phlogopite phenocrysts in matrix of clinopyroxene and sanidine or orthoclase. It is related to granite intrusions, such as minettes in Spanish Peaks, Colorado, or appears as mantle-derived magmas with no related rock types (Navajo Buttes, Arizona). When minette is peralkaline, it is distinguished from lamproite on the basis of phlogopite: 1) phlogopite may show complex mantling or reversed continuous zoning 2) the rims of phlogopite may be depleted in Al and enriched in Fe, Ba, and Ti with regard to the ground mass mica and the cores of the mica phenocrysts. The more intensive phleochroism in core relative to rim is due to Fe enrichment. These features are atypical for lamproites and probably indicate the presence of subsurface magma chambers and magma mixing, respectively. The composition of phlogopite varies, however, between and within minette occurrences (Mitchell and Bergman 1991).

2.2.2 Kimberlites

There are two types of kimberlites, traditionally referred as group I (basaltic kimberlites) and group II (micaceous kimberlites). Mitchell (1995) proposed name orangeite for group II kimberlites which are only found in South Africa. Group I kimberlites are volatile-rich (CO_2 dominates) potassic ultrabasic rocks (Mitchell 1995). Texture is inequigranular due to macrocrysts, and in some instances megacrysts, set in fine-grained matrix. The mega/macrocryst assemblage comprises of anhedral olivine, magnesian ilmenite, Cr-poor titanian pyrope, diopside, phlogopite, enstatite, and Ti-poor chromite. Matrix consists of olivine with one or more of the following phases: monticellite, phlogopite, perovskite, spinel, apatite, and serpentine. Some diopside-free hypabyssal group I kimberlites resemble olivine lamproites, but are distinguishable by their ground mass (Mitchell and Bergman 1991). Group II kimberlites are ultrapotassic peralkaline volatile-rich (H_2O dominates) rocks (Mitchell 1995) which show mineralogical and isotopic similarities to some phlogopite-rich lamproites. Phlogopite occurs as phenocrysts and in the ground mass.

Diopside is commonly primary, spinel, perovskite, calcite, melilite, and primary serpentine are found but monticellite and magnesium-ilmenite are absent. Macrocrystal (visible on bare eyes) olivine is present but megacrysts are rare in relation to the group I kimberlites (Mitchell and Bergman 1991). Group II kimberlite mica is of two types: in type I the Fe content is similar to lamproite mica, but Ti content is lower and Al higher. Micas of type II are similar to phenocrystal mica in Leucite Hills lamproites, but their evolutionary trends are distinguishable.

2.2.2 Lamproites

The geochemical criteria to distinguish a lamproite, referred here briefly, is represented in detail in Mitchell and Bergman (1991, p. 37). Lamproite is ultrapotassic (molar K_2O / Na_2O <3), commonly perpotassic (molar K_2O / Al_2O_3 >0.8), and peralkaline [(molar Na_2O+K_2O)/ Al_2O_3 >0.7]. In addition, Nd and Pb isotopic compositions indicate mantle-derived origin, and that the sources have been enriched in LREE (Y, La, Ce, Pr, Nd, and Pm) and depleted in U for a long period of time. If a rock contains primary plagioclase, melilite, monticellite, kalsilite, nepheline, Na-rich alkalifeldspar, sodalite, nosean, hauyne, melanite, schorlomite, or kimzeyite it can not bee classified as lamproite (Woolley et al. 1996). Melanitic, schorlomitic, and kimzeytic garnets, however, are common in lamprophyres and some group II kimberlites. The following primary phases, in widely varying amounts, characterize lamproites according to Mitchell and Bergman (1991): phenocrystal phlogopite (2-10 wt-% TiO_2, 5-12 wt-% Al_2O_3), groundmass poikilitic tetraferriphlogopite (5-10 wt-% TiO_2), potassium richterite (3-5 wt-% TiO_2, 4-6 wt-% K_2O), forsteritic olivine, diopside (Al_2O_3 and Na_2O-poor), Fe-rich (1-4 wt-% Fe_2O_3) leucite, and Fe-rich sanidine (1-5 wt-% Fe_2O_3). Diamondiferous lamproites are mainly located in areas where Archean and younger lithospheric unit are juxtaposed (White et al. 1995), as in Dronning Maud Land (Groenewald et al. 1995). The types of upper mantle-derived xenoliths and xenocrysts vary depending on the type of the host-lamproite (Mitchell and Bergman 1991). Olivine lamproites contain often dunites as xenoliths and "dogtooth" olivine as xenocrysts. Cognate suite of phlogopite-pyroxenites and diopsides are common in phlogopite- and leucite lamproites. Lherzolite and harzburgite are rarely present in both lamproite types.

2.3 Xenolith problematics

Xenoliths and xenocrysts occur in many plutonic and volcanic igneous rocks. Abundant mantle-derived nodules and crystals have been found especially in mafic and ultramafic volcanic rocks, e.g. kimberlites, lamproites, and basalts. Three principal types of xenoliths and xenocrysts exist: 1) restite material which may represent a residue from partial melting of mantle or crust 2) accidental material, which has been mingled to the magma from the walls of the conduit and 3) cognate material, which has formed from magma in question and is co-magmatic with the host-magma (Shelley 1993). The xenoliths are often referred as accidental and cognate types. If the xenoliths are not in equilibrium with the host-magma, they will dissolve or react. Whether the host-magma becomes significantly contaminated or not, depends on the amount of assimilation compared to the volume of the magma, and on the composition of the assimilant. The absence of xenoliths does not prove that material has not assimilated by the magma; xenoliths might have dissolved completely. According to Tsuchiyama (1986), the composition of partial melt generated in a peridotite xenolith in basaltic melt is not affected by the host magma, and vice versa. The size of the xenolith does not affect the rate in which the xenolith is completely digested, instead it depends on compositional differences between the host-rock and the xenolith. The melting of a simple compound and a compound consisting of solid solution differs from each other. In the former case, mass transfer is not important, but when crystal has to change its composition during melting, the diffusion in solid begins affect. For example, plagioclase may melt only few per cents under its critical temperature, and the produced cotectic melt is albite-rich. Above this critical temperature, which is 1242.5ºC at pressure of 1 atm in system diopside-plagioclase (An_{60}), melting is meta-stable and the plagioclase composition does not change (Tsuchiyama 1986).

In addition to melting, the xenoliths and their minerals are modified by metamorphic reactions; re-crystallization in constant volume and chemical changes. Metasomatism takes place when a metasomatic fluid changes the composition of the protolith. The effect is occasionally visible: if a xenolith contains atypical minerals, reflecting the composition of the fluid, modal metasomatism has taken place (Menzies & Hawkesworth 1986). Cryptic metasomatism applies if the chemical composition of pre-existed minerals changes.

Rudnick (1992) stated that distinctive features for xenoliths transported by kimberlites are green schist to amphibolite facies metamorphism and enrichment in rubidium and/or strontium. Metasomatosis may take place if the original element and isotopic ratio of the xenolithic fragment is lower than the one in the host dyke. Therefore, it is essential to study carefully the host dyke composition before handling the data collected from the xenoliths.

3. MATERIALS AND METHODS

3.1 Materials

Sampling for this study was performed in year 2001 on Kjakebeinet nunatak, on an expedition of the FINNARP. The samples were collected from two lamproite dykes (dyke 1 is the thicker and dyke 2 the narrower dyke), described in section 2.1.3, and the boulders approximately 20 m to southwest from the summit. Dyke 3 (c. 2 km to south from the summit) was used only as reference in this study; the locations of the dykes are shown in fig. 1 (section 1) after Luttinen et al. 2002. Both dykes and boulders contain abundant inclusions. The collected xenolith samples are a rough estimate on the entity of nodules present in the boulders (samples Xe1-Xe16) and in the dyke 1 (samples P1-P9). Ultramafic xenoliths were especially sought after.

3.1.1 Thin sections and hand specimen

18 thin sections on the dyke 2, c. 40 cm in diameter (sample K3O, fig. 36 section 6), were prepared at the Department of Geology, University of Helsinki, by Ms. Helena Korkka. A

Table 1 Hand specimens and preparations. In the first row, from left to right, is sample ID, then follows the types of the preparations, if the hand specimen has been available for this study, and the estimated size of the hand specimen in centimeters or alternatively in kilograms. Sample K3O is from dyke 2.

Sample ID	Preparation	hand specimen	hand specimen size	Sample	Preparation	hand specimen	hand specimen size
XE-1	pt	X	c. 5kg	P-1	pt	X	c. 1x9cm
XE-2	pt	X	c. 6x6x4cm	P-2	pt	X	c. 4x3x2cm
XE-3	pt	X	c. 3x8x4cm	P-3	pt	X	c. 2x4cm
XE-4	pt	X	c. 5x6x5cm	P-4	pt	X	c. 3x4cm
XE-5	pt	X	c. 9x5x3cm	P-5	pt	X	c. 2x4cm
XE-6	pt	X	c. 16x10x6cm	P-6	pt	X	c. 3x5cm
XE-7	pt	X	c. 10x3x5cm	P-7	pt	X	c. 3x2cm
XE-8	pt	X	c. 7x4x4cm	P-8	pt	X	c. 5x4cm
XE-9	pt	X	c. 7x5x5cm	P-9	pt	-	
XE-10	2pt	X	c. 10x7x5cm	K3O	10t+8 pt	X	40x15x10c
XE-11	2pt+m	X	c. 7x7cm	XE=Xenolith from the boulders			
XE-12	pt	X	c. 9x5x5cm	P=Xenolith fron the dyke K3P			
XE-13	pt	X	c. 4x3x4cm	K3O=Cross-section of the dyke K3O			
XE-14	pt	X	c. 5x4cm	t=thin section			
XE-15	3pt+m	X	c. 0,5kg	pt=polished thin section			
XE-16	pt+m	X	c. 4x4cm	m= mineral separation			

40 cm cross-section of dyke 2 is represented by thin sections K3O1-K3O9. Thin sections of dyke 1 (sample AL/KB8-98) and dyke 3 (sample AL/KB21-98) were used to compare the mineralogy and petrography of the dykes. Quantitative mineral chemical data on dyke 2 (sample AL/KB6) and dyke 3 (sample AL/KB21) (Luttinen, unpublished) were also used as reference material. The estimates represented on the xenolith size in table 1 were made from heels of the first 25 polished thin sections. According to table 1, the xenoliths sampled from the boulders are bigger and more abundant than the ones from the dyke 1. The boulders expose a wider surface than the dykes in the outcrop; therefore nodules in them were probably easier to discover and sample. Leucocratic xenoliths were only found from the boulders, not from the two dykes. Moreover, xenoliths extracted from outcrops were only sampled from one location in the dyke 1 (Dr. Arto Luttinen and Dr. Saku Vuori, pers. comm. 2005). It is thus presumable that the samples from boulders are more representative of the crust under WDML than the material sampled from dyke 1.

3.1.2 Mineral separations

Table 2 Mineral fractions used in the samarium, neodymium, rubidium, and strontium isotope determinations. Weight mg is the amount of separate in 10^{-3} grams weighted for analyses.

Sample ID	Fraction	Weight mg	Description	Impurities
Xe-11	Apat	1,2		Micron-scale inclusions
Xe-11	Pl	204,2	Mostly dim grains but clear, transparent ones occur. Less magnetite than in the fraction of Xe-16 plagioclase.	Magnetite
Xe-15	Calc	130,4	Mostly dim grains but clear, transparent ones occur. Some andradite present.	Andradite
Xe-15	Cpx	185	Some andradite occurs, otherwise pure	Andradite
Xe-16	Cpx	176,4	Mixed clinopyroxene-magnetite grains present.	Magnetite
Xe-16	Pl	201,2	Mostly dim grains but clear, transparent ones occur. Some magnetite present.	Magnetite

Abbreviations: Apat apatite, Calc calcite, Cpx clinopyroxene, Pl plagioclase.

Mineral separation procedure is described in section 3.2.7. Most of the fractions contained impurities, but apatite of sample Xe-11 (layered granulite) had only micron-scale inclusions, probably fluid (table 2). In plagioclase fractions and clinopyroxene of sample Xe-16 (garnet granulite) minor mixed magnetite-bearing grains were present. Both plagioclases contained dim and transparent grains; the dim grains dominated. Calcite and clinopyroxene of carbonatite (Xe-15) had minor titanian andradite as impurities. In addition, calcite was dominated by dim grains, but also clear grains were present.

3.2 Methods

3.2.1 Thin section study

The thin sections were studied with a Nikon petrographic microscope to identify the minerals and the rock types, describe their petrography, and choose samples for microprobe analysis. Point counting (1000 points) was made to determine the mode (mineral proportions in volume percentages). In strongly lineated or melted samples, a rough estimate of the mode was made using the thin section and hand specimen. Results on point counting are shown in appendix 3 table 1. Colour index is according to Streckeisen (1973) (cf. Le Maitre et al. 1989), and the index has been determined for samples that were point counted (table 9 section 8). In photomicrographs abbreviation ppl refers to plain polarized light and xpl to polarized light. Thin section study was made at the Department of Geology, University of Helsinki, except for some that were made at the Geological Survey of Finland, Espoo.

3.2.2 Microprobe analyses

Semi-quantitative microprobe analyses on the minerals were made by the author using the JEOL JXA-8600 electron microprobe at the Department of Geology, University of Helsinki. The analyses were performed on polished thin sections covered with carbon in EDS (energy dispersive spectrometer) mode with 15 kV accelerating potential and 1 nA beam current. The beam diameter was 1 μm and time used in a single measurement 100 effective seconds. Microsondlab-software uses the ZAF procedure, which is commonly in use for converting the measured energies to atomic proportions of elements (Waters 2004). Water and carbon can not be measured on EDS alone. Normalized atomic proportions are acquired after the elements have been manually selected. It must be emphasized that amphibole and mica analyses made alone with this equipment are poorly comparable to quantitative data as such (Prof. Ragnar Törnroos pers. comm. 2006).

3.2.3 Recalculation of the mineral chemical data

The oxide weight percentages were calculated on a spreadsheet made by the author. The numbers of ions as well as end-member percentages were calculated from the oxide weight

percentages using the spread sheets by Preston (1999) with some exceptions. I modified some of the spread sheets, e.g. to recalculate the proportion of andradite garnet and ferric iron content in it using the equation (1) after Droop (1987).

$$F=2X*(1-T/S) \quad (1)$$

where F is the number of Fe^{3+} ions per X oxygen atoms, T is the ideal number of cations per formula unit and S is the observed total of cations, with all iron calculated as Fe^{2+}. Pyroxene spread sheet was modified to convert a bug on the recalculation of silicon and aluminium on the site T (appendices 1 and 2, tables 9 and 5). Apatite compositions are given in weight percentages only due to some analyses which contain over 3 wt-% fluorine (fluor-apatite) (appendices 1 and 2, table 1). The carbonate recalculation sheet was compiled by the author. In the case of the dykes 2 and 3, qualitative reference analyses on phlogopite and pyroxenes (Luttinen, unpublished) were available. In the appendices, the semi-quantitative analyses represented are normalized to 100 (appendices 1 and 2). Comparing the mica analyses to reference data (Section 8) analyses made at the University of Helsinki have been normalized to 93.6 because the mean water content measured is 6.4wt-% according to the mean of three mica analyses (Luttinen, unpublished). This same assumption has been applied concerning the mica in sample P-3 (phlogopite rock) and Xe-15 (carbonatite). In the case of water-free minerals, such as pyroxene, the reference data used was recalculated to 100. The whole-rock chemical compositions (Fig. 15 Section 5, appendix 3) were calculated combining the modes and the mineral chemical compositions. In the case of clinopyroxene-feldspar intergrowths the feldspar (8 vol-% of the pyroxene) has been taken into account; the feldspar composition used is the one measured from the respective sample (if several measurements, an arithmetic mean were used), clinopyroxene composition is an arithmetic mean on the clinopyroxene in contact with the plagioclase.

3.2.4 Mineral identification and classification

The minerals were identified on the basis of transmitted-light microscopy and microprobe analyses. Amphibole names and classification are after Leake et al. (1987) and pyroxene analyses were handled according to recommendation established in Morimoto et al. (1989). Feldspar, garnet, mica, and spinel group mineral nomenclatures are after Deer et al. (1992).

3.2.6 Nomenclature of metamorphic rocks

The naming of the metamorphic rock types in this thesis follows recommendations after Schmidt et al. (2004) that concern medium- to high-grade rocks (Coutinho et al. 2004). The references are published as web versions by the IUGS Subcommission on the Systematics of Metamorphic Rocks dated in 2004 and are available at the website of British Geological Survey (http://www.bgs.ac.uk).

3.2.7 Stable isotope analyses and sample preparation

The oxygen and carbon isotopes of a carbonatite inclusion Xe-15, was studied. The whole rock composition was analyzed with gas-source mass spectrometer Thermo Finnigan Delta plus Advantage at the Department of Geology, University of Helsinki with the assistance of M.Sc. Akseli Torppa. The whole rock powder was detached with a drill from three points of the xenolith relatively close to each other, with a varying distance from the lamproite contact. A 0.4 -0.5 mg aliquot of whole rock powder per sample was weighted for analysis. 102% phosphoric acid at 70 °C was used for one hour to release the carbon dioxide for the measurement. The Halpanen calcite was used as a quality standard, and the accuracy and repetitiveness for measured elements, carbon and oxygen, was better than ± 0.1 per mil. The concept of δ value for oxygen is in equation (2) after Rollinson (1993)

$$\delta^{18}O‰ = [(^{18}O/^{16}O\ (\text{sample}) - ^{18}O/^{16}O\ (\text{standard})) * (^{18}O/^{16}O\ (\text{standard}))^{-1} * 1000] \quad (2)$$

For carbon the $^{18}O/^{16}O$ is replaced with value of $^{13}C/^{12}C$. The results are given as $\delta^{18}O$ values relative to the VSMOW standard and as $\delta^{13}C$ values relative to the VPDB standard. The $\delta^{18}O$ values relative to the VPDB standard were recalculated to the VSMOW standard using the equation 3 after Coplen et al. (1983).

$$1.03086 * \delta^{13}C\ \text{VPDB} + 30.01 \quad (3)$$

3.2.7 Radiogenic isotope analyses and sample preparation

Six mineral separates (table 2) and three whole rock samples were studied for their Sm-Nd and Rb-Sr isotope compositions. Two of the samples represent gabbroic xenoliths (fig.15 section 5.1) which are present in the dyke 2 and in the boulders. The third one is a carbonatite for which the oxygen and carbon isotope analysis was also made. Mineral

separates were prepared as follows: The host lamproite was sawn off from the selected samples (Xe-11, Xe-15 and Xe-16). The remaining material consisting only on xenolithic material was milled in an iron swing-mill and sieved to fractions of under 0.075 mm, 0.125-0.250 mm, 0.250-0.5 mm, and over 0.5 mm in diameter. Whole rock powder was made separately in iron swing-mill from undamaged rock, except in the case of the sample Xe-16, where the whole rock powder was milled from the fraction coarser than 0.5 mm, due to the small size of the xenolith. I separated the minerals using hand-magnet, Franz isomagnetic separator, and heavy liquids [sodium polywolframate, thallium malonate formate (Clerici), and bromoform], and hand-picking to get fractions suitable for Sm-Nd and Rb-Sr isotope analyses. The separation with the Clerici solution and bromoform was made at the Geological Survey of Finland, Espoo, with the assistance of Ms. Leena Järvinen. A few XRD analyses were made on the mineral separates by Prof. Martti Lehtinen at the Department of Geology, University of Helsinki. Six mineral fractions and three whole rock powders were chosen for isotope analysis: Apatite and plagioclase from the layered granulite (Xe-11), calcite and clinopyroxene fractions from the carbonatite (Xe-15), and apatite, clinopyroxene and plagioclase from the garnet granulite (Xe-16). Before a leaching procedure the mineral separates were washed with a dilute HNO_3 and apatite in a dilute HCl in an ultrasonic bath. At this stage apatite separate from sample Xe-16 was dissolved and therefore destroyed. The descriptions after the mineral separates are shown in table 2.

The weighted separates (table 2), 150mg (Xe-11 and Xe-16) and 500mg (Xe-15) of whole rock powders, were dissolved in teflon vials in a 1:4 mixture of HNO_3 and HF, calcite in HCl. After evaporation the samples were dissolved in HCl and a clear solution was spiked with ^{149}Sm-^{150}Nd and ^{87}Rb-^{84}Sr in tracers. Rubidium, strontium, and light rare earth elements were separated using standard cation exchange chromatography. After this the LREE (Sm and Nd) were separated from each other on quartz columns. Isotope ratios of Sm, Nd, and Sr were measured on a VG Sector 54 mass spectrometer (those of Nd and Sr in dynamic mode). Isotopic measurements on Rb were performed using a noncommercial Nier-type mass spectrometer built at the Geological Survey of Finland. Repeated analyses of La Jolla Nd standard gave $^{143}Nd/^{144}Nd$ of 0.511847±0.000008 (when measuring the apatite and whole rock powder of sample Xe-11) and 0.511849±0.000008 (mean and

external 2s error of nine measurements) and for the other measurements. External error in the reported ^{143}Nd-^{144}Nd ratios is estimated to be better than 0.0025%. Repeated analyses of NBS987 Sr standard gave $^{87}Sr/^{86}Sr$ of 0.710268±0.000020 (mean and external 2s error of eleven measurements). The ^{87}Sr-^{86}Sr ratios are reported relative to $^{87}Sr/^{86}Sr$ 0.71024 of NBS987 and the external error is probably better than 0.002%. Isotope analyses were made at the Geological Survey of Finland, Espoo, in the guidance of Dr. Hannu Huhma, Ms. Tuula Hokkanen, and Mr. Arto Pulkkinen.

Standards used in calculations as well as the results are represented in section 7 in table 7. Epsilon values for Sr and Nd (at present to make comparisons between the host and other rock types and at 180 Ma to estimate the relationship to the Jurassic basaltic magmatism) were calculated using the following equation after Rollinson (1992):

$$\varepsilon^{t}(^{143}Nd/^{144}Nd)=[(^{143}Nd/^{144}Nd_{sample}-^{143}Nd/^{144}Nd_{standard})/(^{147}Sm/^{144}Nd_{sample}-{}^{147}Sm/^{144}Nd_{standard})+1] \quad (4)$$

When epsilon strontium is calculated $^{143}Nd/^{144}Nd$ is replaced by $^{87}Sr/^{86}Sr$ and $^{147}Sm/^{144}Nd$ by $^{87}Rb/^{86}Sr$ values. The reference used in these calculations is the value of CHUR (value of chondrite uniform reservoir ie. the bulk earth for neodymium isotopes); the specific value used is represented with the results (section 7). In the favourable case the depleted mantle model ages gives the crustal residence age of the magma. These ages were iterated using a spread sheet made by the author. For this, the equations of epsilon value (4) and epsilon value for depleted mantle after DePaolo 1981 (5) were used.

$$\varepsilon^{DM}(T)=0.25T^{2}-3T+8.5 \quad (5)$$

where T is the time at 10^{3} Ma.

The Rb-Sr isotope ratios of the samples as well as the concentrations of these elements (section 7 table 7) were calculated using GWBasic software, those of Sm-Nd using a spread sheet made by M.Sc Jeremy Woodard. The errorchrons were plotted on Isoplot software (Ludwig 1999); the diagrams constructed are shown in section 7.

4. PETROGRAPHY OF THE XENOLITHS

The xenoliths from the boulders and dyke 1 are divided to groups on the basis of their mesoscopic and microscopic appearance. The grouping emphasizes the differences between the xenoliths in terms of their structure, mode, and protolith. The term gneiss is designated here to metamorphic rocks displaying a gneissose structure (Butcher and Frey 1994) regardless of the grain-size (cf. Shelley 1993 p.103). Mineral assemblages and colour indices, if determined, are listed in table 8 (section 8). Mineral chemical analyses for apatite (table 1), amphiboles (table 2), carbonates (table 3), garnet (table 4), mica (table 5), plagioclase (table 6), potassium feldspar (table 7), symplectic feldspar (table 8), pyroxenes (table 9), rutile (table 10), spinel group minerals (table 11), and ilmenite (table 12) are shown in appendix 1. All the xenoliths are rounded and those from the boulders seem to be larger than those from the dyke 2. The shape of xenoliths has probably been modified mechanically during the transportation (Tsuchiyama 1994).

4.1. Tonalite gneisses

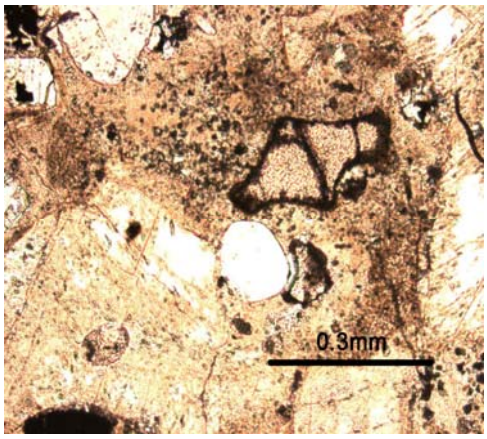

A **B**

Figure 2. Tonalite gneiss Xe-4 in hand specimen (A) On the left is the cut surface, on the right the weathered surface. Scale bar is in centimeters. Xe-4, photomicrograph, ppl (B). The brownish mineral with high relief is garnet, the white mineral below the garnet is quartz, and in the lower left corner is seritized plagioclase.

These samples represent leucocratic, weakly to moderately lineated, fine- to medium-grained gneissic rocks. Characteristic is un-twinned plagioclase, granoblastic texture, and secondary, fibrous orthoclase along the grain boundaries. Orthoclase co-exists with minor, euhedral carbonate. Presence of garnet and signs of partial melting are pointing to high-grade metamorphic conditions.

Sample Xe-1

This sample comprises of plagioclase (60 vol-%) and quartz (29 vol-%). Accessory minerals are magnetite (3.5 vol-%), calcite (2.8 vol-%), apatite (1.2 vol-%), ankerite pseudomorphs after orthopyroxene (1.8 vol-%), chlorite (1.2 vol-%), hematite, and zircon. Plagioclase (An_{0-32}) is anhedral, sericitized, and mostly un-twinned. Some albite twinned crystals are present. Composition based on maximum extinction angle is An_{40}. Quartz shows undulose extinction. Apatite is anhedral. Garnet? is altered completely to silica- (56-59 wt-% SiO_2), iron- (17-21 wt-% FeO) and magnesium-rich (11-15 wt-% MgO), strongly green-yellow pleochroic mixture (mainly chlorite?). Deeply brownish-red hematite contains 6-25 wt-% MgO, which probably refers to coexistence with spinel group mineral magnesioferrite. Metamictic zircon is brownish and rounded.

Sample Xe-4

Minor quartz veinlets are observed in thin section. Plagioclase (56.5 vol-%) and quartz (31.7 vol-%) are the main phases, and fresh, almandine-rich garnet is present. Accessory minerals are ankerite (4.4 vol-%), chlorite (3.1 vol-%), magnetite and pyrite (2.9 vol-%), apatite (0.8 vol-%), hematite (0.6 vol-%), and zircon. Plagioclase (An_{2-25}) is mainly un-twinned, some albite-twinned crystals exists. Plagioclase composition based on maximum extinction angle is An_{37}. Quartz shows undulose extinction. F-bearing apatite is anhedral and has irregular, F-free rim. Chlorite is iron-rich and shows strong green-yellow pleochroism. Hematite is MgO-bearing (6-9 wt-%) and therefore probably coexists with spinel group mineral magnesioferrite. Metamictic zircon is rounded and has overgrowth, probably metamorphic in origin (cf. apatite).

Sample Xe-9

This medium-grained rock contains sparse mafic bands. Granoblastic plagioclase (50 vol-%) and occasionally polycrystalline, undulose quartz (40 vol-%) are the main phases. Accessory minerals are garnet, magnetite, ilmenite, apatite, carbonate, zircon, and aegirine.

The narrow mafic layers are distinguished by garnet, apatite, rutile, aegirine, and titanoferous magnetite. Plagioclase (An_{0-27}) is serisitized, often completely altered. Almandine-rich garnet is partly chloritized and contains red oxide inclusions. Magnetite and ilmenite co-exist and comprise simple exsolution textures. Aggregates of magnetite and chlorite probably replace biotite. Anhedral, greenish agirine occurs along grain boundaries with fibrous orthoclase. The mineral abundances represented are based on visual estimate.

4.2 Augen gneisses

The common denominators of the augen gneisses are augen texture, medium grain size, and abundant potassium feldspar. In hand specimen samples Xe-2, Xe-3, and Xe-12 are similar to each other and different from sample Xe-5. Sample Xe-5 is more leucocratic. Both samples Xe-2 and Xe-3 contain accessory aegirine. Due to strong lineation point counting was not made; dominating phases, however, are potassium feldspar and quartz. Chlorite is occasionally abundant. Microcline is present in all samples. Quartz is mainly polycrystalline and shows undulose extinction. Quartz and strongly altered feldspar comprise granoblastic texture between the coarser potassium feldspar and quartz grains

Figure 3. Augen gneiss Xe-2 in hand specimen. The weathered surface (left) and the cut surface (right). The scale bar is in centimeters.

Sample Xe-2

Anhedral quartz shows undulose extinction and is universally mantled by greenish, acicular mineral (alkali amphibole?). Medium-grained, saussuritized potassium feldspar is mainly cross-hatch twinned microcline with quartz inclusions. Plagioclase has altered to a brown mineral and albite twinning is occasionally observed. Accessory minerals are chlorite, calcite, and zircon.

Sample Xe-3

Quartz shows undulose extinction. Potassium feldspar is rounded and saussuritized, showing either cross-hatch twinning or perthitic texture. Potassium feldspar encloses magnetite crystals. Accessory minerals are anhedral apatite, calcite, magnetite, zircon, sodium pyroxene, chlorite and un-identified phosphate. Zircon is metamictic and brownish, sodium pyroxene shows light green pleochroism. Chlorite is rich in Si and Fe (70 wt-% SiO_2, 17 wt-% FeO) and contains some Mg and Al (7 wt-% MgO and 7 wt-% Al_2O_3).

Sample Xe-5

Microcline is cross-hatch twinned. Quartz shows undulose extinction and encloses probably rutile. Occasional poorly developed ribbon-quartz microstructure is observed. Plagioclase (An_{30}) is serisitized and mainly completely altered, but contains some relict albite-twinnig. Accessory minerals are anhedral apatite, ankerite, metamictic zircon, and iron-rich chlorite. Fibrous orthoclase occurs along the grain boundaries.

Sample Xe-12

This sample is a bit more sheared than the other augen gneisses. Cross-hatch twinned, occasionally perthitic potassium feldspar has pressure shadows of quartz. Quartz shows undulose extinction, some of the grains are polycrystalline. In places the quartz encloses acicular sodium-pyroxene crystals. Plagioclase has altered, as in sample Xe-5, some relict albite-twinning is observed. Accessory minerals are brownish zircon, anhedral apatite, and calcite.

4.3. Alkali feldspar granite gneisses

These xenoliths are medium- to coarse-grained and equigranular. Potassium feldspar is mainly perthitic, and quartz shows undulose extinction. Some brecciation is observed. Secondary, fibrous orthoclase is abundant along the grain boundaries. Occasionally the orthoclase has nearly spherulitic habit. Alteration of the feldspars is strong and it is difficult to distinguish between plagioclase and potassium feldspar. The mineral abundances are based on visual estimates.

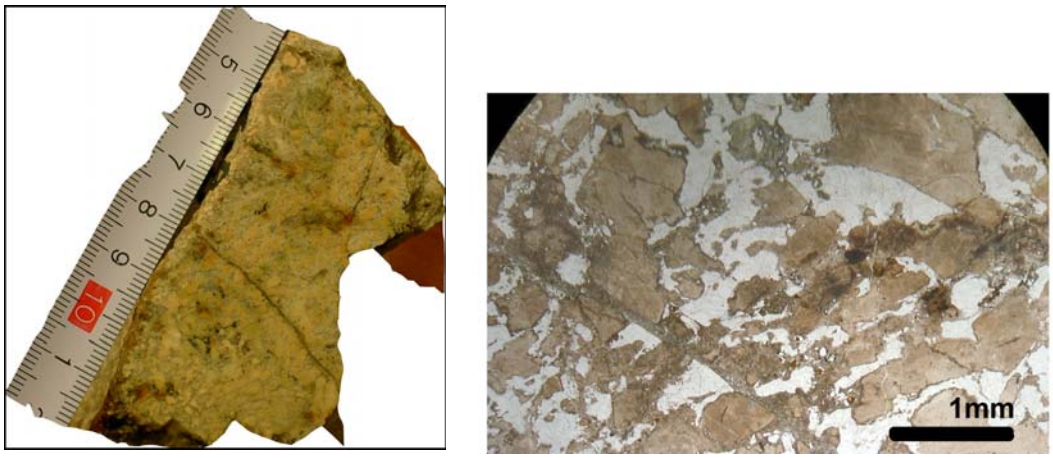

A B

Figure 4. Alkali feldspar granite gneiss Xe-8 in hand specimen (A), cut surface. The scale bar is in centimeters. Photomicrograph on sample Xe-8 (B), ppl. Note that potassium feldspar is strongly altered.

Sample Xe-6

Microcline (60 vol-%) is saussuritized, and poikilitic with plagioclase inclusions. Occasionally corroded quartz (30 vol-%) shows undulose extinction. Albite twinned plagioclase (10 vol-%) is oligoclase according to its maximum extinction angle. Based on the microprobe analyses plagioclase composition is $An_{2\text{-}15}$. A narrow quartz vein is seen in a thin section; it contains corroded, anisotropic, greenish grains with low refractive index compared to quartz. Accessory minerals are apatite, magnetite, and calcite.

Sample Xe-7

Anhedral potassium feldspar (50 vol-%) is strongly saussuritized. Quartz (40 vol-%) shows undulose extinction. Plagioclase (10 vol-%) is altered to brownish, and only relict albite-twinning is observed. Accessory minerals are euhedral, occasionally anhedral calcite, ankerite, chlorite, muscovite, and un-identified phosphate.

Sample Xe-8

This sample is mesoscopically brecciated and sheared. No microprobe analyses have been made because of strong saussuritization and the analogue to the sample Xe-6. Potassium feldspar (50vol-%) is medium-grained, saussuritized, and some signs after cross-hatch twinning exists. Quartz (40vol-%) is medium-grained, shows undulose extinction and is occasionally sheared. Accessory minerals are carbonate, chlorite, opaque mineral, zircon, and plagioclase. Plagioclase is strongly altered showing relict albite twinning.

4.4 Layered granulites

The granoblastic, layered granulites have preserved an igneous layered texture. Samples P-4 and Xe-11 are ultramelanocratic to melanocratic, quartz-free types, and sample Xe-10 is a leucocratic, quartz-bearing rock (fig. 5). In addition to the layering, clinopyroxene in both types has symplectic texture. Hornblende-pyroxenite P-4 probably represents a plagioclase-free part from a rock type similar to sample Xe-11.

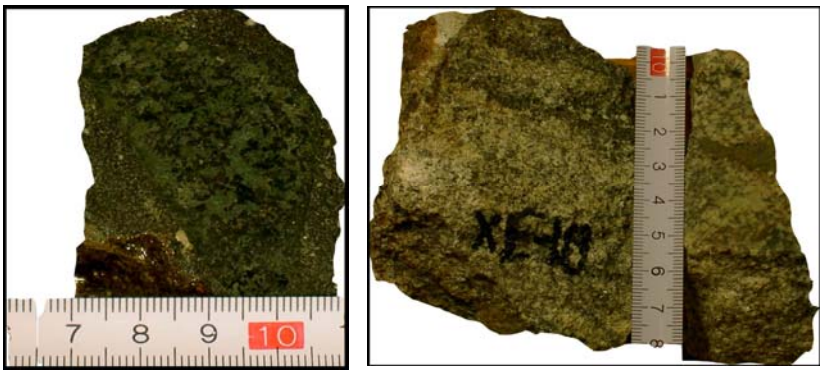

A **B**

Figure 5. The layered granulites. Ultramelanocratic granulite P-4 in hand specimen (A), cut surface. The texture and mineralogy is similar to the one observed in the ultramelanocratic layer of sample Xe-11. Leucocratic granulite Xe-10 in hand specimen (B). The eroded surface (left) and the cut surface (right). The scale bar is in centimetres.

Sample Xe-10 leucocratic granulite

This sample is medium- to coarse grained. Plagioclase (64.8 vol-%), Quartz (13.6 vol-%), and augite (18.3 vol-%) comprise the major phases. Accessory minerals are altered garnet (3.3 vol-%) apatite, magnetite, rutile, carbonate, and zircon. In thin section the grain boundaries are curved, and the present composition of the rock is quartz dioritic. Plagioclase (An_{25-28}) varies between albite-twinned and un-twinned forms. Quartz shows undulose extinction and contains abundant fluid inclusions. Na_2O-bearing (c. 1 wt-%) augite is surrounded by fine-grained, up to 0.25 mm wide symplectic coronae and may occasionally be completely symplectic. Fine-grained magnetite and carbonate occur along the grain boundaries of plagioclase and clinopyroxene. Altered garnet, showing as anhedral opaque phase in thin section (fig. 6) forms sparse, thin layers. These layers are accompanied with fine-grained material, probably originated by partial melting. Otherwise the rock seems to be very homogenous. The composition of the altered garnet resembles

pyrope-almandine garnet; but as in fig. 6 B, the grains comprise very fine-grained material. The altered garnet encloses Ca-poor pyroxene that is symplectic with labradorite (An_{56}). Pyroxene is greenish-light brown pleochroic and Al_2O_3-rich (8-9 wt-%) in composition.

Sample P-4 hornblende-pyroxenite

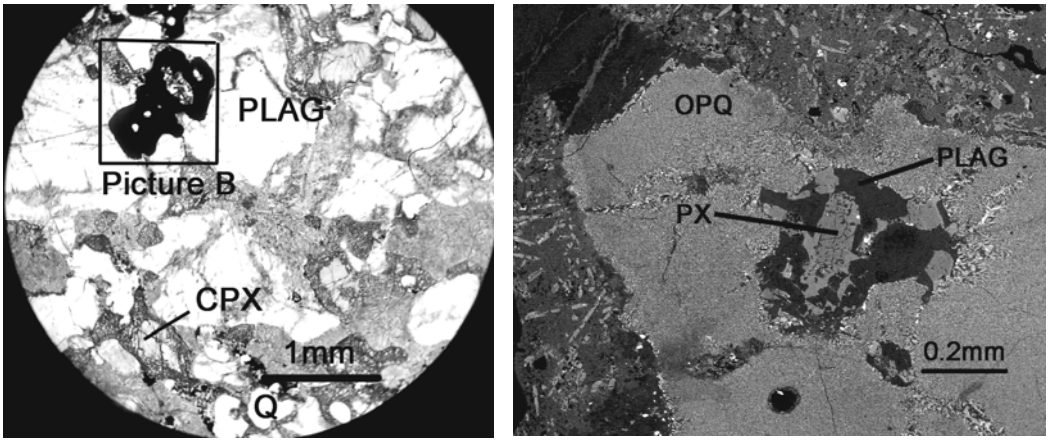

A **B**

Figure 6. Quartz dioritic leucocratic granulite (sample Xe-10) in photomicrograph (A), ppl and in BS-image (B). Area of B is depicted in A. In B the fine-grained material on top, left, is of partially melted part. Abbreviations: PLAG, plagioclase; CPX, augite; Q, quartz; PX, low-calcium pyroxene; and OPQ, optically opaque altered garnet.

Mesoscopically, the xenolith P-4 is well rounded, medium-grained, and has a sharp contact with the dyke. The main phases are diopside (55.7 vol-%), magnesio-hastingsitic hornblende (34.8 vol-%), and titanoferous magnetite (6.3 vol-%). Accessory minerals are dolomite (1.6 vol-%), and apatite (0.3 vol-%). Diopside forms symplectites with potassium-bearing oligoclase (An_{13}). Hornblende is yellow-brownish to yellow pleochroic and relatively altered (fig. 7 B). Fine-grained carbonate and anhedral apatite are enclosed by diopside. Magnesium-rich biotite and titanoferous magnetite occur along the grain boundaries of hornblende.

Sample Xe-11 andesine-hornblende-pyroxenite

This sample is medium-grained and shows both mineralogical and grain-size layering. The layering comprises of clinopyroxenite bands which grade to plagioclase-bearing layers. Contact towards the host-dyke is sharp. Thin section Xe-11.1 represents a clinopyroxenite layer, which is comparable to sample P-4: the main phases are clinopyroxene (48 vol-%) and ferro-pargasitic hornblende (38 vol-%). Accessory minerals are apatite, magnetite, carbonate, biotite, and pyrite. Weakly green pleochroic, Ca-rich diopside forms symplectic

intergrowths with albite (An_7), encloses pyrite and sporadically some carbonate. The composition of vermicular feldspar in symplectite is, now and then, rich in potassium (11-12 wt-% K_2O). Anhedral, altered hornblende (fig. 7), is brownish-yellow to greenish-yellow pleochroic and contains up to 5 wt-% TiO_2. An un-altered, but possibly secondary, overgrowth of hornblende (thin section Xe-11.2) gives the maximum titanium content measured (4.7 wt-%). Hornblende encloses apatite and carbonate. Some biotite has crystallized into cracks. Both clinopyroxene and hornblende contains abundant, tiny magnetite crystals.

In the plagioclase-bearing part (thin section Xe-11.2) the major phases are hornblende (46.4 vol-%), clinopyroxene (34.6 vol-%), and plagioclase (17.9 vol-%). Accessory minerals are magnetite (0.6 vol-%), carbonate (0.5 vol-%) and apatite (not detected in point counting). The vermicular feldspar in symplectites is andesine (An_{49}), and it contains some potassium. Slightly sericitized, anhedral plagioclase (An_{23}) has typically a very fine-grained reaction corona texture: towards the reacted rim composition changes from oligoclase (An_{23}) to albite (An_6). Three types of plagioclase are observed: 1) un-twinned, 2) poikilitic, albite-twinned and 3) interstitial, undulose and fresh. The latter is albite ($An_{3.5}$) in composition. Fine-grained, serpentinized relicts, coated with magnetite, are more abundant in thin section Xe-11.2 than in Xe-11.1. Those are probably pseudomorphs after olivine.

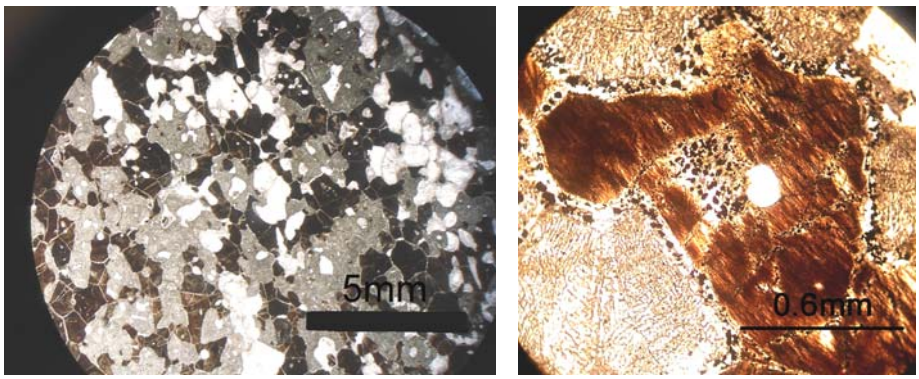

A **B**

Figure 7. Photomicrographs (ppl) of a plagioclase -bearing, melanocratic layer (A) and an ultramelanocratic layer (B) in hornblende-plagioclase-pyroxenite Xe-11. In the middle of B is hornblende with magnetite on grain boundaries. The round mineral inside hornblende is carbonate. On the lower left corner shows clinopyroxene-plagioclase symplectite.

4.5 Meso-melanocratic granulites

Melanocratic, gabbroic mineral assemblage and granoblastic texture typify these samples. Mesoscopically, the medium-grained, garnetiferous samples P-7, P-8, and Xe-16 are similar to each other. Though, sample P-7 has a coarser, re-crystallized rim against the dyke. It differs from the others also by its composition (fig. 15) and presence of subhedral hornblende. Samples P-2 and P-6 are fine-grained, distinguished by albite twinned, relatively Ca-rich plagioclase, fresh clinopyroxene and the lack of garnet. Sample P-2 shows a gneissic, banded structure and contains two types of pyroxene, augite and enstatite.

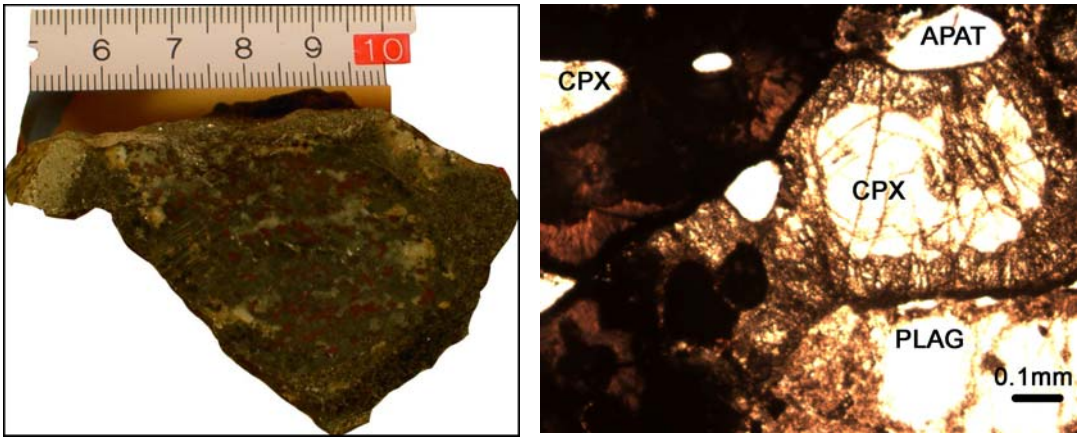

A B

Figure 8. Melanocratic garnet granulites. Sample P-8 in hand specimen (A), cut surface. The scale bar is in centimeters. Sample Xe-16, photomicrograph (B), ppl, shows reaction textures between clinopyroxene and plagioclase. The dark material with fibrous habit on left is pseudomorphs after garnet. Abbreviations: APAT, apatite; CPX, clinopyroxene; and PLAG, plagioclase.

Sample P-7 plagioclase-garnet-augite-hornblende granulite

This sample shows, relative to the core of the xenolith, a coarser-grained boundary towards to the host. Presumably the 2-3 mm thick boundary has re-crystallized due to the magmatic transport. Main phases are plagioclase (50.3 vol-%), pseudomorphs after garnet (17.2 vol-%), augite (15 vol-%) and hornblende (10.4 vol-%). Accessory minerals are opaque (3.2 vol-%), carbonate (1.5 vol-%), apatite (1.3 vol-%), and chlorite (1.10 vol-%). Plagioclase (An_{4-23}) is mainly albite- but occasionally un-twinned. The most calcic composition, An_{23} is found in a crystal enclosed by a pseudomorph after garnet. The anisotropic, dark brown to orange in color, pseudomorphs after garnet consist of tiny particles, sized below 1μm. The composition of the pseudomorph is very close to iron-magnesium garnet, ranging between

45-52 wt-% SiO_2, 23-30 wt-% Al_2O_3, 5-14 wt-% FeO, 2-9 wt-% MgO, 2-9 wt-% CaO, 1-5 wt-% Na_2O, and 0-3 wt-% K_2O. The grains rarely enclose un-altered almandine-pyrope, apatite, augite, and plagioclase. Sodium-free augite occurs symplectically with potassium feldspar (13 wt-% K_2O). When pyroxene is enclosed by a pseudomorph of garnet, it contains 2 wt-% Na_2O. Subhedral hornblende show yellow-yellowish brown pleochroism. Apatite is anhedral and fluorine- and chlorine-bearing in composition.

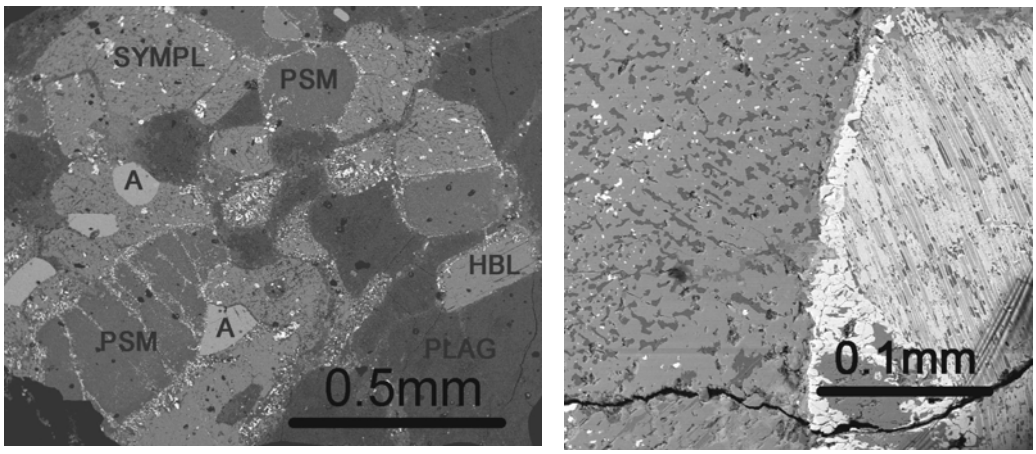

A **B**

Figure 9. Melanocratic garnetiferous granulites. Sample P-7(A) shows granoblastic texture, BS-image. Sample P-8 (B), BS-image. On the left is symplectite of clinopyroxene (light grey) and feldspar (darker grey). White spots are magnetite. On the right, altered ilmenite consists of titanium-bearing (17 vol-% TiO_2) magnetite (almost white lamellae) and rutile (the light grey lamellae). The boundary between the ore and symplectite is titanium-bearing magnetite. Abbreviations: A, apatite; HBL, hornblende; PLAG, plagioclase; PSM, pseudomorph after garnet; and SYMPL; augite-feldspar symplectite.

Sample P-8 plagioclase-clinopyroxene-granulite

Clinopyroxene (42.7 vol-%), plagioclase (25.8 vol-%), Opaque minerals magnetite, ilmenite, and pyrite (15.4 vol-%), and pseudomorphs after garnet (9.90vol-%) comprise the major phases. Accessory minerals are ankerite (4.50 vol-%), apatite (1.7 vol-%), and secondary reddish brown biotite (not detected in point counting). Clinopyroxene, calcic augite-diopside in composition, occur symplectical with albite (An_8). Apatite and opaque are enclosed by pyroxene. Anhedral plagioclase (An_{4-18}) is un-twinned. Altered ilmenite with exsolution lamellae (fig. 9 B) consists of titanian magnetite and rutile. The brown to orange colored pseudomorphs after garnet consist of tiny magnetite grains and a substance

rich in silica, aluminum, and iron. Fine-grained carbonate and orthoclase occur as secondary minerals along the grain boundaries.

Sample Xe-16 Plagioclase-augite-garnet-granulite

The main phases comprise augite (38.4 vol-%), plagioclase (26.9 vol-%), pseudomorphs after garnet (22.1 vol-%), and opaque minerals (7.5 vol-%). The opaques include pyrite, magnetite, and titanoferous magnetite with exsolved rutile. Accessory minerals are apatite (3.6 vol-%), calcite (1.0 vol-%), and amphibole. Clinopyroxene shows 0.1mm wide, clinopyroxene-feldspar symplectic rim. Anhedral plagioclase (An_{20-24}) is mainly un-twinned. As in the other samples, the anisotropic pseudomorph after garnet comprises on fine-grained (~1μm in diameter) material. The pseudomorph encloses almandine-pyrope, clinopyroxene, plagioclase and apatite. Calcite is occasionally prismatic, commonly anhedral. Hornblende is brownish and is observed next to the dyke contact. Apatite is anhedral.

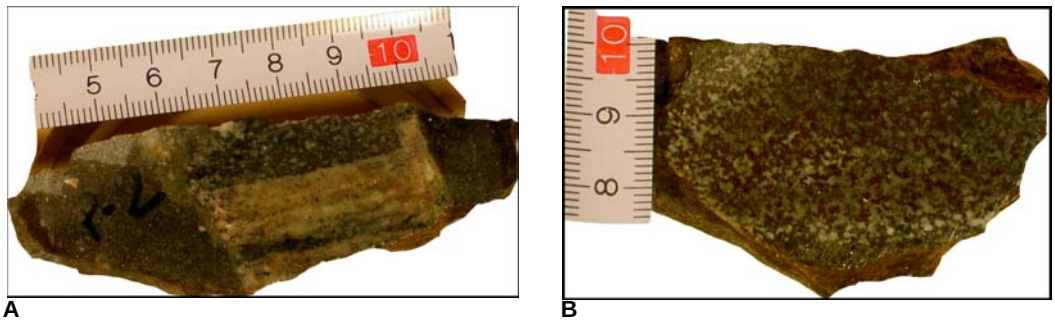

Figure 10. Fine-grained melanocratic granulites Sample P-2 in hand specimen (A), cut surface. Sample P-6 in hand specimen (B), cut surface. Scale bar in the pictures is in centimeters.

Sample P-2 Gabbronoritic granulite gneiss

This sample is gneissic and divided in two parts; melanocratic and leucocratic. In the melanocratic part subhedral plagioclase (An_{15-33}) is albite twinned; the largest extinction angle indicates composition An_{44}. Subhedral pyroxenes, augite and enstatite, comprise c. 20 vol-%. Enstatite has partly, or occasionally totally, altered to chlorite. In leucocratic part the composition of subhedral plagioclase ranges from An_{21} to An_{100} (analyses from albite- and anorthite-rich lamellae). Saussuritized potassium-feldspar is present only in leucocratic layer; clino- and orthopyroxenes are absent. Common for both layers are sericitization of plagioclase, undulose quartz, and accessory minerals biotite, chlorite, magnetite, carbonate, apatite, and rounded, brownish zircon.

Sample P-6 Meta-olivine-gabbro

This sample consists of plagioclase (48.8 vol-%), augite (23.8 vol-%), pseudomorphs after olivine (17.8 vol-%), and biotite (5.1 vol-%). Accessory minerals are magnetite (4.1 vol-%), apatite (0.4 vol-%), and zircon. Plagioclase (An_{0-57}) is mainly albite twinned, sericitized, and interstitial. Augite has weakly developed, c. 0.05 mm wide symplectic grain-boundaries, and contains abundant fluid inclusions. Olivine pseudomorphs consist mainly of talc and magnetite. Biotite is subhedral, magnetite anhedral, apatite anhedral and zircon rounded.

4.6 Kyanite granulites

These strongly altered samples show a mineral assemblage of kyanite, garnet, potassium feldspar, rutile, spinel ± quartz, which is characteristic for high-grade metapelites. The texture, however, indicates partial melting, and shearing after re-crystallization.

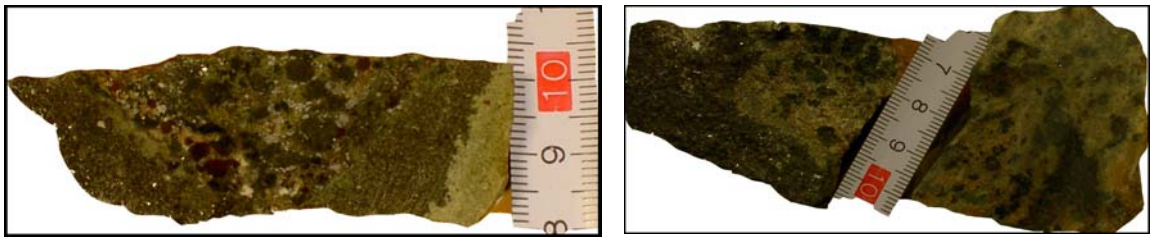

A B

Figure 11. Orthopyroxene-bearing kyanite-granulite P-5 (A) in hand specimen. Kyanite-rich granulite Xe-13 (B) in hand specimen. The common denominator under microscope to these samples is the presence of kyanite and quartz as well as the sheared texture. Scale bar in is in centimetres.

Sample Xe-13 Quartz-potassium feldspar-kyanite-garnet-spinel granulite

This sample contains an assemblage typical of the high granulite facies. Both the undulose quartz and anhedral, relatively fresh potassium feldspar are sheared. Rounded, undulose kyanite, pyrope-almandine, altered to hercynitic spinel and/or magnetite along grain boundaries, comprises the porphyroblasts. Rutile is rounded. The rounded shape and the undulose extinction of kyanite indicate late deformation. Shearing must have occurred at least once, after (re)crystallization of quartz and potassium feldspar.

Sample P-5 Quartz-potassium feldspar-kyanite-orthopyroxene-spinel granulite

The main phases of this high-grade rock are undulose quartz, undulose orthopyroxene, and anhedral kyanite, which show occasionally undulose extinction. Kyanite is also slightly

rounded in shape. The orthopyroxene coexists with dark green, hercynitic spinel and they comprise coarse-grained clots. Spinel, rutile, magnetite, ilmenite, and metamictic rounded zircon are the accessory minerals. Orthoclase of fibrous habit is abundant all over the rock, and the texture implies alteration and shearing. Titanoferous magnetite has reaction boundaries with kyanite and fibrous orthoclase. Garnet might have been present: a completely altered grain is rimmed by iron-rich chlorite and the core comprises of magnetite, spinel, and aluminium silicate. It is predictable that the dyke host has strongly affected this sample; euhedral potassium feldspar, fibrous sodium pyroxene, carbonate, and pyrite occur near to the dyke contact. Carbonate is iron- and magnesium-bearing (25 vol-% FeO, 23 vol-% MgO).

4.7 Metasedimentary rocks

This small, heterogenic group consists of xenoliths of sedimentary protoliths. The lack of muscovite refers to high-grade conditions, but other metamorphic index minerals are mainly lacking. Carbon shale (P-1) has preserved primary structures; in contrast sample Xe-14 is fine-grained and strongly altered.

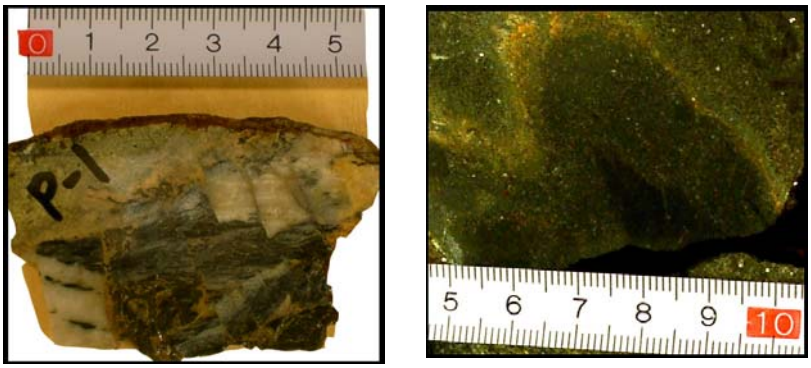

A **B**

Figure 12. Carbon shale P-1 (A) and metagraywacke Xe-14 (B) in hand specimen. Cut surface. The scale bar is in centimeters.

Sample P-1 Carbon shale

This strongly lineated, fine-grained rock comprises deformed coal layers and a quartz veinlet. Between the coal layers polygonal albite is found. Polycrystalline quartz is undulose, and contains opaque dust, probably coal. The fine-grained organic matter

(identified as carbon by microprobe) has probably deposited simultaneously with mineral material and, during metamorphosis or related fluid action, the psammitic part has recrystallized.

Sample P-9 Meta sandstone

The sample shows polygonal granoblastic texture; no lineation is observed. Plagioclase (40 vol-%) has a composition of An_{5-24}. Quartz (20 vol-%) shows undulose extinction. Accessory minerals are calcite (10 vol-%), chlorite, magnetite, jadeitic pyroxene, and zircon. Albite-twinned plagioclase dominates, but also anhedral, polygonal, un-twinned grains are present. Probably secondary calcite is occasionally euhedral. Titanoferous magnetite contains 16 wt-% TiO_2. Radial amphibole is probably metasomatic on the basis of its occurrence.

Sample Xe-14 Meta graywacke

The sample is fine-grained. Well-rounded, corroded and/or sheared, undulose, possibly originally volcanic quartz is present. In hand specimen, grading caused by quartz crystals is observed. The sample also contains lots of opaque, an unidentified iron-silicate material, and the matrix comprises mainly on potassium feldspar. There are minor volcanic rock fragments, which contain fine-grained simple-twinned feldspar. Brownish green to olive green plechroic sodium-pyroxene, slightly altered to chlorite, is observed next to dyke contact. There is also granoblastic albite. Accessory minerals are epidote, barite, apatite, chlorite, magnetite, dolomite, and zeolite. The abundant opaque material contains approximately 55 wt-% SiO_2 and 20 wt-% FeO. The abundant potassium feldspar and sodium-pyroxene co-existing with albite near to the dyke contact are presumably indications of reactions during the magmatic transport. The grading and the separate, angular to rounded, iron- and silica-rich fragments, prior to a sedimentary rock that possibly includes volcanoclastic material. Therefore the sample has been classified as a greywacke with minor volcanoclastic fragments.

4.8 Diopside-schorlomite-carbonatite

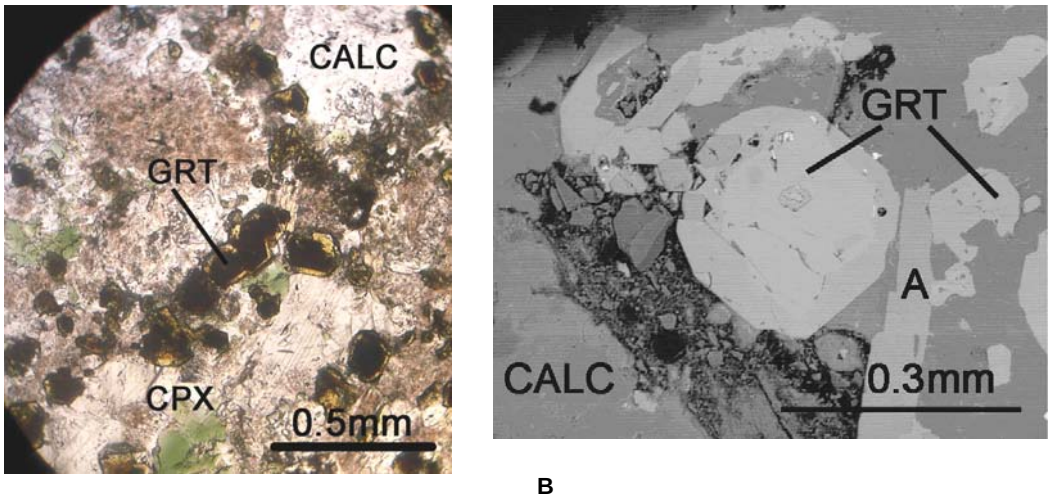

A B

Figure 13. Diopside-schorlomite-carbonatite, thin section Xe-15.1. Microphotograph (A) ppl. Garnet is zoned. BS-image (B) show that core of the garnet is heavier than the rim. Inclusion enclosed by the garnet in the middle is calcium perovskite. Abbreviations: A, apatite; CALC, calcite; CPX, diopside; GRT, garnet.

This xenolith sample (Xe-15) is heterogenic and contains two distinctive parts: clinopyroxene-bearing (thin sections Xe-15.1 and Xe-15.3) and clinopyroxene-rich (thin section Xe-15.2). In both parts calcite comprises at least 50 vol-% (table 1 appendix 3).

The clinopyroxene-bearing part comprises of calcite (52.1 vol-%), garnet (25.5 vol-%), and potassium feldspar (17.3 vol-%). Accessory minerals are biotite (2.2 vol-%), apatite (1.5 vol-%), barite (1.3 vol-%), and titanium oxide (0.1 vol-%). Calcite is mainly euhedral and twinned. The garnet is zoned, titanium-rich andradite (schorlomite according to XRF identification and microprobe analyses) in which the amount of titanium increases towards the core. Significant part of the reddish-brown garnet crystals are mantled by a yellowish, titanium-poor andradite rim. These garnet grains contain a bit less titanium in their cores than the unzoned ones. Anhedral, microperthitic potassium feldspar occurs interstitially. Biotite show pale green-pale brown pleochroism, and phlogopitic composition. Apatite is prismatic.

The main phases in clinopyroxene-rich part are calcite (52.3 vol-%), diopside (23.7 vol-%), biotite (9.3 vol-%), garnet (7.9 vol-%), and opaque minerals (5.9 vol-%). Apatite (0.9 vol-%) and potassium feldspar are accessory minerals. Calcite is anhedral to subhedral, sometimes sheared. Subhedral diopside is mainly weakly bright green pleochroic but occasionally shows colorless zoning. Sodium concentrations range between 0 and 3 wt-%

Na_2O. Reddish-brown schorlomite is mainly of the un-zoned type. A sheared, c. 5 mm wide region was observed in diopside-rich part. In this layer colorless and occasionally twinned diopside has weakly green pleochroic rims. Calcite is sheared and the garnet has mainly been altered to magnetite.

4.9 Phlogopite rock

Sample P-3 Phlogopite-ankerite-rock

This sample has an ellipsoid form and a cryptocrystalline appearance (fig. 14 A). The main phases are phlogopite (82.3 vol-%) and calcite (5.5 vol-%). Accessory minerals are diopside (4.7 vol-%), titanium oxide (0.9 vol-%), potassium richterite (0.8 vol-%), and apatite (0.5 vol-%). Orthoclase and quartz comprise 5.3 vol-%. Euhedral titanoferous phlogopite is occasionally kinked; this indicates deformation. Ankerite is subhedral and contains 18-25 wt-% FeO and 16-21 wt-% MgO. Euhedral diopside has twinned polysynthetically and potassium richterite show yellowish-brown to pale brown pleochroism. Interstitial orthoclase and interstitial quartz are anhedral and undulose. Minor apatite is prismatic.

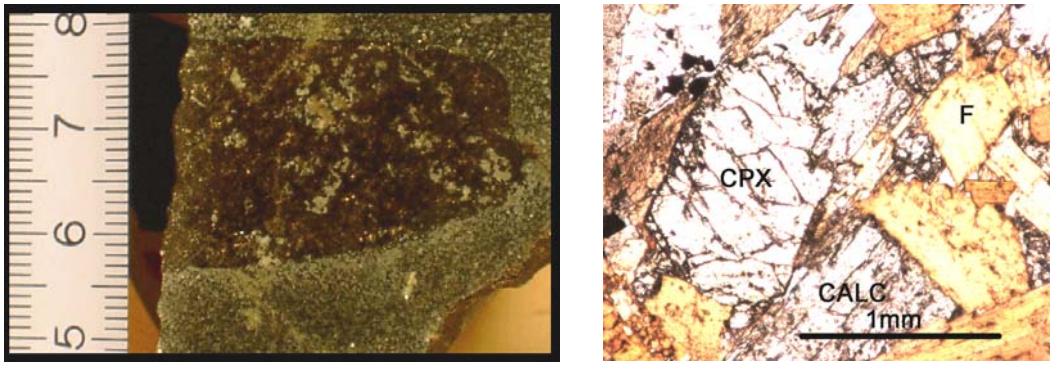

A B

Figure 14. Phlogopite rock. Sample P-3 in hand specimen (A), cut surface. The scale bar is in centimeters. Photomicrograph (B), ppl. Sparse diopside crystals are subhedral and occasionally twinned. Abbreviations: CALC, calcite; CPX, clinopyroxene; F, phlogopite.

5. WHOLE-ROCK AND MINERAL CHEMISTRY OF THE XENOLITHS

5.1 Whole-rock chemistry

Most of the samples have been altered and infiltrated by the dyke material. Therefore, whole-rock compositions were calculated using the mode (table 1 appendix 3) and average compositions of the minerals. This was probably the best way to estimate the whole-rock major element chemistry: it is probable that the compositions determined, shown in fig. 15, are relatively close to the protolith. The TAS-diagram (Total Alkalis-Silica) is used here to distinguish between different metaigneous rock types though originally it is used in classification of unaltered volcanic rocks (Le Maitre et al. 1989) (fig. 15).

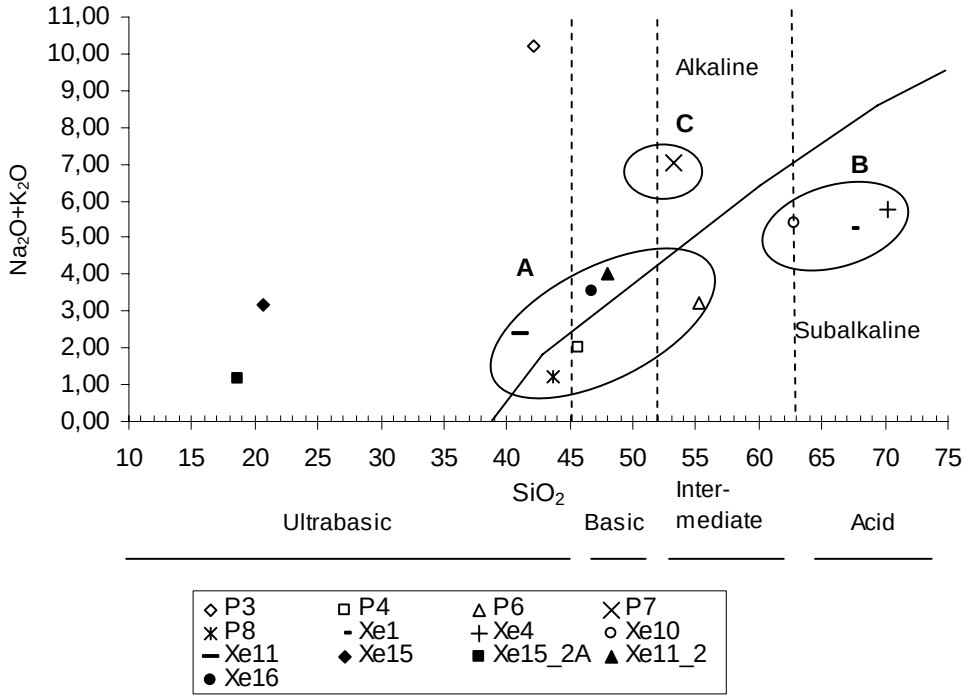

Figure 15. Lamproite-hosted xenoliths in SiO_2 versus Na_2O+K_2O (in wt-%) diagram. The circled area A refers to gabbroic/basaltic, B to granodioritic, and C gabbroic-syenodioritic composition (Cox et al. 1979). The alkaline and sub-alkaline fields were determined by Rickwood (1989). Ultrabasic (below 45 wt-%), basic (45-52 wt-%), intermediate (52-63 wt-%), and acid (over 63 wt-%) rock types are after Le Maitre et al. 1989.

The xenoliths show wide compositional range (SiO_2 19-70 wt-%, TA 1-10 wt-%). Majority show a loose trend along the subalkaline-alkaline boundary (Rickwood 1989). Silica-poor carbonatite (Xe-15) and highly alkaline phlogopite rock (P-3) differ notably from the other xenoliths. Total alkalis content varies mainly between 1 and 3 % reflecting the small amount of feldspars. High TA value in the phlogopite rock (P-3) is due to abundant phlogopite. Ultrabasic to intermediate samples P-4, P-8, Xe-11, and Xe-16 exhibit gabbroic whole-rock compositions, intermediate to acid samples Xe-1, Xe-4, and Xe-10 granodioritic compositions, and intermediate sample P-7 gabbroic-syenodioritic compositions. Carbonatite (Xe-15) and phlogopite rock (P-3) are the ultrabasic rock types. Harker diagrams (fig. 16) show variable degrees of correlation between SiO_2 and the other

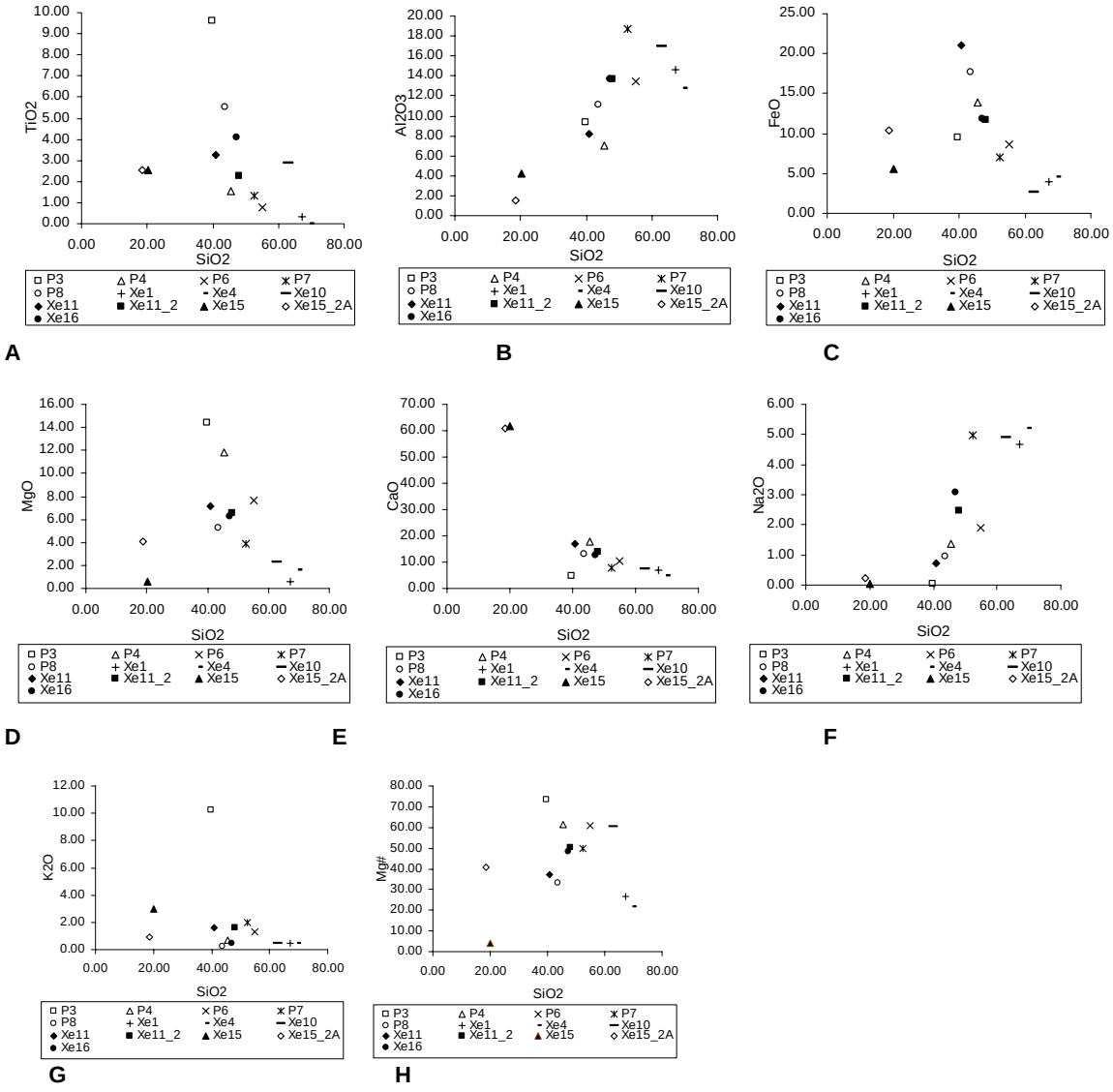

Figure 16 Whole rock compositions of the xenoliths determined by combining modal and mineral chemical data. SiO_2 versus TiO_2, Al_2O_3, FeO (total), MgO, CaO, Na_2O and K_2O (in wt-%) and magnesium number (Mg#).

major oxides. High MgO, FeO, and CaO reflect the high abundance of mafic silicates in the melanocratic granulites (P-4, Xe-11), meso- to melanocratic garnet granulites (P-7, P-8, Xe-16), and the phlogopite rock (P-3), where as the enrichment at Al_2O_3 and Na_2O reflect the high abundance of plagioclase.

5.2 Mineral chemistry

5.2.1 Garnet

The garnet analyses are represented in table 4 in appendix 1. The compositions have been recalculated to ions per 24 oxygen atoms and wt-% of pyrope $Mg_3Al_2Si_3O_{12}$, almandine $Fe_3Al_2Si_3O_{12}$, grossular $Ca_3Al_2Si_3O_{12}$, and spessartine $Mn_3Al_2Si_3O_{12}$ using modified spread sheets of Preston (1999). The sixth end-member, uvarovite Ca_3Cr_2 Si_3O_{12}, was neglected, because no chromium was detected. Xenolith-hosted garnet compositions are shown in fig. 17. The garnets can be divided to almandine-rich and grossular-rich types. Garnet in

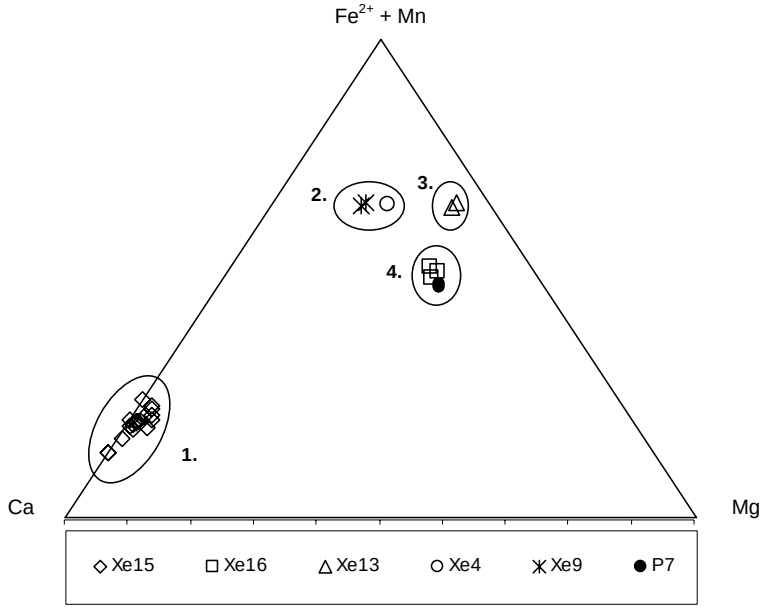

Figure 17. Garnet compositions. The amount of cations (Fe^{2+} + Mn), Ca and Mg recalculated on the basis of 24 oxygen atoms stand for almandine, grossular and pyrope component, respectively. The rock types are indicated 1) diopside-schorlomite-carbonatite, 2) tonalite gneiss 3) melanocratic granulites 4) kyanite granulite.

tonalite gneisses (Xe-4 and Xe-9), melanocratic granulites (P-7 and Xe-16), and kyanite granulite (Xe-13) are almandine-rich. Grossular-rich garnet (andradite) was only found in diopside-schorlomite-carbonatite (Xe-15) (table 4 appendix 1, fig. 17).

Almandine-rich garnet

Almandine-rich garnet shows fairly limited compositional variations ($Alm_{47-66}Gro_{5-20}Py_{14-29}Sp_{0-11}$). In tonalite gneisses, garnet is found as a minor phase. Fresh garnet was found in sample Xe-4, whereas in sample Xe-9 the garnet is partly chloritized. The composition of garnet is $Alm_{55-56}Gro_{16-20}Py_{14-18}Sp_{10-11}$. In kyanite granulite (Xe-13), $Alm_{66}Gro_{5}Py_{29}$ garnet is altered to hercynite and chlorite along the grain boundaries. The melanocratic granulites (P-7 and Xe-16) show the highest pyrope contents; $Alm_{47-50}Gro_{15-16}Py_{32-35}Sp_{2}$. Garnet has altered to orange to dark brown material, which consists of tiny particles. The heaviest phase is titanium-bearing magnetite; lighter material remains unidentified. The presence of rim indicates that the garnet has reacted to yield equilibrium with its surroundings (fig. 18).

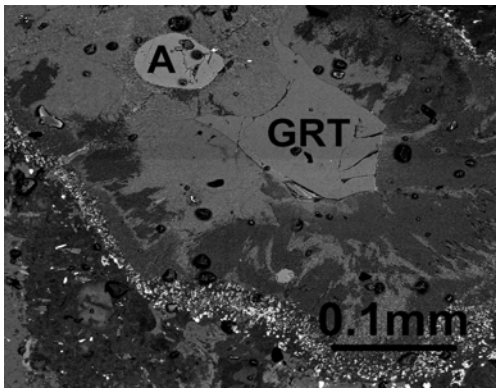

Figure 18. Almandine-rich garnet in melanocratic granulite (sample Xe-16), BS-image. Abbreviations: A, apatite; GRT, garnet.

In melanocratic granulite P-8 fresh garnet has not been observed. It has presumably been consumed in the reaction forming the dark brown alteration rims. Fig. 19 shows that the compositions of the pseudomorphic garnet conform to garnet and montmorillonite-chlorite mixture, being notably similar to the garnet in samples P-7, P-8, and Xe-16. The iron and magnesium content might have been slightly higher in pre-existing garnet in P-8 compared to garnet in samples P-7 and Xe-16.

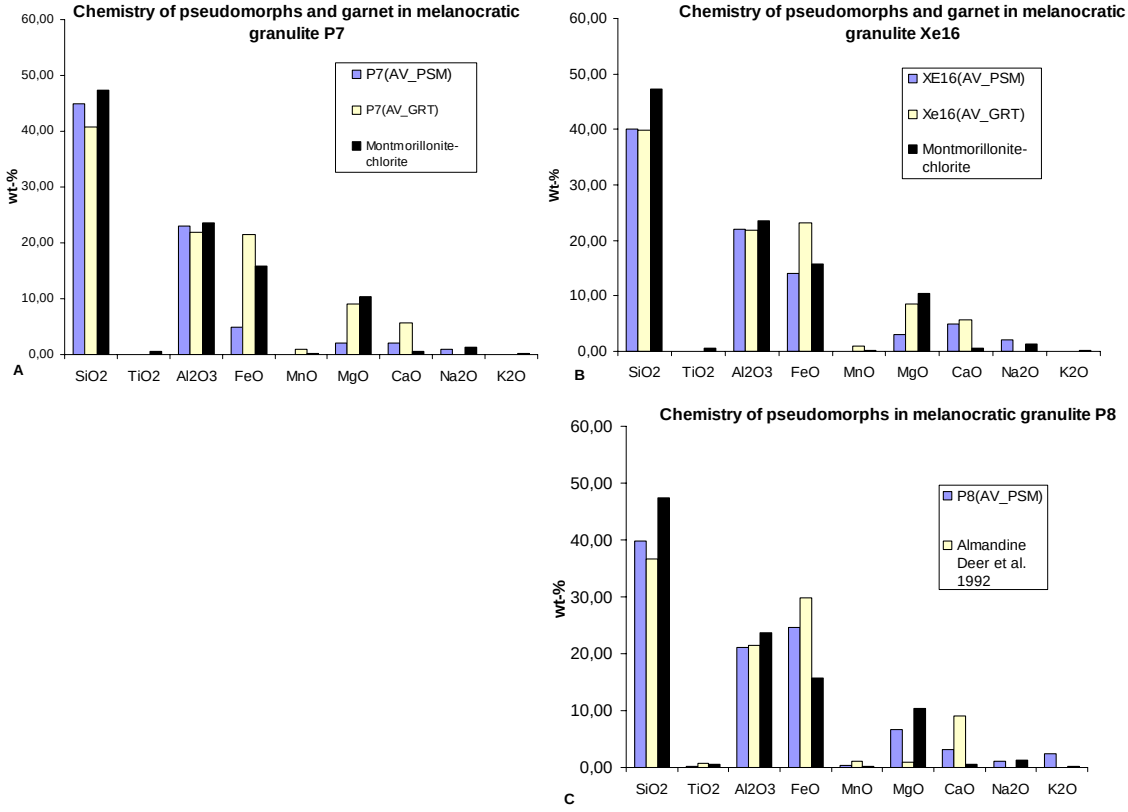

Figure 19. Compositions of the pseudomorphs after garnet in melanocratic granulites (P-7, P-8, and Xe-16) with regard to major oxides (in wt-%). The composition is given as an average of selected analyses. A) Sample P-7: (AV_PSM) the average of pseudomorph (4 analyses), (AV_GRT) the average of garnet (2 analyses), montmorillonite-chlorite is an average from data by Deer et al. 1992. B) Sample Xe16: As in A, pseudomorph 3 analyses, garnet 3 analyses. C) Sample P-8: As in A, pseudomorph 6 analyses, $Alm_{67}Gro_{26}Py_4Sp_3$ garnet from Deer et al. 1992.

The mineral chemical data for the almandine-rich garnet is plotted in Harker diagrams in fig. 20. The Al_2O_3 contents range between 20.5 and 22.5 wt-%, FeO (total) between 21 and 30 wt-%. The highest amount of MnO (4-5 wt-%) is observed in the garnet in tonalite gneisses (Xe-4 and Xe-9). MgO is higher in the melanocratic granulites (P-7 and Xe-16) and kyanite-granulite (Xe-13) than in the tonalite gneisses. CaO comprises only few percents in the kyanite-granulite, whereas 5-7 wt-% of CaO is observed in the other garnets.

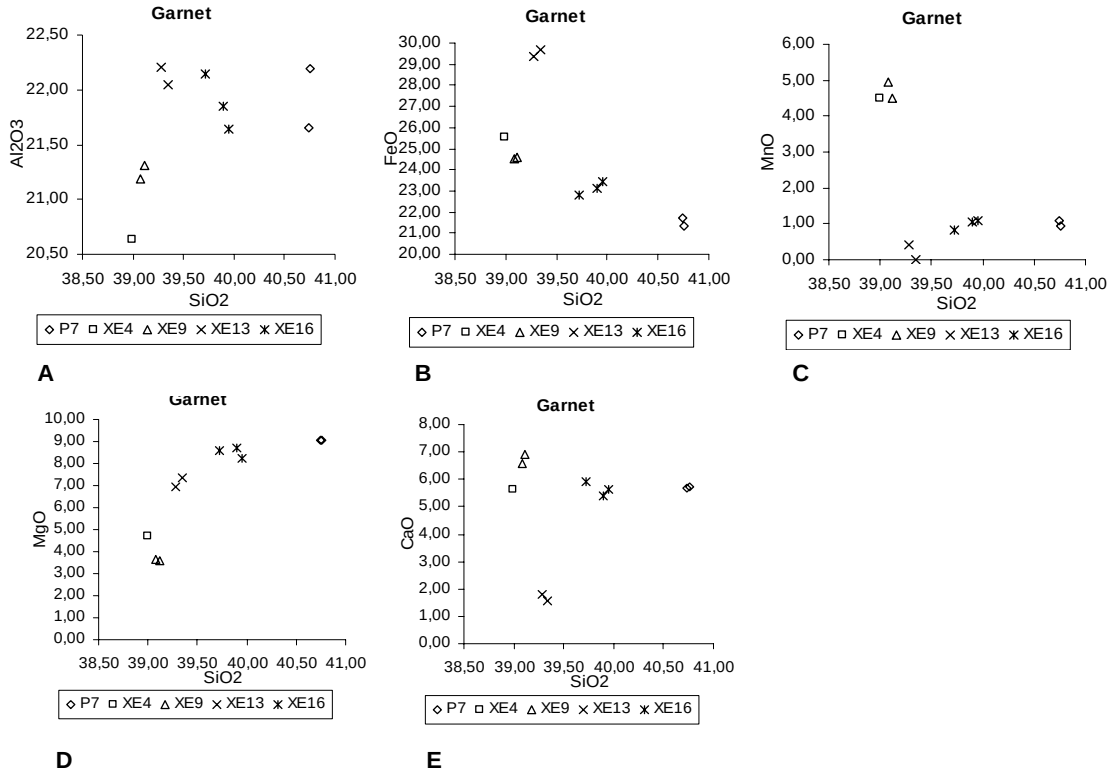

Figure 20. Almandine-rich garnet compositions. SiO_2 versus TiO_2, Al_2O_3, FeO (total), MgO, and CaO (in wt-%).

Titanian andradite

Titanian andradite is found in schorlomite-diopside-carbonatite (Xe-15). The majority of the analyses represent titanium-rich andradites, but schorlomite compositions were observed in the cores of euhedral garnet crystals (fig. 21). The observed compositional range is $Alm_{14-25}Gro_{2-37}Py_{0-4}Sp_{0-4}And_{49-75}$. Schorlomite was defined by Deer et al. (1992) as follows: an andradite garnet which contains c. 15 wt-% TiO_2 or more, and Fe^{3+}< Ti. In addition to the composition, characteristic for schorlomite is a strong reddish brown colour, and a larger cell parameter (a=12.128 Å) relative to the one of andradite (a=12.05Å) (www.webmineral.com). The a-axis measured for a garnet separate was ~12.13Å. Compositional zoning causes variation and is observed in the spectrum (Prof. Martti Lehtinen pers. comm. 2006).

The ferric iron content of andradite (sample Xe-15) ranges between 0.45 and 1.1, and Ti between 0.0 and 1.2 atoms per formula unit (apfu). According to Huggins et al. (1977) ferric iron is responsible of the reddish brown colour in titanian andradite. Analyses 11, 25,

26, and 27, (table 4 appendix 1) from the colourless and yellowish parts of garnet, show a low-titanium (0-0.3 Ti apfu) and relatively high ferric iron (0.67-0.99 Fe^{3+} apfu) content. Analyses from the reddish brown cores of garnet show mainly notably higher Ti (0.8-1.3 apfu) but lower Fe^{3+} (0.45-0.73 apfu) than the rims. Reddish brown, un-zoned garnet in the sheared part (thin section Xe15.2) has also low Fe^{3+} (~0.5 apfu) and high titanium content (0.9-1.2 apfu). Therefore it is probable that in this case titanium causes the strong colour of andradite. Huggins et al. (1977) stated that the majority of titanium substitutes the silicon on the tetrahedral site and hence it has a charge of 4+. Excess titanium in these garnets, however, is in the octahedral site and, consequently, it may be tetra- or trivalent (Dingwell and Brearley 1985). The presence of Ti^{3+} would cause some error on the calculated amount of ferric iron, as the equation after Droop (1987), is based on the assumption that only iron has a varying valence (Waters 2004).

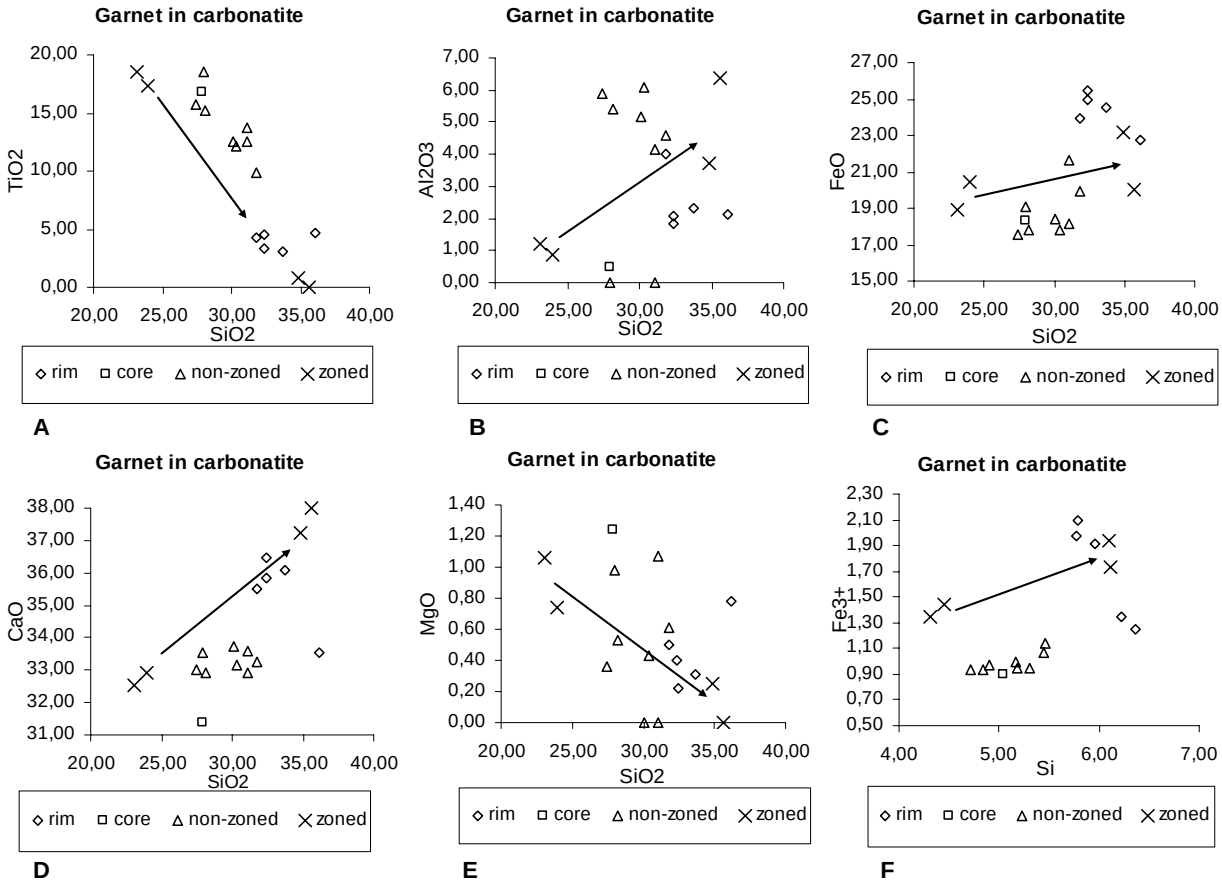

Figure 21. Andradite garnet in carbonatite (Xe-15). A-E) SiO_2 content versus TiO_2, Al_2O_3, FeO (total), CaO, and MgO (in wt-%). F) Number of Si on the basis of 24 oxygen atoms versus number of Fe^{3+} recalculated according to Droop (1987). Arrow shows a zoning trend observed in a single, zoned crystal from core to rim.

Compositional zoning, observed also under microscope, is shown in fig. 21. The arrow indicates the zoning trend in a single, euhedral garnet grain, which has a yellowish outer rim. The direction of the trend is promoted by the other rim and core analyses. The un-zoned garnet comprises a transitional compositional group, which follows loosely the trend of zonation (fig.21). The cores are rich in TiO_2 and have low Al_2O_3 and relatively low CaO contents. Some cores of zoned garnet grains contain 4-5 wt-% ZrO_2. The rims are mainly low in TiO_2, Al_2O_3, and MgO. Relative to the cores the rims are rich in CaO and slightly richer in Al_2O_3, FeO, and ferric iron. Overall, garnet shows wide compositional ranges. TiO_2 varies most, from zero to 19 wt-%. Considerable changes are observed also in Al_2O_3 (1-6 wt-%), FeO (18-26 wt-%), and CaO (31-38 wt-%) contents (fig. 21 A-D). The MgO content is low and varies only slightly (fig. 21 E). Ferric iron comprises 0.45-1.05 apfu of the Fe present. Some garnet grains contain rare sub-microscopic inclusions. The inclusions occur mainly in zoned garnets. Calcium-perovskite (Ca, Na, Fe^{2+}, Ce, Sr) (Ti, Nb) O_3 and leucite $K[AlSi_2O_6]$ have presumably been observed (table 4 R1_4 and R1_17, respectively).

Table 3. Inclusions of the garnet in diopside-schorlomite-carbonatite (Xe-15).

	SiO_2	TiO_2	Al_2O_3	FeO	CaO	Na_2O	K_2O	Nb_2O_5	Cr_2O_3	Cl	Total
Xe15 (R1_4)	1,3	75,9	n.d	2,2	18,8	n.d	n.d	1,8	n.d	n.d	100
Xe15 (R1_5)	77,0	1,6	n.d	5,7	12,2	n.d	n.d	n.d	2,2	1,3	100
Xe15 (R1_6)	91,6	n.d	n.d	1,4	2,3	n.d	n.d	n.d	4,3	0,5	100
Xe15 (R1_17)	48,0	n.d	34,7	3,3	n.d	0,2	13,8	n.d	n.d	n.d	100

n.d.=not detected

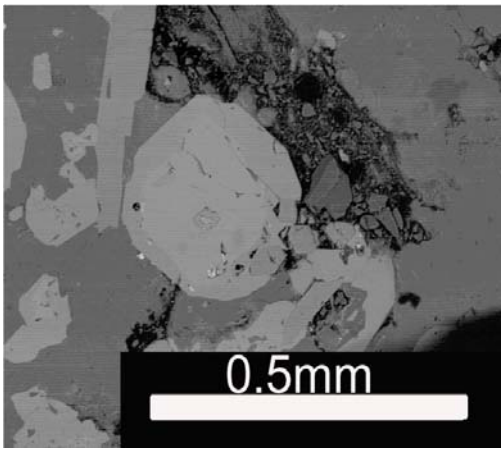

Figure 22. Diopside-schorlomite-carbonatite (Xe-15), zoned garnet, BS-image. On the upper left corner the oblong crystal is extraordinarily large apatite crystal. Darker gray on the back ground is calcite. The diameter of the garnet is c. 0.25 mm; the grain encloses calcium perovskite.

5.2.2 Pyroxene

Pyroxene analyses are shown in appendix 1 in table 9. The compositions have been recalculated to weight percentages of wollastonite (Wo) $Ca_2Si_2O_6$, enstatite (En) $Mg_2Si_2O_6$, ferrosilite (Fs) $Fe_2Si_2O_6$, and aegirine (Ae) $NaFe^{3+}Si_2O_6$ using spread sheets by Preston (1999). The majority of the analyzed pyroxene compositions fit in the field of Ca-Mg-Fe-pyroxenes (figs. 23 and 24). In the Q-J-diagram (fig. 23) four main groups (Ca-, Mg-, and Fe-pyroxenes, Ca-Na-pyroxenes, Na-pyroxenes, and other pyroxenes) are observed (Morimoto et al. 1989).

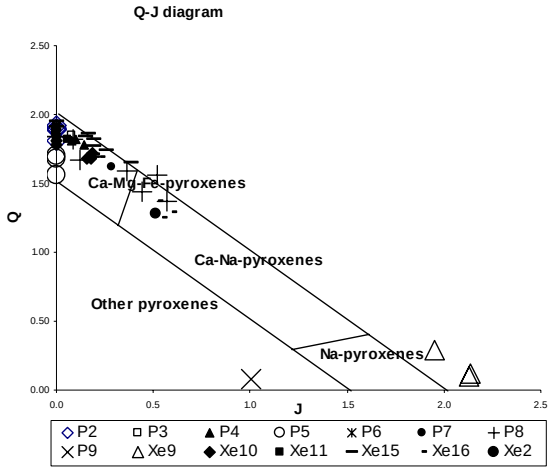

Figure 23. Analyzed pyroxenes on the Q-J diagram, where J= 2* Na cat ions on the basis of six oxygen atoms (x-axis, approximation of the total number of Na and Al, Fe^{3+}, Cr^{3+}, and Sc^{3+}). Q= sum of Ca, Mg, and Fe^{2+} cat ions, calculated on the basis of six oxygen atoms (y-axis). Pyroxene classification and nomenclature is after Morimoto et al. (1989).

Sodium-rich pyroxene

Fig. 23 shows that pyroxene in tonalite gneiss (Xe-9) does not fit in the four main groups. The pyroxene contains 13-14 wt-% Na_2O and 0.6-1.9 wt-% TiO_2 (appendix 1 in table 9). According to the definition of "unusual pyroxenes", (cf. Morimoto et al. 1989) this kind of pyroxene, called ferroan aegirine, contains substituted component $NaR^{2+}{}_{0.5}Ti^{4+}{}_{0.5}Si_2O_6$ (R^{2+} stands for Fe^{2+}). In literature, however, name aegirine-augite is often used (Morimoto et. al. 1989). The accessory pyroxene in the mafic granulites (P-8 and Xe-16) and augen gneiss (Xe-2) shows aegirine-augite composition (fig. 24 A).

The pyroxene in metasandstone (P-9) is on the compositional field of "other pyroxenes" (fig. 23), defined in Morimoto et al. (1989). The pyroxene has a messy, altered appearance

in thin section. It contains 3 wt-% K_2O, and is very aluminium-rich (28 wt-% Al_2O_3) (table 9 in appendix 1). According to Morimoto et al. (1989) replacement of sodium with aluminium may cause placement in the field of other pyroxenes, though the mineral would be sodium pyroxene (fig. 24 A). This is because the value of x-axis (J) (fig. 23) is an approximation of the total number of Na and Al, Fe^{3+}, Cr^{3+}, and Sc^{3+}. Further, the calculated distribution of aluminium to sites T and M1 is deficient to the accuracy of the measurement of silicon (Waters 2004), therefore also the semi-quantitative data may cause error. As in fig. 24 A, the pyroxene in metasandstone, $Na_{0.5}K_{0.13}Ca_{0,02}Al_{0.83}Fe_{0,05}Si_{2.19}O_6$, is classified as jadeite.

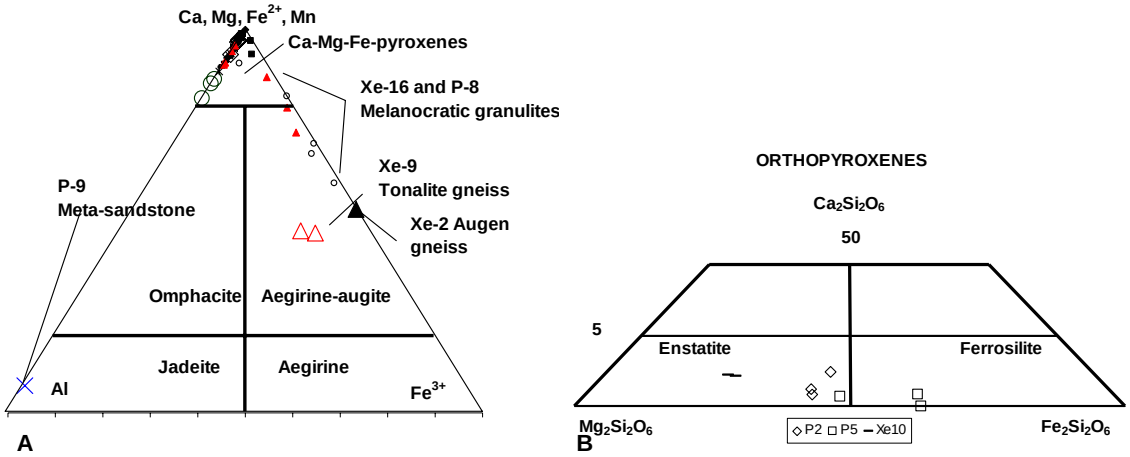

Figure 24. Pyroxene compositions. A) Na- and Ca-rich pyroxene. Majority of the pyroxene compositions is within the field of Ca-Mg-Fe-pyroxenes. B) Low-calcium orthopyroxene. Pyroxene classification and nomenclature is after Morimoto et al. (1989).

Orthopyroxene

Orthopyroxene (low-calcium pyroxene, appendix 1 table 9) is present in three of the studied rock types: gneissic metagabbro (P-2), kyanite granulite (P-5), and layered leucocratic granulite (Xe-10). In the gneissic metagabbro orthopyroxene is partly chloritized and co-exists with augite. In kyanite granulite, orthopyroxene occurs as deformed reaction rims and after melted garnet as hercynite-orthopyroxene symplectites. The compositional range of orthopyroxene in kyanite granulite P-5 (Fs_{48-62}) depends on the co-existing phases: the orthopyroxene in ferrosilite field is symplectic with hercynitic spinel, whereas the one in enstatite field comprises a coronae phase in contact with quartz.

In gneissic metagabbro (P-2) the composition of orthopyroxene is En_{54-57}. The highest enstatite proportion (En_{71}) is observed in layered leucocratic granulite (Xe-10) (fig. 24 B), where the orthopyroxene is enclosed in pseudomorphic garnet.

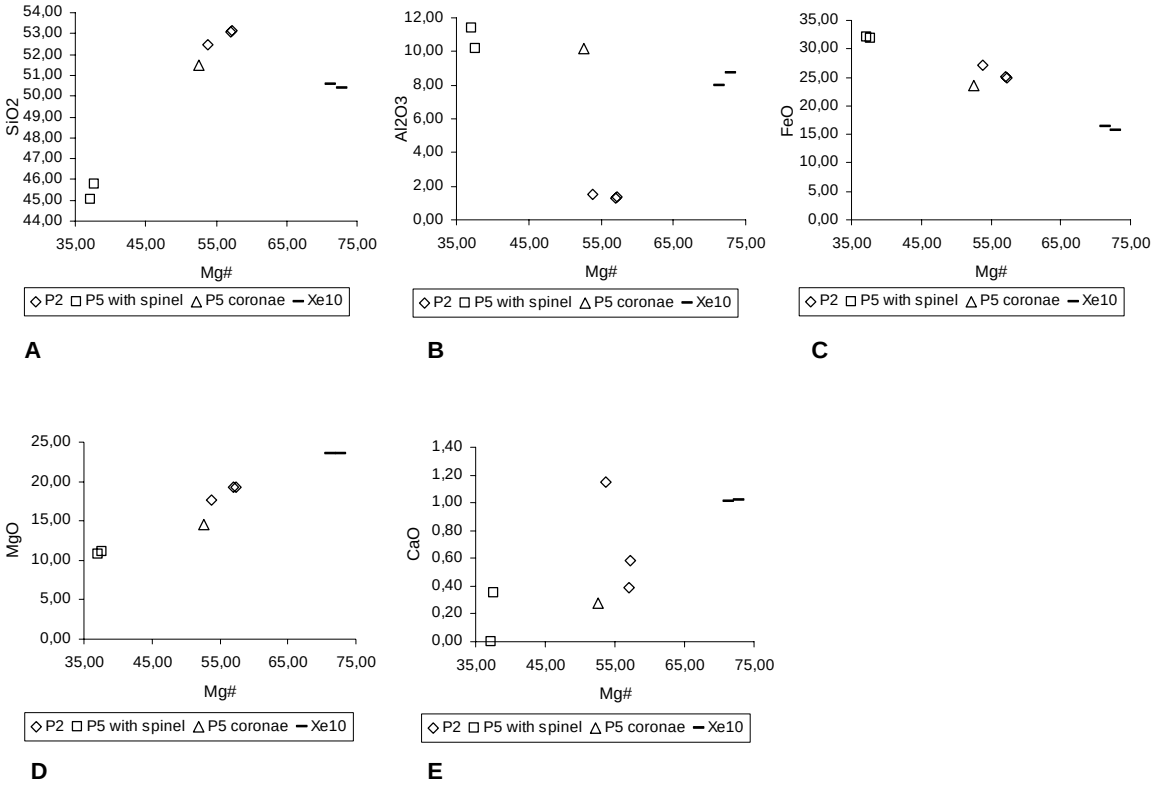

Figure 25. Orthopyroxene. Mg number (Mg#) versus SiO_2, Al_2O_3, FeO (total), MgO, and CaO.

Fig. 25 shows magnesium ratio versus major oxide proportions of orthopyroxene. The orthopyroxene in gneissic metagabbro P-2 and kyanite granulite P-5 are best distinguished from each other by their aluminium content (fig. 25 B). In gneissic metagabbro Al_2O_3 is low (c. 1.5 wt-%), in kyanite granulite relatively high, (10-11 wt-% Al_2O_3). Relatively high Al_2O_3 content (8-9 wt-%) is also observed in layered leucocratic granulite. The varying composition in kyanite granulite P-5 shows in figs.s 25 C and D: orthopyroxene co-existing with hercynitic spinel show higher FeO and lower MgO than the one occurring as coronae phase. Calcium is present as a minor element, CaO ranging from zero to one wt-% (fig. 25).

Clinopyroxene

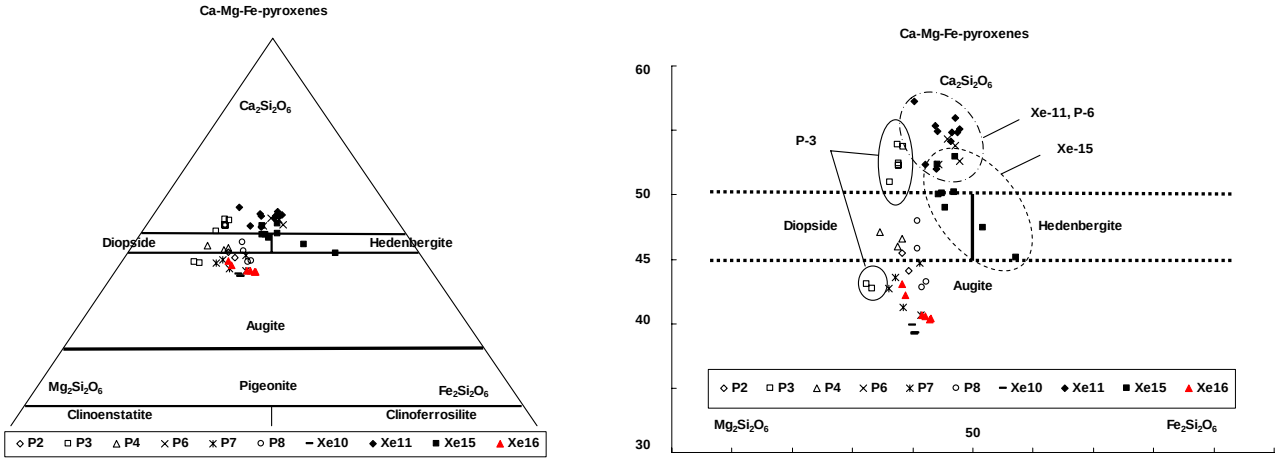

Figure 26. Clinopyroxene composition (A). B is a detail from A. CaO content ranges between 39 and 57 mol-% $Ca_2Si_2O_6$, and the $Mg_2Si_2O_6$ between 52-68 mol-%. Figures are after Morimoto et al. (1989).

Compositions of the clinopyroxene (calcium-pyroxene, appendix 1 table 9) are shown in fig. 26. The variation in Mg and Fe contents is quite small, but Ca varies a lot. Mg ranges mainly between 52 and 68 mol-% $Mg_2Si_2O_6$. The most Fe-rich compositions were observed for the Na-bearing diopside in diopside-schorlomite-carbonatite (Xe-15), comprising 63-68 mol-% $Fe_2Si_2O_6$ (circled in fig. 26 B). Augite in samples P-2, P-7, P-8, Xe-10, and Xe-16 constitute the most uniform group in relation to Ca, Mg, and Fe. Melanocratic granulites P-4, and P-8, and a gneissic metagabbro P-2, show diopsidic compositions. Ca content of the pyroxene in the phlogopite rock P-3 ranges more than 5 mol-% $Ca_2Si_2O_6$ and thus defines two pyroxenes: augite and calcium-rich diopside. The Ca-rich diopside of phlogopite rock P-3, metagabbro P-6, layered melanocratic granulite Xe-11, and diopside-schorlomite-carbonatite Xe-15 show the highest $Ca_2Si_2O_6$ portions. An extreme Ca content (57 mol-% $Ca_2Si_2O_6$) is observed for diopside of sample Xe-11 (table 9 in appendix 1).

Fig. 27 (CaO vs TiO_2, MgO, and FeO diagram of the high Ca clinopyroxene mentioned above) shows relatively high Ti contents (1-2 wt-% TiO_2) which are related to high CaO (Xe-15, P-3). TiO_2 of layered melanocratic granulite (Xe-11) and metagabbro (P-6) varies mainly between 0.5 and 1 wt-%. The layered melanocratic granulite Xe-11 and diopside-schorlomite-carbonatite Xe-15, show positive correlation (fig. 27 A); CaO increases with

increasing MgO content. Opposite trend is observed in phlogopite rock P-3 where lower MgO content reflects higher CaO (fig. 27 B). Samples P-6, Xe-11, and Xe-15 show a loose negative correlation; CaO increases with decreasing FeO (fig. 27 C). Overall, the raised amount of Ca in sample P-3 (phlogopite rock) could occur due to substitution of Mg by Ca, and in other pyroxenes due to substitution of Fe by Ca (the M2 site is occupied with Ca, Mg, Na, Mn, and Fe^{2+}). The lowest values (~23 wt-%) of CaO, however, are observed from the plagioclase-bearing part and the highest (27 wt-%) from ultramelanocratic part of the layered melanocratic granulite (Xe-11). Whether the high CaO in these four samples reflects igneous process or metamorphic recrystallization retains to be determined.

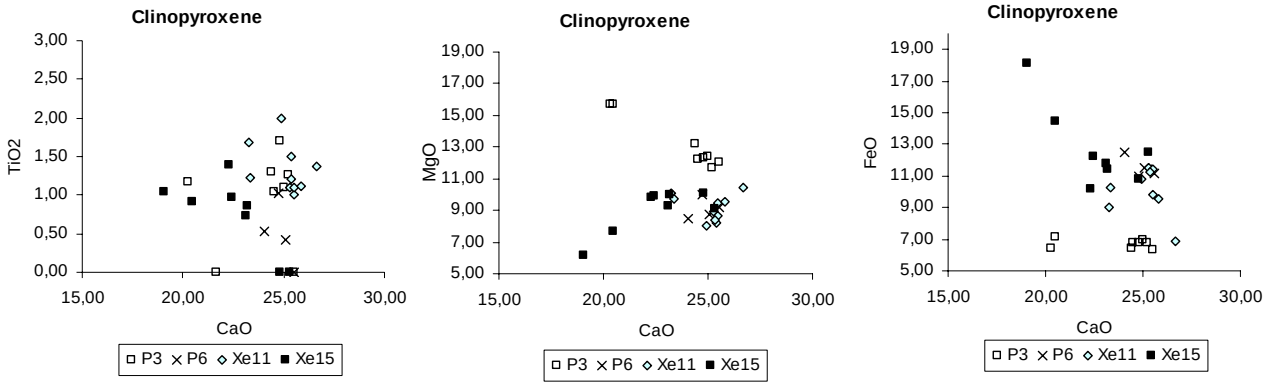

A **B** **C**

Figure 27. CaO versus FeO, TiO_2, and MgO in clinopyroxenes plotting in the field of wollastonite (Morimoto et al. 1989).

Fig. 28 comprises the clinopyroxene analyses. Pyroxene of phlogopite rock (P-3) is rich in SiO_2, TiO_2, MgO, and CaO, and poor in Al_2O_3 and FeO(tot). Layered melanocratic granulite (Xe-11) and diopside-schorlomite-carbonatite (Xe-15) comprise a group rich in TiO_2 (1-2 wt-%) and CaO (fig. 27). FeO- and MgO-content is mainly constant, 9-13 wt-% and 7-11 wt-%, respectively. Majority of the pyroxene contain 2-4 wt-% Al_2O_3; the highest proportions are observed in pyroxene of sample Xe-11 (the plagioclase-bearing part), leucocratic layered granulite Xe-10, and melanocratic granulite P-7 (fig. 28 B). The Al-rich pyroxene seems to correlate with the presence of plagioclase. The pyroxenes comprise an array showing increasing MgO with increasing SiO_2. The magnesium number (Mg#) is highest in phlogopite rock P-3 and melanocratic layered granulite P-4. The lowest values (~55) are found in the melanocratic layered granulite Xe-11 and in meta-gabbro P-6. The

symplectic morphology observed in pyroxenes of melanocratic samples P-4, P-7, P-8, Xe-11, and Xe-16 seems to be relatively independent of the composition.

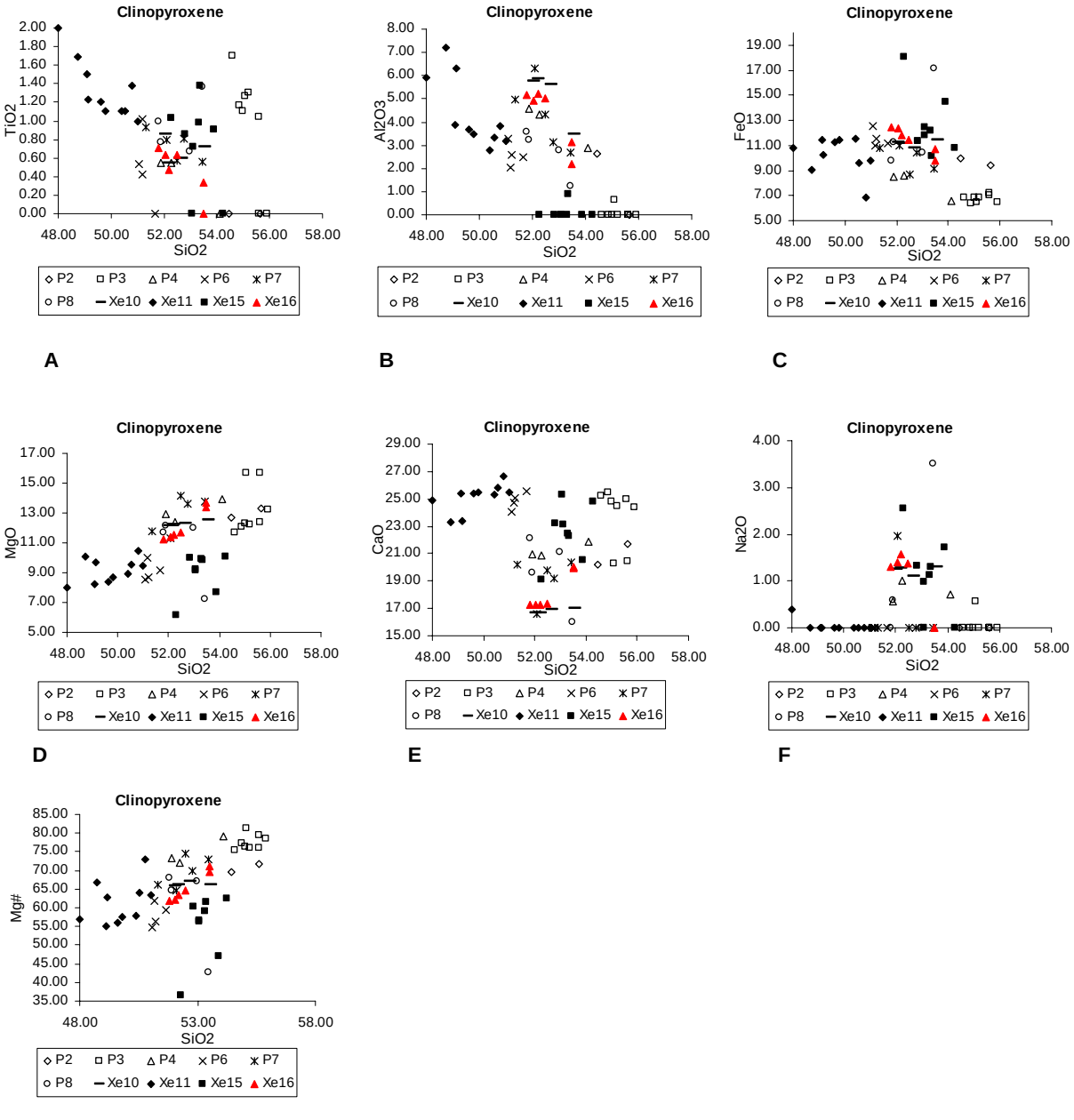

Figure 28. Calcium pyroxene. SiO_2 versus TiO_2, Al_2O_3, FeO (total), MgO, CaO, Na_2O (in wt %) and magnesium number (Mg#).

5.2.3 Amphibole

The amphibole analyses are shown in table 2 in appendix 1. The compositions were recalculated on the basis of 23 anions (O, OH, and F) using a spread sheet of Waters (2004). The amphibole classification (Leake et al. 1978, 1997, 2003) builds on atomic proportions per formula unit. The quality of the analysis, constant sum procedure on recalculation, and the often complicated crystal chemistry of amphibole cause error (Rollinson 1992, Waters 2004). Therefore, a loose grouping to calcic and sodic-calcic amphiboles is used here, instead of a more strict nomenclature. Two groups of amphibole were observed: relatively alkali poor calcic amphiboles and alkali-rich, Ca-poor amphiboles (fig. 29). The calcic amphiboles occur as a major phase in layered granulites P-4 and Xe-11; those show compositions $Na_{0.8\text{-}0.9}K_{0.4}Ca_{1.5}Mg_{2.6}Fe3+_{0.2\text{-}0.4}Ti_{0.2}Si_{6.2\text{-}6.3}Al_{2.5\text{-}2.6}O_{22}(OH)_2$ (magnesio-hastingsite) and $Na_{0.4\text{-}0.5}K_{0.3\text{-}0.6}Ca_{1.5\text{-}1.9}Mg_{1.5\text{-}1.8}Fe^{2+}{}_{1.9\text{-}2.2}Ti_{0.3\text{-}0.5}Si_{6.1\text{-}6.4}Al_{2.5\text{-}2.7}O_{22}(OH)_2$ (ferro-pargasite), respectively. Accessory calcic amphiboles, showing quite

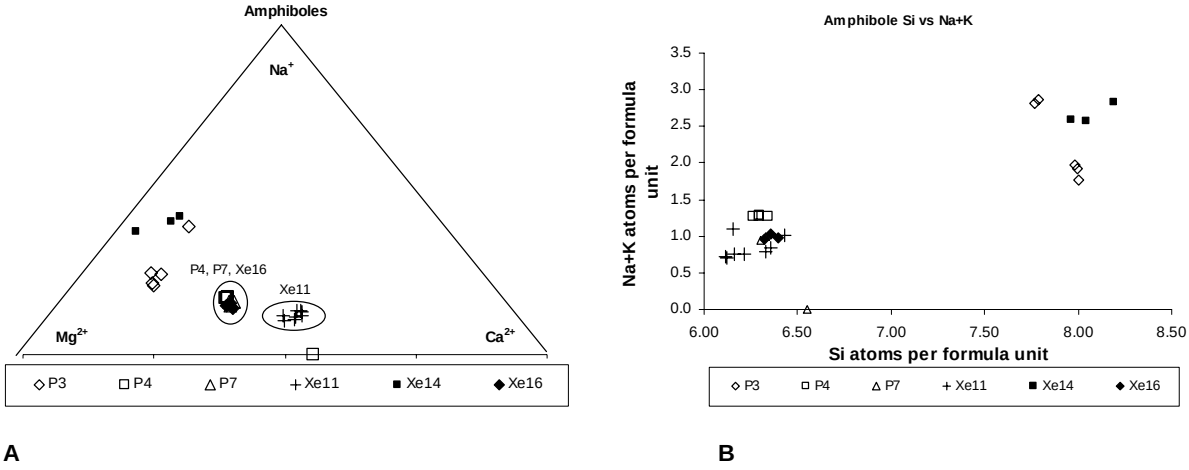

Figure 29. A) Amphibole compositions in relation to Na, Mg, and Ca (apfu). B) Si (apfu) versus Na+K (apfu).

similar compositions to samples P-4 and Xe-16, are observed in melanocratic granulites P-7, P-8 and Xe-16 (fig. 30). The alkali-rich amphiboles were found as accessory phases in phlogopite rock P-3 (potassium richterite) and meta-graywacke Xe-14 (ferro-eckermanite). The amphibole of sample Xe-14 was interpreted as a metasomatic phase; the ferro-eckermanitic composition confirms that.

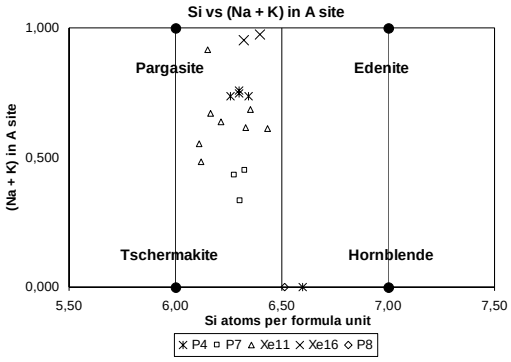

Figure 30. Amphibole of melanocratic granulites plotted with end-member compositions of the calcic amphiboles (Deer et al. 1992).

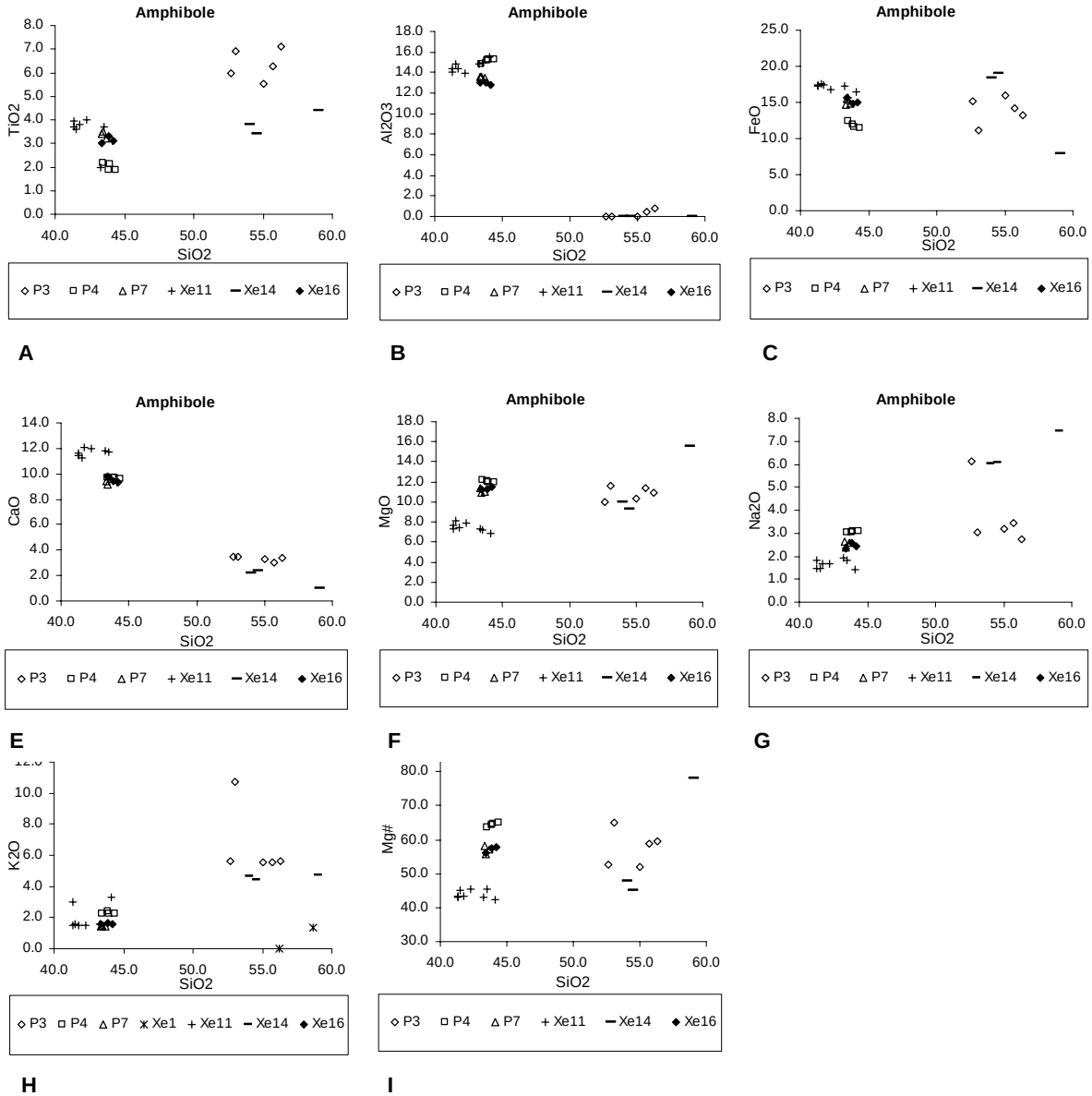

Figure 31. SiO_2 vs. TiO_2, Al_2O_3, FeO (total), MnO, CaO, MgO, Na_2O, K_2O (wt-%) and magnesium number (Mg#) for amphiboles in xenoliths.

The Harker diagrams (fig. 31) show the major divariant trends in the amphiboles. The calcic amphiboles are poor in SiO_2, relatively rich in Al_2O_3 (12-16 wt-%), CaO (8-12 wt-%), and FeO (10-20 wt-%). TiO_2 (2-4 wt-%), Na_2O (2-4 wt-%), and K_2O (1-3 wt-%) were observed. Decreasing magnesium number (fig. 31 F) divides the calcic amphiboles in three groups: P-4 (65), P-7 and Xe-16 (56-58) and Xe-11 (43-45). The alkali-rich amphiboles show more compositional variation. The potassic richerite of phlogopite rock (P-3) is rich in TiO_2 (6-7 wt-%) and Na_2O (3-6 wt-%), but poor in Al_2O_3. K_2O content is high (6-11 wt-%) but varies a lot. Due to high K content, a prefix potassic is used (Leake et al. 1997). The metasomatic amphibole of metagraywacke (Xe-14) is notably similar to P-3 but comprises lower TiO_2 (4-5 wt-%) and mainly higher Na_2O (6-7 wt-%).

5.2.4 Mica

The mica analyses are shown in table 5 in appendix 1. The compositions were recalculated to cations per formula unit on the basis of 22 anions (O, Cl, and F) using spread sheets of Preston (1999). The spread sheet was modified by the author to include barium, which usually replaces potassium in the unit cell.

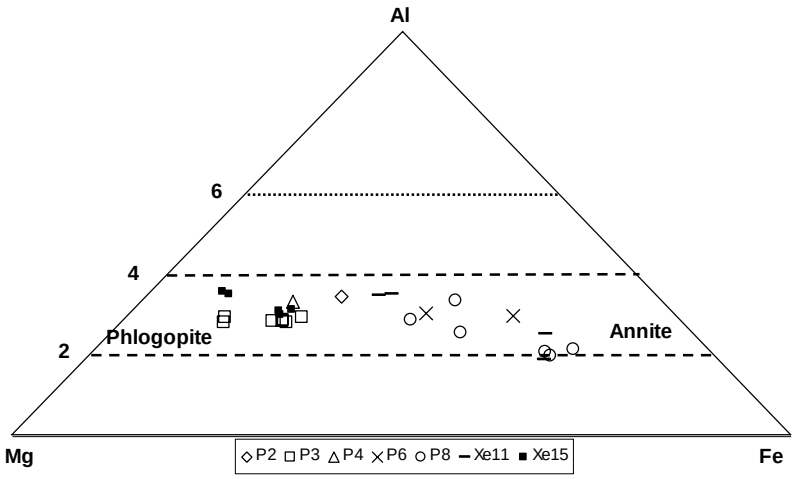

Figure 32. Mica compositions in the xenoliths represented with regard to Al, Mg, and Fe (tot) on the basis of 22 anions. End-members phlogopite and annite are after Deer et al. (1992).

Mica occurs as a major phase in phlogopite rock (P-3) and in calcite rock (Xe-15). In melanocratic granulites the mica, if present occur along grain boundaries. Fig. 32 shows that samples P-3 (phlogopite rock), P-4 (layered melanocratic granulite), and Xe-15

(carbonatite) contain magnesium-rich mica, phlogopite. Compositions closer to annite end-member are observed in melanocratic granulites P-2 (gneissic), P-6, P-8, and Xe-11. Muscovite is rarely observed as retrogressive phase.

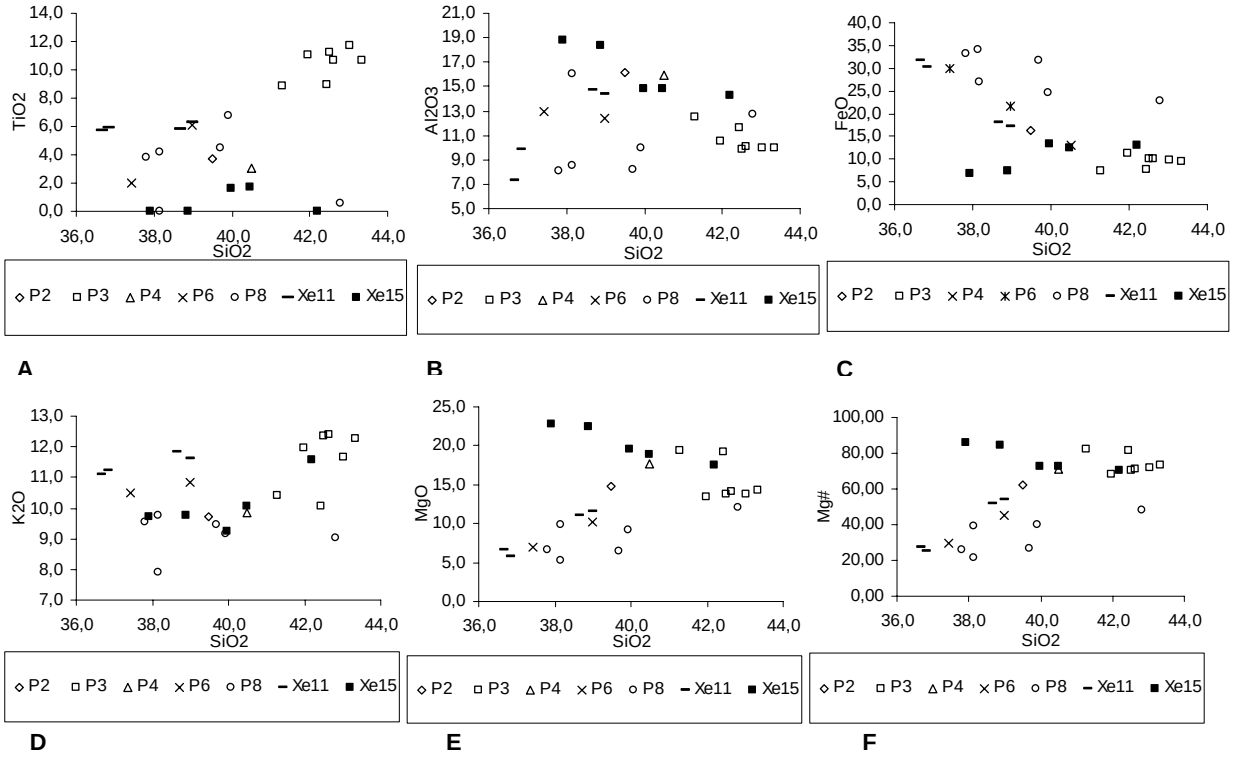

Figure 33. Mica in xenoliths. SiO_2 vs TiO_2, Al_2O_3, FeO (total), K_2O, MgO, (wt-%) and magnesium number (Mg#).

Harker diagrams (figs. 33 A-F) show compositional range of mica from xenoliths. Three groups of mica are observed: 1) Iron-rich [15-35 wt-% FeO (total)] mica in melanocratic granulites P-2, P-6, P-8, and Xe-11) show intermediate TiO_2 (2-7 wt-%) and variable Al_2O_3 contents. 2) TiO_2-rich mica (8-12 wt-% TiO_2) dominates the phlogopite rock (P-3) sample, but is observed also in the layered melanocratic granulite P-4. Intermediate Al_2O_3 (9-13 wt-%), low FeO (5-10 wt-%) and intermediate MgO (12-15 wt-%) are also distinguishable features for group 2. 3). The mica from carbonatite Xe-15, show high MgO and Al_2O_3, low TiO_2 and intermediate FeO.

5.2.5 Plagioclase

Plagioclase analyses are shown in table 6 in appendix 1. The compositions were recalculated to the end-members orthoclase $KAlSi_3O_8$ (Or), anorthite $CaAl_2Si_2O_8$ (An), and albite $NaAlSi_3O_8$ (Ab), using spread sheets by Preston (1999).

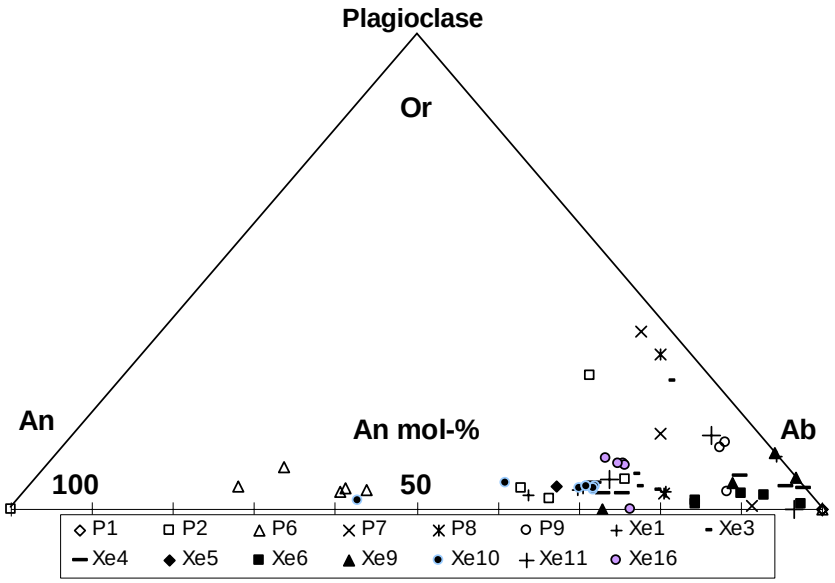

Figure 34. Plagioclase composition relative to mol-% of Or ($KAlSi_3O_8$), An ($CaAl_2Si_2O_8$), and Ab ($NaAlSi_3O_8$).

Plagioclase is a major constituent in the melanocratic and leucocratic granulites (metagabbroic rocks) and the tonalite gneisses. Albite without significant orthoclase component is observed in some of the alkali feldspar granites (Xe-6), augen gneisses (Xe-3), and meta-sedimentary rocks (P-1 and P-9). Relatively fresh, twinned plagioclase is an exception and co-exists always with non-twinned plagioclase, which often show lower anorthite content than the twinned plagioclase. The composition can vary quite much within a rock type, solely albite compositions were observed in carbon shale (P-1). Otherwise albite-oligiclase compositions were present in every plagioclase-bearing sample. Bytownite-anorthosite (An_{54-100}) compositions were observed in mafic granulites P-2 and P-6, and in leucocratic layered granulite Xe-10. There are only few andesine (An_{30-36}) compositions when oligoclase (An_{12-28}) is the most abundant composition (28 out of 64 analyses) (fig. 34, table 6 in appendix 1). For further descriptions on plagioclase see section 5.

5.2.6 Potassium feldspar

Potassium feldspar analyses are shown in table 7 in appendix 1. The compositions were recalculated to the end-members orthoclase $KAlSi_3O_8$ (Or), anorthite $CaAl_2Si_2O_8$ (An), and albite $NaAlSi_3O_8$ (Ab), using spread sheets by Preston (1999).

Fibrous orthoclase along grain boundaries is found as a metasomatic phase in tonalite gneiss, potassium feldspar granite gneiss, and kyanite granulite xenoliths. The melanocratic

granulites occasionally show minor euhedral orthoclase crystallized next to the dyke contact; this reflects metasomatic origin. Non-metasomatic, but presumably re-crystallized potassium feldspar is present in alkali feldspar granites, augen gneisses and kyanite granulite samples. The potassium feldspar in carbonatite (Xe-15) and phlogopite rock (P-3) xenoliths is interpreted as non-metasomatic and it may even be igneous.

24 out of 44 potassium feldspar analyses contain more than 90 mol-% $KAlSi_3O_8$. Minor FeO was observed in phlogopite rock P-3 (2.1 wt-%) and in kyanite granulite P-5 (1.5-2.0 wt-%). Microcline is present in the augen gneisses (Xe-2, Xe-3, Xe-5, and Xe-12); 15-42 mol-% $NaAlSi_3O_8$ (albite) was observed in the form of exsolutions. The albite content in perthitic potassium feldspar ranges between 4 and 43 mol-% (alkali feldspar granites).

5.2.7 Carbonates

Carbonate analyses are shown in table 3 in appendix 1. The compositions were recalculated to cations on the basis of 6 oxygen atoms using spreadsheet made by author. The classification is after Deer et al. (1992). Strontium-bearing (0-3 wt-% SrO) calcite is the main phase in carbonatite (Xe-15). Accessory calcite is present in tonalite gneisses (Xe-1, Xe-4), augen gneisses (Xe-2, Xe-3, and Xe-12), alkali feldspar granite gneisses (Xe-6 and Xe-7), layered granulite (Xe-11), mafic granulite Xe-16, and meta-sandstone P-9. Minor ankerite is present in phlogopite rock (P-3), tonalite gneisses (Xe-1 and Xe-4), augen gneiss (Xe-5), and kyanite granulite (Xe-13). Dolomite occurs accessorily in layered granulite (P-4) and ferroan dolomite in mafic granulite P-8. Metagraywacke (Xe-14) contained Mg- and Fe-rich, Mn-bearing carbonate.

5.2.8 Rutile

Rutile analyses are represented in appendix 1 in table 10. The compositions were recalculated to cations on the basis of 2 oxygen atoms using spread sheets by Preston (1999). Small amounts of Nb (0-2.4 wt-%), V (0-2.9 wt-%), Fe (0-1.4 wt-%), Ca (0-1.4 wt-%), Si (0-0.4 wt-% SiO_2), and Ba (0-2.4 wt-%) were detected occasionally. Majority of rutile observations bases on chemical analyses; only in sample Xe-13 the mineral is identifiable optically.

5.2.9 Spinel group minerals

Analyses of spinel group minerals are shown in table 11 in appendix 1. Most of the spinel analyses represent members of solid-solution series between magnetite and ulvöspinel end-members. The analyses show TiO_2 between 0 and 37 wt-%, FeO 58 and 98 wt-%, Al_2O_3 0

and 8 wt-%, MgO 0 and 9 wt-%, SiO_2 0 and 5wt-%, and Cr_2O_3.0 and 1.5 wt-%. Low Ti-content (below 7 wt-% TiO_2) and presence of Mge is charasteristic to magnetite from tonalite gneisses Xe-1 and Xe-4. The highest Mg-content of magnetite (25 wt-% MgO) was observed in Xe-1; it is probably due to mineral maghemite which is often associated with hematite (Deert et al. 1992). Red iron oxide (hematite) is a typical accessory phase in tonalite gneiss xenoliths. The magnetite of layered melanocratic granulites P-4 and Xe-11 and melanocratic granulite P-6 contained occasionally small amount of Cr, V and Zn were also observed rarely. Hercynite is present in kyanite granulites (P-5 and Xe-13). Spinel from sample P-5 show composition 59-66 wt-% Al_2O_3, 25-37 wt-% FeO, and 4-7 wt-% MgO; in sample Xe-13 the composition is poorer in Al, 17 wt-% Al_2O_3, 75 wt-% FeO, 4wt-% SiO_2 and 2 wt-% MgO.

5.2.10 Ilmenite

Analyses of ilmenite are shown in table 12 in appendix 1. The compositions are recalculated to cations on the basis of 32 and 6 oxygen atoms, respectively, using spread sheets by Preston (1999). Ilmenite occurs as exolution lamellae with Ti-rich magnetite/rutile in kyanite granulite (P-5), mafic granulites P-8 and Xe-16, and metasandstone P-9. TiO_2 content of ilmenite in former samples ranges between 47 and 85 wt-%, FeO between 21-51 wt-%. Minor amounts of Mn, Si, and Mg were observed (table 12 appendix 1).

5.2.11 Apatite, sulphides and sulphates

Apatite analyses are shown in in table 1 appendix 1 (in wt-%). Some Na and Cl were observed in several analyses (in 7 and 5 samples, respectively). Fluorine comprises 5 wt-% of apatite in mafic granulite P-7, 6-9 wt-% in tonalite gneisses Xe-4 and Xe-9, and 4 wt-% in alkali feldspar granite gneiss Xe-5.

Pyrite is a typical accessory mineral in all the xenolith rock types. Chalcopyrite was observed in layered melanocratic granulite (Xe-11). Barite is present in metagreywacke (Xe-14) and carbonatite (Xe-15).

6. PETROGRAPHY AND MINERAL CHEMISTRY OF THE DYKE 2

Dyke 2 is situated on the summit of Kjakebeinet (fig. 1); it is the narrower of the two dykes. A cross-section of this c. 40 cm wide lamproite dyke was studied to identify and describe the phases present. The mesoscopic appearance comprises narrow, c. 3 cm wide, porphyritic margin and a phaneritic, fine-grained core (fig. 35). The microscopic

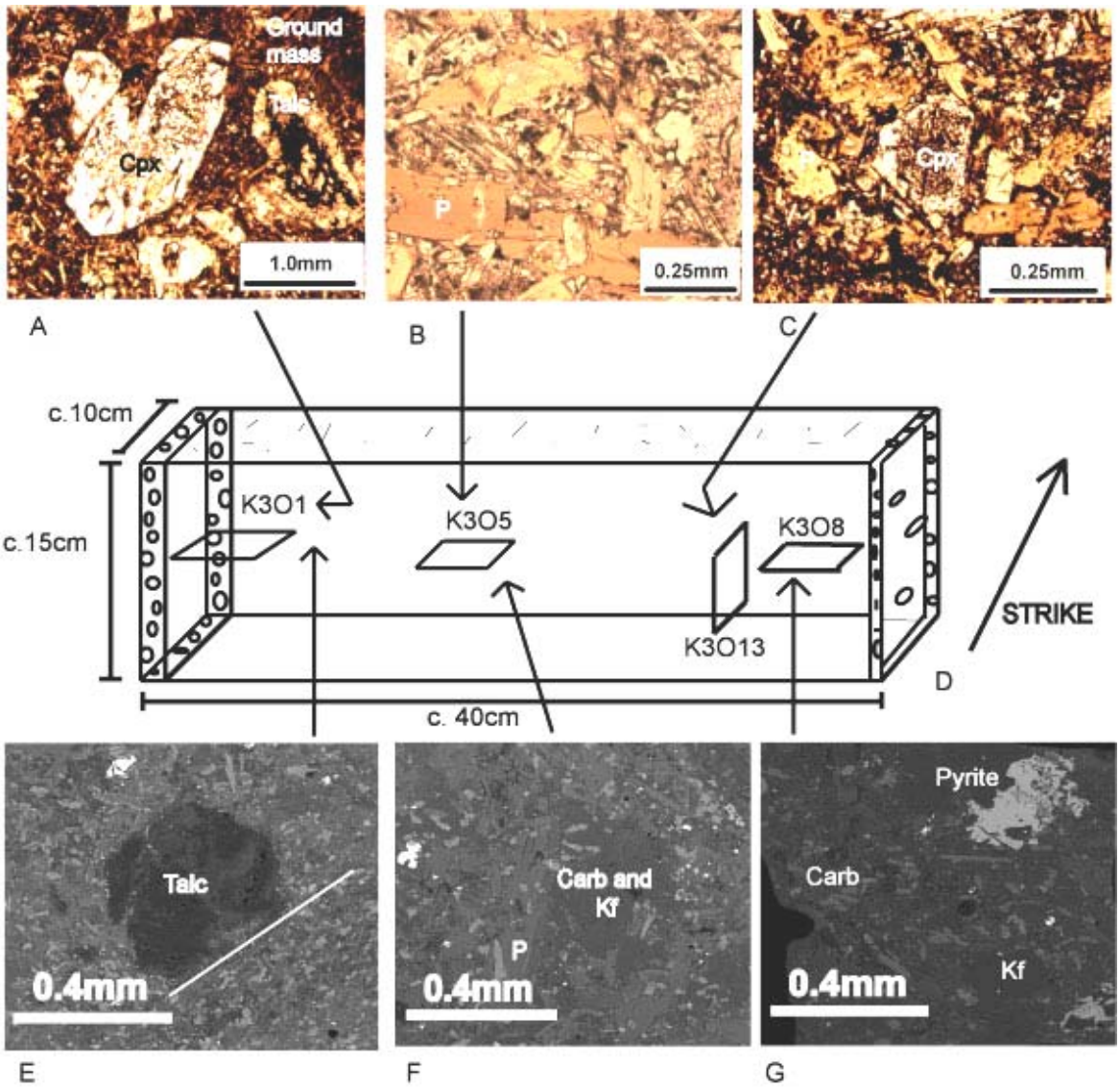

Figure 35. The lamproite dyke 2 hand specimen (cross-section). A-C, photomicrographs, ppl. A shows the porphyritic margin with cryptocrystalline ground mass (ground mass). On the centre of the picture is altered diopside (cpx) and on the right a talc pseudomorph (talc). B is from the core of the dyke where the main phenocryst phase is phlogopite (P). On the picture the phases present in ground mass are diopside, potassium feldspar, apatite, carbonate, and talc. C, on transitional zone between the porphyritic margin abundant opaque minerals exists with zoned phlogopite (Dark areas on the pictures A and C is mainly an effect caused by birefringence and the fine grain size of the ground mass). Minor opaque minerals present are pyrite and iron oxide. D,shows a sketch of the hand specimen. The thin sections (4 out of 18) and phenocrysts are not to scale. E-G, BS-images. White line on E divides the picture to porphyritic margin on the left and fine-grained, sheared zone (c. 2 cm) on the right. Abbreviations: Carb, carbonate; Kf, K-feldspar; P, phlogopite.

study showed that the “porhyritic” margin contains macrocrystal pseudomorphs after olivine and clinopyroxene in phaneritic groundmass. C. 4 cm wide sheared zone is observed next to the porphyritic margin. Towards the core, the grain-size increases and phlogopite shows intensiv zoning; the presence of abundant opaque is related to this phenomenon. This zone, observed under the microscope, is approximately 6 cm wide. The core region is distinguished by abundant phlogopite, subhedral, altered carbonate, and interstitial potassium feldspar.

6.1 Petrography

The mineral assemblage of the dyke (phlogopite, diopside, potassium feldspar, and pseudomorphs after olivine) remains quite constant through out the cross-section, even though the grain size and the appearance of the minerals vary. Carbonate, rutile, apatite, barite, pyrite, and aegirine are accessory phases; Magnetite occurs as an alteration product after olivine and as rare macrocrysts.

Porphyritic margin

The phenocrysts comprises of 0.25 - 1 mm talc and calcite pseudomorphs after olivine (13.6 vol-%) and up to 2.5 mm calcite pseudomorphs with iron oxide (reddish colour) (4.3 vol-%), 0.5 – 1 mm diopside (3.9 vol-%), and potassium feldspar aggregates often co-existing with very fine-grained calcite (10.3 vol-%). Diopside is mainly fresh, euhedral, and occasionally zoned, but c. 1 mm subhedral crystals with altered core (potassium feldspar symplectic and/or rarely sodium-pyroxene-bearing) are found. 0.05 – 0.15 mm individual potassium feldspar grains occur mainly as grain aggregates, occasional 0.5 mm single grains are observed; the appearance is altered and potassium feldspar contains abundant tiny inclusions. Fine-grained groundmass (67.9 vol-%) comprises carbonate, 0.025 – 0.1 mm phlogopite, 0.15 – 0.25 mm euhedral apatite, 0.05 mm twinned, euhedral diopside, talc, potassium feldspar, and rutile occurring as c. 0.05 mm in diameter aggregates, in the order of abundance. Greenish, acicular, sometimes spherulitically oriented, unidentified material occupies the ground mass. Though the grain-size of the ground mass makes observations difficult, the phlogopite seems to be inclusion-free. Potassium feldspar-carbonate mainly comprise irregularly shaped “vesicles” that are rarely polycrystalline, pointing to amygdaloidal origin.

Sheared zone

Adjacent to the porphyritic margin the grain size of the groundmass increases and the pseudomorphs after olivine change anhedral and rounded. Phenocrysts disappear. Calcite occurs only as ground mass phase and its appearance refer to secondary origin. Phlogopite remains quite fine grained; the boundary between the porphyritic margin and the "sheared zone" is sharp and the latter show a lineation parallel to strike (fig. 35 E). Towards the core (comprising c. 6 cm zone) the general grain size increases and phenochrystal, subhedral, intensively zoned phlogopite co-exists with abundant pyrite. Completely altered, euhedral olivine is often surrounded by rim of phlogopite.

Core

The grain size of the phenocrystal phase (phlogopite, apatite, and ankerite) is greatest in the core of the dyke (fig. 35 B and F). The pseudomorphic phases are similar to the porphyritic margin and yield a diameter of 1 mm. The size of subhedral to euhedral phlogopite (39-45 vol-%) ranges between 0.7 and 1 mm. Concentric zoning is observed occasionally, though more rarely than in the zone transitional between the sheared zone and the core. The coarsest phlogopite encloses occasionally euhedral apatite and diopside. Therefore it is possible that morphological forms called groundmass phlogopite (poikilitic, subhedral plates often enclosing diopside, leucite, priderite, apatite and spinel) and phenocrystal phlogopite (strongly phleochroic, inclusion-free type which is often corroded or embayed on margins) (Mitchell and Bergman 1991) are present. The dominating type in dyke 2 is phenocrystal phlogopite. Scarce, medium-grained aggregates of euhedral, sector zoned phlogopite and iron oxide occurs occasionally. There are two types of diopside (13 vol-%): a rare, c. 1 mm in diamerer, subhedral, altered type which sometimes composes monomineralic aggregates (xenocrysts derived from almost decomposed xenoliths?). Single crystals show fresh, unaltered rim which is diopside in composition. The predominant diopside is euhedral, 0.3 mm in diameter, occasionally zoned and fresh (fig. 36).

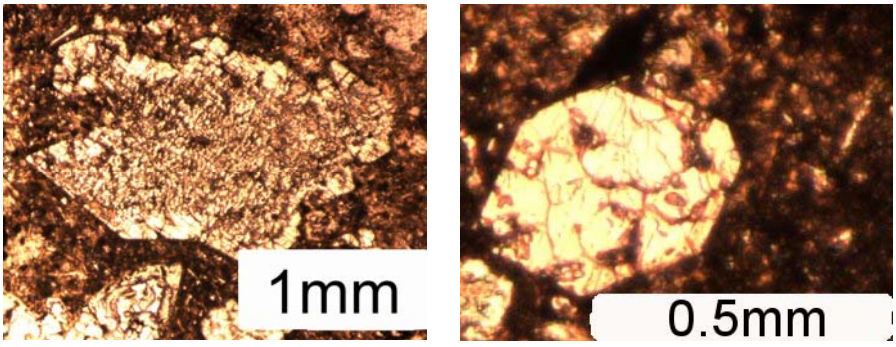

Figure 36. Diopside types of dyke 2: A) Diopside with altered core, B) Euhedral, fresh diopside.

Fine-grained talc pseudomorphs (9-10 vol-%) and interstitial potassium feldspar-carbonate patches (22-27 vol-% and 9 vol-%, respectively) distribute through the cross-section quite equable. Potassium feldspar is less altered and carbonate is coarser-grained on the core than on the margins. The potassium feldspar occurs mainly as polycrystalline, ocelli-like blebs with irregular margins. Euhedral apatite (0.15 – 0.25 mm) occurs throughout the dyke as a ground mass phase and is occasionally partly enclosed by potassium feldspar. Slightly altered ankerite is crystalline and yields 9 vol-%. Fine-grained, euhedral to subhedral rutile, anhedral, titanium-bearing aegirine-augite, anhedral pyrite, and Ti- and Al-bearing magnetite in olivine pseudomorphs comprises the minor phases. Accessory sodium-pyroxene occurs sporadically and rarely inside the altered type of diopside.

6.2 Comparison to dykes 1 and 3

Thin section AL/KB8-98 is from the core of the dyke 1 which hosts the xenoliths identified with P symbols. KB21-98 represents dyke 3 located to south from the summit of Kjakebeinet. A rough petrographical comparison to dyke 2 is made below.

Dyke 1

The mineral assemblage is comparable to dyke 2. There is more and coarser clinopyroxene (probably corresponds to unidentified acicular phase described among the porphyritic margin of dyke 2) which occur mainly as euhedral, oblong crystals. Phlogopite is occasionally strongly zoned. Interstitial carbonate and potassium feldspar are fresher and probably more abundant than in dyke 2. Talc pseudomorphs after olivine are less abundant and no aegirine (bright green pyroxene) is observed. Apatite is subhedral and coarser-grained in dyke 1.

Dyke 3

There are no talc pseudomorphs after olivine in this thin section, AL/KB21. Subhedral phlogopite (0.1-1 mm) is rarely zoned with irregular dark-brown material. Potassium feldspar and carbonate patches are less abundant and their size is smaller than in dyke 2. They occur mainly as ocelli, and carbonate amygdale are present. The ground mass comprises abundant euhedral, rarely phenocrystal, greenish-yellow pleochroic pyroxene, and apatite.

6.3 Mineral chemistry

6.2.1 Pyroxene

Pyroxene analyses are represented in table 5 appendix 2. The recalculation procedure of pyroxene is described in section 5.2.1. Two types of pyroxene were found; aegirine augite and diopside.

Sodium pyroxene

The green sodium-pyroxene does not fit in the four main groups of pyroxenes, when plotted in Q-J diagram. This is probably due to substitution of Na with Ti (Morimoto et al. 1989). Aegirine-augite contains 4-8 wt-% TiO_2, 24-25 wt-% FeO, and 11-13 wt-% Na_2O. The magnesium ratio is very low (0-9).

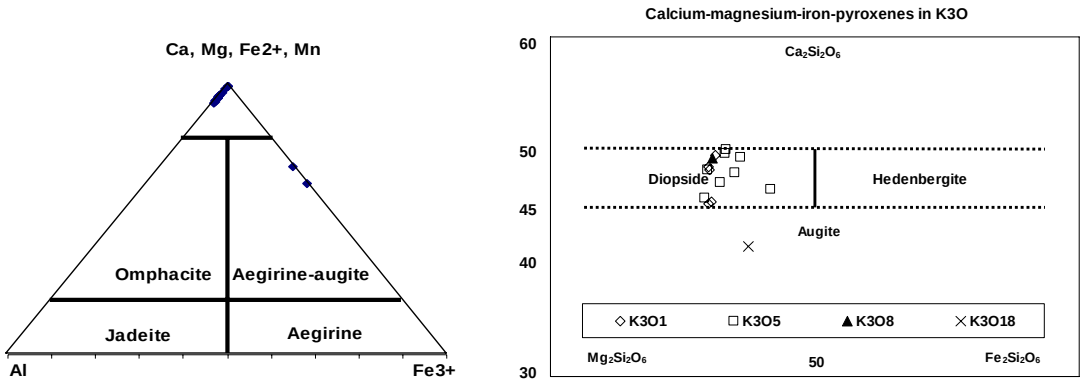

Figure 37. Composition of pyroxene in dyke 2. A) The Ca-Mg-Fe pyroxene. B) The calcium-rich pyroxene in the dyke 2 diopside. Augite was found as an inclusion in magnetite. Nomenclature and classification is after Morimoto et al. (1989).

Clinopyroxene

The major pyroxene is diopside (fig. 37 B) in composition; fig. 38 shows the compositional range of diopside. It is slightly Ti- and Al-bearing (TiO_2 and Al_2O_3 ranges between 0 and 3 wt-%); CaO, FeO, and MgO content ranges between 20-25, 4-10, and 12-17 wt-%, respectively. The magnesium number varies between 78 and 89. Augite enclosed by magnetite is mainly similar to diopside but it has a notably lower magnesium ratio of 72. A minor amount of chromium (c. 0.5 wt-% Cr_2O_3) is observed on the rims of zoned crystals. Summarized, the diopside shows some variation in composition (fig. 38). The unaltered rim of macrocrystal pyroxene shows similar composition to fresh, euhedral diopside (fig. 36).

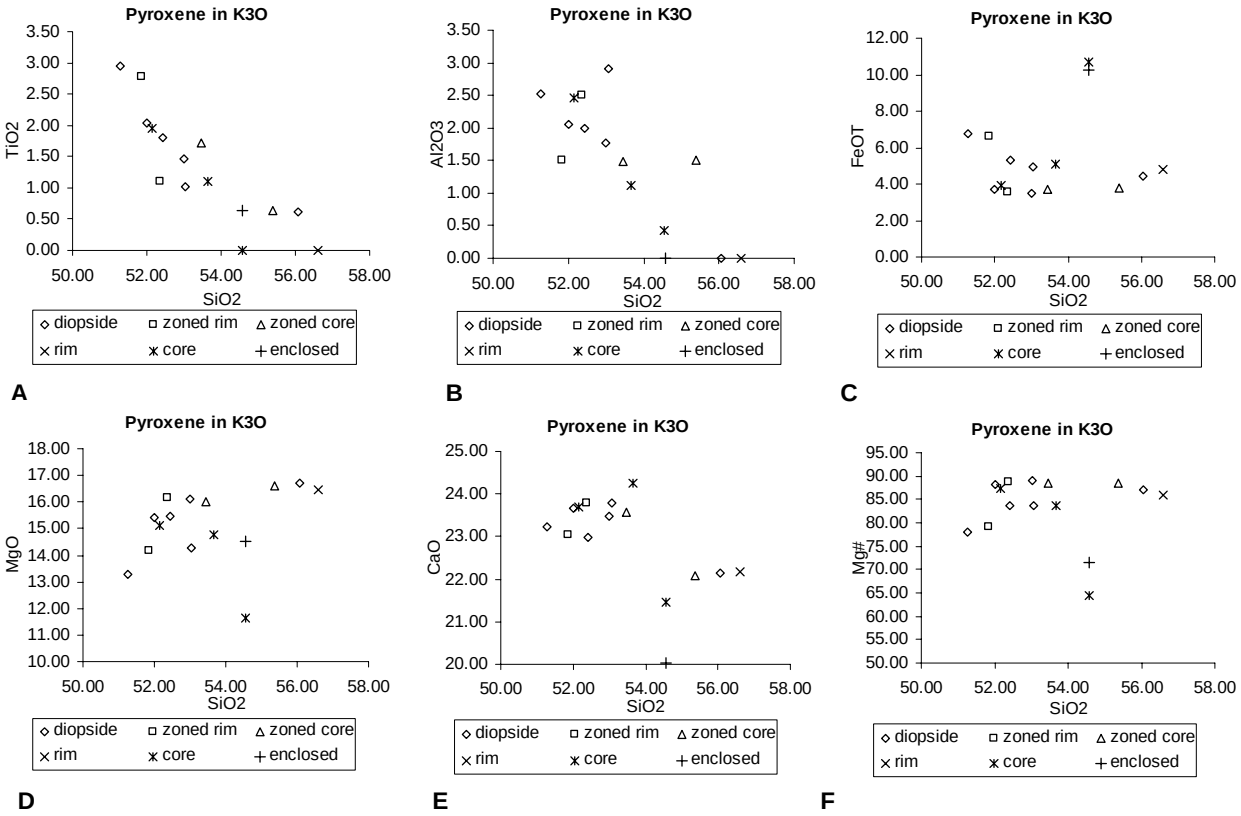

Figure 38. Composition of clinopyroxene in dyke 2, sample K3O. SiO_2 versus TiO_2, Al_2O_3, FeO (total), MgO, CaO, and magnesium number (Mg#). “Enclosed” refer to pyroxene enclosed by an opaque mineral.

6.2.2 Mica

Mica analyses are represented in table 3 appendix 2. The recalculation procedure is described in section 5.2.2. Mica is tri-octahedral (Deer et al. 1992), magnesium-rich (magnesium number 70-82) phlogopite.

Six of the analyses represented in fig. 39 are from the very fine-grained phlogopite from the porphyritic margin of the dyke 2. Phlogopite, associated with magnetite macrocrysts (in thin section K3O18), comprise three analyses; the "vicinity of opaque" in fig. 39 refers to these three analyses and to phlogopite enclosed by magnetite. Other analyses are divided in two with respect to the location of analysis point. In fig. 39 phlogopite composition is shown in relation to Al cations per formula unit. Al content increases with decreasing Si and increasing Ti (fig. 39 A). A slight negative slope is seen among Al versus Fe content (fig. 39 B). Phlogopite of porphyritic margin shows notably constant composition with regard to Al, Si, and Ti. According to Mitchell and Bergman (1991) Al rich and Fe poor compositions refer to less evolved phlogopite. Therefore, the mica in porphyritic margin is slightly less evolved than in other parts of the dyke. In wt-% the compositional range of phlogopite is: TiO_2; 3 - 8 wt-% and Al_2O_3 9 - 14 wt-%;

majority of phlogopite contains 9-12 wt-% FeO and 10 wt-% K_2O. The Mg content is relatively high, 16-21 wt-% MgO (table 3 appendix 2) but the magnesium number varies quite a lot.

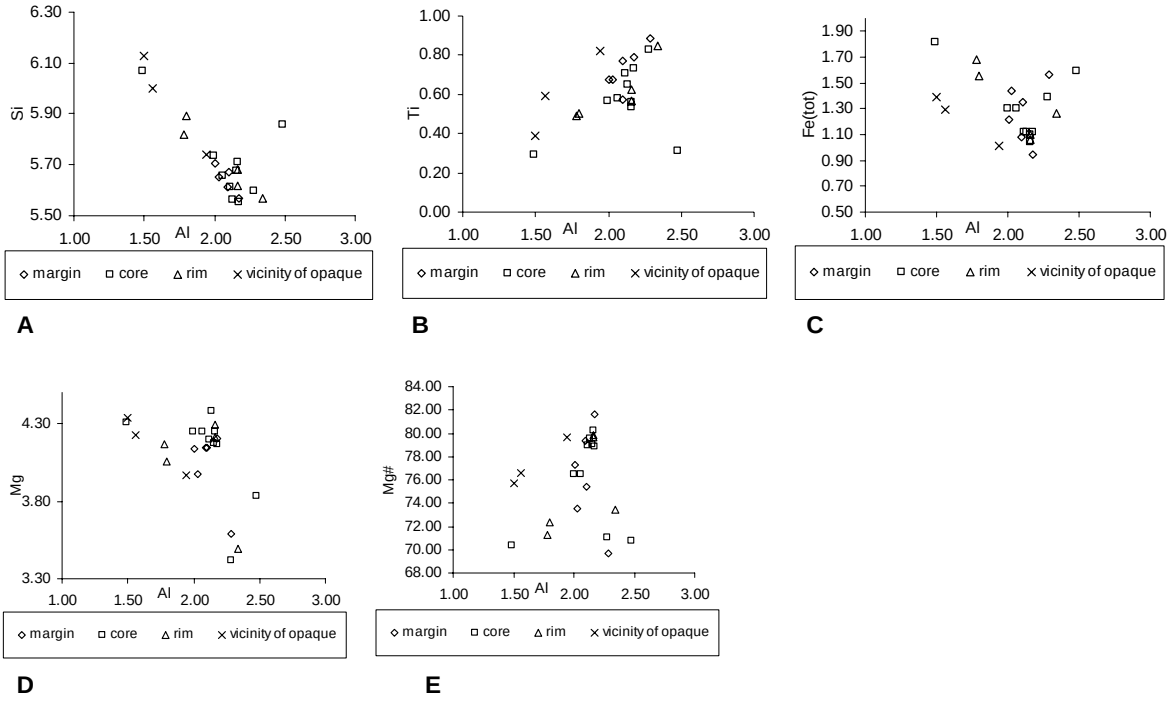

Figure 39. Composition of phlogopite in dyke 2; Al cations versus Si, Ti, FeO (total), Mg (on the basis of 22 oxygen atoms) and magnesium number in phlogopite.

6.2.3 Potassium feldspar

The analyses are represented in table 4 appendix 2. Recalculation procedure is described in section 5.2.4. Potassium feldspar occur interstitally as more or less altered aggregates with carbonate. Sodium and calcium are absent in feldspar and consequently it comprises of pure orthoclase end-member.

6.2.4 Carbonates, oxides, and phosphates

Calcite was observed in the interstices of a magnetite macrocryst; otherwise the carbonate analysed is ankerite (table 2 appendix 2).

Spinel group mineral analyses are represented in table 7 appendix 2. Accessory magnetite contains aluminium and titanium. It occurs with phlogopite in medium-grained aggregates. The compositional range is 79-97 wt-% FeO, 0-12 wt-% TiO_2, 0-9 wt-% Al_2O_3, 0-3 wt-% MgO, and 0-4 wt-% SiO_2. The silicon content is probably derived from impurities. In the core of talc and talc-carbonate-magnetite pseudomorphs magnetite, and a Cr (22 wt-% Cr_2O_3) and Ti (10 wt-% TiO_2) bearing spinel group

mineral is observed. Rutile (table 6 appendix 2) occurs as a euhedral minor phase; Si and Zr in analyses reflacts that it usually contains inclusions.

Apatite is euhedral and on the basis of this study, homogenic; no inclusions were observed. 0-4 wt-% fluorine is observed and a trace of chlorine was measured once.

7. ISOTOPE GEOCHEMISTRY

In this section the melanocratic granulites (Xe-11 layered melanocratic granulite, Xe-16 garnetiferous melanocratic granulite), introduced in section 4, have been referred as metagabbroic samples. Isotopic studies of the carbonatite sample and metagabbroic xenoliths were made to get information on their age and origin. In the study area, a thick, Phanerozoic supracrustal sequence covers the Proterozoic, or older, basement. There is no direct evidence on location of Cambrian-Ordovician suture between Grunehogna craton and Maud belt, and, until now, the bedrock below southern Vestfjella has been unknown. Mafic magmas have repeatedly intruded the crust in Mesoproterozoic to Jurassic times on WDML and adjacent areas; therefore it is not self-evident that the gabbroic xenoliths would represent Jurassic magma types. Nepheline-syenite-complex on Straumsvola, WDML, records Jurassic alkaline magmatism (Harris and Grantham 1993). Oxygen, carbon, and radiogenic isotope data in addition to mineral chemical data was necessary to clarify the relationship between the carbonatite xenolith and the hosting lamproite. The knowledge on crustal compositions is valuable in the study of Jurassic basaltic and lamproitic magmatism.

7.1 Oxygen and carbon

The mineral assemblage and appearance of carbonatite xenolith Xe-15 refers to an igneous rock sample; stable isotopes were used to further characterize the sample and to eliminate the possibility of a sedimentary origin. Whole-rock oxygen and carbon isotopic compositions were determined for the diopside-schorlomite-carbonatite xenolith (Xe-15) (table 4).

Table 4. Whole rock carbon and oxygen isotopic composition of diopside-schorlomite-carbonatite sample Xe-15. Numbers 1, 2, and 3 refer to partial samples.

Sample	δ13C VPDB	δ18O VSMOW
Xe-15-1	-4.25	10.35
Xe-15-2	-3.62	11.16
Xe-15-3	-3.71	11.27

The $\delta^{13}C$ values range from -3.62 to -4.25 ‰ VPDB and the $\delta^{18}O$ values from 10.35 to 11.27 ‰ VSMOW, respectively. The measured values include in the ordinary chondrite

field determined by Wright et al. (1988). Deep-seated carbon reservoir shows $\delta^{13}C$ values between -2 and -8 ‰, which include the mean ratios observed in kimberlites (-4.7±1.2 ‰) and in carbonatites (-5.1±1.8 ‰) (Deines and Gold 1973). According to Javoy et al. (1986), the $\delta^{13}C$ in mantle ranges between -5 and -8 ‰, especially

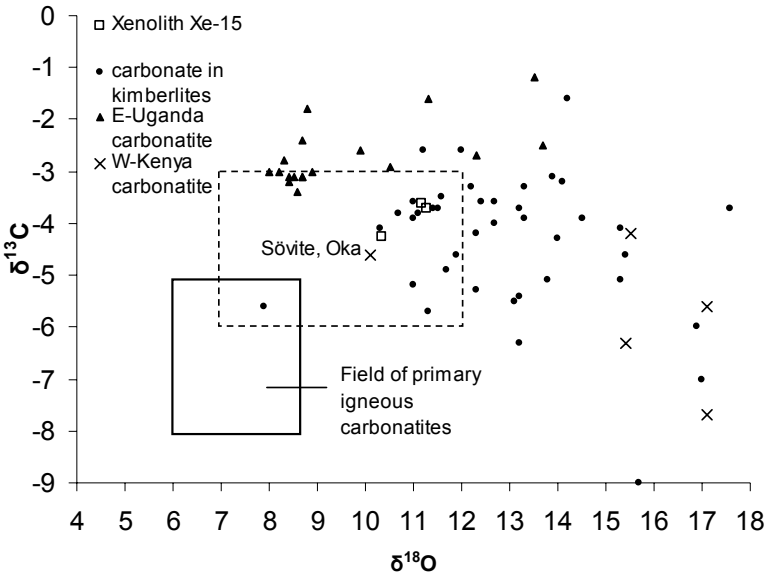

Figure 40. Whole-rock carbon and oxygen isotopic ratio of diopside-schorlomite carbonatite sample Xe-15. Field of primary igneous carbonatites is after Taylor et al. (1967), isotopic ratios of kimberlite carbonate, African carbonatites, and the compositional range of Oka sövites (Ontario) are after Deines and Gold (1973).

carbonatites may show quite a large variation due to isotopic fractionation. The carbon isotope composition of sample Xe-15 shows a strong affinity to deep-seated, mantle-derived carbon, whereas the oxygen isotope ratio 10-11 ‰ VSMOW is higher than the primitive mantle ratio, 5.7±0.3 ‰ VSMOW, determined from chondrite meteorites (Taylor 1980). The $\delta^{18}O$ and $\delta^{13}C$ values measured (table 4), however, show similar values to sövites of Oka, Ontario, and kimberlite carbonates of several continents (fig. 40). The so-called primary igneous carbonatites (Taylor et al. 1967) show lower $\delta^{18}O$ and $\delta^{13}C$ relative to sample Xe-15 isotopic composition. Thus Nelson et al. (1988) argued that, in carbonatites, significant shift in $\delta^{18}O$ and $\delta^{13}C$ from the mantle values reflects a subduction-related origin. Although the igneous values of oxygen isotopic ratios of the sample Xe-15 may have re-equilibrated after crystallization due to 1) the hydrous character of host-lamproite magma and 2) hydrothermal alteration at low temperatures. The petrographical observations are promoted by oxygen and carbon isotopic composition (table 4); the sample Xe-15 shows strong affinity to carbonatites.

7.2 Radiogenic isotopes

The mineral fractions used in Rb-Sr and Sm-Nd isotope measurements were hand picked and mostly free of microscopic inclusions; some impurities were present, however (table 2 section 3.1.2). The appearance of the plagioclase in granulite samples (Xe-11, Xe-16) raises the question whether the separates have contained both metamorphic and igneous plagioclase; the analyses may show mixed isotopic ratios. On the other hand, the Sm-Nd system may well remain closed in granulite facies conditions (Dickin 1995), and thus the state of plagioclase is irrelevant. Clinopyroxene and garnet in the carbonatite (Xe-15) show compositional zoning of unknown origin. Therefore clinopyroxene and whole-rock data may record mixing of isotopic compositions. In addition, the calcite fraction contained a minor amount of mixed calcite-garnet grains (table 2 section 3.1.2.).

Table 5. Isotopic composition of the host dyke and the xenoliths. Data for dyke 2 is from Luttinen et al. 2002.

		$^{87}Rb/^{86}Sr$	$^{87}Sr/^{86}Sr$	Rb ppm	Sr ppm	$^{147}Sm/^{144}Nd$	$^{143}Nd/^{144}Nd$	Sm ppm	Nd ppm
Dyke 2	lamproite	0.08572	0.705517	92.4	2828.0	0.08629	0.512219	33.3	242.1
Xe-15	carbonatite	0.08210	0.705307	76.1	2672.0	0.10838	0.512250	14.5	81.2
Xe-11	granulite	0.19329	0.704369	49.0	730.7	0.13921	0.512455	6.26	27.3
Xe-16	granulite	0.09232	0.704712	44.1	1375.0	0.11607	0.512108	15.3	79.7

The xenoliths have been transported by lamproite dyke enriched in REE (table 5). The host, presumably similar to dyke 2, shows higher amounts of Rb (92 ppm), Sr (2828 ppm), Sm (33 ppm), and Nd (242 ppm) (table 5 and 6) relative to the xenoliths studied (table 5). The REE concentrations of the dyke indicate that the strongest lamproite-derived contaminants were Sr and Nd. Rudnick (1992) stated that Rb and/or Sr enrichment is typical of granulite xenoliths transported by kimberlites due to high concentrations of these elements in kimberlite magma. Therefore the Rb-Sr results on the melanocratic granulites, especially the whole-rock analyses, should be viewed with caution (Rudnick 1992).

According to Powell et al. (1966) carbonate-rock xenoliths do not contaminate by Sr during kimberlite transportation, though the hosting dyke would show higher Sr concentrations. In addition, the amount of radiogenic Sr would increase only slightly in case Rb concentrations would rise because of the long half-life of rubidium (49000 Ma) compared to the age of the dyke (160 Ma, Luttinen et al. 2002). Therefore, the $^{87}Sr/^{86}Sr$ ratio of the carbonatite (Xe-15) should reflect the igneous composition.

Radiogenic isotope ratios, REE concentrations, epsilon values of present day for Nd and Sr, and Nd depleted mantle model-ages (DePaolo 1981), are shown in table 6.

Table 6. REE concentrations, isotopic composition, epsilon values of Nd and Sr, and Nd depleted mantle model ages for metagabbroic (Xe-11 and Xe-16) and carbonatite (Xe-15) xenoliths.

Sample	Fraction	Sm ppm	Nd ppm	$^{147}Sm/^{144}Nd$	$^{143}Nd/^{144}Nd$	εNd(0)	Rb ppm	Sr ppm	$^{87}Rb/^{86}Sr$	$^{87}Sr/^{86}Sr$	εSr(0)	T_{DM}
Xe11	WR	6,3	27,3	0,1392	0.512455±9	-3,6	49,0	730,7	0,19329	0.704369±15	-1,9	1204
Xe11	Apat	115,3	731,8	0,0956	0.512419±11	-4,3	15,9	4330,9	0,01058	0.703271±14	-17,4	816
Xe11	Pl	0,5	4,0	0,0786	0.511880±10	-14,8	44,1	1643,6	0,07737	0.703815±14	-9,7	1310
Xe15	WR	14,5	81,2	0,1084	0.512250±9	-7,6	76,1	2672,1	0,08210	0.705307±14	11,5	1149
Xe15	Calc	13,8	106,5	0,0785	0.512252±9	-7,6	4,6	5976,6	0,00222	0.705042±14	7,7	898
Xe15	Cpx	15,3	63,5	0,1461	0.512252±10	-7,6	28,4	844,5	0,09693	0.70542±14	13,1	1776
Xe16	WR	15,3	79,7	0,1161	0.512108±13	-10,4	44,1	1375,0	0,09232	0.704712±19	3,0	1456
Xe16	Cpx	15,6	59,5	0,1590	0.512139±9	-9,8	11,7	194,6	0,17386	0.704829±13	4,7	2535
Xe16	Pl	2,6	17,9	0,0879	0.512053±11	-11,5	44,4	1959,2	0,06532	0.704916±13	5,9	1199

Estimated error for $^{147}Sm/^{144}Nd$ and $^{87}Rb/^{86}Sr$ is 0.4%. $^{143}Nd/^{144}Nd$ is normalized to $^{146}Nd/^{144}Nd=0.7219$, $^{87}Sr/^{86}Sr$ to $^{86}Sr/^{84}Sr=0.1194$. εNd and εSr values were calculated using present day values $^{143}Nd/^{144}Nd=0.51264$ and $^{147}Sm/^{144}Nd=0.1966$, and $^{87}Sr/^{86}Sr=0.7045$ and $^{87}Rb/^{86}Sr=0.0816$ for CHUR (Chondrite Uniform Reservoir) according to Hamilton et al. (1983). Depleted mantle model-age (T_{DM}) is after DePaolo (1981). Abbreviations for fractions: WR=whole rock powder, apat=apatite, calc=calcite, cpx=clinopyroxene, and pl=plagioclase.

7.2.1 Carbonatite (Xe-15)

The carbonatite (Xe-15) whole rock sample contains 15 ppm Sm, 81 ppm Nd, and 76 ppm Rb (table 6). It shows notably high Sr concentrations which range from 845 ppm (clinopyroxene) to 5977 ppm (calcite). Calcite has the highest Nd contents (107 ppm). All of the analysed fractions yielded similar $^{143}Nd/^{144}Nd$ ratios with present day epsilon Nd value of -7.6. The depleted mantle model-age for Nd (DePaolo 1981) varies between 900 and 1780 Ma; the whole rock model age is 1150 Ma. The present day epsilon Sr value ranges between +7.7 and +13.1; the whole rock epsilon Sr value is +11.5.

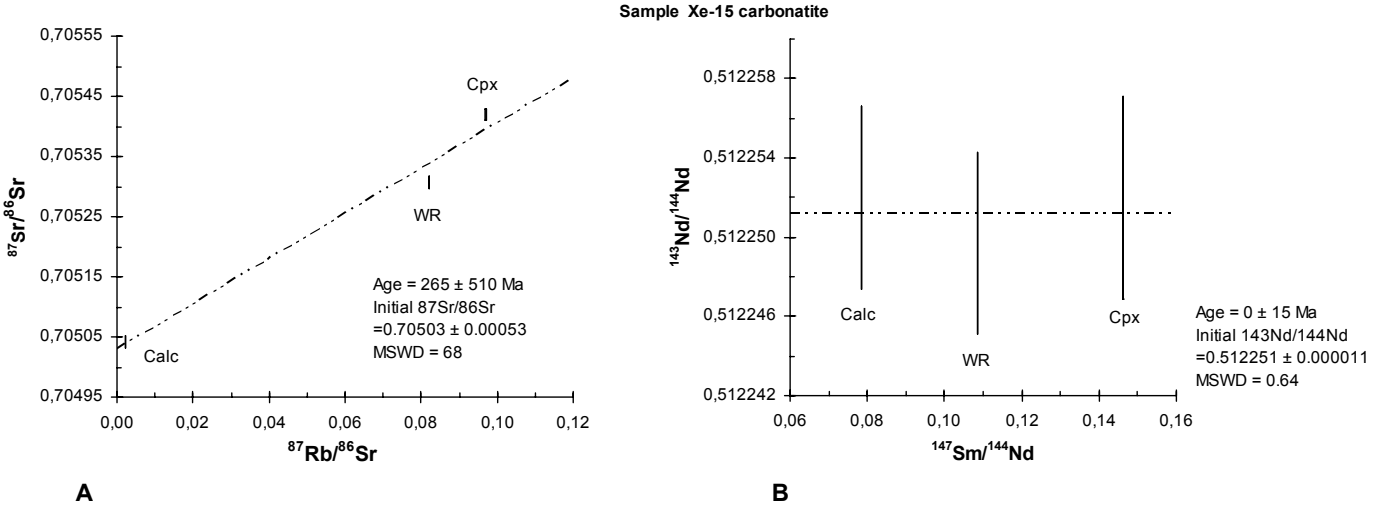

Figure 41. $^{87}Rb/^{86}Sr$ versus $^{87}Sr/^{86}Sr$ (A) and $^{147}Sm/^{144}Nd$ versus $^{143}Nd/^{144}Nd$ (B) diagrams for carbonatite sample Xe-15. Analytical error on $^{87}Sr/^{86}Sr$ and $^{143}Nd/^{144}Nd$ is indicated by the line. Abbreviations: Calc, calcite; cpx, clinopyroxene; WR, whole rock.

A plot of $^{87}Rb/^{86}Sr$ versus $^{87}Sr/^{86}Sr$ (fig. 41 A) shows positive correlation between the data points (fig. 41 A). The poorly constrained regression line corresponds with an age of 265 Ma. The calcite fraction shows notably low $^{87}Sr/^{86}Sr$ which probably is close to initial $^{87}Sr/^{86}Sr$ value. Fig. 41 B shows that the $^{143}Nd/^{144}Nd$ ratios of different fractions of sample Xe-15 are identical within error. The closure time of Sm-Nd system is probably too young to be determined.

7.2.2 Layered metagabbro (Xe-11)

The whole rock of the layered metagabbro (Xe-11) contains 6 ppm Sm, 27 ppm Nd, 49 ppm Rb, and 730 ppm Sr (table 6). Apatite shows the highest Nd (730 ppm) and Sr (4331 ppm) concentrations. Apatite and whole rock have almost identical $^{143}Nd/^{144}Nd$ ratios. The present day epsilon Nd value ranges between -3.6 (whole rock) and -14.8 (plagioclase). The depleted mantle model-age for Nd (DePaolo 1981) is youngest for apatite (820 Ma) and oldest for plagioclase (1310 Ma). The epsilon Sr values range between -1.9 (whole rock) and -17.4 (apatite). The high abundance of fluid inclusions

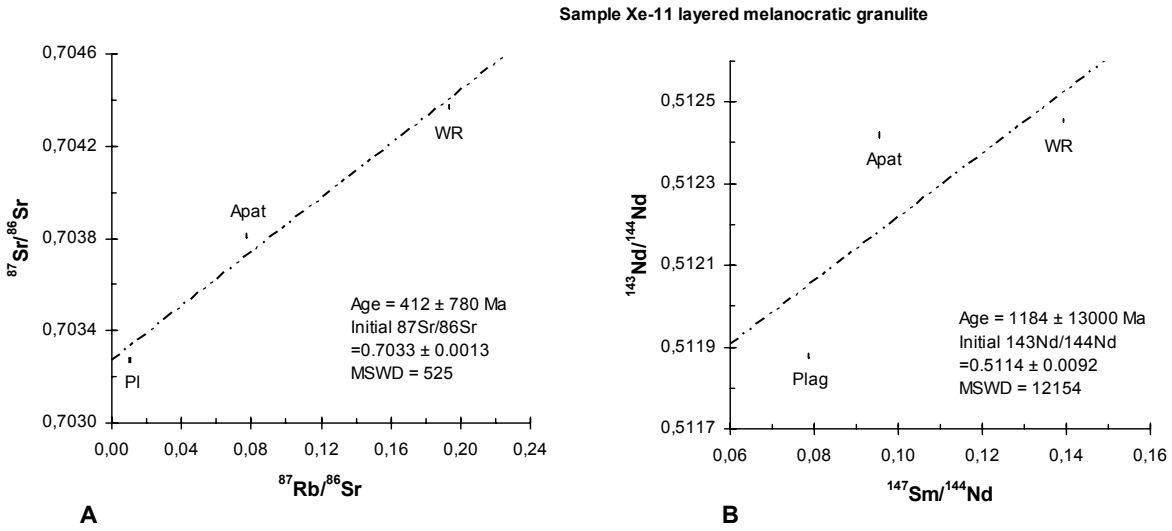

Figure 42. $^{87}Rb/^{86}Sr$ versus $^{87}Sr/^{86}Sr$ (A) and $^{147}Sm/^{144}Nd$ versus $^{143}Nd/^{144}Nd$ (B) diagrams for metagabbroic sample Xe-11. Analytical error on $^{87}Sr/^{86}Sr$ and $^{143}Nd/^{144}Nd$ is indicated by the line. Abbreviations: Apat, apatite; pl, plagioclase; WR, whole rock.

suggests that apatite has equilibrated with metamorphic/metasomatic fluids and therefore the apatite does not reflect igneous compositions. A plot of $^{87}Rb/^{86}Sr$ versus $^{87}Sr/^{86}Sr$ (fig. 42 A) shows positive correlation between the data points; the regression line, however, is poorly constrained. The apatite depleted mantle-model age 820 Ma (table 6) and lamproite emplacement age 160 Ma (Luttinen et al. 2002) are included in the Rb-Sr "age" 412±780 Ma. Fig. 42 B shows that plot of $^{147}Sm/^{144}Nd$ versus $^{143}Nd/^{144}Nd$ does not show correlation and the system does not yield meaningful ages.

The very low $^{143}Nd/^{144}Nd$ value of plagioclase refers to old enriched component and the depleted mantle model age of plagioclase (1310 Ma) may well broadly correspond with the age of the protolith.

7.2.3 Garnetiferous metagabbro (Xe-16)

The whole rock sample of garnetiferous metagabbro (Xe-11) contains 15 ppm Sm, 80 ppm Nd, 44 ppm Rb, and 1375 ppm Sr (table 6). The whole rock and plagioclase fractions show high Rb concentrations (1375 ppm and 1959 ppm, respectively). The depleted mantle model-age for Nd is youngest for plagioclase (1199 Ma) and oldest for clinopyroxene (2535 Ma). The present day epsilon Nd value varies between -9.8 (clinopyroxene) and -11.5 (plagioclase) and epsilon Sr between +3.0 (whole rock) and +5.9 (plagioclase). A plot of $^{87}Rb/^{86}Sr$ versus $^{87}Sr/^{86}Sr$ (fig. 43 A) does not show correlation whereas $^{147}Sm/^{144}Nd$ versus $^{143}Nd/^{144}Nd$ plot (43 B) shows correlation and corresponds with an age of 179 Ma, although, the age is poorly constrained.

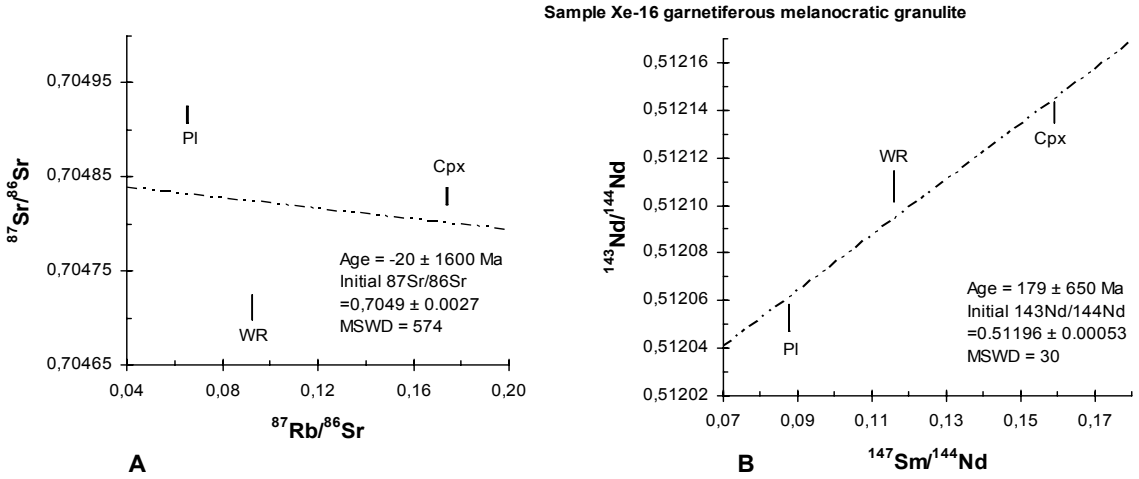

Figure 43. $^{87}Rb/^{86}Sr$ versus $^{87}Sr/^{86}Sr$ (A) and $^{147}Sm/^{144}Nd$ versus $^{143}Nd/^{144}Nd$ (B) diagrams for garnetiferous metagabbroic sample Xe-16. Analytical error on $^{87}Sr/^{86}Sr$ and $^{143}Nd/^{144}Nd$ is indicated by the line. Abbreviations: Cpx, clinopyroxene; pl, plagioclase; WR, whole rock.

7.3 Age constraints

The Rb-Sr and Sm-Nd isotopic studies did not yield precise age data for the studied xenoliths; a range of feasible ages were constrained and those are represented below. The behaviour of the isotopic systems constrains the interpretations made; Sm and Nd are less mobile than Rb and Sr and, therefore, less sensitive to hydrothermal alteration (Dickin 1995). The Rb-Sr system is often used to define metamorphic crystallization/cooling ages whereas Nd-Sm system often preserves information on

igneous crystallization. The latter may, however, also start to behave as an open system under high granulite facies conditions.

7.3.1 Carbonatite (Xe-15)

Several lines of evidence support a genetic link between the carbonatite xenolith and the lamproite. The epsilon Nd value at 160 Ma (-5.7) and depleted mantle model age 1154 Ma of the xenolith, is similar to the initial epsilon Nd and depleted mantle model age of lamproite, (-6.0) and 1100 Ma, respectively (Luttinen et al. 2002). The $^{147}Sm/^{144}Nd$ and $^{87}Sr/^{86}Sr$ isotopic ratios of the xenolith are also close to lamproite (table 5); these facts promote the mineralogical interpretation that the xenolith could be cogenetic with lamproite. Such a facts are in agreement with the undifferentiated $^{143}Nd/^{144}Nd$ ratios and $^{87}Rb/^{86}Sr$ versus $^{87}Sr/^{86}Sr$ plots (fig. 44 A and B), where relatively young ages (221-291 Ma) are probably reliable. This result does not preclude the possibility of carbonatite xenolith as an autolithic inclusion.

7.3.2 Layered metagabbro Xe-11

In this xenolith the Rb-Sr system has presumably been disturbed by the lamproite derived Rb and Sr; however, the age of 571 Ma for apatite-plagioclase plot (fig. 45 A) is

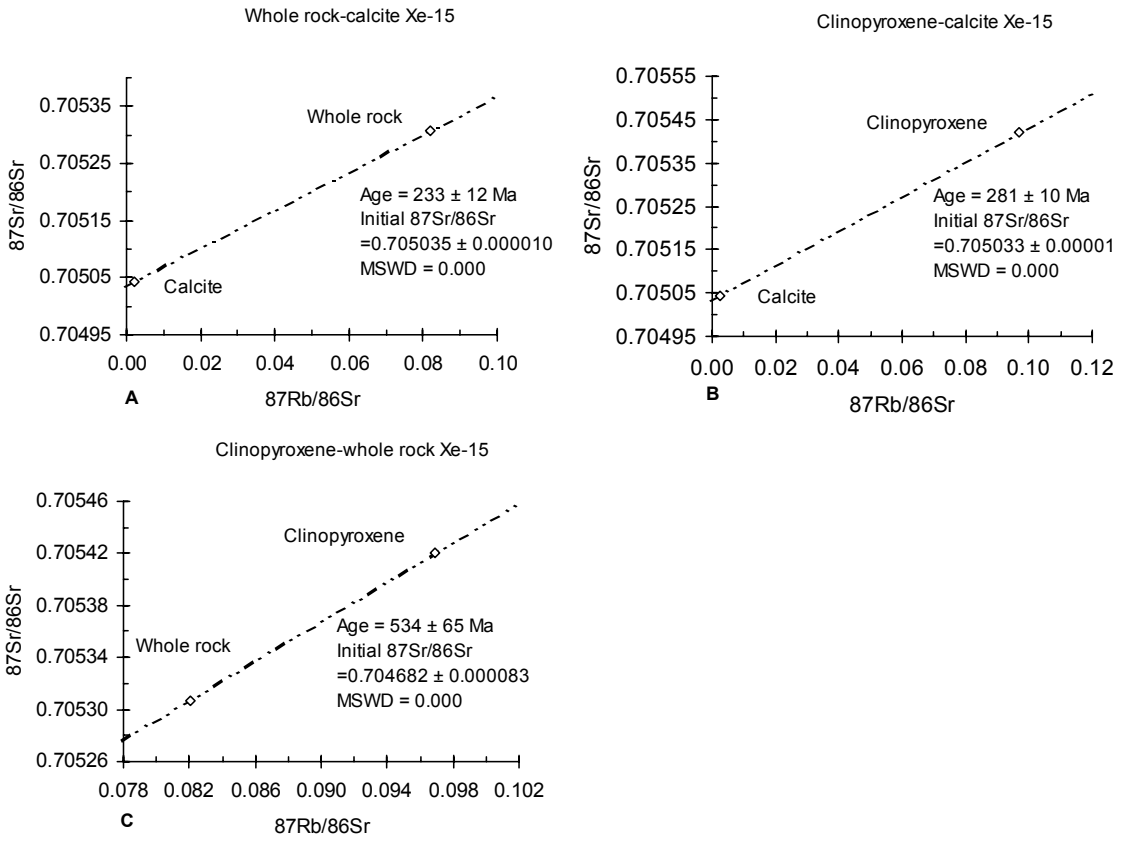

Figure 44. $^{87}Rb/^{86}Sr$ versus $^{87}Sr/^{86}Sr$ diagrams for sample Xe-15 (carbonatite). A) Calcite – whole-rock; B) Calcite – clinopyroxene; C) whole-rock - clinopyroxene.

close to c. 500 Ma Pan-African ages observed e.g. on the central Dronning Maud Land (Jacobs et al. 1998). The magnitude of the depleted mantle model age of 1310 Ma for plagioclase is promoted by fig. 45 B which shows age of 1446 Ma. The low $^{143}Nd/^{144}Nd$ ratio of plagioclase, and c. 570 Ma metamorphic Rb-Sr age, are in consistence with the feasible Mesoproterozoic crystallization of this sample.

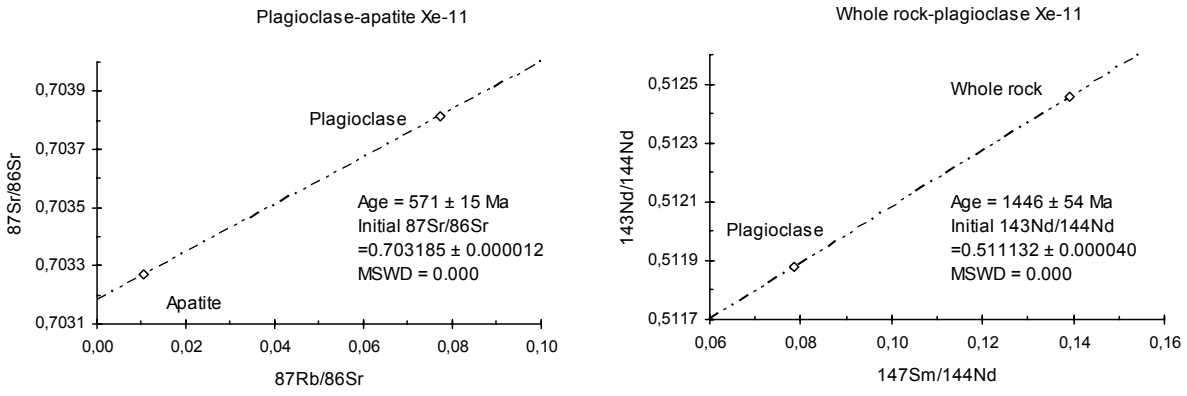

Figure 45. $^{87}Rb/^{86}Sr$ versus $^{87}Sr/^{86}Sr$ and $^{147}Sm/^{144}Nd$ versus $^{143}Nd/^{144}Nd$ diagrams for layered metagabbro sample Xe-11. A) Apatite – plagioclase; B) Whole rock - plagioclase.

7.3.3 Garnetiferous metagabbro Xe-16

The whole rock $^{143}Nd/^{144}Nd$ of this xenolith (Xe-16) has presumably slightly increased

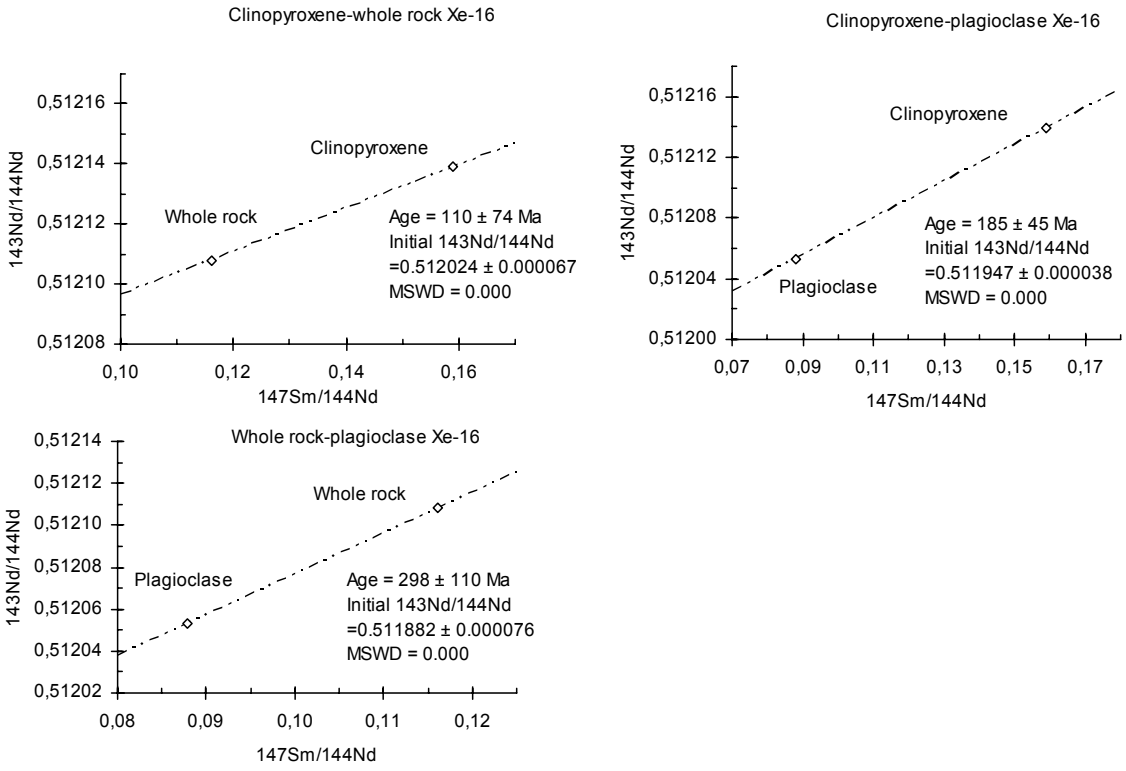

Figure 46. $^{147}Sm/^{144}Nd$ versus $^{143}Nd/^{144}Nd$ diagrams for sample Xe-16 (garnetiferous metagabbro). A) whole- rock - clinopyroxene; B) plagioclase - clinopyroxene; C) whole-rock - plagioclase.

due to contamination by the more radiogenic Nd derived from the host dyke. This is consistent with fig.46; fig. 46 A (shows age of 110 Ma) would show steeper slope and yield older age if the whole rock $^{143}Nd/^{144}Nd$ would be less radiogenic. Fig. 46 C (shows age of 298 Ma) would respectively show shallower slope and yield younger age in relation to fig. 46 B (shows age of 185 Ma). The depleted mantle model-ages for this sample are Proterozoic to Archean (table 6); this is consistent with depleted mantle model ages calculated from the Nd isotopic data of the Jurassic gabbroic intrusions of Vestfjella (Vuori 2004). In summary, the observed 185 Ma age reflects feasibly the latest closure of Sm-Nd system of this xenolith. Presumably this xenolith represents Jurassic mafic magmas crystallized in the lower crust though mixed isotopic ratios or complete opening of the Sm-Nd system in high granulite facies conditions can not be precluded.

7.4. The metagabbroic xenoliths versus Vestfjella gabbros and Lesotho xenoliths

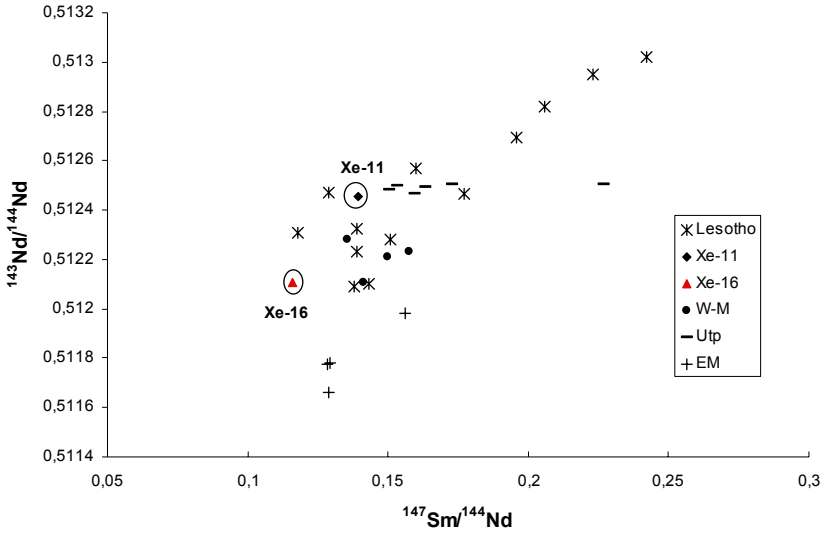

Figure 47. Sm-Nd (present day) whole rock isotopic composition of basic metagabbroic xenoliths (Xe-11 and Xe-16) relative to basic granulite xenoliths of Lesotho (Lesotho), after Rogers and Hawkesworth 1982, and East-Muren (E-M), West-Muren (W-M), and Utpostane (Utp) isotopic compositions for Jurassic gabbroic intrusions, after Vuori 2004.

Fig. 47 shows $^{147}Sm/^{144}Nd$ versus $^{143}Nd/^{144}Nd$ diagram on present day values of the Kjakebeinet metagabbroic xenoliths and Lesotho basic granulite xenoliths after Rogers and Hawkesworth (1982). The Sm-Nd isotopic compositions of the Vestfjella Jurassic intrusions, after Vuori 2004, are also shown. The Kjakebeinet xenoliths (two analyses)

show affinity to Lesotho Proterozoic granulite xenoliths but also to East- and West-Muren Jurassic intrusions.

Table 7. Comparison of Kjakebeinet xenolihs, southern Vestfjella gabbroic intrusions, and Lesotho basic granulite xenolith (isotopic compositions).

	$^{87}Rb/^{86}Sr$	$^{87}Sr/^{86}Sr$	εSr (180Ma)	$^{147}Sm/^{144}Nd$	$^{143}Nd/^{144}Nd$	εNd (180Ma)
1 Xe-11WR	0.19329	0.704369±15	-6	0.13921	0.512455±9	-2
2 Xe-11Pl	0,07737	0.703815±14	-10	0,07860	0.511880±10	-12
3 Xe-16 WR	0.09232	0.704712±19	+3	0.11607	0.512108±13	-9
4 Xe-16 Cpx	0,17386	0.704829±13	+1	0,15899	0.512139±9	-9
5 Xe-16 Pl	0,06532	0.704916±13	+7	0,08785	0.512053±11	-9
6 West Muren	0.09-0.12	0.7061-0.7073	+15-+38	0.1358-0.1574	0.51211-0.51228	-6 - -9
7 East Muren	0.04-0.17	0.7063-0.7108	+27 -+86	0.1285-0.1562	0.51166-0.51198	-12--18
8 Utpostane	0.03-0.13	0.7051-0.7066	+11-+33	0.1505-0.2271	0.51246-0.51251	-2 - -3
9 Lesotho		0.70359-0.70507		0.118-0.242	0.512092-0.513019	+9.4- -9.3

References:
1-5 The fractions of layered melatagabbro (Xe-11) and garnetiferous metagabbro(Xe-16). Abbreviations: WR, whole rock; Cpx, clinopyroxene; Pl, plagioclase.
6-8 Gabbroic intrusions of Vestfjella, Luttinen et al. 2004. Comparison to basalt types of Vestfjella after Vuori 2004.
9 Range of 13 Lesotho basic granulites after Rogers and Hawkesworth 1982.

As in table 7, sample Xe-16 (garnetiferous metagabbro) show similar and constant epsilon Nd relative to West Muren gabbro; whole rock of layered sample Xe-11 is instead similar to Utpostane intrusion. Both samples are within range of Lesotho basic granulites. Layered sample Xe-11 whole rock and plagioclase fraction show lower $^{87}Sr/^{86}Sr$ ratio than garnetiferous sample Xe-16. According to Rudnick (1992), an elevated $^{87}Sr/^{86}Sr$ ratio may generate in recent granulite facies metamorphism or mixing of crust and mantle materials, if the rock is a relatively young underplated cumulate. High Sr ratio is also distinctive for granulite xenoliths derived from the lower crust. The possible relatively young, cumulate origin is consistent with age speculations, based on mineral errorchrons, made on garnetiferous granulite Xe-16. Both samples, Xe-11 and Xe-16, have metamorphosed in granulite facies. Though the gabbroic xenoliths record enrichment in Sr induced during the dyke transport, their $^{87}Sr/^{86}Sr$ ratio and epsilon value for Sr are notably lower than those of the gabbroic intrusions of southern Vestfjella, which show wide variation in epsilon Sr (+11 - +86) (Vuori 2004) (table 7). This may indicate that sample Xe-16 (garnetiferous metagabbro) was less contaminated by the crust components than the Jurassic gabbroic rocks and could therefore represent a product crystallized in deeper levels.

8. DISCUSSION

The protoliths, the conditions of re-crystallization, and the geological setting of the xenoliths are discussed in sections 8.1 and 8.2. The mineral chemistry of some Kjakebeinet lamproites is discussed in 8.3. The xenoliths comprise of two groups: accidental xenoliths of crustal origin and cognate xenoliths, which show mineralogy characteristic for mantle-derived material. The mineralogy of the xenoliths is shown in table 8, mode, and whole rock chemistry in appendix 3.

Table 8. Mineralogy of the xenoliths.

Sample	Point count	M´	Mineral assemblage	Accessory phases	Rock type	Sample	Point count	M´	Mineral assemblage	Accessory phases	Rock type
XE-1	x	10,5	Pl+Q	Opx?+Grt?+ Apat+Zirc	Tonalite gneiss	XE-14			Q+Kfs+Opq+ VRF		Metagraywacke
XE-2			Kfs+Q+Pl	Na-Ca-px+Zirc	Augen gneiss	XE-15.1	x	29,1	Calc+Grt+Kfs+Biot	Phl+Rut+ Apat+Ba	Carbonatite
XE-3			Kfs+Q	Na-px+Apat+Zirc	Augen gneiss	XE-15.2		46,8	Calc+Cpx+Biot+ Grt+Mt	Apat+Ba	Carbonatite
XE-4	x	11,8	Pl+Q+Grt	Grt+Opx?+ Apat+Zirc	Tonalite gneiss	XE-16	x	68,5	Cpx+Pl+ Grt+ Opq	Apat+Ca-Na-px+Amf	Metagabbro
XE-5			Kfs+Q+Pl	Apat+Zirc	Augen gneiss	P-1			Coal+Q+Pl	Pl	Coal shale
XE-6		<10	Kfs+Q+Pl	Apat	Alkali feldspar granite gneiss	P-2			*Pl+Cpx+Opx+Q +Biot	Bi+Apat+ Zirc	Metagabbro
XE-7		<10	Kfs+Q+Pl		Alkali feldspar granite gneiss	P-3	x	88,7	Phlg+Calc+Cpx+ Rut+K-Rich	Kfs+Q+Cpx+ Rut+K-Rich	Phlogopite rock
XE-8		<10	Kfs+Q	Pl+Zirc	Alkali feldspar granite gneiss	P-4	x	98,4	Cpx+Hbl+Mt	Opx?+Carb+ Apat	Metagabbro
XE-9			Pl+Q+Grt+Rut	Grt+Rut+Na-px+Apat+Zirc	Tonalite gneiss	P-5			Q+Opx+Kya+ Spl	Spl+Rut+ Zirc	Metapelite
XE-10	x	21,6	Pl+Q+Cpx	Apat+Mt+Rut + Zirc	Metagabbro	P-6	x	50,8	Pl+Cpx+Ol?	Bi+Mt+ Apat+Zirc	Metagabbro
XE-11.1	x	99	Cpx+Hbl+Mt	Carb+Apat	Metagabbro	P-7	x	46,9	Pl+Grt+Cpx+ Hbl	Apat	Metagabbro
XE-11.2	x	81,6	Hbl+Cpx+Pl	Mt+Carb	Metagabbro	P-8	x	68	Cpx+Pl+Opq+ Grt?	Apat+Na-Ca-px	Metagabbro
XE-12			Kfs+Q	Na-px+Zirc	Augen gneiss	P-9		<10	Pl+Q+Jad	Jad+Mt+ Amf+Zirc	Metasandstone
XE-13			Kfs+Q+Kya+ Rut+ Grt+Spl	Spl	Metapelite						

Retrograde chlorite and mica, and metasomatic minerals, are neglected in this table. Accessory phases comprise less than 5 vol-%. Colour index after Le Maitre et al. (1989): M´=0-30 leucocratic, 30-60 mesocratic, and 60-100 melanocratic (Neuendorf et al. 2005). Abbreviations: x=point count (1000points) has been made. M´=Colour index after Le Maitre et al. (1989).Question mark (?) after mineral abbreviation, pseudomorphic appearance; (*) in P-2, the mineralogy of the paleosome. Apat, apatite; Ba, barite; Bi, biotite; Calc, calcite; carb, carbonate; Cpx, clinopyroxene; Grt, garnet; Kfs, potassium feldspar; Jad, jadeite; K-Rich, potassium richterite; Mt, magnetite; Na-px, aegirine; Na-Ca-px, aegirine-augite; Opx, orthopyroxene; Phl, phlogopite; Pl, plagioclase; Q, quartz; Rut, rutile; Spl, spinel group mineral; VFR, volcanic rock fragment; Zirc, zircon.

Section 5 described the xenoliths in detail. Here the groups of tonalite and alkali feldspar granite gneisses are combined to leucocratic metaigneous rock types (8.1.1). The layered granulites (P-4, Xe-10, and Xe-11) and melanocratic granulites (P-2, P-6, P-7, P-8, and Xe-16) are referred as metagabbroic samples (8.1.2). Kyanite granulites (P-5 and Xe-13) and metasedimentary rocks (P-1, P-9, and Xe-14) comprise the metasedimentary group (8.1.3). Augen gneisses show little evidence on their protolith and are therefore handled shortly (8.1.4). Carbonatite Xe-15 (8.2.1) and phlogopite rock (8.2.2) comprise a section of their own.

Most of the xenoliths have re-crystallised in the granulite facies conditions. As commonly known, metapelites form several distinctive mineral assemblages that indicate the metamorphic grade, whereas metabasites have fewer assemblages with wider stability fields: therefore, the mineralogy of metabasites is less informative in relation to prevailed pressure-temperature conditions. Also felsic metaigneous rocks often lack index minerals. Characteristic granulite facies mineral assemblages and index minerals for metabasites are orthopyroxene, which occurs in low-pressure mafic granulites, or the higher-pressure assemblage plagioclase, clinopyroxene, garnet ± quartz. In metapelites, annite+quartz reacts forming orthopyroxene+potassium feldspar+water in temperatures of c. 800 °C. Metapelitic granulites in the lower continental crust (P<8 kbar, T <800 °C) are characterized by the assemblage orthopyroxene+sillimanite+quartz+garnet. Co-existing orthopyroxene and kyanite requires pressures above 10 kbar (Butcher and Frey 1994). High-grade metamorphic mineral assemblages of the xenoliths have not been developed during lamproite transportation; greenschist to lower amphibolite facies metamorphism characterizes the alteration which occurs in xenoliths hosted by potassium-rich ultrabasic dykes such as kimberlites and lamproites (Rudnick 1992). Retrograde reactions, however, might have taken place after or during the dyke transport. In general, retrograde reactions make the determination of peak metamorphic conditions difficult. The high probability of metasomatic changes in the mineral chemistry of the xenoliths, lack of suitable mineral pairs and mineral assemblages, makes usage of thermobarometry problematic on these samples. Further quantitative mineral chemical data is required for exact determinations. Therefore approximations using phase diagrams are represented in this work. The detailed recognition of different tectonic settings requires undisturbed trace element data and

knowledge on the relationships between the rock types. The former was not collected to this study and the latter is not available. Isotopic data on two metagabbroic xenoliths and a carbonatite is handled in section 7. The following text is based mainly on the major element chemistry of the minerals affected by alteration that was caused by the host rock and probably also affected by fluids in crustal levels.

8.1 Crustal xenoliths

8.1.1 Leucocratic metaigneous rocks

Tonalite gneisses (Xe-1 and Xe-4, Xe-9) and alkali feldspar granite gneisses (Xe-6, Xe-7, Xe-8, and Xe-12) are the acid rock types with igneous protolith. Samples Xe-1 and Xe-4 plot in the field of sub-alkaline series (fig. 15 section 5). The usefulness of this classification along metamorphic, sometimes cumulate rock types in origin is questionable, but is used in this thesis to make some distinction between the xenolith types. The composition of garnet promotes the connection between sample Xe-9 and other tonalite gneisses.

Tonalite gneisses

Due to re-crystallization in granulite facies conditions the texture of the rock is quite un-informative: the samples do not provide evidence for the origin of these gneisses as intrusive or extrusive igneous rocks (fig. 2 section 4). Garnet composition, however, is distinctive to metaigneous garnet: CaO content of the almandine is high (6-7 wt-%) in relation to the few percentages observed in garnet in pelitic rocks (Miyashiro 1973) such as in sample Xe-13 (fig. 47 B). Moreover, according to Coleman et al. (1965) and Deer et al (1992) the observed garnet composition in tonalite gneisses ($Alm_{55}Gro_{16\text{-}20}Py_{14\text{-}18}Sp_{10}$) is similar to garnet in granulites and charnockites (fig. 47 A).

The presence of metamorphic garnet and partially melted grain boundaries (occupied with fibrous orthoclase), which yield to a volume of a few percentages, refer to high grade conditions and beginning of the anatexis. Though, some small-scale melting has taken place during magmatic transport (cf. Tsuchiyama 1986). Partial melting of a water saturated tonalite starts at 650 °C in pressures above 5 kbars (ca. 18 km depth in the crust), and the

garnet starts to nucleate at c. 14 kbars (ca. 50 km depth in the crust) (Schmidt and Thompson 1996). As is commonly known, the presence of water lowers the reaction temperatures, so if the rock would be "dry" temperature needed to melt it would be higher. In summary, these tonalite gneisses have presumably re-crystallized in pressures corresponding to middle crustal levels.

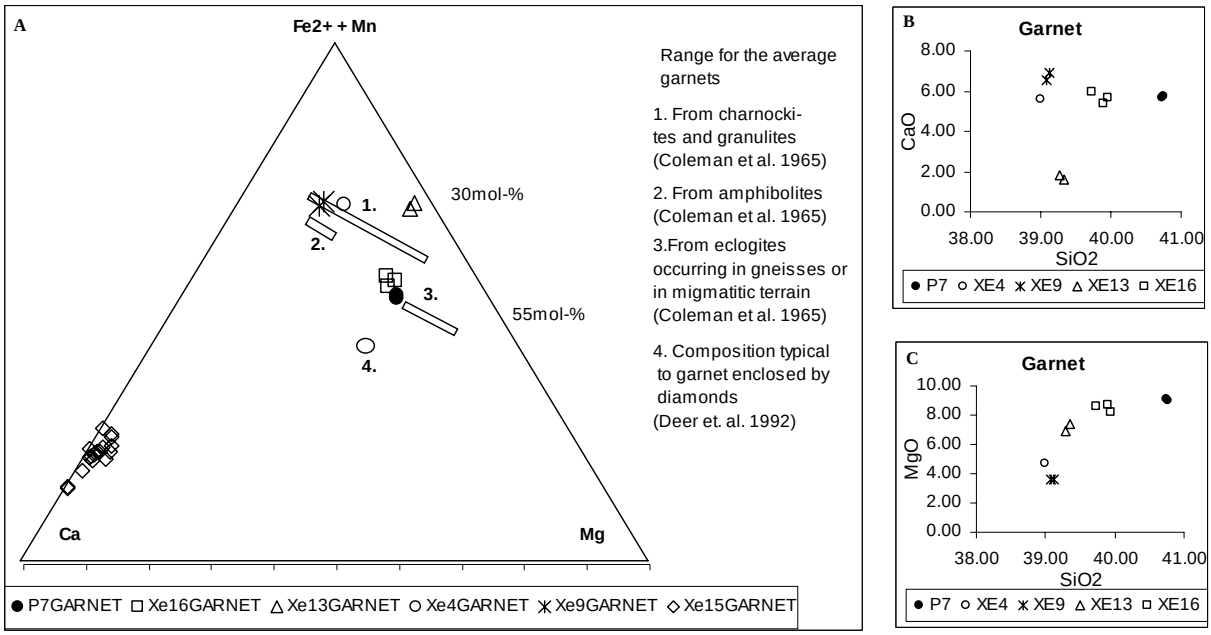

Figure 48. Garnet compositions A) With regard to almandine (Fe2+ +Mn), grossulare (Ca) and pyrope (Mg) content (mol-%). Figure is modified after Coleman et al. (1965) (garnet compositions are from Tröger 1959). B) SiO_2 versus CaO C) SiO_2 versus MgO. Oxides are in wt-%.

U-Pb zircon age determined for samples Xe-1 and Xe-4 is c. 1000 Ma (Dr. Arto Luttinen pers. comm. 2006). The nearest exposed Precambrian locality, Heimefrontfjella c. 120 km east from Kjakebeinet consists on 900-1200 Ma gneisses of metavolcanic origin (Weber et al. 1987 and Thomas 1994 as referred in Groenewald et al. 1995); moreover, the Mesoproterozoic Maud belt was interpreted to made up mainly on volcanic arc systems (Thomas 1989, as referred in Groenewald et al. 1995). Consequently, these tonalite gneisses probably represent samples of collision-related calc-alkaline magmatism which took place during the Kibaran/Grenvillean orogeny and formed the 1000 Ma Maud orogenic belt. These observations are consistent with geophysical data that shows that the Mesoproterozoic formations extend below the basaltic rocks of southern Vestfjella.

Alkali feldspar granite gneisses

Macroscopically sample Xe-6 resembles a cumulate or a pegmatic rock but samples Xe-7, Xe-8, and Xe-12 show sheared appearance indicated by round, notably stretched potassium feldspar. The absence of cross-hatch twinned potassium feldspar refers preferentially to fresh rock of magmatic or high grade metamorphic origin, instead of un-deformed pegmatitic vein (Deer et al. 1992). Alkaline intrusive and extrusive rocks are often related to early stages of the continental rifting due to the small scale melting which occurs when the upwelling asthenosphere undergoes decompression melting. The increased heat flow and uplift of the crust also causes melting of the silica, aluminium, and alkaline rich crust (White and McKenzie 1989; McKenzie 1989). This produces alkaline rocks types; relatively extent, layered complexes have been reported. Alkali feldspar layers have been described e.g. in Gardar Province, Greenland, which is a layered intrusion complex related to continental intra-plate rifting (Upton et al. 1996). On WDML Harris and Grantham (1993) described two 170 Ma nepheline syenite plutons at Straumsvola, c. 500 km NNE from Kjakebeinet. These alkaline rocks show leucocratic and mafic layering, and foids are often present. Though the alkali granite xenoliths are presently rich in quartz it does not prove that the protolith did not contain foids. There is no reason why the xenoliths could not have derived from an alkali rich cumulate layer of some layered igneous system. However, according to Groenewald et al. (1995) several authors have reported Mesoproterozoic granitoids, mostly A-type granites, on the H.U Sverdrupfjella area, located on the eastern side of Jutul-Penck Through. Pegmatitic granites are observed, oldest of them being strongly deformed and often gneissose. From this point of view the least deformed sample Xe-6 could represent a piece of pegmatitic granite, when the others show more petrographical affinity for the older, deformed granitoids. The dominating potassium feldspar makes these xenoliths rich in K and poor in Ca. Minerals distinctive for A-type granite such as fayalite, annite, apatite, and fluorite (Clemens et al. 1986) have not been observed. However, the co-existing meta-gabbroic xenoliths and extensive anorogenic basaltic magmatism, post-dated by intrusion of Straumsvola syenites, comprise a typical association for A-type granites (Barker et al. 1975, Collins et al. 1982, as referred to in Clemens et al. 1986). Therefore, these samples could well be related to Mesozoic rifting.

8.1.2Metagabbroic xenoliths

The petrographic similarities and differences between the metagabbroic xenoliths, listed on page 77, are discussed in this section. These xenoliths show ultrabasic to intermediate compositions; on the basis of their texture and appearance, however, the medium-grained metagabbroic rocks are interpreted as cumulated rocks. Therefore, the whole-rock compositions represented must be used with caution; they cannot represent the composition of the primary gabbroic magma due to cumulate origin and high metamorphic grade of the xenoliths. Absence of amphibole or its composition refers to granulite facies metamorphism of these xenoliths; this is discussed in detail below. The gabbroic xenoliths can be divided in two groups 1) garnet-bearing (P-7, P-8, and Xe-16) and 2) garnet-free (P-2, P-4, P-6, Xe-10, and Xe-11). The garnet-free xenoliths show two subgroups: 2a) fine-grained samples (P-2 and P-6) and 2b) medium-grained layered samples (P-4, Xe-10, and Xe-11). Group 1 sample Xe-16 show Mesozoic age (Sm-Nd mineral errorchron) and group 2 sample Xe-11 Proterozoic age (Sm-Nd mineral errorchron). As is commonly known, even in similar pressure and temperature conditions the nucleation of metamorphic minerals may occur only in certain areas, e.g. layers, with suitable composition or with adequate nucleation centers. Garnet composition in general (fig. 47 section 8.1.2), is close to one in eclogites within gneisses (Coleman et al. 1965), but this is probably due to similar bulk chemistry. Only the silica under saturated samples, distinguished by the absence of quartz, olivine, and orthopyroxene (or pseudomorphs after those minerals), contain garnet. However, the absence of garnet in the silica over saturated types is interpreted to occur due

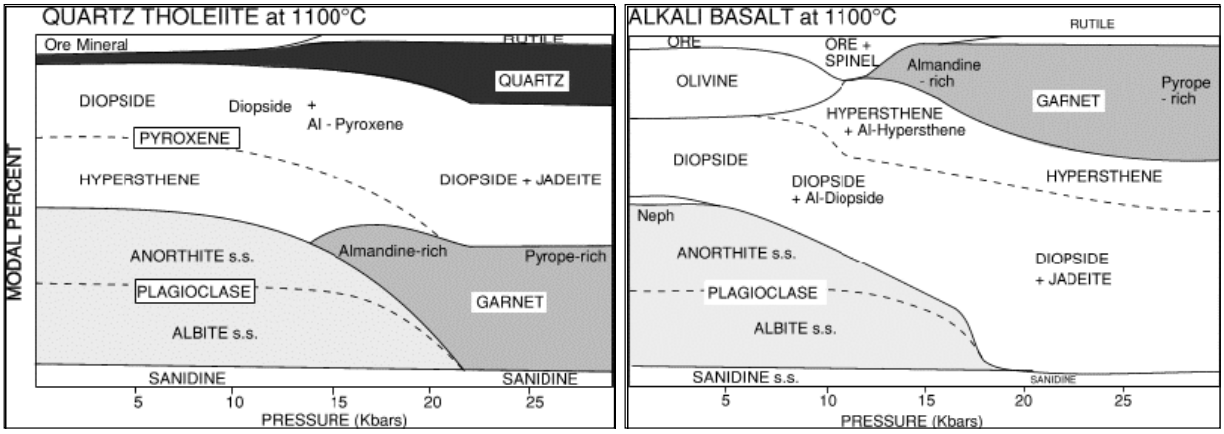

Figure 49. The mineralogy of the quartz tholeiite and alkali olivine basalt with increasing pressure. The metamorphic grade increases from the lower granulite facies on the left to eclogite facies on the right. Figure is after Green and Ringwood (1967).

to higher pressures needed to produce garnet than what in silica under saturated rocks (fig. 49, Green and Ringwood 1967).

G1; garnet-bearing metagabbros

The samples P-7, P-8, and Xe-16 range on whole-rock composition (fig. 15 section 5.1) from subalkaline (P-8) to perceptibly alkaline (P-7) and show affinity to layered metagabbros P-4 and Xe-11. Sample P-7 is richer in plagioclase (table 9) than other metagabbroic samples and contains pargasitic hornblende as a major phase; therefore the silica and alkali contents of this xenolith are high. The mineral chemistry of pyroxenes varies between the samples (fig. 28 section 5.2.2). Quartz, olivine, and orthopyroxene are absent, and therefore these samples are considered as silica under saturated. Alkaline affinity of these samples, however, is also indicated by the presence of aegirine-augite on samples P-8 and Xe-16, and some pargasitic hornblende (fig. 30 section 5.2.3) in all the three samples. Similar hornblende, which is stabile in granulite facies (Kesson and Price 1972), occurs as a major phase in layered metagabbros P-4 and Xe-11. The (re)-crystallization conditions were estimated using fig. 49 (alkali basalt): the presence of relatively almandine-rich garnet, aluminous augite, sodic plagioclase (mainly oligoclase) and abundant opaque minerals (ore) refer to pressures between c. 11 and 17 kbars (ca. 40-60 km depth in the crust) in samples P-7, P-8 and Xe-16 (cf. Green and Ringwood 1967).

G2a; fine-grained, garnet-free metagabbros

The gneissic sample P-2 and meta-olivine-augite-gabbro (P-6) are silica oversaturated to saturated on the basis of the presence of quartz and orthopyroxene in P-2 and pseudomorphic olivine in P-6. The gneissic appearance of sample P-2 refers to partial melting of the sample. The lack of amphibole and muscovite on these samples strongly refers to high-grade metamorphosis. Moreover, the relatively fine-grained appearance refers to a finer grained protolith in relation to the other metagabbroic xenoliths. Vuori (2004) reported fine to medium-grained hornfelses in the margins of the gabbroic intrusions; sample P-6 could represent a low-P (<4 kbar) pyroxene-hornfels facies rock (Butcher and Frey 1994).

Huang and Wyllie (1986) stated that the solidus temperature of olivine tholeiitic gabbro is approximately 650 °C in the pressure of 15 kbars (ca. 54 km depth in the crust) with

presence of 5-50 wt-% H_2O. Combining the former statement to fig. 49 (quartz tholeiite), and if the affect of other fluid than water is neglected, following estimates concerning samples P-2 and P-6 were made. 1) The absence of garnet reflects re-crystallization in pressures below c. 14 kbar (fig. 48, Quartz tholeiite) though the temperature would differ from 1100°C, because the nucleation of garnet is more pressure than temperature dependent (O´Brien and Rötzler 2003); 2) Absence of amphibole refers to temperatures higher than in amphibolite facies; 3) The melting of partially melted sample P-2 has started at minimum 650 °C temperature, if the pressure has been lower than 15 kbars; 4) The low Al-content of orthopyroxene in P-2 (fig. 25 section 5.2.2) refers to lower temperatures than in higher granulite facies, though the presence of orthopyroxene does indicate that the metamorphism has taken place in granulite facies conditions (Deer et al. 1992); 5) The mineral assemblage in P-6 could represent both granulite facies and pyroxene-hornfels facies. The absence of orthopyroxene, however, refers preferentially to too low silica content for orthopyroxene to form. Olivine, altered to talc, is present. Therefore sample P-6 has re-crystallized in granulite facies not in hornfels facies.

G2b) layered, garnet-free samples

Samples P-4 and Xe-11 are ultrabasic to basic in whole-rock composition, and both are placed next to alkaline-subalkaline boundary in fig. 15 section 5.1. The absence of quartz, orthopyroxene, and olivine, and presence of over 30 vol-% pargasitic-magnesiohastingsitic-hornblende in mode refer to silica undersaturated composition. These samples, however, show layering and clinopyroxene composition (fig.28 section 5.2.2) similar to intermediate leucocratic sample Xe-10. Therefore it is precluded that these rock types could represent the same rock type, though sample Xe-10 is silica over saturated, and shows the most evolved mineralogy. A geochronological study on the layered leucocratic granulite could resolve the age of this sample and promote the isotopic results from the basic sample Xe-11.

Melanocratic layered samples P-4 and Xe-11

As in fig. 49 the absence of garnet in silica under-saturated rocks refers to re-crystallization pressures below 11 kbar (ca. 36 km depth in the crust). The layered appearance, however,

leaves the possibility that there is a garnet-free layer in question. If the amphibole is a primary phase, pressure should be somewhat higher to access the same mineral assemblage in temperature of 1100 °C (Ernst 1968). The igneous origin of the pargasitic hornblende is promoted by Kesson and Price (1972), who stated that titanious pargasite, common phase in alkaline rocks, is a near liquidus phase occurring even in pressures of 25-30 kbar. Though pargasite, as amphiboles in general, has a wide stability field with upper phase boundary at 835 °C in 1 kbar pressure, the temperature decreasing with increasing fugasity of oxygen (Ernst 1968). Abundant magnetite and absence of hematite in the samples P-4 and Xe-11 refer to rather reducing environment. The high Ti (0.2-0.5 apfu) and Al (2.4-2.7 apfu) content observed in samples P-4 and Xe-11 is typical to hornblende in granulite facies conditions (Spear 1981). Moreover, Tribuzio et al. (2000) argued, based on compositional evidence, that high temperatures of formation refers to igneous origin of amphiboles in ophiolites. In the case of extensive, high heat flow environment of Jurassic WDML it is not axiomatic that only magmatic rocks would have crystallized in high temperatures. The Sm-Nd isotope errorchrons refer that sample Xe-11 could be Proterozoic in origin (section 7). This is consistent with fact that layered intrusions, including massive anorthosites, can also occur in continental and arc-related settings (Davidson 1990, Hall 1996, Rivers 1997). The Maud belt (fig. 1) formed during the Grenvillean/Kibaran orogeny (c. 1000 Ma) (Groenewald et al. 1995); it is highly probable that basement of Kjakebeinet is Proterozoic in age.

Leucocratic layered sample Xe-10

This sample shows presently quartz dioritic composition, but the mineralogy promotes gabbroic origin. Clinopyroxene composition of this sample is similar to slightly alkaline pyroxene in garnet granulite Xe-16 (fig. 50 section 8.1.3). Part of the quartz is probably metamorphic in origin, produced by reaction orthopyroxene + plagioclase = garnet + clinopyroxene + quartz (Griffin and Heier 1973, Deer et. al 1992), which takes place when accessing to high granulite facies conditions. In this case the orthopyroxene would have been used up during the reaction that formed a reaction rim consisting mainly on garnet. The presence of this pseudomorphic garnet rim (fig. 6 section 4.4), enclosing both low-calcium pyroxene and labradorite support the above assumption. The following

interpretatios are 1) layering has formerly comprised of major orthopyroxene; 2) igneous plagioclase has been richer in anorthite component, for example ~An_{56}, which is the plagioclase composition enclosed by pseudomorphic garnet; 3) the protolith for this rock was, presuming that the plagioclase composition would be greater than An_{50}, orthopyroxene gabbro (Le Maitre et al. 1989).

The sample differs from the tonalite gneisses by its layering, interpreted as igneous one, presence of clinopyroxene, relict orthopyroxene and bytownite, and the andesitic plagioclase showing occasional albite twinning. Though andesitic plagioclase has been described from the felsic marginal unit of the West Muren Jurassic gabbroic intrusion (Vuori et al. 2004) quartz, when present, is un-deformed (Dr. Saku Vuori pers. comm. 2006). Moreover, neither the composition of metamorphic plagioclase is comparable to igneous one nor is its behaviour similar in low- and high-grade conditions (Goldscmidt 1982). The appearance and composition of this rock refers to a deformed, mildly alkaline gabbroic rock, which presumably is older than 180 Ma. Gabbroic and charnockitic rocks have intruded to the Mesoproterozoic (1600-1000 Ma) basement complex on Kirwanveggen (Tingey 1991). The felsic granulite might be cognate to tonalite gneisses and/or represent a part of a gabbroic layered intrusion or even an anorthosite (Sighinolfi and Gorgoni 1975). On the basis of major element data it is impossible to say if the tonalite gneisses or the metagabbros really represented a co-magmatic series with this sample. However, anorthositic complexes are found from extensive areas related to either back-arc extension or collapse of a collisional orogen (Rivers 1997). Therefore, this sample could represent post-Grenvillean layered intrusive or a fractionated magma chamber related to 500 Ma Pan-African orogeny. In summary the felsic and melanocratic rock types could be related as follows in the mid-continental rift-related, 1100 Ma Duluth Complex in Minnesota. It comprises anorthositic, felsic, and individual mafic intrusions with tholeiitic affinity. These are often intruded to significantly older anorthositic series (Miller and Ripley 1996). Charnocktites, which have common compositional features with the tonalite gneisses of this study, have also been described in relation to anorthosites in the Grenville front of Ontario (Davidson 1990).

Constraints to petrogenesis

Pargasitic hornblende, typical for alkaline rocks crystallized even in extremely high T and P (Kesson and Price 1972) is present as a major phase in samples Xe-11, P-4, and P-7; modal amount of Hbl diminishes in order. The composition of the hornblende ranges from ferro-pargasite in Xe-11 to magnesio-hastingsite in P-4; the compositions are similar to hornblende in samples P-7, P-8, and Xe-16 but different from amphibole of Straumsvola alkaline complex (fig. 50).

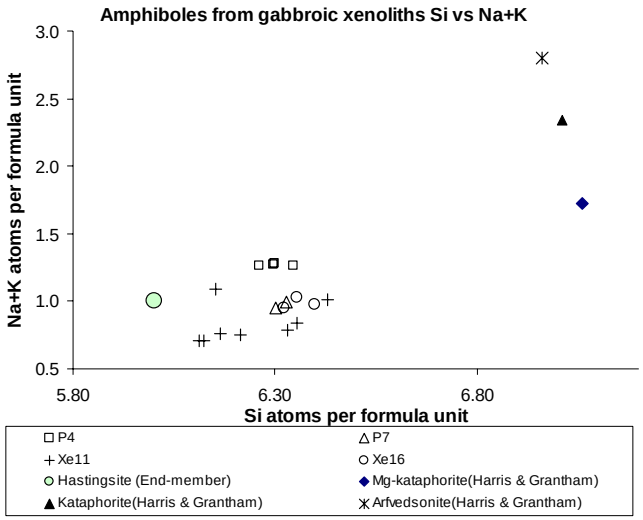

Figure 50. Si versus Na+K cations per formula unit. Amphibole analyses from the xenoliths and magnesio-kataphorite, kataphorite and arfvedsonite from Straumsvola alkaline complex after Harris & Grantham, 1993.

The subhedral to euhedral morphology (exception in samples P-8 and Xe-16 where hornblende is a minor phase), alteration, and the fact that, according to Yoder and Tilley (1962), the amount of crystallizing amphibole increases with decreasing amount of pyroxene, is referring to primary origins. However, the major oxide data does not give unambiguous information on the origin of the hornblende (cf. Coogan et al. 2001; Tribuzio et al. 2000). Pargasite compositions have been reported as primary phases in alkaline ring dyke complex of Alnö (Morogan and Lindblom 1995) and as metamorphic or subsolidus phase (e.g., Otten 1984). Coogan et al. (2001) reported magmatic and hydrothermal types of Hbl in basalts of mid-ocean ridges with low spreading rate. In summary, hornblende could have crystallized from mantle-derived, potassium- and titanium-rich hydrous fluid (Oxburgh 1964) and the xenoliths could represent pieces of alkaline magma (Kesson and

Price 1972) or a primary, Ti-rich amphibole, such as kaersutite or titanious pargasite, could have altered due to external, potassium-rich fluid. The latter diverges with observation that hornblende show fresh Ti-rich overgrowth (observed in sample Xe-11).

Symplectite textures of cpx and ab

Several metagabbroic samples (P-4, Xe-10, Xe-11, P-7, and P-8) show clinopyroxene-plagioclase symplectites. The symplectic texture in sample Xe-10 is well developed, but in sample Xe-16 only the grain boundary of clinopyroxene has reacted. Symplectites of clinopyroxene and plagioclase are common in retrogressed eclogite facies rocks; the textures develop when omphacite (clinopyroxene with jadeite component) breaks down to

Table 9 Bulk composition of the clinopyroxene-feldspar symplectites (Sympl), when the volume of plagioclase in symplectite is 8 %. The cpx (clinopyroxene) eclogite is after Miyashiro & Seki (1958) according to Deer et al. (1963), sodian augite after Deer et al. (1963) and omphacite after Morogan 1970 according to Deer et al. 1992. Oxides are in wt-%.

	SiO_2	TiO_2	Al_2O_3	Fe_2O_3	FeO	MgO	CaO	Na_2O	K_2O
P4 (Sympl)	52.22	0.51	6.85		7.87	12.08	19.84	0.63	0.00
P7 (Sympl)	53.69	0.63	4.65		9.07	12.62	18.22	0.07	1.03
P8 (Sympl)	53.11	0.77	5.11		9.35	10.91	20.00	0.74	0.01
Xe11 (Sympl)	50.96	1.13	5.50		8.75	8.80	23.93	0.21	0.59
Xe16 (Sympl)	54.52	0.00	3.52		9.81	12.58	18.40	0.29	0.88
Augite in P2	54.46	0.00	2.62		9.96	12.73	20.24	0.00	0.00
Cpx eclogite	51.86	0.20	1.02	0.99	1.73	25.24	17.09	0.08	0.06
Sodian augite	50.09	1.15	5.34	4.23	6.13	10.49	19.17	2.78	0.04
Ompha-cite	56.02	0.38	12.74	0.88	1.64	8.01	12.45	7.05	0.40

low sodium clinopyroxene and sodic plagioclase due to decreasing pressure (Dirks and Sithole 1999, Deer et al. 1992). Similar textures are also recorded in the sheared marginal parts of relatively un-deformed garnet-granulite pods (Treloar 1990). Table 10 show a comparison between bulk composition of the symplectic clinopyroxene grains and “common augite” of sample P-2, clinopyroxene from eclogite (Miyashiro & Seki 1958), sodian augite (Deer et al. 1963) and omphacite (Deer et al. 1992). However, no relicts after omphacite were observed, but as in table 10 (cpx eclogite) clinopyroxene in eclogite does not necessarily contain abundant sodium. The composition of the clinopyroxene-

plagioclase symplectites corresponds to augite of gneissic metagabbro P-2 (table 10). Though, during the formation, some mobile elements may have been lost; the sodian augite composition is richer in Na_2O than the symplectites. Secondary aegirine observed in samples P-8 and Xe-16 could have 1) formed from mobilized Na derived from the erupting volcanic rocks; 2) crystallized at the presence of seawater; it also might 3) imply the primary composition of the magma; or the Na could have 4) released from cpx during the symplectite-forming process. Anyway, the symplectite composition differs remarkably from the eclogite clinopyroxene and omphacite represented in table 10.

Tectonic symplectites reported are very fine-grained (Treloar 1990) and the metagabbroic samples of this study lack other textures indicating shear. Therefore my proposal is that a jadeite-bearing clinopyrone would have reacted due to decompression and formed the symplectites. Following facts promote the hypothesis: Pyroxene with c. 13 mol-% jadeite component $NaAlSi_2O_6$, which is the highest composition recorded in the calcium pyroxenes of xenoliths (sample P-8) (analysis 32 table 9 appendix 1), is not stable with plagioclase in pressures above c. 10 kbar (ca. 36 km depth in the crust) (Holland 1983). On the basis of pressure estimates, done using phase diagram of Green and Ringwood (1967), these samples could record relatively high temperatures and pressures. Also the geological setting promotes particularly the high temperatures, further, the xenolithic origin makes high pressure conditions possible.

8.1.3. Summary; metagabbroic rocks

The group 1 and 2b metagabbroic rocks, except leucocratic granulite Xe-10, show variable alkaline affinity: layered samples P-4 and Xe-11 and garnet granulite P-7 may be considered as metamorphosed alkali gabbros when the rest of garnetiferous samples reflect mildly alkaline compositions. Group 2a, fine-grained, garnet-free metagabbros do not represent cumulated xenoliths; those show quartz tholeiitic (P-2) and olivine tholeiitic gabbro compositions. Clinopyroxene-plagioclase symplectites in group 1 and 2b reflect subsolidus reactions taken place in decreasing pressure. The formation due to decreasing pressure is promoted by thick dark brown alteration rim around scarce unaltered garnet. Griffin et al. (1987) as referred in Rudnick (1992) stated that the rim could have formed in lower crust due to localized heating. The lower crust of WDML has probably been heated at least twice: on Jurassic due to underplating of the mafic magmas and during the Kibaran

orogeny (1000 Ma); Proterozoic heating was observed in Namaqualand, where 1150 Ma granulites were formed (Waters 1992). The symplectite, however, seem to have formed before the xenolith entrainment into the lamproitic melt; it is improbable that reaction as wide as this could have taken place during the rapid ascent of the dyke. The K observed in symplectic plagioclase (table 8 appendix 1) definitely refers to lamproite contamination; metasomatic carbonate and phlogopite was also observed in these samples. Though *sensu stricto* eclogites do not occur among these xenoliths, eclogite facies conditions have possibly occurred due to increased heat flow during Mesozoic extensive phase and/or Proterozoic collisional orogeny, taking place before considerable lithospheric thinning. Summarized, the xenoliths record high grade metamorphism but origin as retrogressed eclogites is highly improbable. This is analogous with the observations that eclogite xenoliths have not been observed in lamproite dykes (Mitchell and Bergman 1991).

The ages determined using Sm-Nd mineral errorchrons are inaccurate; however, they do show that metagabbroic xenoliths represent two age groups. Because the gabbroic samples have the same contaminant, the lamproite dyke 2, the isotopic compositions are comparable: Group 2b sample Xe-11 shows higher $^{147}Sm/^{144}Nd$ and lower initial (best estimates on figs. 45 B and 46 B) $^{143}Nd/^{144}Nd$ than group 1 sample Xe-16. This promotes that the xenoliths were derived from different sources; the older sample Xe-11 should show lower $^{147}Sm/^{144}Nd$ and higher $^{143}Nd/^{144}Nd$ if the source was the same. The Proterozoic age of layered sample Xe-11 promotes the idea of leucocratic granulite as older gabbroic rock, which is related to the samples P-4 and Xe-11. Sample Xe-16, on the basis of Jurassic age, should represent material fractionated from the Jurassic melts. Therefore the isotopic composition gives information on the primary melts emplaced on Jurassic, if the fractionation and lamproite contamination would be removed by modelling; the appearance of this garnet granulite refers to lower crustal origin and therefore it would be less contaminated by old crustal components in relation to e.g. gabbroic rocks of southern Vestfjella. The strong contamination by crustal material of the preceding rock types shows at 1) high epsilon Sr (Vuori 2004) 2) crustal residence times ranging between 1400 and 2850 Ma, when zircon U-Pb age is 180 Ma.

8.1.4 Meta-sedimentary rocks

Four types of metasedimentary rocks were found among the xenoliths. The metapelites (described as kyanite granulites P-5 and Xe-13) record high granulite facies conditions; the absence of cordierite in these two relatively Mg-poor samples, migmatitic appearance, and presence of kyanite ± garnet refer to temperatures close to 800°C and pressures of 8-11 kbar (Spear 1993; Koester et al. 2002; Le Breton and Thompson 1988; Clemens and Wall 1981, Clemens 1984 as referred to Spear 1993 pp. 368). The pressure is consistent with c. 30 km depth in the crust. The appearance and high-grade assemblage show that the metapelites represent different environment from the other metasedimentary xenoliths. When Proterozoic metaigneous xenoliths are found among the xenoliths, I propose, that these samples would represent buried sediments from a basin or accretionary prism related to Grenvillean orogeny.

The metasandstone (P-9) shows well-developed granoblastic texture; coal shale (P-1) on the contrary shows relict primary layering. Xenolithic pieces of sandstone are found from both of the lamproite dykes (Dr. Saku Vuori pers. comm. 2005) and in Jurassic basalts of southern Vestfjella, giving crustal residence age of 1550Ma (Luttinen and Furnes 2000). Juckes (1972) reports sandstone layers and lenses as inter-layered the lava horizons and coal layers with Permian fossils in the Heimefrontfjella area. On the basis of the preserved primary features on the coal shale it probably represents the Permian sediments outcropped eg. on Ahlmanryggen. The meta-sandstone might as well represent Permian as Proterozoic sedimentary rocks.

8.1.4 Augen gneisses

Augen gneisses, listed on page 81, do not give much information on their protolith; the abundant low-Al chlorite-like alteration product refers to pre-existence of ferro-magnesian minerals. Sheared, augen gneissic texture refers to the beginning of the ductile deformation process, which takes place approximately in 10-20 km depth in the crust (Twiss and Moores 2000), depending e.g. on the regional geothermal gradient and pore fluid pressure. During the episode of the Mesozoic continental rifting the heat flow was high; consequently the ductile deformation would have taken place in shallower depths A rough estimate 20 km (lithostatic pressure of 5.6 kbar) could represent the definite maximum

depth for these rocks. However the augen gneisses could have formed in any time before the dyke intrusion, e.g. in detachment faulting which shows as normal faults on the surface and is particularly common process when passive continental margins are formed (Lister et al. 1986).

8.2 Ultrabasic xenoliths

Rudnick (1992) has reviewed types of xenoliths occurring in kimberlitic rock types (lamproites, kimberlites, and minettes). Mafic granulites and mafic garnet granulites have been recorded all around world, felsic granulites and paragneisses are also common. Eclogites or mica-amphibole-ilmenite-rutile (MARID) xenoliths have not been observed in lamproites and the latter are only found in South African micaceous (group II) kimberlites (Mitchell & Bergman 1991). Therefore the carbonatite xenolith is the only type not commonly found in lamproites, phlogopite rock is probably an autolithic inclusion.

8.2.1 Schorlomite-diopside-carbonatite

The texture and mineralogy of the inclusion refers to magmatic origin though diopside and andradite garnet are common minerals in contact metamorphosed calc-silicate and carbonate rocks (Deer et al. 1992). Some cryptic and/or modal metasomatism might have taken place during the dyke transport, but microperthitic potassium feldspar has also been recorded as a primary phase in alkaline intrusive rocks (McKenzie et al. 1982). Magmatic origin of garnet and its relation to alkaline rocks are promoted by following facts: 1) practically titanium free and homogenous, light yellow rim around garnet is unlikely to form via partial melting of the titanium-rich schorlomite garnet; 2) King and Sutherland (1966) described pyroxenite-related ijolite showing similar textures and microstructures than the xenolith. Melanite garnet (andradite with over c. 15 wt-% TiO_2) is often zoned with a light colored rim; 3) perovskite, considered as a mantle derived mineral, is enclosed by garnet though it is absent from the dyke, and the possible leucite inclusion promotes silica-poor crystallization environment (table 4 section 5.2.1); and 4) recently melanite-schorlomite garnet has been described by Gwalani et al. (2000) from a plug in carbonatite-alkalic diatreme (from Deccan igneous province, India) and by Chakhmouradian and Zaitsev (2002) in calcite-amphibole-clinopyroxene rock in Kola Peninsula, Russia. The

diopside shows textural and compositional affinity to clinopyroxene in alkaline rock types: 1) King and Sutherland (1966) described clinopyroxene as bands or bordering dyke intrusions in ijolite rocks of Napak area, eastern Uganda; 2) melanite garnet co-existing with aegirine or aegirine augite, sometimes with diopside with sodium-bearing outer rim, calcite, nepheline or leucite, have been reported as constituents of several alkaline rock types, mainly ijolite series (nepheline-clinopyroxene rocks); 3) pyroxene shows often "salitic" cores rimmed by green aegirine-augite in lamproites (Mitchell and Bergman 1991) – this microtexture is observed in "sheared" thin section Xe-15.2; and 4) the sodium-bearing diopside shows slight affinity against the pyroxene from Ugandan co-magmatic series of nepheline-leucitite, carbonate nodule and amphibole pyroxenite (fig. 51).

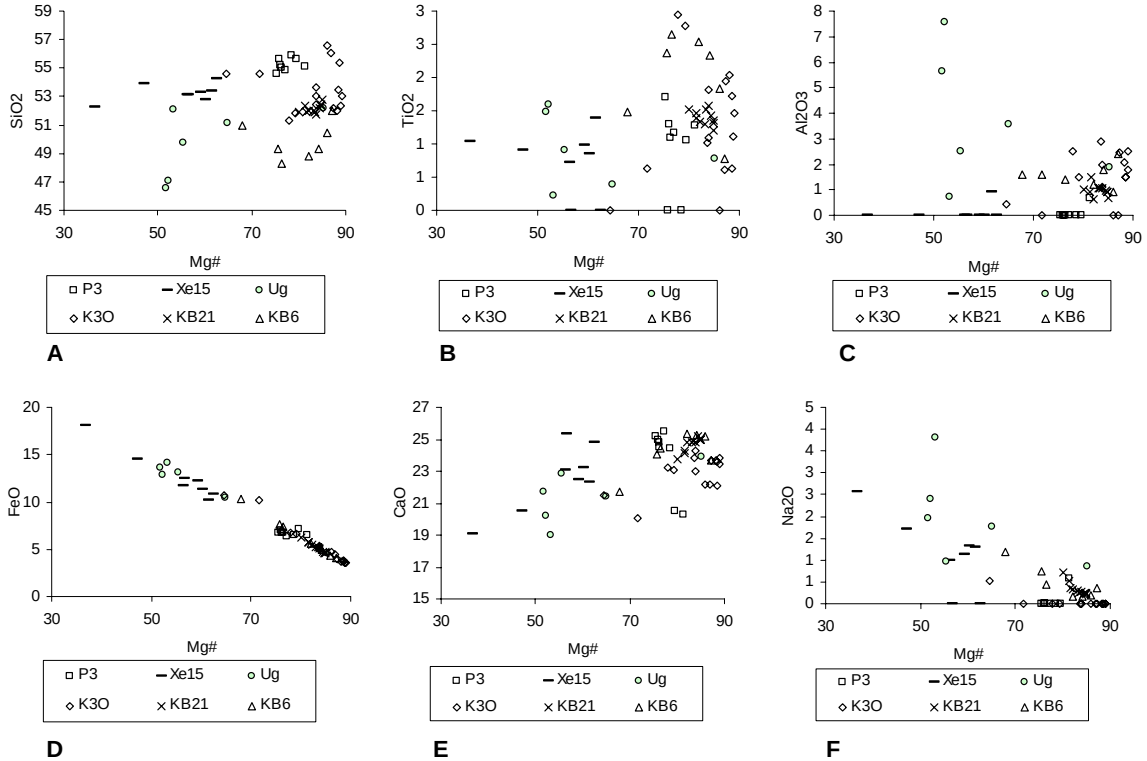

Figure 51. Clinopyroxene in xenoliths P-3 and Xe-15, in the dyke K3O, KB6 the dyke K3O quantitative analyses (Luttinen, unpublished data), dyke KB21, and selected alkaline rocks from East Africa rift, Uganda (Lloyd 1981). Abbreviations: Ug=Ugandan pyroxene.

Phlogopite (up to 9 vol-%) composition (fig. 52) of carbonatite xenolith differs from the one observed in phlogopite rock inclusion (P-3) and in Kjakebeinet lamproite dykes. On the other hand, the compositions, in relation to Al_2O_3, FeO and TiO_2 content, show strong affinity with group II kimberlite mica but also against the minette mica compositions

represented in Mitchell and Bergman (1991). They state that primitive micas are characterized by higher aluminium and lower iron content than the evolved ones. Therefore, higher aluminium and low titanium content of the mica of the carbonatite xenolith could refer to deep crystallization of lamproite material; maybe when the possible silicate and carbonate melts were segregated.

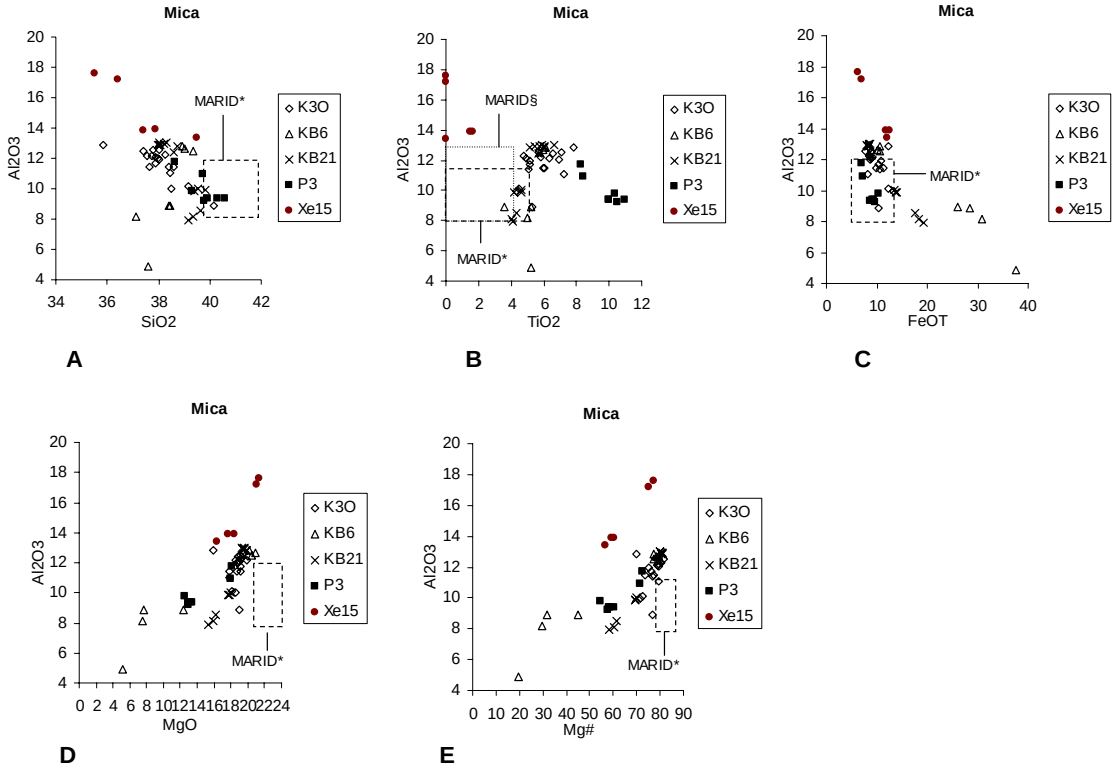

Figure 52. Mica composition of the xenoliths P-3, Xe-15, and the dykes of Kjakebeinet; Al_2O_3 versus SiO_2, TiO_2, FeO (total), MgO, and magnesium number (Mg#). Abbreviations: K3O, dyke 2 semi-quantitative data; KB6, dyke 1, quantitative data; KB21, dyke 3; MARID*, range in phlogopite composition from 12 mica-amphibole-rutile-ilmenite-diopside inclusions from South African kimberlites (Waters 1987); MARID§, MARID-suite composition after Dawson and Smith (1977) as referred to Mitchell and Bergman (1991).

The stable isotope study of carbonatite xenolith (table 5 section 7.1) points to carbonatite or lamproite origin and radiogenic isotopes (table 6 section 7.2) show a strong affinity to the Kjakebeinet lamproite dyke 2. The Rb-Sr mineral age based on two data points (fig. 44 p. 77) is 271-201 Ma. A question is risen whether the xenolithic material could be the source of the abundant carbonate, atypical for lamproites (Luttinen et al. 2002), in the dykes. The isotopic composition (table 6 section 7.2) combined with the mineral chemical data show that carbonatite xenolith Xe-15 is co-magmatic to the Kjakebeinet lamproite.

8.2.2 Phlogopite rock (P-3)

Diopside from Kjakebeinet lamproites and the phlogopite rock (P-3) are notably similar, though calcite rock records a higher FeO content and lower magnesium ratio (fig. 51). The whole rock chemistry of phlogopite rock resembles the chemistry of the Kjakebeinet lamproites. The xenolith is richer in titanium (10 wt-% TiO_2) and potassium (10 wt-% K_2O) and depleted in calcium (5 wt-% CaO) in relation to dykes 1 and 2, and notably richer in titanium and depleted in silica with regard to lamproite averages (Bergman 1987 as referred to Luttinen et al. 2002). This could refer to crystallization from melt generated by a smaller-scale partial melting than the lamproites. The mineral assemblage titanium-rich phlogopite, potassic richterite, and diopside are similar to those of lamproites (Michell and Bergman 1991) and MARID (mica-amphibole-rutile-ilmenite-diopside) inclusions that are only found from South African kimberlites: though, ilmenite is missing and TiO_2 phase present is anatase. Waters (1990) suggested that MARID xenoliths were crystallized from lamproite magma and this explains the similarity of the mineral assemblages. Twinned diopside, atypical for rapidly cooled Leucite Hills lamproites but common in slowly cooled West-Kimberley lamproites, refers to crystallization slower relative to the host-lamproite. The diopside composition is similar to the dykes 1 and 2 of Kjakebeinet (fig. 51). Phlogopite composition (fig. 52) with regard to aluminium oxide, silica, and iron oxide contents, however, is similar to MARID inclusions from South African kimberlites (cf. Waters 1987). On the basis of the major element chemistry, phlogopite rock is a cognate xenolith, but trace element study and more material is needed to do further conclusions, e.g., on the MARID proposal and the micaceous kimberlite connection. The presence of low-pressure TiO_2 polymorph anatase indicates crystallization of the xenolith in relatively low pressures but presence of ankerite, on the other hand, is consistent with high temperatures. The relatively high Al_2O_3 content of the phlogopite combined to the proposal of high-T low-P crystallization environment could refer to the origin of the xenolith as low-pressure cumulate crystallized from relatively un-evolved magma.

8.3 Mineral chemistry of the Kjakebeinet lamproites

On the basis of mineral abundances the dyke 2 (sample K3O) is a phlogopite-sanidine-diopside-olivine-lamproite. Classification based on mineral chemistry requires still further studies although the dyke 2 shows affinity to madupitic lamproites.

8.3.1 Phlogopite

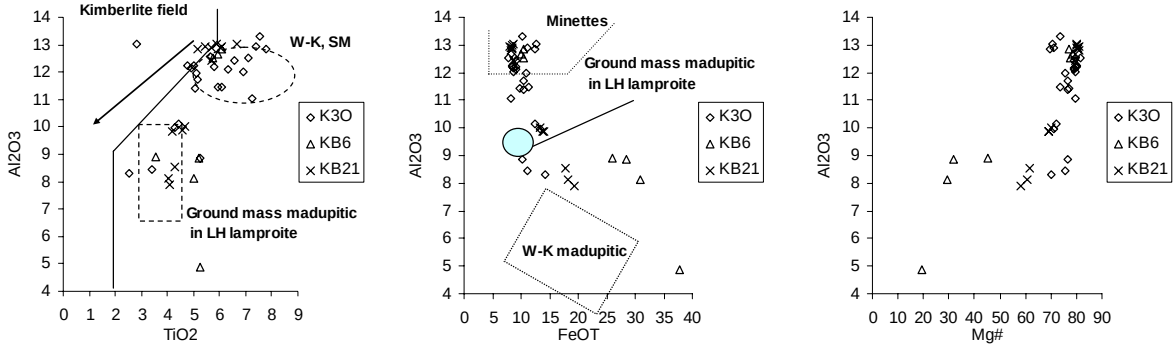

Figure 53. Phlogopite of the Kjakebeinet lamproites, Al_2O_3 versus TiO_2, FeOT (total) and magnesium number. K3O=dyke 2, semi-quantitative analyses, KB6=dyke 2 quantitative analyses (Luttinen unpublished data) and KB21=dyke 3 quantitative analyses (Luttinen unpublished data). A) The field of kimberlite mica, W-K SM= mica from lamproites of West Kimberley, Australia and Smoky Butte, Montana, ground mass madupitic mica in Leucite Hills (LH) lamproite, and an arrow indicating zoning trend in group II kimberlites Mitchell (1995). B) Minette field (bases on several authors and areas) and West Kimberley madupitic lamproite from Mitchell and Bergman (1991).

The majority of mica compositions, partly due to irregular distribution of analysis points, are similar with regard to aluminium and titanium content (fig. 53 A) to the ones from West Kimberley and Smoky Butte lamproites. The compositions from the rims (KB6 and KB21) are similar to madupitic ground mass phlogopite from Leucite Hills lamproites (Mitchell and Bergman 1991) showing lower aluminium and slightly lower titanium content in relation to other analyses (fig. 53 A). Another compositional group resembles West-Kimberley and Smoky Butte micas. According to zonation trend, represented by Mitchell and Bergman (1991), the compositional variation of Kjakebeinet dykes is nearly perpendicular to trend in other lamproites (Mitchell and Bergman 1991 p.215), but almost parallel to the trend of the group II kimberlites (Mitchell 1995).

The total iron oxide versus aluminium oxide diagram (fig. 53 B) shows that the mica composition ranges between the field of minettes (several areas and authors, see Mitchell and Bergman 1991 p. 213) and West Kimberley madupitic lamproite compositions (Mitchell and Bergman 1991). Whether this is due to magma mixing or assimilation requires further studies. Fig. 53 C shows that rims of the KB6 phlogopite are the most evolved ones on the basis of very low magnesium ratio, and decreasing aluminium with increasing iron content (Mitchell and Bergman 1991).

It is essential in the future to specify between the morphological forms of phenocrystal and groundmass phlogopite (Mitchell and Bergman 1991) when working with the mineral analyses and also distinguish between the lamproite groups.

8.3.2. Clinopyroxene

The diopside compositions (table 5 appendix 2) are typical of lamproites (Mitchell and Bergman 1991, p.242), though phlogopite shows affinity for minettes. Scarce, fine-grained diopside enclosed by fine-grained phlogopite in the core region of the dyke provides evidence for the presence of transitional of madupitic mica (Mitchell and Bergman 1991, p.233); this is also indicated by the phlogopite composition (fig. 53 B). Bright green aegirine-augite is observed in Leucite Hills lamproites, and its occasional presence inside altered diopside (fig. 37 A section 6.1) is probably due to crystallization from a vapour phase (Kuehner 1980 and Mitchell 1985 as referred to in Mitchell and Bergman 1991).

8.3.3 Olivine

Olivine is completely altered to talc, occasionally to calcite-iron oxide pseudomorphs. It is mainly found as phenocrystal and euhedral. This is common for lamproites. The amount of olivine ranges between 9 and 18 vol-% (section 6.1).

9. CONCLUSIONS

The xenoliths studied from Kjakebeinet ultrapotassic, mica-rich lamproite dykes represent several lower to upper crustal rock types; tonalite, alkali feldspar granite, and augen gneisses, metagabbros and metasedimentary xenoliths were observed. Two of the xenoliths, carbonatite, and phlogopite rock, are cognate to the host-dyke, however.

Generalizing, mineral assemblages of the xenoliths indicate high-grade metamorphism. The garnetiferous metagabbros and the metapelitic xenoliths were probably derived from the lower crust. The metagabbroic series; the layered metagabbros, the fine-grained, garnet-free metagabbros, and garnetiferous metagabbros record successively higher pressures. The tonalite gneiss samples were probably metamorphosed at middle-crustal levels. The Sm-Nd isotopic study provides evidence of two different age groups among the metagabbroic samples; Mesozoic and Proterozoic. Based on unpublished U-Pb zircon (SHRIMP) data the tonalite gneisses are Proterozoic (1000 Ma) and may represent calc-alkaline magmatic activity during the Grenvillean/Kibaran orogeny. The alkali feldspar granite gneisses most probably represent Proterozoic metaigneous rocks. The metasandstone, the coal shale, and the meta-greywacke may record Permian strata which is widespread in the area.

The dyke 2 (sample K3O) can be classified as phlogopite-sanidine-diopside-olivine lamproite. Phlogopite compositions show compositional affinity to madupitic lamproites and group II kimberlites. The cognate phlogopite xenolith is particularly typical of phlogopite lamproites, but carbonatite nodules have not been reported in lamproites before. These samples do offer material for petrogenetic studies of the Kjakebeinet lamproites.

Overall, the xenoliths indicate heterogeneity of the crust and presence of differentiated metaigneous rocks in the basement. They also show that Proterozoic formations extend below the southern Vestfjella.

10. ACKNOWLEDGEMENTS

I wish to thank my supervisor Dr. Arto Luttinen as he gave the opportunity to study these interesting rocks, as well as his patience and discussion during the work. Dr. Tapani Rämö gave comments on the text and corrected language at the end which is greatly appreciated. I thank Dr. Juha Karhu on comments concerning the stable isotope work. Dr. Ragnar Törnroos made it possible to use EDS equipment at the University of Helsinki and Dr. Hannu Huhma offered access to the Isotope laboratory of Geological Survey of Finland, Espoo, and helped with isotope data processing. Several persons, my warmest thanks to you, assisted and gave advice on the lab work; Ms. Tuula Hokkanen, Ms. Leena Järvinen, and Mr. Arto Pulkkinen from Geological Survey of Finland, Espoo; Dr. Martti Lehtinen, Mr. Akseli Torppa, Mr. Pasi Heikkilä, Ms. Tuija Vaahtojärvi, Ms Helena Korkka, and Dr. Matti Poutiainen from University of Helsinki. Support of friends and relatives was indispensable. Financially this study was supported by Academy of Finland, facilitating e.g. sampling by FINNARP crew 1997/1998 and 2000/2001, Hämäläis-osakunta (Hämäläisten ylioppilasäätiön rahasto, Oskari ja Siiri Vilamon rahasto, Ester ja Knut Polónin rahasto, Sampsa Mantereen rahasto), and Matematiikan ja luonnontieteiden rahasto.

REFERENCES

Arndt N.T. and Goldstein S.L. 1987. Use and abuse of crust-formation ages. Geology 15, 893-895.

Barth T.F.W. and Ramberg I.B. 1966. The Fen Circular Complex. In: Tuttle O.F. and Gittins J. 1966. Carbonatites. Interscience publishers. 591p., pp. 225-257.

Boyd W.W. 1987. Crustal evolution in the Pensacola Mountains: inferences from chemistry and petrology of the igneous rocks and nodule-bearing lamprophyre dykes. In: Geological Evolution of Antarctica. Thomson M.R.A, Crame J.A., Thomson J.W. (Eds) proceedings of the Fifth International Symposium on Antarctic Earth Sciences.

British Geological Survey. Site visited 27.3.2006. http://www.bgs.ac.uk/scmr/scmr_products.html.

Butcher K. and Frey M. 1994. Petrogenesis of Metamorphic Rocks. Springer-Verlag, Germany. 318p.

Chakhmouradian A.R. and Zaitsev N.A. 2002. Calcite-amphibole-clinopyroxene rock from the Africanda Complex, Kola Peninsula, Russia: Mineralogy and a possible link to carbonatites. III. Silicate minerals. The Canadian Mineralogist 40, 1347-1374.

Clemens J.D., Holloway J.R. and White A.J.R. 1986. Origin of an A-type granite: Experimental constraints. American Mineralogist 71, 317-324.

Coleman R.G., Lee D.E., Beatty L.B. and Brannock W.W. 1965. Eclogites and Eclogites: Their Differences and Similarities. Geological Society of America Bulletin 76, 483-508.

Coogan L.A., Wilson R.N., Gillis K.M., and MacLeod C.J. 2001. Near-solidus evolution of oceanic gabbros: insights from amphibole geochemistry. Geochimica et Cosmochimica Acta 65, 4339-4357.

Coplen T.B., Kendall C., and Hopple J. 1983. Comparison of stable isotope reference standards. Nature 302, 236-238.

Corner B. 1994. Geological evolution of western Dronning Maud Land within a Gondwana framework: Geophysics subprogramme. Final project report to SACAR. Department of Geophysics, Whitwaterstrand University, South Africa. 21p.

Coutinho J M V, Kräutner, H G, Sassi, F, Schmid R and Sen, S: A systematic nomenclature for metamorphic rocks: 8. Amphibolite and granulite. Recommendations by the IUGS Subcommission on the Systematics of Metamorphic Rocks. Recommendations, web version of 01.05.2004. Site visited 27.3.2006. http://www.bgs.ac.uk/scmr/scmr_products.html.

Cox K.G., Bell J.D, and Pankhurst R.J. 1979. The Interpretation of the Igneous Rocks. George Allen & Unwin Ltd, London. 450p.
Davidson A. 1990. Two transects across the Grenville front, Killarney and Tyson Lake areas, Ontario. In: Salisbury M.H. and Fountain D.M. (Eds) 1990. Exposed Cross-sections of the Continental Crust. Kluwer Academic Publishers, Neatherlands. pp. 343-400.

Deer W.A., Howie R.A., and Zussman J. 1963. Rock Forming Minerals Volume 2 Chain silicates. Longmans Green and CO ltd, London. 379p.

Deer W.A., Howie R.A., and Zussman J. 1992. An Introduction to the Rock Forming Minerals. Longman Scientific and Technical, London, 696p.

Deines P and Gold D.P. 1973. The isotopic composition of carbonatite and kimberlite carbonates and their bearing on the isotopic composition of deep seated carbon. Geochimica et Cosmochimica acta 37, 1709-1733.

DePaolo J.D. 1981. Neodynium isotopes in the Colorado Front Range and crust-mantle evolution in the Proterozoic. Nature 291, 193-195.

Dickin A.P. 1995. Radiogenic isotope geology. Cambridge University Press, Cambridge. 452p., pp. 39-103, 173-201.

Dingwell D.B. and Brearley M. 1985. Mineral chemistry of igneous melanite garnets from analcite-bearing volcanic rocks, Alberta, Canada. Contributions to Mineralogy and Petrology 90, 29-35.

Dirks P.H.G.M and Sithole T.A. 1999. Eclogites in the Makuti gneisses of Zimbabwe: implications for the tectonic evolution of the Zambezi Belt in southern Africa. Journal of metamorphic Geology 17, 593–612.

Droop G. 1987. A general equation for estimating Fe 3+ concentrations in ferromagnesian silicates and oxides from microprobe analyses, using stoichiometric criteria. Mineralogical Magazine 51, 431-43.

Duncan R.A., Hooper P.R., Rehacek J., Marsh J.S. and Duncan A.R. 1997. The timing and duration of the Karoo igneous event, southern Gondwana. Journal of Geophysical Research 102, 18127-18138.

Ernst W.G. 1968. Amphiboles. Springer-Verlag, New York.125pp.

Goldscmidt J.R. 1982. Plagioclase stability at elevated temperatures and water pressures. American Mineralogist 67, 653-675.

Green D.H. and Ringwood A.E. 1967. An experimental investigation of the gabbro to eclogite transformation and its petrological applications. Geochimica et Cosmochimica Acta 31, 767-833.

Griffin W.L. & Heier K.S. 1973. Petrological implications of some corona structures. Lithos 6, 315-335.

Groenewald P.B., Moyes A.B., Grantham G.H., and Krynauw J.G. 1995. East Antarctic crustal evolution: geological constraints and modelling in western Dronning Maud Land. Precambrian Research 75, 231-250.

Gwalani L.G., Rock N.M.S., Ramasamy R., Griffin B.J, and Mulai B.P. 2000. Complexly zoned Ti-rich melanite-schorlomite garnets from Ambadungar carbonatite-alkalic complex, Deccan Igneous Province, Gujarat State, Western India. Journal of Asian Earth Sciences 18, 163-176.

Hall A. 1996. Igneous Petrology. Addison Wesley Publishing Company. 550p.

Hamilton P.J., O'Nions R.K., Bridgwater D. and Nutman A. 1983. Sm-Nd studies of Archean metasediments and metavolcanics from West Greenland and their implications for the Earth's early history. Earth and Planetary Science Letters 62, 263-272.

Harris C. and Grantham G.H. 1993. Geology and petrogenesis of the Straumsvola nepheline syenite complex, Dronning Maud Land, Antarctica. Geological Magazine 130, 513-532.

Huang W-L.H., and Wyllie P.J. 1986. Phase relationships of gabbro-tonalite-granite-water at 15 kbar with application to differentiation and anatexis. American Mineralogist 71, 301-316.

Huggins F.E., Virgo D., and Huckenholz H.G. 1977. Titanium-containing silicate garnets. II. The crystal chemistry of melanites and schorlomites. American Mineralogist 62, 646-665.

Jacobs J., Fanning C.M.., Henjes-Kunst F., Olesch M.., and Paech H. 1998, Continuation of the Mozambique belt into East Antarctica: Grenville-age Metamorphism and polyphase Pan-African high-grade events in central Dronning Maud Land. Journal of Geology 106, 385-406.

Jacobs J., Bauer W., Spaeth G., Thomas R. J., and Weber K. 1996. Lithology and structure of the Grenville-aged (~1.1 Ga) basement of Heimefrontfjella (East Antarctica) Geologische Rundschau 85, 800-821.

Javoy M., Pineau F., and Delorme H. 1986. Carbon and nitrogen isotopes in the mantle. Chemical Geology 57, 41-62.

Juckes L.M. 1972. The geology of north-eastern Heimefrontfjella, Dronning Maud Land. British Antarctic survey scientific reports 65.

Kesson S. and Price R.C. 1972. The Major and Trace Element Chemistry of Kaersutite and Its Bearing on the Petrogenesis of Alkaline Rocks. Contributions to Mineralogy and Petrology 35, 119-124.

King B.C. and Sutherland D.S. 1966. The carbonatite complexes of Eastern Uganda. In: Tuttle O.F. and Gittins J. 1966 Carbonatites. Interscience publishers, New York, 591p., pp. 73-126.

Koester E., Pawley A.R., Fernandes L.A., Porcher C.C. and Soliani Jr E. 2002. Experimental Melting of Cordierite Gneiss and the Petrogenesis of Syntranscurrent Peraluminous Granites in Southern Brazil. Journal of Petrology 43, 1595-1616.

Leat P.T., Riley T.R., Storey B.C., Kelley S.P., and Millar I.L. 2000. Middle Jurassic ultramafic lamprophyre dyke within the Ferrar magmatic province, Pensacola Mountains, Antarctica. Mineralogical Magazine 64, 95-95.

Le Breton N. & Thompson A. B. 1988. Fluid-absent (dehydration) melting of biotite in metapelites in the early stages of crustal anatexis. Contributions to Mineralogy and Petrology 99, 226–237.

Le Maitre, R.W., Bateman, B., Dudek, A., Keller, J., Lameyre, J., Le Bas, M.J., Sabine, P.A., Schmid, R., Sørensen, H., Streckeisen, A., Woolley, A.R. & Zanettin, B. 1989. A Classification of Igneous Rocks and Glossary of Terms: Recommendations of the International Union of Geological Sciences Subcomission on the Systematics of Igneous Rocks. Blackwell Scientific Publications.

Leake B.E. 1978. Nomenclature of amphiboles. American Mineralogist 63, 1023-1052.

Leake B.E., Woolley A.R., Arps C.E.S., Birch W.D., Gilbert M.C., Grice J.D., Hawthorne F.C., Kato A., Kisch H.J., Krivovichev V.G., Linthout K., Laird J., Mandarino J.A., Maresch W.V., Nickel E.H., Rock N.M.S., Schumacher J.C., Smith D.C., Stephenson N.C.N., Ungaretti L., Whittaker E.J.W., and Guo Y.Z. 1997. Nomenclature of amphiboles: Report of the subcommittee on amphiboles of the international mineralogical association, commission on new minerals and mineral names. The Canadian Mineralogist 35, 219-246.

Lister G.S., Etheridge M.A., and Symonds P.A. 1986. Detachment faulting and the evolution of passive continental margins. Geology 14, 246-250.

Lloyd F.E. 1981. Upper-mantle metasomatism beneath a continental rift:clinopyroxenes in alkali mafic lavas and nodules from South West Uganda. Mineralogical Magazine 44: 315-23.

Luttinen A.V., Vuori S.K., Mänttäri I., & Huhma H. 2004. U-Pb chronology and Nd and Sr isotope geology of gabbroic intrusions from Dronning Maud Land, Antarctica: implications for tectono-magmatic evolution of the Karoo Large Igneous Province. In: Vuori S.K. 2004, Petrogenesis of the Jurassic gabbroic intrusions of Vestfjella, Dronning Maud Land, Antarctica. University of Helsinki (PhD thesis).

Luttinen A.V, Zhang X., and Foland K.A. 2002. 159Ma Kjakebeinet lamproites (Dronning Maud Land, Antarctica) and their implications for Gondwana breakup processes. Geological Magazine 139, 525-539.

Luttinen A.V. and Furnes H. 2000. Flood Basalts of Vestfjella: Jurassic Magmatism Across an Archean Proterotzoic Lithospheric Boundary in Dronning Maud Land, Antarctica.

Luttinen A.V. 2000. Origin of Jurassic Vestfjella flood basalts, Dronning Maud Land, Antarctica. Academic dissertation. University printing house, Helsinki.

Luttinen A.V. & Siivola J.U. 1997. Geochemical Charasteristics of Mesozoic Lavas and Dikes from Vestfjella, Dronning Maud Land: Recognition of Three Distinct Chemical Types. The Antarctic Region: Geological Evolution and Processes, 495-503.

McKenzie D.P. 1989. Some remarks on the movement of small melt fractions in the mantle. Earth and Planetary Science Letters 95, 53-72.

McKenzie W.S., Donaldson C.H., and Guilford C. 1982. Atlas of igneous rocks and their textures. Longman Group Limited, England. 148p.

Menzies M.A. and Hawkesworth C. J. 1986. Mantle metasomatism. Academic press geology series, London. 472 p.

Mitchell R.H. 1995. Kimberlites, orangeites, and related rocks. Plenum Press, New York, 410 p.

Mitchell R.H. 1994. The lamprophyre facies. Mineralogy and Petrology 51, 137-146.

Mitchell R.H. & Bergman S.C. 1991. Petrology of lamproites, Plenum Press, New York, 441p.

Miller J.D. and Ripley E.M. 1996. Layered Intrusions of the Duluth Complex, Minnesota, USA. In: Cawthorn R.G. (ed.) 1996 Layered Intrusions. Elsevier Science B.V. Netherlands. 531p.

Miyashiro A. 1973. Metamorphism and metamorphic belts. George Alka & Unwin Ltd, London, 492 p.

Morimoto N., Fabries J., Ferguson A.K, Ginzburg I.V., Ross M., Seifeit F.A., and Zussman J. 1989. Nomenclature of pyroxenes. Canadian Mineralogist 27,143-156.

Morogan V. and Lindblom S. 1995. Volatiles associated with the alkaline - carbonatite magmatism at Alnö, Sweden: a study of fluid and solid inclusions in minerals from the Laångarsholmen ring complex. Contributions to Mineralogy and Petrology 122, 262-274.

Nelson D.R., Chivas A.R., Chappell B.W, and McCulloch M.T., 1987. Geochemical and isotopic systematics in carbonatites and implications for the evolution of ocean-island sources. Geochimica et Cosmochimica acta 72, 1-17.

Neuendorf K.K.E, Mehl J.P. Jr., and Jackson J.A. 2005. Glossary of Geology. Fifth edition. American geological institute, Alexandria, Virginia.

O´Brien P.J. and Rötzler J. 2003. High-pressure granulites: formation, recovery of peak conditions and implications for tectonics. Journal of Metamorphic Geology 21, 3-20.

Otten T. 1984. The origin of brown hornblende in the Artfjället gabbro and dolerites. Contributions to Mineralogy and Petrology 86, 189-199.

Oxburgh E.R. 1964. Petrological evidence for the presence of amphibole in the upper mantle and its petrogenetic and geophysical implications. Geological Magazine 101, 1-19.

Powell J.L., Hurley P.M., and Fairbairn H.W. 1966. The Strontium Isotopic Composition and Origin of Carbonatites. In: Tuttle O.F. and Gittins J. 1966. Carbonatites. Interscience publishers, New York, 591p., pp. 365-378.

Rickwood, P.C. 1989, Boundary lines within petrologic diagrams which
use oxides of major and minor elements. Lithos 22, 247-263.

Riley T.R., Leat P.T., Storey B.C., Parkinson I.J., and Millard I.L. 2003. Ultramafic lamprophyres of the Ferrar large igneous province: evidence for a HIMU mantle component. Lithos 66, 63-76.

Rivers T.1997. Lithotectonic elements of the Grenville Province: review and tectonic implications. Precambrian Research 86, 117-154.

Rogers N.W. & Hawkesworth C.J. 1982. Proterozoic age and cumulate origin for granulite xenoliths, Lesotho. Nature 299, 409-413.

Rollinson H.R. 1993. Using Geochemical Data: Evaluation, Presentation, Interpretation. Longman Group UK Limited, England. 352p.

Rudnick R.L. 1992. Xenoliths - Samples of the lower continental crust. In: Fountain D.M., Arculus R., and Kay R.W. (eds.) 1992. Elsevier, Amsterdam, 485p., pp. 269-313.

Schmid R., Fettes D., Harte B., Davis E., Desmons J., Meyer-Marsilius H-J., and Siivola J.A. Systematic nomenclature for metamorphic rocks: How to name a metamorphic rock. Recommendations by the IUGS Subcommission on the Systematics of Metamorphic Rocks. Recommendations, web version of 01.05.2004. Site visited 27.3.2006. http://www.bgs.ac.uk/scmr/scmr_products.html.

Schmidt M.W. and Thompson A.B. 1996. Epidote in calc-alkaline magmas: An experimental study of stability, phase relationships, and the role of epidote in magmatic evolution. American Mineralogist 81, 462-474.

Shelley D. 1993. Igneous and metamorphic rocks under the microscope. Chapman & Hall, Cambridge. 445p.

Sighinolfi G.P. and Gorgoni C. 1975. Genesis of Massif-Type Anorthosites- The Role of High-Grade Metamorphism. Contributions to Mineralogy and Petrology 51, 119-126.

Spear, F.S. 1993. Metamorphic phase equilibria and pressure–temperature–time paths. Mineralogical Society of America, Monographs 1, 799p.

Spear F.S. 1981. An experimental study of hornblende stability and compositional variability in amphibolite. American Journal of Science 281, 697-734.

Spry A. 1969. Metamorphic textures. Pergamon press. 350p.
Sweeney R.J., Thompson A. B., and Ulmer P. 1993. Phase relations of a natural MARID composition and implications for MARID genesis, lithospheric melting and mantle metasomatism. Contributions to mineralogy and petrology 115, 225 -241.

Sörensen H. (ed.) 1974. The alkaline rocks. John Wiley, London. 622pp.

Taylor H.P. Jr, Frechen J., and Degens E.T. 1967. Oxygen and carbon isotope studies of carbonatites from the Laacher See District, West Germany and the Alnö District, Sweden. Geochimica et Cosmochimica acta 31, 407-430.

Taylor H.P. 1980. The effects of assimilation of country rocks by magmas on $^{18}O/^{16}O$ and $^{87}Sr/^{86}Sr$ systematics in igneous rocks. Earth and Planetary Science Letters 47, 243-254.

Tingey R.J. 1991, The regional geology of Archaean and Proterozoic rocks in Antarctica. In: Tingey, R.J. (ed.). The Geology of Antarctica. Clarendon Press, Oxford 680p., pp.1-73.

Treloar P.J., Carney J.N., Crow M.J., Evans J.A., and Barton C.N. 1990. Pressure-temperature-time paths of granulite metamorphism and uplift, Zambesi Belt, N.E. Zimbabwe. In: Vielzeuf D. and Videl Ph. (eds.) 1990. Granulites and Crustal Evolution, 585p., pp.223-241. Kluwer academic Publishers, Neatherlands.

Tribuzio R., Tiepolo M, and Thirlwall M.F. 2000. Origin of titanian pargasite in gabbroic rocks from the Northern Apennine ophiolites (Italy): insights into the late-magmatic evolution of a MOR-type intrusive sequence. Earth and Planetary Science Letters 176, 281-293.

Tröger W.E. 1959. Optische bestimmung der gesteinbildenden Minerale, Teil 1, Bestimmungs Tabellen, Stuttgart. 147p.

Tsuchiyama A. 1986. Melting and dissolution kinetics - Application to partial melting and dissolution of xenoliths. Journal of Geophysical Research 91**,** 9395-9406.

Twiss R.J. and Moores E.M. 2000. Structural Geology. Freeman and Company, New York, 532 p.

University of Helsinki, Department of Geology. Ohjeita geologian pro gradu-tutkielman ja muiden kirjallisten opinnäytteiden laatimista varten. Versio 31.8.2004.

Upton B.G., Parsons I., Emeleus C.H., and Hodson M.E. 1996. Layered Alkaline Igneous Rocks of the Gardar Province, South Greenland. In: Cawthorn R.G. (ed.) 1996 Layered Intrusions. Elsevier Science B.V. Netherlands. 531 p.

Vuori S. K. 2004. Petrogenesis of the Jurassic gabbroic intrusions of Vestfjella, Dronning Maud Land, Antarctica. University of Helsinki (PhD thesis).

Vuori S.K., Johanson B.S., and Pakkanen L.K. 2004 In: Vuori S.K. 2004, Petrogenesis of the Jurassic gabbroic intrusions of Vestfjella, Dronning Maud Land, Antarctica. University of Helsinki (PhD thesis).
Waters D. 2004. http://www.earth.ox.ac.uk/~davewa/pt/. Site visited 25.2.2006.

Waters D.J. 1990. Thermal history and tectonic setting of the Namaqualand granulites, Southern Africa: Clues to Proterozoic crustal development. In: Vielzeuf D. and Videl Ph. (eds.) 1990. Granulites and Crustal Evolution, 585p., pp. 243-256. Kluwer academic Publishers, Neatherlands.

Waters F.G. 1987. A suggested origin of MARID xenoliths in kimberlites by high pressure crystallization of an ultrapotassic rock such as lamproite. Contributions to Mineralogy and Petrology 95, 523-533.

Webmineral. http://www.webmineral.com. Site visited latest 4.5.2006.

White R.S. 1997. Mantle plume origin for the Karoo and Ventersdorp flood basalts, South Africa. South African Journal of Geology 100, 271-282.

White R. and McKenzie D. 1989. Magmatism at Rift Zones: The Generation of Volcanic Continental Margins and Flood Basalts. Journal of geophysical research 94, 7685-7729.

Woolley A.R., Bergman S.C., Edgar A.D., Le Bas M.J., Mitchell R.H., Rock N.M.S., and Scott Smith B.H. 1996. Classification of lamprophyres, lamproites, kimberlites, and the kalsilitic, melilitic, and leucitic rocks. The Canadian Mineralogist 43, 175-186.

Wright I.P., Monica M., and Pillinger C.T. 1988. Carbon, oxygen and nitrogen isotopic composition of possible martian weathering products in EETA 79001. Geochimica et Cosmochimica Acta 52, 917-924.

Yoder H.S. and Tilley C.E. 1962. Origin of basalt magmas. Journal of Petrology 3, 342-532.

APPENDIX 1

Table 1 apatite analyses

	1	2	3	4	5	6	7	8	9	10
	P3	P7	P7	P8	P8	P8	Xe1	Xe1	Xe4	Xe4
Sample	(R3_7)	(R2_10)	(R3_4)	(R3_4)	(R4_5)	(R5_9)	(R3_2)	(R3_4)	(R1_3)	(R1_4)
CaO	56,67	52,90	51,78	56,45	54,58	57,07	56,20	55,82	50,88	56,99
Na_2O	0,41	0,57	0,41	0,49	0,34	0,41	0,00	0,00	0,00	0,00
FeO	0,00	0,00	0,00	0,67	1,43	0,96	0,39	0,64	0,62	0,00
MnO	0,00	0,00	0,00	0,00	0,00	0,00	0,00	0,43	0,00	0,00
MgO	0,00	0,51	0,50	0,00	0,61	0,00	0,00	0,00	0,77	0,00
P_2O_5	42,92	40,64	40,93	42,01	42,41	41,55	43,41	43,11	40,54	43,01
SiO_2	0,00	0,00	0,00	0,00	0,00	0,00	0,00	0,00	0,00	0,00
Cl	0,00	0,00	1,58	0,38	0,62	0,00	0,00	0,00	0,19	0,00
F	0,00	5,39	4,79	0,00	0,00	0,00	0,00	0,00	7,00	0,00
total	100,0	100,0	100,0	100,0	100,0	100,0	100,0	100,0	100,0	100,0

	11	12	13	14	15	16	17	18	19	20
	Xe4	Xe5	Xe9	Xe11	Xe11	Xe15	Xe15	Xe16	Xe16	Xe16
Sample	(R1_10)	(R1_1)	(R3_1)	(R5_9)	(R5_14)	(R1_8)	(R1_13)	(R1_1)	(R1_5)	(R2_5)
CaO	53,05	37,56	51,79	60,04	59,59	58,39	58,28	55,85	55,03	55,04
Na_2O	0,00	0,00	0,34	0,52	0,00	0,00	0,33	0,00	0,38	0,00
FeO	0,00	0,00	0,62	0,00	0,00	0,00	0,00	0,00	0,56	0,97
MnO	0,00	0,00	0,00	0,00	0,00	0,00	0,00	0,00	0,00	0,00
MgO	0,00	0,00	0,00	0,28	0,00	0,00	0,00	0,39	0,39	0,38
P_2O_5	41,02	57,95	40,01	39,16	40,41	40,54	38,61	42,87	42,60	43,16
SiO_2	0,00	0,00	0,00	0,00	0,00	1,07	2,77	0,00	0,00	0,00
Cl	0,00	0,00	0,66	0,00	0,00	0,00	0,00	0,92	1,04	0,45
F	5,93	4,48	6,59	0,00	0,00	0,00	0,00	0,00	0,00	0,00
total	100,0	100,0	100,0	100,0	100,0	100,0	100,0	100,0	100,0	100,0

Table 2 amphibole analyses

	1	2	3	4	5	6	7	8	9	10
	P3	P3	P3	P3	P3	P4	P4		P4	P7
Sample	(R1_5)	(R1_7)	(R2_9)	(R2_10)	(R2_1)	(R2_6)	(R3_1)	P4 R3_4)	(R3_5)	(R2_2)
SiO_2	53,06	56,30	52,66	55,01	55,72	44,36	43,47	43,84	43,96	43,67
TiO_2	6,93	7,10	5,97	5,53	6,26	1,88	2,18	1,87	2,13	3,21
Al_2O_3	0,00	0,81	0,00	0,00	0,47	15,29	14,84	15,16	15,26	13,52
Cr_2O_3	0,00	0,00	0,00	0,00	0,00	0,00	0,00	0,00	0,00	0,00
FeO	11,18	13,20	15,11	15,89	14,14	11,47	12,35	11,97	11,59	14,90
MnO	0,00	0,00	1,05	1,16	0,00	0,00	0,00	0,00	0,00	0,00
MgO	11,63	10,86	10,03	10,34	11,38	11,99	12,17	12,08	11,97	11,05
CaO	3,46	3,39	3,44	3,34	3,00	9,65	9,67	9,69	9,69	9,62
Na_2O	3,03	2,72	6,13	3,16	3,45	3,07	3,05	3,02	3,11	2,60
K_2O	10,71	5,62	5,59	5,56	5,58	2,29	2,26	2,38	2,29	1,42
total	100,00	100,00	100,00	100,00	100,00	100,00	100,00	100,00	100,00	99,99
Number of cations on the basis of 23 oxygen atoms										
Si	7,79	8,00	7,76	8,00	7,98	6,32	6,21	6,25	6,27	6,24
Al	0,00	0,00	0,00	0,00	0,02	1,68	1,79	1,75	1,73	1,76
Al	0,00	0,14	0,00	0,00	0,06	0,89	0,70	0,80	0,84	0,52
Fe(iii)	0,00	0,00	0,00	0,00	0,00	0,18	0,41	0,31	0,19	0,62
Ti	0,76	0,76	0,66	0,61	0,67	0,20	0,23	0,20	0,23	0,35
Cr	0,00	0,00	0,00	0,00	0,00	0,00	0,00	0,00	0,00	0,00
Fe(ii)	1,37	1,57	1,86	1,93	1,69	1,18	1,06	1,12	1,20	1,16
Mn	0,00	0,00	0,13	0,14	0,00	0,00	0,00	0,00	0,00	0,00
Mg	2,55	2,30	2,21	2,24	2,43	2,55	2,59	2,57	2,55	2,35
Ca	0,54	0,52	0,54	0,52	0,46	1,47	1,48	1,48	1,48	1,47
Na	0,86	0,75	1,75	0,89	0,96	0,85	0,84	0,83	0,86	0,72
K	2,01	1,02	1,05	1,03	1,02	0,42	0,41	0,43	0,42	0,26
TOTAL	15,88	15,05	15,98	15,36	15,29	15,74	15,73	15,75	15,76	15,45
Mg#	64,97	59,47	52,51	51,92	58,93	65,09	63,72	64,28	64,80	56,94

	11	12	13	14	15	16	17	18	19	20
Sample	P7 (R2_8)	P7 (R3_8)	Xe11 (R2_9)	Xe11 (R4_1)	Xe11 (R4_20)	Xe11 (R4_21)	Xe11 (R5_10)	Xe11 (R5_13)	Xe11 (R5_22)	Xe11 (R5_23)
SiO_2	43,41	43,33	41,31	43,29	41,53	41,32	41,74	43,52	42,24	44,09
TiO_2	3,51	3,42	3,97	1,95	3,58	3,72	3,79	3,68	4,02	3,10
Al_2O_3	13,54	13,63	14,41	14,86	14,77	14,08	14,33	14,94	13,96	15,55
Cr_2O_3	0,00	0,00	0,00	0,00	0,00	0,00	0,00	0,00	0,00	0,00
FeO	15,51	14,71	17,42	17,32	17,64	17,30	17,40	15,59	16,80	16,45
MnO	0,00	0,00	0,58	0,00	0,00	0,00	0,00	0,00	0,00	0,00
MgO	10,94	11,39	7,71	7,34	8,17	7,36	7,48	7,25	7,85	6,80
CaO	9,19	9,45	11,61	11,76	11,28	11,42	12,11	11,71	11,96	9,32
Na_2O	2,38	2,64	1,49	1,90	1,45	1,83	1,66	1,81	1,66	1,41
K_2O	1,51	1,43	1,51	1,57	1,57	2,97	1,50	1,50	1,50	3,29
total	99,99	100,00	100,00	100,00	100,00	100,00	100,00	100,00	100,00	100,00
Number of cations on the basis of 23 oxygen atoms										
Si	6,18	6,17	6,11	6,36	6,10	6,15	6,16	6,33	6,21	6,43
Al	1,82	1,83	1,89	1,64	1,90	1,85	1,84	1,67	1,79	1,57
Al	0,45	0,46	0,62	0,93	0,65	0,62	0,66	0,89	0,63	1,10
Fe(iii)	0,88	0,76	0,00	0,00	0,21	0,00	0,00	0,00	0,00	0,00
Ti	0,38	0,37	0,44	0,22	0,40	0,42	0,42	0,40	0,45	0,34
Cr	0,00	0,00	0,00	0,00	0,00	0,00	0,00		0,00	0,00
Fe(ii)	0,97	0,99	2,16	2,13	1,96	2,15	2,15	1,90	2,07	2,01
Mn	0,00	0,00	0,07	0,00	0,00	0,00	0,00	0,00	0,00	0,00
Mg	2,32	2,42	1,70	1,61	1,79	1,63	1,65	1,57	1,72	1,48
Ca	1,40	1,44	1,84	1,85	1,77	1,82	1,92	1,83	1,88	1,46
Na	0,66	0,73	0,43	0,54	0,41	0,53	0,47	0,51	0,47	0,40
K	0,27	0,26	0,28	0,29	0,29	0,56	0,28	0,28	0,28	0,61
TOTAL	15,33	15,43	15,55	15,56	15,48	15,74	15,55	15,38	15,51	15,40
Mg#	55,70	57,99	43,29	43,05	45,24	43,15	43,40	45,34	45,45	42,44

	21	22	23	24	25	26
Sample	Xe14 (R1_3)	Xe14 (R1_4)	Xe14 (R1_7)	Xe16 (R3_1)	Xe16 (R3_2)	Xe16 (R3_5)
SiO_2	59,02	54,51	54,01	43,83	44,18	43,40
TiO_2	4,38	3,42	3,79	3,30	3,09	3,02
Al_2O_3	0,00	0,00	0,00	13,04	12,84	12,97
Cr_2O_3	0,00	0,00	0,00	0,00	0,00	0,00
FeO	7,85	19,06	18,46	14,86	15,00	15,67
MnO	0,00	0,92	0,93	0,00	0,00	0,00
MgO	15,58	9,26	10,00	11,30	11,51	11,27
CaO	1,03	2,35	2,17	9,46	9,37	9,77
Na_2O	7,45	6,06	6,03	2,58	2,43	2,34
K_2O	4,69	4,42	4,63	1,63	1,59	1,57
total	100,00	100,00	100,00	100,00	100,00	100,00
Number of cations on the basis of 23 oxygen atoms						
Si	8,19	8,04	7,96	6,35	6,40	6,32
Al	0,00	0,00	0,00	1,65	1,60	1,68
Al	0,00	0,00	0,00	0,58	0,59	0,55
Fe(iii)	0,00	0,00	0,00	0,00	0,00	0,00
Ti	0,46	0,38	0,42	0,36	0,34	0,33
Cr	0,00	0,00	0,00	0,00	0,00	0,00
Fe(ii)	0,91	2,35	2,28	1,80	1,82	1,91
Mn	0,00	0,12	0,12	0,00	0,00	0,00
Mg	3,22	2,04	2,20	2,44	2,49	2,45
Ca	0,15	0,37	0,34	1,47	1,45	1,53
Na	2,00	1,73	1,72	0,72	0,68	0,66
K	0,83	0,83	0,87	0,30	0,29	0,29
TOTAL	15,77	15,86	15,91	15,68	15,66	15,71
Mg#	77,96	45,22	47,90	57,55	57,78	56,18

Mg#= magnesium ratio

1-5 Accessory, subhedral, brownish in ppl (=plain polarized light)

6-12 Pale yellow-brownish to yellow pleochroic ppl, abundant tiny inclusions with varying density.

13-20 Pale yellow-brownish to yellow pleochroic ppl.

21-23 Accessory, subhedral, occurs with accessory alkalic pyroxene, TiO_2, and barite

24-26 Accessory, brownish-yellow ppl, alteration product?

Table 3 carbonate analyses

	1	2	3	4	5	6	7	8	9	10
	P3	P3	P3	P3	P4	P8	P9	Xe1	Xe1	Xe2
Sample	(R1_8)	(R1_9)	(R2_7)	(R2_11)	(R2_7)	(R1_12)	(R1_4)	(R1_2)	(R2_4)	(R1_6)
FeO	25,65	18,10	21,93	20,03	7,00	13,76	1,36	1,91	33,98	1,06
MnO	0,00	0,00	1,18	1,21	3,98	1,49	0,00	0,00	1,24	1,82
MgO	16,30	20,65	18,78	19,72	30,61	26,71	0,00	0,00	15,40	0,00
CaO	58,04	60,86	58,11	59,05	58,41	57,46	98,64	98,09	49,37	97,12
SrO	0,00	0,39	0,00	0,00	0,00	0,00	0,00	0,00	0,00	0,00
total	99,99	100,00	100,00	100,01	100,00	99,42	100,00	100,00	99,99	100,00
The number of cations on the basis of 6 oxygen atoms										
Fe	0,51	0,36	0,44	0,40	0,14	0,28	0,03	0,04	0,68	0,02
Mn	0,00	0,00	0,02	0,02	0,08	0,03	0,00	0,00	0,02	0,04
Mg	0,33	0,41	0,38	0,39	0,61	0,53	0,00	0,00	0,31	0,00
Ca	1,16	1,22	1,16	1,18	1,17	1,15	1,97	1,96	0,99	1,94
Sr	0,00	0,01	0,00	0,00	0,00	0,00	0,00	0,00	0,00	0,00
Total	2,00	2,00	2,00	2,00	2,00	1,99	2,00	2,00	2,00	2,00
Mg/Ca	0,28	0,34	0,32	0,33	0,52	0,46	0,00	0,00	0,31	0,00
Fe/Ca	0,44	0,30	0,38	0,34	0,12	0,24	0,01	0,02	0,69	0,01

	11	12	13	14	15	16	17	18	19	20
	Xe2	Xe3	Xe4	Xe4	Xe4	Xe4	Xe5	Xe5	Xe6	Xe7
Sample	(R2_1)	(R2_3)	(R1_5)	(R1_7)	(R2_5)	(R3_4)	(R1_2)	(R2_2)	(R1_1)	(R1_2)
FeO	0,00	0,00	32,98	32,47	34,97	3,41	26,66	29,26	0,91	0,00
MnO	0,00	2,35	2,20	1,93	0,89	0,83	0,00	0,00	0,00	0,87
MgO	0,00	0,00	13,33	12,74	15,29	0,00	17,98	15,35	0,00	0,00
CaO	100,00	97,48	51,49	52,86	48,85	95,55	55,26	55,38	99,09	99,13
SrO	0,00	0,18	0,00	0,00	0,00	0,20	0,10	0,00	0,00	0,00
total	100,00	100,01	100,00	100,00	100,00	99,99	100,00	99,99	100,00	100,00
The number of cations on the basis of 6 oxygen atoms										
Fe	0,00	0,00	0,66	0,65	0,70	0,07	0,53	0,59	0,02	0,00
Mn	0,00	0,05	0,04	0,04	0,02	0,02	0,00	0,00	0,00	0,02
Mg	0,00	0,00	0,27	0,25	0,31	0,00	0,36	0,31	0,00	0,00
Ca	2,00	1,95	1,03	1,06	0,98	1,91	1,11	1,11	1,98	1,98
Sr	0,00	0,00	0,00	0,00	0,00	0,00	0,00	0,00	0,00	0,00
Total	2,00	2,00	2,00	2,00	2,00	2,00	2,00	2,00	2,00	2,00
Mg/Ca	0,00	0,00	0,26	0,24	0,31	0,00	0,33	0,28	0,00	0,00
Fe/Ca	-	-	0,64	0,61	0,72	0,04	0,48	0,53	0,01	-

	21	22	23	24	25	26	27	28	29	30	31
	Xe7	Xe11	Xe12	Xe13	Xe13	Xe14	Xe15	Xe15	Xe15_2	Xe16	Xe16
Sample	(R2_1)	(R1_4)	(R2_1)	(R1_8)	(R3_2)	(R1_6)	(R2_2)	(R4_6)	(R1_1)	(R1_4)	(R4_4)
FeO	0,73	0,00	0,00	26,95	28,64	11,84	0,00	0,00	0,00	0,00	0,00
MnO	2,73	0,00	0,00	1,48	1,67	1,02	0,00	0,00	0,00	1,45	0,00
MgO	1,02	0,39	0,00	17,17	19,38	27,91	0,00	0,00	0,00	0,00	0,34
CaO	95,51	99,61	99,91	54,39	50,30	59,23	100,00	96,73	99,76	98,42	99,66
SrO	0,00	0,00	0,09	0,00	0,00	0,00	0,00	3,27	0,24	0,13	0,00
total	99,99	100,00	100,00	99,99	99,99	100,00	100,00	100,00	100,00	100,00	100,00
The number of cations on the basis of 6 oxygen atoms											
Fe	0,01	0,00	0,00	0,54	0,57	0,24	0,00	0,00	0,00	0,00	0,00
Mn	0,05	0,00	0,00	0,03	0,03	0,02	0,00	0,00	0,00	0,03	0,00
Mg	0,02	0,01	0,00	0,34	0,39	0,56	0,00	0,00	0,00	0,00	0,01
Ca	1,91	1,99	2,00	1,09	1,01	1,18	2,00	1,93	2,00	1,97	1,99
Sr	0,00	0,00	0,00	0,00	0,00	0,00	0,00	0,07	0,00	0,00	0,00
Total	2,00	2,00	2,00	2,00	2,00	2,00	2,00	2,00	2,00	2,00	2,00
Mg/Ca	0,01	0,00	0,00	0,32	0,39	0,47	0,00	0,00	0,00	0,00	0,00
Fe/Ca	0,01	-	-	0,64	1,48	0,42	-	-	-	-	-

Table 4 Garnet analyses

	1	2	3	4	5	6	7	8	9	10
Sample	P7 (R4_1)	P7 (R4_2)	Xe4 (R4_1)	Xe9 (R2_1)	Xe9 (R2_6)	Xe13 (R4_1)	Xe13 (R4_2)	Xe16 (R2_6)	Xe16 (R5_3)	Xe16 (R5_5)
SiO_2	40,76	40,74	39,00	39,12	39,08	39,28	39,34	39,72	39,95	39,90
TiO_2	0,00	0,00	0,00	0,00	0,00	0,00	0,00	0,00	0,00	0,00
Al_2O_3	22,20	21,65	20,63	21,32	21,19	22,21	22,05	22,14	21,65	21,85
FeO	21,34	21,74	25,57	24,55	24,55	29,37	29,68	22,82	23,42	23,10
MnO	0,94	1,10	4,51	4,50	4,95	0,42	0,00	0,81	1,09	1,06
MgO	9,04	9,07	4,68	3,58	3,65	6,92	7,35	8,58	8,25	8,71
CaO	5,72	5,70	5,61	6,93	6,58	1,81	1,58	5,93	5,64	5,38
Total	100,00	100,00	100,00	100,00	100,00	100,00	100,00	100,00	100,00	100,00
Number of cations on the basis of 24 oxygen atoms										
Si	6,15	6,17	6,13	6,14	6,14	6,08	6,09	6,05	6,11	6,08
Ti	0,00	0,00	0,00	0,00	0,00	0,00	0,00	0,00	0,00	0,00
Al	3,95	3,86	3,82	3,94	3,92	4,05	4,02	3,98	3,90	3,93
Fe(2+)	2,69	2,75	3,36	3,22	3,22	3,80	3,84	2,91	2,99	2,95
Mn	0,12	0,14	0,60	0,60	0,66	0,05	0,00	0,10	0,14	0,14
Mg	2,03	2,05	1,10	0,84	0,85	1,60	1,70	1,95	1,88	1,98
Ca	0,92	0,92	0,95	1,16	1,11	0,30	0,26	0,97	0,92	0,88
Total	15,87	15,90	15,96	15,89	15,90	15,89	15,90	15,96	15,94	15,95
End-members per cent										
Pyp	35,24	34,91	18,29	14,38	14,61	28,34	29,25	32,87	31,65	33,31
Alm	46,66	46,93	55,97	55,33	55,17	65,85	66,22	49,04	50,42	49,57
Gro	16,02	15,76	15,75	20,01	18,95	5,82	4,52	16,32	15,55	14,80
Spe	2,08	2,40	10,00	10,28	11,26	0,00	0,00	1,77	2,38	2,31
Total	100,00	100,00	100,00	100,00	100,00	100,00	100,00	100,00	100,00	100,00

	11	12	13	14	15	16	17	18	19	20
Sample	Xe15 (R1_1)	Xe15 (R1_2)	Xe15 (R1_14)	Xe15 (R1_15)	Xe15 (R1_16)	Xe15 (R1_18)	Xe15 (R2_1)	Xe15 (R2_4)	Xe15 (R2_6)	Xe15 (R3_3)
SiO_2	36,12	27,91	37,10	33,71	31,79	32,41	30,37	27,44	31,09	31,81
TiO_2	4,65	16,79	3,90	3,09	4,21	3,38	12,19	15,78	12,58	9,81
Al_2O_3	2,14	0,48	2,60	2,31	4,02	2,08	6,07	5,88	4,14	4,61
FeO	22,75	18,35	22,44	24,50	23,95	25,44	17,81	17,53	18,18	19,90
MnO	0,00	0,00	0,00	0,00	0,00	0,00	0,00	0,00	0,00	0,00
MgO	0,78	1,24	0,64	0,31	0,50	0,22	0,43	0,36	1,07	0,61
CaO	33,56	31,38	33,31	36,08	35,52	36,47	33,14	33,02	32,94	33,27
ZrO2	0,00	3,85	0,00	0,00	0,00	0,00	0,00	0,00	0,00	0,00
Total	100,00	100,00	100,00	100,00	100,00	100,00	100,01	100,00	100,00	100,00
Number of cations on the basis of 24 oxygen atoms										
Si	6,23	5,05	6,36	5,96	5,62	5,79	5,18	4,72	5,31	5,47
Ti	0,60	2,28	0,50	0,41	0,56	0,45	1,56	2,04	1,62	1,27
Al	0,43	0,10	0,53	0,48	0,84	0,44	1,22	1,19	0,83	0,93
Fe2+	1,94	1,88	1,97	1,70	1,60	1,71	1,60	1,59	1,65	1,71
Fe3+	1,34	0,89	1,25	1,92	1,94	2,10	0,94	0,93	0,95	1,14
Mn	0,00	0,00	0,00	0,00	0,00	0,00	0,00	0,00	0,00	0,00
Mg	0,20	0,33	0,16	0,08	0,13	0,06	0,11	0,09	0,27	0,16
Ca	6,20	6,08	6,11	6,83	6,72	6,98	6,05	6,08	6,03	6,12
Total	16,95	16,62	16,88	17,39	17,41	17,53	16,65	16,65	16,66	16,80
End-members per cent										
Pyp	2,41	4,03	1,99	0,96	1,57	0,67	1,41	1,19	3,44	1,95
Alm	23,22	22,66	23,85	19,77	18,93	19,49	20,58	20,46	20,76	21,44
Gro	13,57	2,31	17,11	13,56	19,96	11,68	25,54	22,41	18,60	21,37
Spe	0,00	0,00	0,00	0,00	0,00	0,00	0,00	0,00	0,00	0,00
And	60,80	71,00	57,05	65,70	59,54	68,15	52,46	55,93	57,21	55,25
Total	100,00	100,00	100,00	100,00	100,00	100,00	100,00	100,00	100,00	100,00

	21	22	23	24	25	26	27	28	29
	Xe15	Xe15	Xe15	Xe15	Xe15	Xe15	Xe15	Xe15.2	Xe15.2
Sample	(R3_4)	(R3_5)	(R6_1)	(R6_2)	(R6_3)	(R6_4)	(R6_12)	(R1_2)	(R2_2)
SiO_2	30,06	28,14	23,11	23,93	34,88	35,64	32,40	27,94	31,07
TiO_2	12,59	15,23	18,57	17,35	0,81	0,00	4,53	18,47	13,71
Al_2O_3	5,17	5,42	1,18	0,86	3,70	6,37	1,84	0,00	0,00
FeO	18,44	17,78	18,93	20,47	23,14	19,99	25,00	19,05	21,62
MnO	0,00	0,00	0,00	0,00	0,00	0,00	0,00	0,00	0,00
MgO	0,00	0,53	1,06	0,74	0,25	0,00	0,40	0,98	0,00
CaO	33,74	32,90	32,55	32,94	37,22	37,99	35,83	33,55	33,60
ZrO2	0,00	0,00	4,60	3,71	0,00	0,00	0,00	0,00	0,00
Total	100,00	100,00	100,00	100,00	100,00	100,00	100,00	100,00	100,00
Number of cations on the basis of 24 oxygen atoms									
Si	5,16	4,84	4,32	4,45	6,11	6,11	5,77	4,89	5,45
Ti	1,63	1,97	2,61	2,43	0,11	0,00	0,61	2,43	1,81
Al	1,05	1,10	0,26	0,19	0,76	1,29	0,39	0,00	0,00
Fe2+	1,66	1,62	1,62	1,74	1,45	1,13	1,75	1,82	2,11
Fe3+	0,99	0,93	1,34	1,45	1,94	1,73	1,97	0,97	1,06
Mn	0,00	0,00	0,00	0,00	0,00	0,00	0,00	0,00	0,00
Mg	0,00	0,13	0,30	0,21	0,07	0,00	0,11	0,26	0,00
Ca	6,21	6,06	6,51	6,57	6,98	6,98	6,84	6,30	6,31
Total	16,69	16,65	16,95	17,03	17,41	17,24	17,43	16,67	16,74
End-members per cent									
Pyp	0,00	1,72	3,50	2,43	0,78	0,00	1,22	3,06	0,00
Alm	21,06	20,75	19,20	20,43	17,04	13,98	20,18	21,77	25,02
Gro	22,55	21,27	4,80	0,00	22,31	36,69	10,25	0,00	0,00
Spe	0,00	0,00	0,00	3,59	0,00	0,00	0,00	0,00	0,00
And	56,39	56,26	72,50	73,55	59,88	49,33	68,35	75,17	74,98
Total	100,00	100,00	100,00	100,00	100,00	100,00	100,00	100,00	100,00

KEY: Pyp=pyrope Alm=almandine Gro=grossulare Spe=spessartine And=andradite in molecular percentages. Oxide proportions are in weight percents End-members per cent = molecular proportion of the end-member. Analysis point in the core: 12,14,15,21,23,24. In rim: 11,13,16,20,22. In colourless rim: 25,26,27.

Table 5 mica analyses

	1	2	3	4	5	6	7	8	9	10
	P2			P3	P3	P3	P3	P3	P4	P6
Sample	(R2_6)	P3 (k2_1)	P3 (k2_2)	(R2_4)	(R2_6)	(R2_15)	(R3_5)	(R3_6)	(R2_2)	(R3_3)
SiO_2	39,49	43,35	43,03	42,63	42,52	41,97	42,43	41,28	40,50	37,43
TiO_2	3,74	10,70	11,69	10,67	11,24	11,05	8,98	8,86	3,03	2,01
Al_2O_3	16,12	9,99	10,02	10,03	9,85	10,48	11,67	12,56	15,92	12,98
FeO	16,19	9,34	9,78	10,11	10,22	11,11	7,64	7,45	12,93	30,03
MnO	0,00	0,00	0,00	0,00	0,00	0,00	0,00	0,00	0,00	0,00
MgO	14,73	14,36	13,80	14,18	13,81	13,41	19,22	19,42	17,75	7,03
BaO	0,00	0,00	0,00	0,00	0,00	0,00	0,00	0,00	0,00	0,00
K_2O	9,72	12,27	11,68	12,38	12,36	11,98	10,06	10,43	9,86	10,52
total	100,00	100,01	100,00	100,00	100,00	100,00	100,00	100,00	100,00	100,00
Numbers of cations on the basis of 22 anions.										
Si	5,61	6,06	6,01	5,99	5,98	5,92	5,82	5,68	5,67	5,75
Al (Z)	2,39	1,64	1,65	1,66	1,63	1,74	1,89	2,04	2,33	2,25
Al (Y)	0,31	0,00	0,00	0,00	0,00	0,00	0,00	0,00	0,29	0,10
Ti	0,40	1,12	1,23	1,13	1,19	1,17	0,93	0,92	0,32	0,23
Fe(ii)	1,92	1,09	1,14	1,19	1,20	1,31	0,88	0,86	1,51	3,86
Mn	0,00	0,00	0,00	0,00	0,00	0,00	0,00	0,00	0,00	0,00
Mg	3,12	2,99	2,87	2,97	2,90	2,82	3,93	3,98	3,70	1,61
K	1,76	2,19	2,08	2,22	2,22	2,15	1,76	1,83	1,76	2,06
Ba	0,00	0,00	0,00	0,00	0,00	0,00	0,00	0,00	0,00	0,00
total	15,52	15,09	14,98	15,16	15,12	15,12	15,19	15,30	15,58	15,87
Mg#	61,86	73,27	71,56	71,43	70,67	68,27	81,77	82,29	71,00	29,45

	11	12	13	14	15	16	17	18	19	20
	P6	P8	P8	P8	P8	P8	P8	Xe11	Xe11	Xe11
Sample	(R4_1)	(R1_6)	(R1_7)	(R2_6)	(R4_12)	(R5_10)	(R5_11)	(R1_5)	(R2_1)	(R2_2)
SiO_2	38,97	39,92	37,82	42,80	39,69	38,15	38,16	36,65	38,66	38,98
TiO_2	6,13	6,74	3,83	0,62	4,48	4,14	0,00	5,72	5,77	6,28
Al_2O_3	12,34	10,01	8,05	12,73	8,20	8,56	16,09	7,35	14,69	14,43
FeO	21,57	24,61	33,17	22,81	31,70	34,06	27,02	31,69	18,05	17,17
MnO	0,00	0,42	0,99	0,00	0,00	0,00	0,93	0,82	0,00	0,00
MgO	10,12	9,14	6,57	12,03	6,49	5,31	9,91	6,68	10,97	11,51
BaO	0,00	0,00	9,57	9,02	9,44	9,77	7,90	11,09	11,86	11,62
K_2O	10,86	9,17	0,00	0,00	0,00	0,00	0,00	0,00	0,00	0,00
total	100,00	100,00	100,00	100,00	100,00	100,00	100,00	100,00	100,00	100,00
Numbers of cations on the basis of 22 anions.										
Si	5,75	5,93	5,94	6,20	6,11	5,98	5,67	5,80	5,63	5,65
Al (Z)	2,15	1,75	1,49	1,80	1,49	1,58	2,33	1,37	2,37	2,35
Al (Y)	0,00	0,00	0,00	0,38	0,00	0,00	0,49	0,00	0,16	0,11
Ti	0,68	0,75	0,45	0,07	0,52	0,49	0,00	0,68	0,63	0,68
Fe(ii)	2,66	3,06	4,36	2,76	4,08	4,47	3,36	4,19	2,20	2,08
Mn	0,00	0,05	0,13	0,00	0,00	0,00	0,12	0,11	0,00	0,00
Mg	2,23	2,02	1,54	2,60	1,49	1,24	2,20	1,58	2,38	2,49
K	2,04	1,74	1,92	1,67	1,86	1,95	1,50	2,24	2,20	2,15
BaO	0,00	0,00	0,00	0,00	0,00	0,00	0,00	0,00	0,00	0,00
Total	15,52	15,31	15,82	15,48	15,55	15,72	15,67	15,96	15,57	15,51
Mg#	45,55	39,42	25,53	48,46	26,73	21,76	38,73	26,81	52,01	54,44

Sample	21 Xe11 (R2_10)	22 Xe15 (R3_6)	23 Xe15 (R3_7)	24 Xe15 (R4_1)	25 Xe15 (R4_3)	26 Xe15 (R6_8)
SiO_2	36,83	38,88	37,92	40,48	39,98	42,19
TiO_2	5,90	0,00	0,00	1,74	1,63	0,00
Al_2O_3	9,91	18,36	18,83	14,86	14,81	14,30
FeO	30,35	7,48	6,71	12,50	13,44	12,91
MnO	0,00	0,00	0,00	0,00	0,00	0,59
MgO	5,78	22,52	22,78	18,91	19,64	17,46
BaO	11,24	9,78	9,72	10,08	9,23	11,59
K_2O	0,00	2,98	4,04	1,43	1,28	0,96
total	100,00	100,00	100,00	100,00	100,01	100,00
Numbers of cations on the basis of 22 anions.						
Si	5,74	5,43	5,33	5,73	5,66	6,00
Al (Z)	1,82	2,57	2,67	2,27	2,34	2,00
Al (Y)	0,00	0,46	0,45	0,21	0,13	0,39
Ti	0,69	0,00	0,00	0,19	0,17	0,00
Fe(ii)	3,95	0,87	0,79	1,48	1,59	1,53
Mn	0,00	0,00	0,00	0,00	0,00	0,07
Mg	1,34	4,69	4,77	3,99	4,14	3,70
K	2,23	1,74	1,74	1,82	1,67	2,10
BaO	0,00	0,16	0,22	0,08	0,07	0,05
Total	15,78	15,93	15,98	15,76	15,70	15,80
Mg#	25,34	84,30	85,82	72,95	72,26	69,74

KEY: Oxides in weight percentages. Al(Z)=aluminium in Z site. Al(Y)=aluminium in Y site.
Mg#=magnesium ratio (Mg/(Mg+Fe+Mn

Table 6 plagioclase analyses

Sample	1 P1 (R2_1)	2 P1 (R2_6)	3 P2 (R1_1)	4 P2 (R1_4)	5 P2 (R2_2)	6 P2 (R3_2)	7 P2 (R3_3)	8 P6 (R1_4)	9 P6 (R1_5)	10 P6 (R4_4)
SiO_2	68,60	69,05	64,81	62,26	59,14	59,75	59,71	56,51	68,41	57,83
Al_2O_3	19,36	19,38	27,30	26,02	28,55	25,63	25,56	26,45	25,21	26,29
FeO	0,00	0,00	0,00	0,00	0,00	0,00	0,00	0,40	0,00	0,00
CaO	0,00	0,00	7,27	3,71	2,57	7,08	6,80	13,18	0,00	11,49
Na_2O	12,04	11,57	0,00	7,06	5,58	6,81	7,54	2,69	6,39	2,98
K_2O	0,00	0,00	0,62	0,95	4,16	0,73	0,39	0,78	0,00	1,41
Total	100,00	100,00	100,00	100,00	100,00	100,00	100,00	100,00	100,01	100,00
Number of cations on the basis of 32 oxygen atoms										
Si	11,99	12,04	9,45	10,95	10,54	10,65	10,65	10,20	10,00	10,38
Al	3,99	3,98	7,96	5,39	6,00	5,39	5,37	5,62	7,37	5,56
Fe	0,00	0,00	0,00	0,00	0,00	0,00	0,00	0,06	0,00	0,00
Ca	0,00	0,00	1,06	0,70	0,49	1,35	1,30	2,55	0,00	2,21
Na	4,08	3,91	0,00	2,41	1,93	2,35	2,61	0,94	1,87	1,04
K	0,00	0,00	0,18	0,21	0,95	0,17	0,09	0,18	0,00	0,32
Total	20,06	19,93	18,66	19,66	19,90	19,91	20,01	19,55	19,24	19,52
End-members per cent										
An	0,00	0,00	100,00	21,05	14,58	34,91	32,50	69,49	0,00	61,90
Ab	100,00	100,00	0,00	72,50	57,29	60,78	65,27	25,61	100,00	29,06
Or	0,00	0,00	0,00	6,45	28,13	4,31	2,23	4,89	0,00	9,03

	11	12	13	14	15	16	17	18	19	20
	P6	P6	P6	P7	P7	P7	P8	P8	P8	P8
Sample	(R4_6)	(R4_7)	(R4_8)	(R2_1)	(R2_3)	(R3_9)	(R1_5)	(R2_1)	(R4_9)	(R4_10)
SiO_2	62,52	61,72	61,68	59,66	67,22	62,79	58,83	63,79	64,05	64,10
Al_2O_3	23,79	24,31	24,12	27,74	18,98	23,95	27,51	22,75	24,12	22,65
FeO	0,00	0,00	0,00	1,25	0,41	0,00		0,00	0,00	0,00
CaO	9,20	9,67	9,94	0,62	1,87	2,43	1,15	3,75	0,65	3,13
Na_2O	3,91	3,69	3,70	5,46	11,36	8,10	12,22	9,11	6,29	9,17
K_2O	0,58	0,62	0,56	5,28	0,17	2,74	0,28	0,60	4,90	0,96
Total	100,00	100,00	100,00	100,00	100,00	100,00	100,00	100,00	100,01	100,01
Number of cations on the basis of 32 oxygen atoms										
Si	11,05	10,93	10,93	10,68	11,85	11,16	10,49	11,28	11,35	11,33
Al	4,95	5,07	5,04	5,85	3,94	5,01	5,78	4,74	5,04	4,72
Fe	0,00	0,00	0,00	0,19	0,06	0,00	0,00	0,00	0,00	0,00
Ca	1,74	1,83	1,89	0,12	0,35	0,46	0,22	0,71	0,12	0,59
Na	1,34	1,27	1,27	1,89	3,88	2,79	4,22	3,12	2,16	3,14
K	0,13	0,14	0,13	1,21	0,04	0,62	0,06	0,14	1,11	0,22
Total	19,21	19,24	19,25	19,94	20,13	20,04	20,77	19,98	19,77	19,99
End-members per cent										
An	54,19	56,63	57,47	3,67	8,26	11,94	4,87	17,90	3,64	15,00
Ab	41,71	39,07	38,66	58,83	90,85	72,05	93,70	78,69	63,71	79,52
Or	4,10	4,30	3,87	37,50	0,89	16,01	1,43	3,41	32,65	5,48

	21	22	23	24	25	26	27	28	29	30
	P9	P9	P9	P9	Xe1	Xe1	Xe1	Xe1	Xe1	Xe3
Sample	(R1_1)	(R1_2)	(R1_3)	(R1_5)	(R1_3)	(R1_4)	(R2_5)	(R4_3)	(R4_4)	(R1_4)
SiO_2	64,33	65,73	67,04	65,52	62,13	62,44	66,31	59,13	63,93	63,11
Al_2O_3	22,77	22,94	21,55	22,96	24,17	23,59	24,11	25,15	22,89	22,91
FeO	0,00	0,00	0,00	0,00	0,00	0,00	0,00	0,72	0,00	0,00
CaO	4,59	0,88	1,88	1,12	5,59	5,56	0,00	7,29	3,58	4,16
Na_2O	7,51	8,25	8,97	8,36	7,42	7,65	8,03	7,21	8,93	8,54
K_2O	0,79	2,20	0,56	2,05	0,68	0,76	1,55	0,49	0,67	1,29
Total	99,99	100,00	100,00	100,01	100,00	100,00	100,00	100,00	100,00	100,00
Number of cations on the basis of 32 oxygen atoms										
Si	11,34	11,53	11,71	11,50	11,01	11,07	11,53	10,60	11,29	11,20
Al	4,73	4,74	4,44	4,75	5,05	4,93	4,94	5,32	4,76	4,79
Fe	0,00	0,00	0,00	0,00	0,00	0,00	0,00	0,11	0,00	0,00
Ca	0,87	0,17	0,35	0,21	1,06	1,06	0,00	1,40	0,68	0,79
Na	2,57	2,81	3,04	2,85	2,55	2,63	2,71	2,51	3,06	2,94
K	0,18	0,49	0,12	0,46	0,15	0,17	0,34	0,11	0,15	0,29
Total	19,67	19,74	19,66	19,77	19,82	19,86	19,52	20,05	19,94	20,02
End-members per cent										
An	24,01	4,78	10,01	5,99	28,19	27,36	0,00	34,83	17,41	19,67
Ab	71,08	81,01	86,44	80,95	67,70	68,20	88,75	62,36	78,71	73,08
Or	4,92	14,21	3,55	13,06	4,11	4,44	11,25	2,81	3,88	7,25

	31	32	33	34	35	36	37	38	39	40
Sample	Xe3 (R1_5)	Xe3 (R3_2)	Xe3 (R3_3)	Xe4 (R1_1)	Xe4 (R1_2)	Xe4 (R2_1)	Xe4 (R2_2)	Xe4 (R3_6)	Xe4 (R3_7)	Xe5 (R1_5)
SiO_2	64,27	63,86	63,55	62,55	62,32	67,32	62,17	67,77	65,91	60,79
Al_2O_3	22,81	22,78	22,81	23,75	23,71	21,06	23,77	20,58	22,07	25,06
FeO	0,42	0,00	0,00	0,00	0,00	0,00	0,00	0,00	0,00	0,00
CaO	1,01	3,83	4,26	5,16	4,84	0,45	5,23	0,00	1,34	6,13
Na_2O	7,13	8,82	8,58	7,95	8,54	10,36	7,87	10,85	9,49	7,20
K_2O	4,35	0,71	0,81	0,59	0,59	0,81	0,96	0,80	1,20	0,82
Total	100,00	100,00	100,00	100,00	100,00	100,00	100,00	100,00	100,01	100,00
Number of cations on the basis of 32 oxygen atoms										
Si	11,43	11,28	11,25	11,08	11,05	11,78	11,04	11,85	11,57	10,81
Al	4,78	4,74	4,76	4,96	4,96	4,34	4,97	4,24	4,57	5,25
Fe	0,06	0,00	0,00	0,00	0,00	0,00	0,00	0,00	0,00	0,00
Ca	0,19	0,73	0,81	0,98	0,92	0,08	0,99	0,00	0,25	1,17
Na	2,46	3,02	2,94	2,73	2,94	3,51	2,71	3,68	3,23	2,48
K	0,99	0,16	0,18	0,13	0,13	0,18	0,22	0,18	0,27	0,19
Total	19,91	19,93	19,94	19,88	20,00	19,90	19,94	19,95	19,89	19,90
End-members per cent										
An	5,30	18,58	20,53	25,48	23,05	2,23	25,37	0,00	6,72	30,43
Ab	67,55	77,31	74,82	71,05	73,60	92,98	69,09	95,37	86,12	64,71
Or	27,14	4,11	4,64	3,47	3,35	4,78	5,54	4,63	7,16	4,86

	41	42	43	44	45	46	47	48	49	50
Sample	Xe6 (R1_3)	Xe6 (R1_4)	Xe6 (R1_5)	Xe6 (R2_1)	Xe6 (R2_2)	Xe9 (R1_3)	Xe9 (R1_4)	Xe9 (R2_7)	Xe9 (R3_2)	Xe10 (R1_1)
SiO_2	66,09	64,06	64,50	64,28	68,29	61,80	64,83	65,86	66,64	61,91
Al_2O_3	21,29	22,58	22,32	22,32	20,37	23,71	22,65	22,73	23,02	24,17
FeO	0,00	0,00	0,00	0,00	0,00	0,00	0,00	0,34	0,00	0,00
CaO	1,25	3,12	3,19	3,18	0,42	5,83	1,69	0,00	0,00	5,20
Na_2O	10,86	9,21	9,77	9,89	10,74	8,65	9,84	9,18	9,32	7,88
K_2O	0,51	1,03	0,23	0,33	0,18	0,00	0,99	1,88	1,01	0,84
Total	100,00	100,00	100,00	100,00	100,00	100,00	100,00	100,00	100,00	100,00
Number of cations on the basis of 32 oxygen atoms										
Si	11,62	11,33	11,37	11,35	11,90	10,98	11,42	11,56	11,61	10,99
Al	4,41	4,71	4,64	4,65	4,18	4,96	4,70	4,70	4,73	5,06
Fe	0,00	0,00	0,00	0,00	0,00	0,00	0,00	0,05	0,00	0,00
Ca	0,23	0,59	0,60	0,60	0,08	1,11	0,32	0,00	0,00	0,99
Na	3,70	3,16	3,34	3,39	3,63	2,98	3,36	3,13	3,15	2,71
K	0,11	0,23	0,05	0,07	0,04	0,00	0,22	0,42	0,22	0,19
Total	20,08	20,01	20,00	20,06	19,84	20,03	20,02	19,86	19,71	19,93
End-members per cent										
An	5,80	14,85	15,08	14,80	2,11	27,14	8,18	0,00	0,00	25,43
Ab	91,37	79,32	83,64	83,38	96,84	72,86	86,13	88,13	93,33	69,65
Or	2,83	5,84	1,28	1,82	1,05	0,00	5,69	11,87	6,67	4,91

	51	52	53	54	55	56	57	58	59	60
Sample	Xe10 (R2_7)	Xe10 (R2_9)	Xe10 (R3_2)	Xe10 (R4_1)	Xe10 (R4_2)	Xe10 (R4_6)	Xe10 (R5_5)	Xe11_2(R1_1)	Xe11_2(R1_2)	Xe11_2(R1_3)
SiO_2	61,69	54,66	61,56	61,86	61,60	61,72	63,15	62,50	65,56	67,38
Al_2O_3	24,20	28,71	24,19	24,09	24,16	24,16	23,19	26,18	22,38	22,24
FeO	0,00	0,63	0,00	0,00	0,00	0,00	0,39	0,00	0,00	0,00
CaO	5,42	11,13	5,43	5,66	5,56	5,48	6,60	0,70	4,14	0,99
Na_2O	7,98	4,56	8,05	7,65	7,87	7,82	5,84	10,62	7,01	7,23
K_2O	0,71	0,32	0,76	0,74	0,82	0,82	0,84	0,00	0,92	2,16
Total	100,00	100,00	100,00	100,00	100,00	100,00	100,00	100,00	100,00	100,00
Number of cations on the basis of 32 oxygen atoms										
Si	10,96	9,87	10,94	10,98	10,95	10,97	11,17	10,97	11,50	11,75
Al	5,07	6,11	5,07	5,04	5,06	5,06	4,83	5,41	4,62	4,57
Fe	0,00	0,10	0,00	0,00	0,00	0,00	0,06	0,00	0,00	0,00
Ca	1,03	2,15	1,03	1,08	1,06	1,04	1,25	0,13	0,78	0,18
Na	2,75	1,60	2,77	2,63	2,71	2,69	2,00	3,61	2,38	2,44
K	0,16	0,07	0,17	0,17	0,19	0,19	0,19	0,00	0,21	0,48
Total	19,96	19,90	20,00	19,90	19,97	19,94	19,51	20,13	19,49	19,43
End-members per cent										
An	26,17	56,32	25,98	27,75	26,74	26,61	36,33	3,52	23,09	5,95
Ab	69,73	41,77	69,66	67,92	68,56	68,67	58,17	96,48	70,80	78,63
Or	4,10	1,91	4,35	4,34	4,69	4,72	5,50	0,00	6,11	15,43

	61	62	63	64	65
Sample	Xe16 (R1_2)	Xe16 (R1_6)	Xe16 (R2_7)	Xe16 (R2_8)	Xe16 (R5_6)
SiO_2	62,73	62,87	62,67	62,51	63,61
Al_2O_3	23,37	23,26	23,46	23,37	23,55
FeO	0,00	0,00	0,00	0,00	0,00
CaO	4,12	4,07	4,34	4,28	4,61
Na_2O	8,13	8,19	7,68	8,16	8,23
K_2O	1,65	1,62	1,86	1,67	0,00
Total	100,00	100,00	100,00	100,00	100,00
Number of cations on the basis of 32 oxygen atoms					
Si	11,14	11,17	11,14	11,12	11,20
Al	4,89	4,87	4,91	4,90	4,89
Fe	0,00	0,00	0,00	0,00	0,00
Ca	0,78	0,77	0,83	0,82	0,87
Na	2,80	2,82	2,64	2,81	2,81
K	0,37	0,37	0,42	0,38	0,00
Total	20,00	19,99	19,94	20,03	19,76
End-members per cent					
An	19,80	19,57	21,21	20,34	23,62
Ab	70,73	71,16	67,97	70,20	76,38
Or	9,47	9,27	10,82	9,46	0,00

KEY An=CaAl2Si2O8 Ab=NaAlSi3O8 Or=KAlSi3O8. The oxides are in weight percentages.

Table 7 potassium feldspar analyses

	1	2	3	4	5	6	7	8	9	10
	P1	P1	P1	P1	P2	P3	P5	P5	P5	P5
Sample	(R1_1)	(R2_2)	(R3_1)	(R3_3)	(R1_5)	(R1_4)	(R2_3)	(R2_6)	(R2_9)	(R3_4)
SiO_2	65,2	66,0	65,8	65,7	58,7	64,2	65,9	65,6	65,9	65,6
Al_2O_3	18,9	18,2	18,7	18,8	15,6	15,4	16,7	17,1	18,7	19,2
FeO	0,0	0,0	0,0	0,0	0,0	2,1	2,0	1,5	0,0	0,0
CaO	0,0	0,0	0,0	0,0	0,3	0,0	0,0	0,0	0,0	0,0
Na_2O	0,3	0,3	0,0	0,3	0,3	0,0	0,6	0,8	1,1	2,0
K_2O	15,6	15,5	15,6	15,2	25,2	18,2	14,9	15,0	14,3	13,2
Total	100,0	100,0	100,0	100,0	100,0	100,0	100,0	100,0	100,0	100,0
Number of cations on the basis of 32 oxygen atoms										
Si	12,0	12,1	12,1	12,0	11,6	12,2	12,2	12,1	12,1	12,0
Al	4,1	3,9	4,0	4,1	3,6	3,4	3,6	3,7	4,0	4,1
Fe	0,0	0,0	0,0	0,0	0,0	0,3	0,3	0,2	0,0	0,0
Ca	0,0	0,0	0,0	0,0	0,1	0,0	0,0	0,0	0,0	0,0
Na	0,1	0,1	0,0	0,1	0,1	0,0	0,2	0,3	0,4	0,7
K	3,7	3,6	3,6	3,6	6,4	4,4	3,5	3,5	3,3	3,1
Total	19,8	19,8	19,7	19,8	21,8	20,3	19,9	19,9	19,8	19,9
End-members per cent										
An	0,0	0,0	0,0	0,0	0,9	0,0	0,0	0,0	0,0	0,0
Ab	2,5	2,6	0,0	3,1	1,6	0,0	5,7	7,2	10,1	18,9
Or	97,5	97,4	100,0	96,9	97,5	100,0	94,3	92,8	89,9	81,1

	11	12	13	14	15	16	17	18	19	20
	P8	P8	P8	Xe1	Xe2	Xe2	Xe2	Xe2	Xe2	Xe3
Sample	(R3_7)	(R4_1)	(R4_2)	(R1_5)	(R1_1)	(R1_3)	(R1_4)	(R1_7)	(R2_4)	(R2_1)
SiO_2	65,3	65,0	65,5	72,3	66,8	66,5	66,8	66,9	66,8	67,1
Al_2O_3	18,6	20,6	19,5	15,0	18,7	19,1	18,9	18,9	18,8	18,7
FeO	0,0	0,0	0,0	0,0	0,0	0,0	0,0	0,0	0,0	0,0
CaO	0,0	0,0	0,0	0,0	0,0	0,0	0,0	0,0	0,0	0,0
Na_2O	0,4	0,4	0,3	0,5	4,3	3,9	4,2	4,6	4,5	3,7
K_2O	15,8	14,1	14,7	12,2	10,2	10,5	10,0	9,6	9,9	10,6
Total	100,0	100,0	100,0	100,0	100,0	100,0	100,0	100,0	100,0	100,0
Number of cations on the basis of 32 oxygen atoms										
Si	12,0	11,8	12,0	12,9	12,1	12,0	12,0	12,0	12,0	12,1
Al	4,0	4,4	4,2	3,2	4,0	4,1	4,0	4,0	4,0	4,0
Fe	0,0	0,0	0,0	0,0	0,0	0,0	0,0	0,0	0,0	0,0
Ca	0,0	0,0	0,0	0,0	0,0	0,0	0,0	0,0	0,0	0,0
Na	0,1	0,1	0,1	0,2	1,5	1,4	1,5	1,6	1,6	1,3
K	3,7	3,3	3,4	2,8	2,3	2,4	2,3	2,2	2,3	2,4
Total	19,9	19,7	19,7	19,0	19,9	19,9	19,8	19,8	19,9	19,8
End-members per cent										
An	0,0	0,0	0,0	0,0	0,0	0,0	0,0	0,0	0,0	0,0
Ab	3,4	3,7	3,3	5,3	39,2	36,2	39,1	42,0	40,7	34,5
Or	96,6	96,3	96,7	94,7	60,8	63,8	60,9	58,0	59,3	65,5

	21	22	23	24	25	26	27	28	29	30
Sample	Xe3 (R2_2)	Xe4 (R3_5)	Xe4 (R1_6)	Xe5 (R2_1)	Xe6 (R1_2)	Xe6 (R2_3)	Xe7 (R1_3)	Xe7 (R2_3)	Xe7 (R2_5)	Xe7 (R2_7)
SiO_2	65,8	65,9	66,2	66,8	65,9	67,2	65,7	66,5	66,8	69,3
Al_2O_3	18,7	18,5	18,6	18,5	18,4	18,8	18,6	18,9	18,7	16,7
FeO	0,0	0,0	0,0	0,0	0,0	0,0	0,0	0,0	0,0	0,0
CaO	0,0	0,0	0,0	0,0	0,0	0,0	0,0	0,0	0,0	0,0
Na_2O	1,6	0,0	1,2	2,2	0,4	4,7	0,4	2,5	3,6	0,3
K_2O	13,9	15,6	14,0	12,5	15,3	9,3	15,4	12,1	11,0	13,8
Total	100,0	100,0	100,0	100,0	100,0	100,0	100,0	100,0	100,0	100,0
Number of cations on the basis of 32 oxygen atoms										
Si	12,0	12,1	12,1	12,1	12,1	12,1	12,1	12,1	12,1	12,5
Al	4,0	4,0	4,0	4,0	4,0	4,0	4,0	4,0	4,0	3,6
Fe	0,0	0,0	0,0	0,0	0,0	0,0	0,0	0,0	0,0	0,0
Ca	0,0	0,0	0,0	0,0	0,0	0,0	0,0	0,0	0,0	0,0
Na	0,6	0,0	0,4	0,8	0,1	1,6	0,1	0,9	1,2	0,1
K	3,2	3,6	3,3	2,9	3,6	2,1	3,6	2,8	2,5	3,2
Total	19,9	19,7	19,8	19,7	19,8	19,8	19,8	19,8	19,8	19,3
End-members per cent										
An	0,0	0,0	0,0	0,0	0,0	0,0	0,0	0,0	0,0	0,0
Ab	14,6	0,0	11,4	20,7	3,6	43,3	3,7	24,0	33,0	2,8
Or	85,4	100,0	88,6	79,3	96,4	56,7	96,3	76,0	67,0	97,2

	31	32	33	34	35	36	37	38	39	40
Sample	Xe12 (R1_1)	Xe12 (R2_2)	Xe13 (R2_8)	Xe13 (R3_5)	Xe14 (R1_2)	Xe14 (R1_8)	Xe14 (R3_2)	Xe14 (R3_3)	Xe15 (R1_11)	Xe15 (R2_3)
SiO_2	66,3	66,3	66,5	66,5	66,4	66,0	66,3	66,1	65,8	65,5
Al_2O_3	18,5	18,4	18,3	20,0	15,4	18,2	16,7	17,9	18,1	17,8
FeO	0,0	0,0	0,0	0,0	0,0	0,0	0,0	0,0	0,0	0,0
CaO	0,0	0,0	0,0	0,0	2,4	0,0	1,7	0,6	0,0	0,0
Na_2O	1,8	2,1	0,0	2,9	0,3	0,4	0,3	0,2	0,0	0,7
K_2O	13,4	13,1	15,3	10,7	15,5	15,4	15,0	15,1	16,1	16,1
Total	100,0	100,0	100,0	100,0	100,0	100,0	100,0	100,0	100,0	100,0
Number of cations on the basis of 32 oxygen atoms										
Si	12,1	12,1	12,2	12,0	12,3	12,1	12,2	12,1	12,1	12,1
Al	4,0	4,0	3,9	4,2	3,4	3,9	3,6	3,9	3,9	3,9
Fe	0,0	0,0	0,0	0,0	0,0	0,0	0,0	0,0	0,0	0,0
Ca	0,0	0,0	0,0	0,0	0,5	0,0	0,3	0,1	0,0	0,0
Na	0,7	0,7	0,0	1,0	0,1	0,1	0,1	0,1	0,0	0,2
K	3,1	3,1	3,6	2,5	3,6	3,6	3,5	3,5	3,8	3,8
Total	19,8	19,8	19,7	19,7	19,9	19,8	19,8	19,7	19,8	20,0
End-members per cent										
An	0,0	0,0	0,0	0,0	11,1	0,0	8,5	3,4	0,0	0,0
Ab	17,3	19,6	0,0	28,8	2,9	3,3	2,9	1,9	0,0	6,0
Or	82,7	80,4	100,0	71,2	86,0	96,7	88,6	94,7	100,0	94,0

Sample	41 Xe15 (R2_3)	42 Xe15 (R3_1)	43 Xe15 (R3_2)	44 Xe15_2 (R4_1)
SiO_2	65,5	65,9	65,9	65,4
Al_2O_3	17,8	18,4	18,7	17,3
FeO	0,0	0,0	0,0	0,0
CaO	0,0	0,0	0,0	0,0
Na_2O	0,7	0,0	0,0	0,2
K_2O	16,1	15,7	15,5	17,0
Total	100,0	100,0	100,0	100,0
Number of cations on the basis of 32 oxygen atoms				
Si	12,1	12,1	12,1	12,1
Al	3,9	4,0	4,0	3,8
Fe	0,0	0,0	0,0	0,0
Ca	0,0	0,0	0,0	0,0
Na	0,2	0,0	0,0	0,1
K	3,8	3,7	3,6	4,0
Total	20,0	19,8	19,7	20,0
End-members per cent				
An	0,0	0,0	0,0	0,0
Ab	6,0	0,0	0,0	2,2
Or	94,0	100,0	100,0	97,8

KEY An=CaAl2Si2O8 Ab=NaAlSi3O8 Or=KAlSi3O8. The oxides are in weight percentages

Table 8 symplectic feldspar analyses

Sample	1 P4 (R2_4)	2 P7 (R2_5)	3 P7 (R2_7)	4 P8 (R4_15)	5 P8 (R5_3)	6 Xe10 (R2_2)	7 Xe10 (R4_4)	8 Xe11 (R1_7)	9 Xe11_2 (R2_2)	10 Xe16 (R2_2)
SiO_2	56,05	56,34	64,60	60,62	62,20	55,17	65,10	66,14	58,75	66,33
Al_2O_3	32,92	29,10	20,06	26,21	28,30	28,04	19,28	26,26	26,36	19,09
FeO	0,94	1,52	0,00	0,71	0,00	1,15	0,68	0,00	0,72	0,00
CaO	2,03	0,00	0,87	1,84	1,40	9,99	0,68	0,91	8,93	0,00
Na_2O	6,76	0,29	1,41	10,38	8,20	4,93	3,72	6,69	5,00	3,59
K_2O	1,31	12,76	13,06	0,23	0,00	0,73	10,55	0,00	0,25	10,99
Total	100,00	100,00	100,00	99,99	100,10	100,00	100,00	100,00	100,00	100,00
Number of cations on the basis of 32 oxygens										
Si	9,93	10,37	11,79	10,76	10,82	9,98	11,84	11,37	10,49	12,00
Al	6,87	6,31	4,32	5,48	5,80	5,98	4,13	5,32	5,55	4,07
Fe	0,14	0,23	0,00	0,11	0,00	0,17	0,10	0,00	0,11	0,00
Ca	0,39	0,00	0,17	0,35	0,26	1,94	0,13	0,17	1,71	0,00
Na	2,32	0,10	0,50	3,57	2,77	1,73	1,31	2,23	1,73	1,26
K	0,30	3,00	3,04	0,05	0,00	0,17	2,45	0,00	0,06	2,54
Total	19,94	20,02	19,82	20,31	19,66	19,97	19,97	19,09	19,63	19,86
End-members per cent										
An	12,85	0,00	4,59	8,80	8,62	50,51	3,39	6,96	48,87	0,00
Ab	77,31	3,34	13,49	89,88	91,38	45,11	33,73	93,04	49,52	33,19
Or	9,84	96,66	81,92	1,31	0,00	4,38	62,89	0,00	1,62	66,81

Sample	11 P4 (R2_11)	12 Xe11 (R5_12)	13 Xe11 (R5_25)
SiO_2	50,25	55,94	53,08
Al_2O_3	34,49	25,89	29,41
FeO	2,85	5,57	3,44
MgO	2,91	1,42	1,29
CaO	1,31	0,00	0,63
Na_2O	3,37	0,39	0,65
K_2O	4,81	10,80	11,49
Total	100,00	100,00	100,00

Oxides in weight percentages.
Analyses represent vermicular intergrowths occuring in/with clinopyroxene. Pyroxene in analysis 6 is exceptionally orthopyroxene which is enclosed by opaque mineral. Analyses 11-13 contain magnesium propably because the analysed area has been too narrow and the beam (1µm) has hit the pyroxene.

Table 9 pyroxene analyses

	1	2	3	4	5	6	7	8	9	10
	P2	P2	P2	P2	P2	P3	P3	P3		P3
Sample	(R2_1)	(R2_3)	(R2_4)	(R2_5)	(R3_1)	(R1_1)	(R1_2)	(k3_1)	P3 (k3_2)	(R2_2)
SiO_2	55,63	53,06	54,46	52,44	53,14	55,60	54,86	55,00	55,90	54,60
TiO_2	0,00	0,00	0,00	0,00	0,00	0,00	1,17	1,10	0,00	1,70
Al_2O_3	0,00	1,26	2,62	1,55	1,34	0,00	0,00	0,00	0,00	0,00
Cr_2O_3	0,00	0,00	0,00	0,00	0,00	0,00	0,00	0,00	0,00	0,00
FeO	9,37	25,18	9,96	27,15	24,87	7,00	6,37	6,80	6,45	6,80
MnO	0,00	0,77	0,00	0,00	0,77	0,00	0,00	0,00	0,00	0,00
MgO	13,33	19,34	12,73	17,72	19,30	12,40	12,08	12,30	13,23	11,70
CaO	21,66	0,39	20,24	1,15	0,58	25,00	25,52	24,80	24,42	25,20
Na_2O	0,00	0,00	0,00	0,00	0,00	0,00	0,00	0,00	0,00	0,00
K_2O	0,00	0,00	0,00	0,00	0,00	0,00	0,00	0,00	0,00	0,00
Total	100,00	100,00	100,00	100,00	100,00	100,00	100,00	100,00	100,00	100,00
Number of cations on the basis of 6 oxygens										
Si	2,06	2,00	2,01	1,99	2,00	2,06	2,03	2,03	2,06	2,02
Al (T)	0,00	0,00	0,00	0,01	0,00	0,00	0,00	0,00	0,00	0,00
Al (M1)	0,00	0,05	0,11	0,06	0,06	0,00	0,00	0,00	0,00	0,00
Fe(3+)	0,00	0,00	0,00	0,00	0,00	0,00	0,00	0,00	0,00	0,00
Cr	0,00	0,00	0,00	0,00	0,00	0,00	0,00	0,00	0,00	0,00
Ti	0,00	0,00	0,00	0,00	0,00	0,00	0,03	0,03	0,00	0,05
Fe(2+)	0,29	0,80	0,31	0,87	0,79	0,22	0,20	0,21	0,20	0,21
Mn	0,00	0,02	0,00	0,00	0,02	0,00	0,00	0,00	0,00	0,00
Mg	0,74	1,09	0,70	1,00	1,08	0,68	0,67	0,68	0,73	0,65
Ca	0,86	0,02	0,80	0,05	0,02	0,99	1,01	0,98	0,96	1,00
Na	0,00	0,00	0,00	0,00	0,00	0,00	0,00	0,00	0,00	0,00
K	0,00	0,00	0,00	0,00	0,00	0,00	0,00	0,00	0,00	0,00
total	3,95	3,98	3,94	3,98	3,98	3,95	3,94	3,94	3,95	3,93
Mg#	71,72	57,05	69,51	53,78	57,29	75,95	77,17	76,33	78,53	75,42
Per cent end-members										
Wo	45,48	0,81	44,13	2,43	1,23	52,31	53,78	52,42	50,78	53,75
En	38,94	56,43	38,63	52,31	56,42	36,10	35,51	36,18	38,52	34,73
Fs	15,58	42,75	17,24	45,26	42,36	11,59	10,70	11,40	10,71	11,53
Ae	0,00	0,00	0,00	0,00	0,00	0,00	0,00	0,00	0,00	0,00
total	100,00	100,00	100,00	100,00	100,00	100,00	100,00	100,00	100,00	100,00

	11	12	13	14	15	16	17	18	19	20
	P3	P3	P3	P4	P4	P4	P5	P5	P5	P6
Sample	(R2_3)	(R3_1)	(R3_3)	(R2_3)	(R2_10)	(R3_2)	(R4_3)	(R4_5)	(R5_3)	(R1_2)
SiO_2	55,20	55,08	55,61	51,88	52,27	54,09	45,04	45,79	51,47	51,08
TiO_2	1,30	1,27	1,05	0,55	0,54	0,00	0,00	0,00	0,00	0,54
Al_2O_3	0,00	0,66	0,00	4,59	4,33	2,87	11,36	10,18	10,19	3,28
Cr_2O_3	0,00	0,00	0,00	0,00	0,00	0,00	0,00	0,00	0,00	0,00
FeO	6,80	6,45	7,18	8,48	8,60	6,55	32,10	31,80	23,48	12,53
MnO	0,00	0,00	0,00	0,00	0,00	0,00	0,65	0,82	0,00	0,00
MgO	12,20	15,67	15,68	12,95	12,37	13,94	10,86	11,05	14,58	8,50
CaO	24,50	20,31	20,49	20,98	20,88	21,84	0,00	0,35	0,28	24,07
Na_2O	0,00	0,57	0,00	0,57	1,01	0,70	0,00	0,00	0,00	0,00
K_2O	0,00	0,00	0,00	0,00	0,00	0,00	0,00	0,00	0,00	0,00
total	100,00	100,01	100,00	100,00	100,00	100,00	100,00	100,00	100,00	100,00
Number of cations on basis of 6 oxygens										
Si	2,04	2,01	2,03	1,92	1,94	1,98	1,76	1,79	1,90	1,94
Al (T)	0,00	0,00	0,00	0,08	0,06	0,02	0,24	0,21	0,10	0,06
Al (M1)	0,00	0,03	0,00	0,12	0,13	0,11	0,28	0,26	0,34	0,09
Fe(3+)	0,00	0,00	0,00	0,00	0,00	0,00	0,00	0,00	0,00	0,00
Cr	0,00	0,00	0,00	0,00	0,00	0,00	0,00	0,00	0,00	0,00
Ti	0,04	0,03	0,03	0,02	0,02	0,00	0,00	0,00	0,00	0,02
Fe(2+)	0,21	0,20	0,22	0,26	0,27	0,20	1,05	1,04	0,75	0,40
Mn	0,00	0,00	0,00	0,00	0,00	0,00	0,02	0,03	0,00	0,00
Mg	0,67	0,85	0,85	0,71	0,68	0,76	0,63	0,64	0,80	0,48
Ca	0,97	0,79	0,80	0,83	0,83	0,86	0,00	0,01	0,01	0,98
Na	0,00	0,04	0,00	0,04	0,07	0,05	0,00	0,00	0,00	0,00
K	0,00	0,00	0,00	0,00	0,00	0,00	0,00	0,00	0,00	0,00
total	3,93	3,96	3,94	3,99	3,99	3,98	3,99	3,98	3,90	3,97
Mg#	76,18	81,24	79,57	73,15	71,93	79,14	37,15	37,65	52,54	54,74
Per cent end-members										
Wo	52,26	41,98	42,68	44,95	44,77	45,83	0,00	0,85	0,71	52,59
En	36,21	45,18	45,46	38,61	36,89	40,71	37,04	37,21	51,41	25,86
Fs	11,54	10,59	11,86	14,23	14,43	10,79	62,96	61,94	47,88	21,55
Ae	0,00	2,25	0,00	2,21	3,91	2,67	0,00	0,00	0,00	0,00
total	100,00	100,00	100,00	100,00	100,00	100,00	100,00	100,00	100,00	100,00

	21	22	23	24	25	26	27	28	29	30
	P6	P6	P6	P7	P7	P7	P7	P7	P8	P8
Sample	(R1_3)	(R4_2)	(R4_5)	(R2_4)	(R2_6)	(R2_9)	(R3_5)	(R3_7)	(R1_1)	(R1_2)
SiO_2	51,21	51,17	51,66	52,77	53,44	52,49	52,09	51,34	50,25	53,87
TiO_2	0,43	1,02	0,00	0,80	0,56	0,57	0,79	0,94	1,49	0,94
Al_2O_3	2,58	2,05	2,49	3,15	2,70	4,30	6,29	4,97	5,59	0,15
Cr_2O_3	0,00	0,00	0,00	0,00	0,00	0,00	0,00	0,00	0,00	0,00
FeO	11,56	10,98	11,13	10,47	9,13	8,68	10,97	10,79	10,18	18,33
MnO	0,42	0,00	0,00	0,00	0,00	0,00	0,00	0,00	0,00	0,45
MgO	8,71	10,02	9,17	13,65	13,79	14,17	11,27	11,80	10,75	6,53
CaO	25,10	24,76	25,55	19,16	20,38	19,79	16,62	20,16	21,74	14,91
Na_2O	0,00	0,00	0,00	0,00	0,00	0,00	1,97	0,00	0,00	4,82
K_2O	0,00	0,00	0,00	0,00	0,00	0,00	0,00	0,00	0,00	0,00
total	100,00	100,00	100,00	100,00	100,00	100,00	100,00	100,00	100,00	100,00
Number of cations on basis of 6 oxygens										
Si	1,95	1,94	1,96	1,96	1,97	1,93	1,93	1,91	1,88	2,08
Al (T)	0,05	0,06	0,04	0,04	0,03	0,07	0,07	0,09	0,01	0,00
Al (M1)	0,07	0,03	0,07	0,09	0,09	0,12	0,20	0,13	0,23	0,01
Fe(3+)	0,00	0,00	0,00	0,00	0,00	0,00	0,00	0,00	0,00	0,21
Cr	0,00	0,00	0,00	0,00	0,00	0,00	0,00	0,00	0,00	0,00
Ti	0,01	0,03	0,00	0,02	0,02	0,02	0,02	0,03	0,04	0,03
Fe(2+)	0,37	0,35	0,35	0,33	0,29	0,27	0,34	0,34	0,32	0,37
Mn	0,01	0,00	0,00	0,00	0,00	0,00	0,00	0,00	0,00	0,01
Mg	0,49	0,57	0,52	0,75	0,76	0,78	0,62	0,66	0,60	0,38
Ca	1,02	1,01	1,04	0,76	0,81	0,78	0,66	0,80	0,87	0,62
Na	0,00	0,00	0,00	0,00	0,00	0,00	0,14	0,00	0,00	0,36
K	0,00	0,00	0,00	0,00	0,00	0,00	0,00	0,00	0,00	0,00
total	3,98	3,98	3,98	3,96	3,96	3,96	3,99	3,96	3,96	4,06
Mg#	56,44	61,94	59,50	69,92	72,93	74,44	64,69	66,09	65,31	38,25
Per cent end-members										
Wo	53,85	52,35	54,32	41,28	43,56	42,70	37,38	44,70	48,60	31,63
En	25,99	29,47	27,13	40,91	41,03	42,54	35,28	36,40	33,44	19,27
Fs	20,16	18,18	18,55	17,81	15,41	14,76	19,33	18,90	17,96	30,58
Ae	0,00	0,00	0,00	0,00	0,00	0,00	8,01	0,00	0,00	18,52
total	100,00	100,00	100,00	100,00	100,00	100,00	100,00	100,00	100,00	100,00

	31	32	33	34	35	36	37	38	39	40
	P8	P8	P8	P8	P8	P8	P8	P9	Xe2	Xe9
Sample	(R1_3)	(R1_4)	(R1_11)	(R2_2)	(R4_16)	(R4_19)	(R5_2)	(R2_1)	(R1_5)	(R1_5)
SiO_2	53,43	53,45	53,84	51,88	52,98	51,88	51,80	65,68	53,54	56,48
TiO_2	2,89	1,37	2,05	0,77	0,67	0,63	1,00	0,00	3,59	0,86
Al_2O_3	0,91	1,25	0,40	3,21	2,77	3,34	3,60	21,09	0,00	0,00
Cr_2O_3	0,00	0,00	0,00	0,00	0,00	0,00	0,00	0,00	0,00	0,00
FeO	17,64	17,18	20,77	11,26	10,46	12,37	9,80	1,80	26,92	28,31
MnO	0,00	0,00	0,00	0,55	0,00	0,00	0,00	0,00	0,00	0,00
MgO	5,92	7,23	4,59	12,17	12,01	11,63	11,70	0,00	6,66	0,00
CaO	13,24	16,02	10,81	19,58	21,11	19,48	22,10	0,62	0,69	1,58
Na_2O	5,98	3,51	7,54	0,58	0,00	0,67	0,00	7,79	6,78	12,77
K_2O	0,00	0,00	0,00	0,00	0,00	0,00	0,00	3,02	1,82	0,00
total	100,00	100,01	100,00	100,00	100,00	100,00	100,00	100,00	100,00	100,00
Number of cations on basis of 6 oxygens										
Si	2,05	2,04	2,09	1,94	1,97	1,95	1,93	2,19	2,09	2,23
Al (T)	0,00	0,00	0,00	0,06	0,03	0,00	0,07	0,00	0,00	0,00
Al (M1)	0,04	0,06	0,02	0,09	0,09	0,15	0,09	0,83	0,00	0,00
Fe(3+)	0,20	0,05	0,36	0,00	0,00	0,00	0,00	0,00	0,30	0,66
Cr	0,00	0,00	0,00	0,00	0,00	0,00	0,00	0,00	0,00	0,00
Ti	0,08	0,04	0,06	0,02	0,02	0,02	0,03	0,00	0,11	0,03
Fe(2+)	0,35	0,49	0,29	0,35	0,33	0,39	0,31	0,05	0,56	0,22
Mn	0,00	0,00	0,00	0,02	0,00	0,00	0,00	0,00	0,00	0,00
Mg	0,34	0,41	0,27	0,68	0,67	0,65	0,65	0,00	0,39	0,00
Ca	0,54	0,66	0,45	0,79	0,84	0,78	0,88	0,02	0,03	0,07
Na	0,44	0,26	0,57	0,04	0,00	0,05	0,00	0,50	0,51	0,98
K	0,00	0,00	0,00	0,00	0,00	0,00	0,00	0,13	0,09	0,00
total	4,06	4,02	4,10	3,99	3,95	3,99	3,96	3,72	4,08	4,18
Mg#	37,46	42,87	28,28	64,74	67,18	62,63	68,04	0,00	30,62	0,00
Per cent end-members										
Wo	28,88	34,99	23,23	41,72	45,77	42,04	47,93	3,83	1,61	3,48
En	17,98	21,98	13,72	36,13	36,22	35,10	35,31	0,00	21,71	0,00
Fs	29,53	29,16	33,76	19,84	18,01	20,10	16,76	9,31	47,97	45,82
Ae	23,61	13,87	29,29	2,31	0,00	2,77	0,00	86,86	28,71	50,70
total	100,00	100,00	100,00	100,00	100,00	100,00	100,00	100,00	100,00	100,00

	41	42	43	44	45	46	47	48	49	50
	Xe9	Xe9	Xe10	Xe10	Xe10	Xe10	Xe10	Xe10	Xe11	Xe11
Sample	(R3_3)	(R3_5)	(R2_1)	(R2_3)	(R2_6)	(R3_1)	(R4_3)	(R4_5)	(R4_19)	(R5_11)
SiO_2	55,97	55,69	50,36	50,56	52,05	52,20	53,56	52,68	48,00	50,55
TiO_2	1,84	0,58	0,58	0,00	0,86	0,55	0,72	0,60	2,00	1,11
Al_2O_3	0,00	0,00	8,73	7,96	5,77	5,84	3,48	5,63	5,90	3,35
Cr_2O_3	0,00	0,00	0,00	0,00	0,00	0,00	0,00	0,00	0,00	0,00
FeO	28,24	29,48	15,71	16,44	11,21	11,17	11,43	10,77	10,80	9,59
MnO	0,00	0,00	0,00	0,48	0,00	0,00	0,00	0,00	0,00	0,00
MgO	0,00	0,00	23,60	23,55	12,19	12,25	12,50	12,28	8,00	9,56
CaO	0,00	0,44	1,02	1,01	16,68	16,72	17,00	16,95	24,90	25,83
Na_2O	13,95	13,80	0,00	0,00	1,24	1,27	1,31	1,10	0,40	0,00
K_2O	0,00	0,00	0,00	0,00	0,00	0,00	0,00	0,00	0,00	0,00
total	100,00	100,00	100,00	100,00	100,00	100,00	100,00	100,00	100,00	99,99
Number of cations on basis of 6 oxygens										
Si	2,21	2,22	1,82	1,83	1,93	1,93	1,98	1,94	1,83	1,91
Al (T)	0,00	0,00	0,18	0,17	0,07	0,07	0,02	0,06	0,17	0,09
Al (M1)	0,00	0,00	0,19	0,17	0,18	0,18	0,14	0,19	0,09	0,06
Fe(3+)	0,75	0,83	0,00	0,00	0,00	0,00	0,00	0,00	0,00	0,00
Cr	0,00	0,00	0,00	0,00	0,00	0,00	0,00	0,00	0,00	0,00
Ti	0,05	0,02	0,02	0,00	0,02	0,02	0,02	0,02	0,06	0,03
Fe(2+)	0,12	0,08	0,48	0,50	0,35	0,35	0,36	0,34	0,34	0,30
Mn	0,00	0,00	0,00	0,01	0,00	0,00	0,00	0,00	0,00	0,00
Mg	0,00	0,00	1,27	1,27	0,67	0,68	0,69	0,67	0,45	0,54
Ca	0,00	0,02	0,04	0,04	0,66	0,66	0,67	0,67	1,02	1,05
Na	1,07	1,06	0,00	0,00	0,09	0,09	0,09	0,08	0,03	0,00
K	0,00	0,00	0,00	0,00	0,00	0,00	0,00	0,00	0,00	0,00
total	4,21	4,23	3,99	4,00	3,97	3,98	3,97	3,96	4,00	3,98
Mg#	0,00	0,00	72,81	71,28	65,96	66,17	66,10	67,03	56,91	63,99
Per cent end-members										
Wo	0,00	0,94	2,22	2,15	37,32	37,29	37,15	38,07	55,10	55,37
En	0,00	0,00	71,12	69,73	37,94	38,03	38,02	38,39	24,63	28,52
Fs	45,01	45,73	26,67	28,12	19,73	19,58	19,66	19,08	18,67	16,12
Ae	54,99	53,33	0,00	0,00	5,02	5,11	5,17	4,45	1,60	0,00
total	100,00	100,00	100,00	100,00	100,00	100,00	100,00	100,00	100,00	100,00

	51	52	53	54	55	56	57	58	59	60
	Xe11	Xe11	Xe11	Xe11	Xe11	Xe11	Xe11_2	Xe11_2	Xe15_2	Xe15_2
Sample	(R5_24)	(R1_6)	(R2_3)	(R4_2)	(R4_3)	(R4_5)	(R2_1)	(R2_3)	(R1_1)	(R1_3)
SiO_2	49,62	50,80	49,10	51,00	50,40	49,80	48,73	49,15	54,27	53,09
TiO_2	1,20	1,38	1,50	1,00	1,10	1,10	1,69	1,23	0,00	0,00
Al_2O_3	3,67	3,84	3,90	3,20	2,80	3,50	7,21	6,29	0,00	0,00
Cr_2O_3	0,00	0,00	0,00	0,00	0,00	0,00	0,00	0,00	0,00	0,00
FeO	11,25	6,87	11,40	9,80	11,50	11,40	9,01	10,28	10,82	12,48
MnO	0,51	0,00	0,50	0,00	0,00	0,00	0,00	0,00	0,00	0,00
MgO	8,39	10,45	8,20	9,50	8,90	8,70	10,10	9,70	10,11	9,12
CaO	25,36	26,66	25,40	25,50	25,30	25,50	23,26	23,35	24,81	25,32
Na_2O	0,00	0,00	0,00	0,00	0,00	0,00	0,00	0,00	0,00	0,00
K_2O	0,00	0,00	0,00	0,00	0,00	0,00	0,00	0,00	0,00	0,00
total	100,00	100,00	100,00	100,00	100,00	100,00	100,00	100,00	100,00	100,00
Number of cations on basis of 6 oxygens										
Si	1,90	1,90	1,88	1,93	1,92	1,90	1,82	1,85	2,04	2,02
Al (T)	0,10	0,10	0,12	0,07	0,08	0,10	0,18	0,15	0,00	0,00
Al (M1)	0,06	0,07	0,06	0,07	0,05	0,06	0,14	0,13	0,00	0,00
Fe(3+)	0,00	0,00	0,00	0,00	0,00	0,00	0,00	0,00	0,00	0,00
Cr	0,00	0,00	0,00	0,00	0,00	0,00	0,00	0,00	0,00	0,00
Ti	0,03	0,04	0,04	0,03	0,03	0,03	0,05	0,03	0,00	0,00
Fe(2+)	0,36	0,22	0,37	0,31	0,37	0,36	0,28	0,33	0,34	0,40
Mn	0,02	0,00	0,02	0,00	0,00	0,00	0,00	0,00	0,00	0,00
Mg	0,48	0,58	0,47	0,53	0,51	0,49	0,56	0,54	0,57	0,52
Ca	1,04	1,07	1,04	1,03	1,03	1,04	0,93	0,94	1,00	1,03
Na	0,00	0,00	0,00	0,00	0,00	0,00	0,00	0,00	0,00	0,00
K	0,00	0,00	0,00	0,00	0,00	0,00	0,00	0,00	0,00	0,00
total	3,99	3,98	3,99	3,98	3,99	3,99	3,97	3,98	3,96	3,98
Mg#	55,97	73,06	55,11	63,35	57,98	57,64	66,67	62,71	62,49	56,57
Per cent end-members										
Wo	54,82	57,14	55,06	54,93	54,18	54,81	52,38	51,98	52,34	52,96
En	25,23	31,27	24,74	28,48	26,52	26,02	31,66	30,04	29,66	26,54
Fs	19,94	11,59	20,20	16,59	19,30	19,17	15,95	17,98	18,01	20,50
Ae	0,00	0,00	0,00	0,00	0,00	0,00	0,00	0,00	0,00	0,00
total	100,00	100,00	100,00	100,00	100,00	100,00	100,00	100,00	100,00	100,00

	61	62	63	64	65	66	67	68	69	70
Sample	Xe15_2 (R2_1)	Xe15_2 (R2_4)	Xe15_2 (R2_5)	Xe15_2 (R3_2)	Xe15_2 (R3_3)	Xe15_2 (R3_4)	Xe16 (R1_4)	Xe16 (R2_1)	Xe16 (R2_4)	Xe16 (R5_2)
SiO_2	53,31	52,82	52,28	53,09	53,88	53,36	52,48	53,49	53,49	52,21
TiO_2	0,98	0,85	1,03	0,73	0,91	1,38	0,64	0,00	0,34	0,48
Al_2O_3	0,00	0,00	0,00	0,00	0,00	0,91	5,03	2,17	3,11	5,23
Cr_2O_3	0,00	0,00	0,00	0,00	0,00	0,00	0,00	0,00	0,00	0,00
FeO	12,20	11,39	18,08	11,78	14,50	10,19	11,47	10,66	9,75	11,78
MnO	0,00	0,41	0,82	1,05	0,84	0,75	0,00	0,00	0,00	0,00
MgO	9,92	10,00	6,14	9,26	7,66	9,82	11,70	13,68	13,38	11,51
CaO	22,45	23,21	19,09	23,10	20,49	22,29	17,32	20,00	19,93	17,24
Na_2O	1,14	1,32	2,56	0,99	1,71	1,31	1,36	0,00	0,00	1,56
K_2O	0,00	0,00	0,00	0,00	0,00	0,00	0,00	0,00	0,00	0,00
total	100,00	100,00	100,00	100,00	100,00	100,00	100,00	100,00	100,00	100,00
Number of cations on basis of 6 oxygens										
Si	2,02	2,01	2,04	2,02	2,06	2,01	1,95	1,99	1,98	1,94
Al (T)	0,00	0,00	0,00	0,00	0,00	0,00	0,05	0,01	0,02	0,06
Al (M1)	0,00	0,00	0,00	0,00	0,00	0,04	0,17	0,08	0,11	0,17
Fe(3+)	0,00	0,05	0,09	0,00	0,00	0,00	0,00	0,00	0,00	0,00
Cr	0,00	0,00	0,00	0,00	0,00	0,00	0,00	0,00	0,00	0,00
Ti	0,03	0,02	0,03	0,02	0,03	0,04	0,02	0,00	0,01	0,01
Fe(2+)	0,39	0,31	0,50	0,38	0,47	0,32	0,36	0,33	0,31	0,37
Mn	0,00	0,01	0,03	0,03	0,03	0,02	0,00	0,00	0,00	0,00
Mg	0,56	0,57	0,36	0,53	0,44	0,55	0,65	0,76	0,74	0,64
Ca	0,91	0,95	0,80	0,94	0,84	0,90	0,69	0,80	0,79	0,69
Na	0,08	0,10	0,19	0,07	0,13	0,10	0,10	0,00	0,00	0,11
K	0,00	0,00	0,00	0,00	0,00	0,00	0,00	0,00	0,00	0,00
total	3,99	4,02	4,03	3,99	3,98	3,98	3,98	3,97	3,95	3,99
Mg#	59,18	60,17	36,68	56,26	47,08	61,53	64,52	69,58	70,97	63,53
Per cent end-members										
Wo	46,91	47,66	40,68	48,30	44,26	47,51	38,42	42,17	43,08	38,06
En	28,85	28,58	18,22	26,96	23,02	29,13	36,12	40,13	40,24	35,35
Fs	19,94	18,85	31,24	20,99	26,02	18,30	19,99	17,70	16,68	20,36
Ae	4,30	4,91	9,86	3,75	6,70	5,06	5,48	0,00	0,00	6,23
total	100	100	100	100	100	100	100	100	100	100

	71	72	73	74	75
Sample	Xe16 (R5_7)	Xe16 (R2_3)	Xe16 (R4_1)	Xe16 (R4_2)	Xe16 (R4_3)
SiO_2	52,06	51,80	54,29	53,77	55,84
TiO_2	0,63	0,71	2,68	3,25	2,86
Al_2O_3	4,92	5,18	0,81	0,41	0,44
Cr_2O_3	0,00	0,00	0,00	0,00	0,00
FeO	12,38	12,47	20,11	18,86	18,44
MnO	0,00	0,00	0,00	0,00	0,43
MgO	11,37	11,27	4,60	5,37	3,54
CaO	17,24	17,28	9,52	11,28	11,05
Na_2O	1,40	1,30	7,99	7,06	7,40
K_2O	0,00	0,00	0,00	0,00	0,00
total	100,00	100,00	100,00	100,00	100,00
Number of cations on basis of 6 oxygens					
Si	1,94	1,93	2,09	2,07	2,14
Al (T)	0,06	0,07	0,00	0,00	0,00
Al (M1)	0,16	0,16	0,04	0,02	0,02
Fe(3+)	0,00	0,00	0,32	0,26	0,14
Cr	0,00	0,00	0,00	0,00	0,00
Ti	0,02	0,02	0,08	0,09	0,08
Fe(2+)	0,39	0,39	0,31	0,33	0,45
Mn	0,00	0,00	0,00	0,00	0,01
Mg	0,63	0,63	0,26	0,31	0,20
Ca	0,69	0,69	0,39	0,47	0,45
Na	0,10	0,09	0,60	0,53	0,55
K	0,00	0,00	0,00	0,00	0,00
total	3,98	3,98	4,09	4,08	4,04
Mg#	62,09	61,70	28,95	33,67	25,07
Per cent end-members					
Wo	38,06	38,32	20,86	24,56	25,14
En	34,94	34,77	14,01	16,27	11,22
Fs	21,42	21,69	33,47	31,35	33,15
Ae	5,58	5,21	31,66	27,82	30,49
total	100,00	100,00	100,00	100,00	100,00

Following analyses contain ferric iron. FeO and Fe2O3 content in weight percentages:

Analysis	30	31	32	33
Fe2O3	7,36	7,11	1,91	12,79
FeO	11,71	11,24	15,46	9,25
Analysis	42,00	62,00	63,00	73,00
Fe2O3	29,92	1,74	3,02	11,35
FeO	2,56	9,82	15,37	9,90

Analysis	39	40	41
Fe2O3	10,42	23,58	27,03
FeO	17,54	7,09	3,92
Analysis	74	75	
Fe2O3	9,31	4,79	
FeO	10,48	14,12	

KEY: Wt-%=weight percentage. FeO is total iron. Number of cations on the basis of 6 oxygens: Al(T)=Aluminium on T site, Al(M1)=aluminium on M1 site, Fe3+, Cr and Ti on M1 site, Ca, Na and Mn on M2 site, Fe2+ and Mg the distribution between M1 and M2 not defined. Mg#=magnesium ratio Mg/(Mg+Fetot+Mn). Per cent end-members: $Wo=Ca_2Si_2O_6$ $En=Mg_2Si_2O_6$ $Fs=Fe_2Si_2O_6$ $Ae=NaFe^{3+}Si_2O_6$, modified from spread sheets by Preston (1999) using Morimoto et. al, 1989. Iron oxide weight percentages are calculated according to equation $FeO(tot)=FeO+0,8998*Fe_2O_3$.

Table 10 rutile analyses

	1	2	3	4	5	6	7	8	9	10
	P3	P3	P8	Xe1	Xe10	Xe10	Xe13	Xe13	Xe13	Xe14
Sample	(R1_6)	(R2_8)	(R5_4)	(R1_1)	(R3_3)	(R3_4)	(R1_6)	(R2_1)	(R2_10)	(R1_1)
SiO_2	0,00	0,00	0,00	0,00	0,00	0,00	0,43	0,00	0,00	0,00
TiO_2	96,85	97,27	98,81	99,72	98,27	98,86	96,70	98,55	99,02	98,88
Al_2O_3	0,00	0,00	0,00	0,00	0,00	0,00	0,00	0,00	0,00	0,00
Cr_2O_3	0,00	0,00	0,00	0,00	0,00	0,00	0,00	0,00	0,00	0,00
FeO	0,00	0,00	1,04	0,00	1,09	0,00	0,00	0,00	0,00	0,00
MgO	0,00	0,00	0,00	0,00	0,00	0,00	0,00	0,00	0,00	0,00
CaO	0,00	0,00	0,00	0,28	0,00	0,24	0,00	0,00	0,00	0,00
V_2O_5	0,71	0,83	0,14	0,00	0,00	0,00	2,87	1,45	0,98	0,00
ZnO	0,00	0,00	0,00	0,00	0,00	0,00	0,00	0,00	0,00	1,12
Nb_2O_5	2,44	1,90	0,00	0,00	0,64	0,91	0,00	0,00	0,00	0,00
BaO	0,00	0,00	0,00	0,00	0,00	0,00	0,00	0,00	0,00	0,00
Total	100,00	100,00	100,00	100,00	100,00	100,00	100,00	100,00	100,00	100,00
The number of cations on the basis of 2 oxygen atoms										
Si	0,00	0,00	0,00	0,00	0,00	0,00	0,01	0,00	0,00	0,00
Ti	0,97	0,98	0,99	1,00	0,99	0,99	0,96	0,98	0,99	0,99
Al	0,00	0,00	0,00	0,00	0,00	0,00	0,00	0,00	0,00	0,00
Cr	0,00	0,00	0,00	0,00	0,00	0,00	0,00	0,00	0,00	0,00
Fe(tot)	0,00	0,00	0,01	0,00	0,01	0,00	0,00	0,00	0,00	0,00
Mg	0,00	0,00	0,00	0,00	0,00	0,00	0,00	0,00	0,00	0,00
Ca	0,00	0,00	0,00	0,00	0,00	0,00	0,00	0,00	0,00	0,00
V	0,01	0,01	0,00	0,00	0,00	0,00	0,03	0,01	0,01	0,00
Zn	0,00	0,00	0,00	0,00	0,00	0,00	0,00	0,00	0,00	0,01
Nb	0,02	0,01	0,00	0,00	0,00	0,01	0,00	0,00	0,00	0,00
Ba	0,00	0,00	0,00	0,00	0,00	0,00	0,00	0,00	0,00	0,00
Total	1,00	1,00	1,01	1,00	1,01	1,00	0,99	1,00	1,00	1,01

	11	12
	Xe15	Xe16
Sample	(R4_5)	(R3_5)
SiO_2	0,44	0,00
TiO_2	94,56	98,59
Al_2O_3	0,00	0,00
Cr_2O_3	0,00	0,00
FeO	0,00	1,41
MgO	0,00	0,00
CaO	1,35	0,00
V_2O_5	1,25	0,00
ZnO	0,00	0,00
Nb_2O_5	0,00	0,00
BaO	2,40	0,00
Total	100,00	100,00
The number of cations on the basis of 2 oxygen atoms		
Si	0,01	0,00
Ti	0,96	0,99
Al	0,00	0,00
Cr	0,00	0,00
Fe(tot)	0,00	0,02
Mg	0,00	0,00
Ca	0,02	0,00
V	0,01	0,00
Zn	0,00	0,00
Nb	0,00	0,00
Ba	0,01	0,00
Total	1,01	1,01

Table 11 Spinel group mineral analyses

	1	2	3	4	5	6	7	8	9	10
	P4	P4	P4	P5	P5	P5	P5	P6	P6	P7
Sample	(R2_5)	(R2_8)	(R3_3)	(R3_5)	(R4_3)	(R4_4)	(R5_1)	(R2_4)	(R3_4)	(R4_6)
SiO_2	1,54	1,52	0,77	2,44	0,00	0,00	1,44	0,00	3,12	2,36
TiO_2	11,40	6,12	8,98	26,69	0,00	0,00	0,00	24,01	0,00	27,48
Al_2O_3	0,63	0,92	4,36	3,26	59,95	58,97	66,55	5,89	0,00	1,84
Cr_2O_3	1,56	0,62	0,00	0,00	0,00	0,00	0,00	1,52	0,00	0,00
V_2O_5	0,00	0,00	0,00	0,00	0,00	0,00	0,00	3,33	0,00	0,00
FeO	84,28	90,41	85,30	67,61	35,26	36,74	25,09	65,25	96,32	67,39
MnO	0,00	0,00	0,00	0,00	0,00	0,00	0,00	0,00	0,00	0,92
MgO	0,00	0,00	0,00	0,00	4,79	4,29	6,92	0,00	0,56	0,00
CaO	0,59	0,41	0,59	0,00	0,00	0,00	0,00	0,00	0,00	0,00
ZnO	0,00	0,00	0,00	0,00	0,00	0,00	0,00	0,00	0,00	0,00
Total	100,00	100,00	100,00	100,00	100,00	100,00	100,00	100,00	100,00	100,00
The number of cations on the basis of 32 oxygen atoms										
Si	0,44	0,44	0,22	0,71	0,00	0,00	0,31	0,00	0,89	0,69
Ti	2,47	1,32	1,92	5,81	0,00	0,00	0,00	5,19	0,00	6,03
Al	0,21	0,31	1,46	1,11	15,81	15,65	16,93	2,00	0,00	0,63
Cr	0,36	0,14	0,00	0,00	0,00	0,00	0,00	0,35	0,00	0,00
V	0,00	0,00	0,00	0,00	0,00	0,00	0,00	0,77	0,00	0,00
Fe3+	9,59	12,04	10,28	1,85	0,19	0,35	0,00	2,50	14,23	1,94
Fe2+	10,74	9,63	9,95	14,52	6,40	6,56	4,53	13,19	8,65	14,49
Mn	0,00	0,00	0,00	0,00	0,00	0,00	0,00	0,00	0,00	0,23
Mg	0,00	0,00	0,00	0,00	1,60	1,44	2,23	0,00	0,24	0,00
Ca	0,18	0,13	0,18	0,00	0,00	0,00	0,00	0,00	0,00	0,00
Zn	0,00	0,00	0,00	0,00	0,00	0,00	0,00	0,00	0,00	0,00
Total	24,00	24,00	24,00	24,00	24,00	24,00	24,00	24,00	24,00	24,00

	11	12	13	14	15	16	17	18	19	20
	P8	P8	P8	P8	P8	P8	P8	P9	Xe1	Xe1
Sample	(R2_8)	(R3_1)	(R3_2)	(R3_3)	(R4_6)	(R5_1)	(R5_5)	(R2_3)	(R2_1)	(R2_2)
SiO_2	3,83	0,51	1,12	0,38	0,00	1,14	0,00	0,47	0,00	4,11
TiO_2	0,00	15,68	77,24	31,43	30,45	9,97	21,80	16,65	4,18	0,00
Al_2O_3	0,00	6,95	0,00	1,83	4,26	3,47	3,94	1,28	3,61	0,00
Cr_2O_3	0,00	0,00	0,00	0,00	0,00	0,00	0,00	0,00	0,00	0,00
V_2O_5	0,00	0,00	0,00	0,00	0,00	0,00	0,96	0,00	0,00	0,00
FeO	94,98	76,09	20,62	65,98	64,88	84,05	73,30	81,60	90,81	88,63
MnO	0,00	0,78	0,71	0,00	0,00	0,00	0,00	0,00	0,00	0,00
MgO	1,18	0,00	0,32	0,39	0,41	0,00	0,00	0,00	1,40	7,26
CaO	0,00	0,00	0,00	0,00	0,00	0,00	0,00	0,00	0,00	0,00
ZnO	0,00	0,00	0,00	0,00	0,00	1,38	0,00	0,00	0,00	0,00
Total	100,00	100,00	100,00	100,00	100,00	100,00	100,00	100,00	100,00	100,00
The number of cations on the basis of 32 oxygen atoms										
Si	1,08	0,14	0,35	0,11	0,00	0,32	0,00	0,14	0,00	1,11
Ti	0,00	3,34	17,98	6,93	6,64	2,14	4,74	3,63	0,88	0,00
Al	0,00	2,32	0,00	0,63	1,46	1,17	1,34	0,44	1,20	0,00
Cr	0,00	0,00	0,00	0,00	0,00	0,00	0,00	0,00	0,00	0,00
V	0,00	0,00	0,00	0,00	0,00	0,00	0,22	0,00	0,00	0,00
Fe3+	13,84	6,72	0,00	1,30	1,27	9,90	4,97	8,02	13,04	13,78
Fe2+	8,58	11,30	5,34	14,87	14,46	10,18	12,74	11,77	8,30	6,19
Mn	0,00	0,19	0,18	0,00	0,00	0,00	0,00	0,00	0,00	0,00
Mg	0,50	0,00	0,15	0,17	0,18	0,00	0,00	0,00	0,58	2,92
Ca	0,00	0,00	0,00	0,00	0,00	0,00	0,00	0,00	0,00	0,00
Zn	0,00	0,00	0,00	0,00	0,00	0,29	0,00	0,00	0,00	0,00
Total	24,00	24,00	24,00	24,00	24,00	24,00	24,00	24,00	24,00	24,00

	21	22	23	24	25	26	27	28	29	30
	Xe1	Xe1	Xe1	Xe1	Xe3	Xe3	Xe4	Xe4	Xe4	Xe9
Sample	(R3_1)	(R4_1)	(R4_2)	(R4_6)	(R1_6)	(R3_1)	(R2_3)	(R3_1)	(R3_2)	(R1_1)
SiO_2	0,00	0,00	1,04	0,43	0,41	0,36	4,64	0,00	3,42	0,62
TiO_2	4,68	7,24	0,00	37,45	0,00	0,00	0,00	0,00	0,00	15,84
Al_2O_3	2,72	3,91	0,00	1,39	0,41	0,00	0,00	0,00	0,00	2,51
Cr_2O_3	0,00	0,00	0,00	0,00	0,00	0,00	0,00	0,00	0,00	0,00
V_2O_5	0,00	0,00	0,00	0,00	0,00	0,00	0,00	0,00	0,00	0,00
FeO	91,84	88,19	73,23	58,04	98,44	99,15	88,62	85,71	89,53	81,02
MnO	0,00	0,00	0,00	0,00	0,00	0,00	1,11	1,70	0,00	0,00
MgO	0,77	0,65	25,04	2,69	0,74	0,49	5,26	9,03	6,22	0,00
CaO	0,00	0,00	0,69	0,00	0,00	0,00	0,37	3,56	0,82	0,00
ZnO	0,00	0,00	0,00	0,00	0,00	0,00	0,00	0,00	0,00	0,00
Total	100,00	100,00	100,00	100,00	100,00	100,00	100,00	100,00	100,00	100,00
The number of cations on the basis of 32 oxygen atoms										
Si	0,00	0,00	0,25	0,13	0,12	0,10	1,27	0,00	0,93	0,18
Ti	1,00	1,54	0,00	8,17	0,00	0,00	0,00	0,00	0,00	3,44
Al	0,91	1,31	0,00	0,47	0,14	0,00	0,00	0,00	0,00	0,85
Cr	0,00	0,00	0,00	0,00	0,00	0,00	0,00	0,00	0,00	0,00
V	0,00	0,00	0,00	0,00	0,00	0,00	0,00	0,00	0,00	0,00
Fe3+	13,10	11,61	15,50	0,00	15,63	15,79	13,47	16,00	14,14	7,92
Fe2+	8,67	9,27	-0,86	14,07	7,80	7,90	6,76	3,03	6,17	11,62
Mn	0,00	0,00	0,00	0,00	0,00	0,00	0,26	0,38	0,00	0,00
Mg	0,32	0,28	8,93	1,16	0,31	0,21	2,14	3,57	2,52	0,00
Ca	0,00	0,00	0,18	0,00	0,00	0,00	0,11	1,01	0,24	0,00
Zn	0,00	0,00	0,00	0,00	0,00	0,00	0,00	0,00	0,00	0,00
Total	24,00	24,00	24,00	24,00	24,00	24,00	24,00	24,00	24,00	24,00

	31	32	33	34	35	36	37	38	39	40
	Xe9	Xe9	Xe9	Xe10	Xe11	Xe11	Xe11	Xe13	Xe15_2	Xe16
Sample	(R2_3)	(R2_5)	(R3_6)	(R3_6)	(R4_15)	(R4_16)	(R5_27)	(R1_9)	(R1_5)	(R1_1)
SiO_2	0,55	0,00	0,00	0,44	1,50	0,00	0,00	4,41	0,00	0,00
TiO_2	1,09	6,46	6,97	36,71	8,00	11,72	13,79	0,44	18,12	14,64
Al_2O_3	6,57	6,38	7,66	0,00	3,78	2,89	7,41	16,91	0,00	0,00
Cr_2O_3	0,00	0,00	0,00	0,00	0,00	0,00	0,55	0,00	0,00	0,00
V_2O_5	0,00	0,00	0,00	0,00	0,00	0,00	0,00	0,00	0,00	0,00
FeO	90,17	84,90	82,42	62,85	86,72	83,95	77,74	75,13	81,60	84,60
MnO	1,00	1,38	0,56	0,00	0,00	1,45	0,00	0,00	0,00	0,77
MgO	0,38	0,87	2,39	0,00	0,00	0,00	0,00	2,27	0,00	0,00
CaO	0,25	0,00	0,00	0,00	0,00	0,00	0,52	0,84	0,28	0,00
ZnO	0,00	0,00	0,00	0,00	0,00	0,00	0,00	0,00	0,00	0,00
Total	100,00	100,00	100,00	100,00	100,00	100,00	100,00	100,00	100,00	100,00
The number of cations on the basis of 32 oxygen atoms										
Si	0,15	0,00	0,00	0,13	0,43	0,00	0,00	1,15	0,00	0,00
Ti	0,23	1,36	1,44	8,22	1,71	2,53	2,93	0,09	3,98	3,21
Al	2,15	2,10	2,48	0,00	1,27	0,98	2,46	5,21	0,00	0,00
Cr	0,00	0,00	0,00	0,00	0,00	0,00	0,12	0,00	0,00	0,00
V	0,00	0,00	0,00	0,00	0,00	0,00	0,00	0,00	0,00	0,00
Fe3+	13,09	11,18	10,63	0,00	10,46	9,97	7,56	8,31	8,04	9,59
Fe2+	7,91	8,67	8,33	15,65	10,14	10,18	10,77	8,12	11,89	11,02
Mn	0,23	0,33	0,13	0,00	0,00	0,35	0,00	0,00	0,00	0,19
Mg	0,16	0,36	0,98	0,00	0,00	0,00	0,00	0,88	0,00	0,00
Ca	0,08	0,00	0,00	0,00	0,00	0,00	0,16	0,23	0,09	0,00
Zn	0,00	0,00	0,00	0,00	0,00	0,00	0,00	0,00	0,00	0,00
Total	24,00	24,00	24,00	24,00	24,00	24,00	24,00	24,00	24,00	24,00

	41	42	43
	Xe16	Xe16	Xe16
Sample	(R1_2)	(R3_4)	(R5_1)
SiO_2	0,51	0,78	0,00
TiO_2	84,84	26,36	32,97
Al_2O_3	0,00	2,91	1,87
Cr_2O_3	0,00	0,00	0,00
V_2O_5	0,00	0,00	0,00
FeO	14,65	69,94	59,37
MnO	0,00	0,00	4,31
MgO	0,00	0,00	1,48
CaO	0,00	0,00	0,00
ZnO	0,00	0,00	0,00
Total	100,00	100,00	100,00
The number of cations on the basis of 32 oxygens			
Si	0,16	0,23	0,00
Ti	20,00	5,77	7,21
Al	0,00	1,00	0,64
Cr	0,00	0,00	0,00
V	0,00	0,00	0,00
Fe3+	0,00	3,01	0,93
Fe2+	3,84	13,99	13,51
Mn	0,00	0,00	1,06
Mg	0,00	0,00	0,64
Ca	0,00	0,00	0,00
Zn	0,00	0,00	0,00
Total	24,00	24,00	24,00

Table 12 ilmenite analyses

Ilmenite	1	2	3
	P5	Xe9	Xe16
Sample	(R5_5)	(R1_2)	(R1_2)
SiO_2	0,00	0,32	0,51
TiO_2	56,59	47,24	84,84
Al_2O_3	0,00	0,00	0,00
Cr_2O_3	0,00	0,00	0,00
V_2O_5	0,00	0,00	0,00
FeO	40,92	50,71	14,65
MnO	1,72	1,73	0,00
MgO	0,77	0,00	0,00
CaO	0,00	0,00	0,00
ZnO	0,00	0,00	0,00
Total	100,00	100,00	100,00
The number of cations on the basis of 6 oxygens			
Si	0,00	0,02	0,02
Ti	2,09	1,85	2,74
Al	0,00	0,00	0,00
Cr	0,00	0,00	0,00
V	0,00	0,00	0,00
Fe(2+)	1,69	1,75	0,53
Fe(3+)	0,00	0,47	0,00
Mn	0,07	0,08	0,00
Mg	0,06	0,00	0,00
Ca	0,00	0,00	0,00
Zn	0,00	0,00	0,00
Total	3,91	4,16	3,28

APPENDIX 2

Table 1 apatite analyses

	1	2	3	4	5	6
Sample	K3O1 (R1_2)	K3O1 (R2_3)	K3O1 (R2_8)	K3O1 (R3_2)	K3O8 (R1_6)	K3O8 (R2_3)
CaO	54,49	60,52	56,11	57,23	57,33	56,15
Na2O	0,00	0,00	0,00	0,00	0,00	0,00
SrO	0,00	0,00	0,00	0,00	0,00	0,00
FeO	0,00	0,00	0,00	0,00	0,00	0,00
MnO	0,00	0,00	0,00	0,00	0,00	0,00
MgO	0,29	0,00	0,00	0,38	0,40	0,00
P2O5	40,66	39,48	40,23	42,39	41,02	40,21
SiO2	0,00	0,00	0,00	0,00	1,06	0,00
Cl	0,00	0,00	0,00	0,00	0,19	0,00
F	4,26	0,00	3,66	0,00	0,00	3,28
total	100	100	100	100	100	100

Table 2 carbonate analyses

	1	2	3	4
Samp-le	K3O5 (R1_3)	K3O5 (R1_7)	K3O5 (R4_2)	K3O18 (R2_5)
FeO	18,59	24,82	19,33	1,82
MnO	0,00	1,18	0,92	1,31
MgO	26,74	21,83	25,08	0,00
CaO	54,67	51,57	54,67	96,32
SrO	0,00	0,00	0,00	0,00
total	100,00	99,39	100,00	99,45
The number of cations on the basis of 6 oxygen atoms				
Fe	0,41	0,57	0,43	0,04
Mn	0,00	0,03	0,02	0,03
Mg	1,05	0,89	0,99	0,00
Ca	1,54	1,51	1,56	2,93
Sr	0,00	0,00	0,00	0,00
Total	3,00	3,00	3,00	3,00
Mg/Ca	0,68	0,59	0,64	0,00
Fe/Ca	0,27	0,38	0,28	0,01
Mg/Fe	2,56	1,57	2,31	0,00

Table 3 mica analyses

	1	2	3	4	5	6	7	8	9	10	11
Sample	K3O1 (R1_3)	K3O1 (R1_7)	K3O1 (R1_11)	K3O1 (R2_4)	K3O1 (R3_3)	K3O1 (R3_5)	K3O1 (R4_1)	K3O5 (R1_4)	K3O5 (R2_1)	K3O5 (R2_2)	K3O5 (R3_4)
SiO2	40,63	38,31	40,55	41,00	40,38	40,22	42,89	40,45	40,09	40,61	40,88
TiO2	5,46	8,33	7,38	6,47	7,60	6,36	5,63	6,75	6,19	6,01	5,08
Al2O3	12,78	13,74	12,84	12,23	13,39	12,24	9,48	12,93	13,03	13,41	13,10
FeO	11,57	13,22	9,33	10,47	8,21	12,20	11,03	9,62	9,68	9,48	8,96
MnO	0,00	0,00	0,00	0,00	0,00	0,00	0,00	0,00	0,00	0,00	0,00
MgO	19,90	17,06	20,07	19,93	20,47	18,97	20,27	20,30	21,18	20,84	20,38
CaO	0,00	0,00	0,00	0,00	0,00	0,00	0,00	0,00	0,00	0,00	0,00
Na2O	0,00	0,00	0,00	0,00	0,00	0,00	0,00	0,00	0,00	0,00	0,00
K2O	9,66	9,33	9,82	9,89	9,94	10,00	10,70	9,95	9,83	9,64	10,04
BaO	0,00	0,00	0,00	0,00	0,00	0,00	0,00	0,00	0,00	0,00	1,56
total	100,00	100,00	100,00	100,00	100,00	100,00	100,00	100,00	100,00	100,00	100,00
Mg#	75,41	69,70	79,31	77,24	81,63	73,49	76,61	79,00	79,60	79,67	80,23
Numbers of cations on the basis of 22 anions.											
Si	5,67	5,41	5,61	5,70	5,57	5,65	6,00	5,61	5,57	5,62	5,71
Al	2,10	2,29	2,10	2,01	2,18	2,03	1,56	2,11	2,13	2,18	2,16
Al	0,00	0,00	0,00	0,00	0,00	0,00	0,00	0,00	0,00	0,00	0,00
TiO2	0,57	0,88	0,77	0,68	0,79	0,67	0,59	0,70	0,65	0,63	0,53
Fe(ii)	1,35	1,56	1,08	1,22	0,95	1,43	1,29	1,12	1,12	1,10	1,05
Mn	0,00	0,00	0,00	0,00	0,00	0,00	0,00	0,00	0,00	0,00	0,00
Mg	4,14	3,59	4,14	4,13	4,21	3,98	4,23	4,20	4,38	4,30	4,25
Ca	0,00	0,00	0,00	0,00	0,00	0,00	0,00	0,00	0,00	0,00	0,00
Na	0,00	0,00	0,00	0,00	0,00	0,00	0,00	0,00	0,00	0,00	0,00
K	1,72	1,68	1,74	1,75	1,75	1,79	1,91	1,76	1,74	1,70	1,79
Ba	0,00	0,00	0,00	0,00	0,00	0,00	0,00	0,00	0,00	0,00	0,09
total	15,56	15,41	15,44	15,49	15,43	15,56	15,58	15,51	15,59	15,52	15,49

	12	13	14	15	16	17	18	19	20	21	22
Sample	K3O5 (R3_5)	K3O5 (R5_3)	K3O5 (R5_5)	K3O8 (R1_3)	K3O8 (R1_7)	K3O18 (R1_1)	K3O18 (R1_2)	K3O18 (R2_1)	K3O18 (R2_2)	K3O18 (R2_7)	K3O18 (R2_8)
SiO2	41,82	41,09	40,30	41,21	40,48	39,98	41,11	43,50	42,59	41,98	40,50
TiO2	4,75	7,76	5,27	5,42	5,50	7,03	4,58	3,64	2,69	2,99	5,37
Al2O3	10,83	11,80	12,99	12,19	12,52	13,29	10,66	9,05	8,87	13,91	13,06
FeO	13,19	8,68	9,37	11,21	11,18	9,63	14,20	11,83	15,25	13,60	9,04
MnO	0,00	0,00	0,00	0,00	0,00	0,00	0,00	0,00	0,00	0,00	0,00
MgO	19,33	19,03	19,86	20,49	20,41	20,13	19,76	20,65	20,29	18,42	20,13
CaO	0,00	0,00	0,00	0,00	0,00	0,00	0,00	0,00	0,00	0,00	0,00
Na2O	0,00	0,00	0,00	0,00	0,00	0,00	0,00	0,00	0,00	0,00	0,00
K2O	10,07	10,03	9,95	9,49	9,91	9,94	9,68	10,48	10,32	9,09	10,26
BaO	0,00	1,62	2,28	0,00	0,00	0,00	0,00	0,86	0,00	0,00	1,64
total	100,00	100,00	100,00	100,00	100,00	100,00	100,00	100,00	100,00	100,00	100,00
Mg#	72,31	79,63	79,08	76,51	76,49	78,84	71,27	75,68	70,34	70,72	79,89
Numbers of cations on the basis of 22 anions.											
Si	5,89	5,74	5,68	5,73	5,66	5,55	5,82	6,13	6,07	5,86	5,68
Al	1,80	1,94	2,16	2,00	2,06	2,18	1,78	1,50	1,49	2,14	2,16
Al	0,00	0,00	0,00	0,00	0,00	0,00	0,00	0,00	0,00	0,14	0,00
TiO2	0,50	0,82	0,56	0,57	0,58	0,73	0,49	0,39	0,29	0,31	0,57
Fe(ii)	1,55	1,01	1,10	1,30	1,31	1,12	1,68	1,39	1,82	1,59	1,06
Mn	0,00	0,00	0,00	0,00	0,00	0,00	0,00	0,00	0,00	0,00	0,00
Mg	4,06	3,97	4,17	4,25	4,25	4,17	4,17	4,34	4,31	3,83	4,21
Ca	0,00	0,00	0,00	0,00	0,00	0,00	0,00	0,00	0,00	0,00	0,00
Na	0,00	0,00	0,00	0,00	0,00	0,00	0,00	0,00	0,00	0,00	0,00
K	1,81	1,79	1,79	1,68	1,77	1,76	1,75	1,88	1,87	1,62	1,84
Ba	0,00	0,09	0,13	0,00	0,00	0,00	0,00	0,05	0,00	0,00	0,09
total	15,61	15,27	15,45	15,54	15,62	15,51	15,68	15,63	15,84	15,49	15,50

	23	24
Sample	K3O18 (R2_11)	K3O18 (R2_12)
SiO2	39,99	39,91
TiO2	7,91	8,08
Al2O3	13,80	14,24
FeO	11,86	10,84
MnO	0,00	0,00
MgO	16,38	16,80
CaO	0,00	0,00
Na2O	0,00	0,00
K2O	10,06	10,13
BaO	0,00	0,00
total	100,00	100,00
Mg#	71,11	73,42
Numbers of cations on the basis of 22 anions.		
Si	5,60	5,57
Al	2,28	2,34
Al	0,00	0,00
TiO2	0,83	0,85
Fe(ii)	1,39	1,26
Mn	0,00	0,00
Mg	3,42	3,49
Ca	0,00	0,00
Na	0,00	0,00
K	1,80	1,80
Ba	0,00	0,00
total	15,32	15,32

Table 4 potassium feldspar analyses

	1	2	3	4	5
sample	K3O1 (R2_5)	K3O1 (R2_6)	K3O8 (R1_4)	K3O8 (R1_5)	K3O18 (R1_3)
SiO2	63,72	64,22	64,69	65,42	65,60
Al2O3	19,89	18,32	19,04	18,47	17,85
FeOT	1,07	0,63	0,40	0,44	0,51
CaO	0,00	0,00	0,00	0,00	0,00
Na2O	0,00	0,00	0,00	0,00	0,00
K2O	15,33	15,50	15,86	15,67	16,03
Number of cations on the basis of 32 oxygen atoms					
Si	11,77	12,00	11,93	12,04	12,11
Al	4,33	4,03	4,14	4,01	3,88
Fe	0,17	0,10	0,06	0,07	0,08
Ca	0,00	0,00	0,00	0,00	0,00
Na	0,00	0,00	0,00	0,00	0,00
K	3,61	3,69	3,73	3,68	3,77
total	19,87	19,83	19,86	19,79	19,84
End-member percentage					
An	0,00	0,00	0,00	0,00	0,00
Ab	0,00	0,00	0,00	0,00	0,00
Or	100,00	100,00	100,00	100,00	100,00

Table 5 pyroxene analyses

	1	2	3	4	5	6	7	8	9	10	11
Sample	K3O1 (R1_5)	K3O1 (R1_9)	K3O1 (R1_10)	K3O1 (R2_1)	K3O1 (R6_3)	K3O5 (R1_1)	K3O5 (R1_2)	K3O5 (R1_5)	K3O5 (R1_6)	K3O5 (R2_4)	K3O5 (R3_2)
SiO2	56,06	52,37	53,45	56,60	52,16	55,39	51,85	52,43	53,71	53,01	53,66
TiO2	0,61123	1,10819	1,72741	0	1,95326	0,62802	2,77438	1,80889	7,88377	1,46	1,09
Al2O3	0,00	2,50	1,49	0,00	2,47	1,50	1,50	1,99	0,00	1,78	1,12
Cr2O3	0,00	0,50	0,00	0,00	0,69	0,00	0,00	0,00	0,00	0,63	0,00
FeO	4,47	3,60	3,72	4,76	3,93	3,81	6,64	5,33	23,51	3,52	5,09
MnO	0,00	0,00	0,00	0,00	0,00	0,00	0,00	0,00	0,00	0,00	0,00
MgO	16,72	16,14	16,03	16,47	15,10	16,60	14,20	15,48	0,00	16,12	14,78
CaO	22,14	23,80	23,58	22,17	23,70	22,07	23,04	22,97	2,30	23,48	24,26
Na2O	0,00	0,00	0,00	0,00	0,00	0,00	0,00	0,00	11,21	0,00	0,00
K2O	0,00	0,00	0,00	0,00	0,00	0,00	0,00	0,00	1,38	0,00	0,00
Total	100,00	100,00	100,00	100,00	100,00	100,00	100,00	100,00	100,00	100,00	100,00
Number of cations on the basis of 6 oxygens											
Si	2,03	1,92	1,95	2,05	1,91	2,00	1,92	1,93	2,10	1,94	1,97
Al (T)	0,00	0,08	0,05	0,00	0,09	0,00	0,07	0,07	0,00	0,06	0,03
Al (M1)	0,00	0,02	0,01	0,00	0,02	0,07	0,00	0,01	0,00	0,01	0,02
Fe(3+)	0,00	0,00	0,00	0,00	0,00	0,00	0,00	0,00	0,36	0,00	0,00
Cr	0,00	0,01	0,00	0,00	0,02	0,00	0,00	0,00	0,00	0,02	0,00
Ti	0,02	0,03	0,05	0,00	0,05	0,02	0,08	0,05	0,23	0,04	0,03
Fe(2+)	0,14	0,11	0,11	0,15	0,12	0,12	0,21	0,16	0,39	0,11	0,16
Mn	0,00	0,00	0,00	0,00	0,00	0,00	0,00	0,00	0,00	0,00	0,00
Mg	0,90	0,88	0,87	0,89	0,83	0,89	0,78	0,85	0,00	0,88	0,81
Ca	0,86	0,93	0,92	0,86	0,93	0,85	0,91	0,90	0,10	0,92	0,96
Na	0,00	0,00	0,00	0,00	0,00	0,00	0,00	0,00	0,85	0,00	0,00
K	0,00	0,00	0,00	0,00	0,00	0,00	0,00	0,00	0,07	0,00	0,00
total	3,95	3,99	3,97	3,95	3,97	3,95	3,97	3,98	4,10	3,98	3,97
Mg#	86,95	88,89	88,48	86,04	87,25	88,58	79,21	83,81	0,00	89,10	83,80
Per cent end-members											
Wo	45,25	48,50	48,30	45,39	49,57	45,81	47,98	47,17	5,70	48,24	49,69
En	47,53	45,77	45,70	46,90	43,96	47,93	41,13	44,24	0,00	46,09	42,11
Fs	7,22	5,73	6,00	7,71	6,47	6,26	10,88	8,59	44,07	5,67	8,20
Ae	0,00	0,00	0,00	0,00	0,00	0,00	0,00	0,00	50,22	0,00	0,00
total	100,00	100,00	100,00	100,00	100,00	100,00	100,00	100,00	100,00	100,00	100,00

	12	13	14	15	16	17
Sample	K3O5 (R4_1)	K3O5 (R4_3)	K3O5 (R4_4)	K3O5 (R5_4)	K3O8 (R2_2)	K3O18 (R2_4)
SiO2	54,56	53,05	56,00	51,27	52,01	54,57
TiO2	0,00	1,01	3,98	2,95	2,03	0,64
Al2O3	0,42	2,90	0,00	2,52	2,05	0,00
Cr2O3	0,00	0,00	0,00	0,00	1,13	0,00
FeO	10,72	4,97	25,12	6,73	3,69	10,25
MnO	0,68	0,00	0,00	0,00	0,00	0,00
MgO	11,62	14,26	1,43	13,30	15,42	14,50
CaO	21,47	23,80	0,91	23,22	23,66	20,04
Na2O	0,52	0,00	12,55	0,00	0,00	0,00
K2O	0,00	0,00	0,00	0,00	0,00	0,00
Total	100,00	100,00	100,00	100,00	100,00	100,00
Number of cations on the basis of 6 oxygens						
Si	2,04	1,94	2,18	1,90	1,91	2,02
Al (T)	0,00	0,06	0,00	0,10	0,09	0,00
Al (M1)	0,02	0,07	0,00	0,01	0,00	0,00
Fe(3+)	0,00	0,00	0,51	0,00	0,00	0,00
Cr	0,00	0,00	0,00	0,00	0,03	0,00
Ti	0,00	0,03	0,12	0,08	0,06	0,02
Fe(2+)	0,34	0,15	0,27	0,21	0,11	0,32
Mn	0,02	0,00	0,00	0,00	0,00	0,00
Mg	0,65	0,78	0,08	0,74	0,84	0,80
Ca	0,86	0,93	0,04	0,92	0,93	0,80
Na	0,04	0,00	0,95	0,00	0,00	0,00
K	0,00	0,00	0,00	0,00	0,00	0,00
total	3,97	3,97	4,14	3,96	3,97	3,96
Mg#	64,48	83,66	9,24	77,89	88,16	71,61
Per cent end-members						
Wo	0,00	50,05	2,05	49,36	49,27	41,49
En	4,21	41,73	4,49	39,36	44,69	41,78
Fs	46,76	8,22	42,28	11,28	6,04	16,73
Ae	49,02	0,00	51,17	0,00	0,00	0,00
total	100,00	100,00	100,00	100,00	100,00	100,00

KEY: Wt-%=weight percentage. Number of cations on the basis of 6 oxygens: Al(T)=Aluminium on T site, Al(M1)=aluminium on M1 site, Fe3+, Cr and Ti on M1 site, Ca, Na and Mn on M2 site, Fe2+ and Mg the distribution between M1 and M2 not defined. Mg#=magnesium number Mg/(Mg+Fetot+Mn). Per cent end-members: Wo=Ca2Si2O6 En=Mg2Si2O6 Fs=Fe2Si2O6 Ae=NaFe3+Si2O6, modified from spread sheets by Preston (1999) using Morimoto et. al, 1989.

Table 6 rutile analyses

	1	2
Sample	K3O1 (R5_1)	K3O5 (R3_1)
SiO2	0,46	3,48
TiO2	96,64	90,26
Al2O3	0,00	0,50
Cr2O3	0,00	0,71
FeO	1,19	3,88
MgO	0,00	0,69
CaO	0,23	0,47
ZrO2	1,49	0,00
Total	100,00	100,00
The number of cations on the basis of 2 oxygen atoms		
Si	0,01	0,05
Ti	0,98	0,91
Al	0,00	0,01
Cr	0,00	0,01
Fe(tot)	0,01	0,04
Mg	0,00	0,01
Ca	0,00	0,01
Zr	0,01	0,00
Total	1,01	1,04

Table 7 spinel group mineral analyses

	1	2	3	4	5	6	7	8
	K3O1	K3O5	K3O8	K3O8	K3O8	K3O18	K3O18	K3O18
Sample	(R6_1)	(R5_2)	(R1_1)	(R1_8)	(R1_9)	(R2_6)	(R2_9)	(R2_10)
SiO2	0,97	1,26	1,92	0,85	0,67	4,06	0,48	0,00
TiO2	10,08	1,44	0,54	7,51	7,34	0,00	12,09	12,90
Al2O3	4,17	0,00	0,90	8,91	9,02	0,40	2,49	2,93
Cr2O3	21,65	0,00	0,00	0,00	0,00	0,00	0,00	0,46
V2O5	2,71	0,00	0,00	0,67	0,00	0,00	0,00	0,00
FeO	57,23	96,91	96,29	79,11	79,58	94,61	83,34	81,02
MnO	3,19	0,00	0,00	0,54	0,90	0,00	0,59	0,00
MgO	0,00	0,40	0,35	2,40	2,50	0,00	1,01	2,69
CaO	0,00	0,00	0,00	0,00	0,00	0,93	0,00	0,00
Total	100,00	100,00	100,00	100,00	100,00	100,00	100,00	100,00
The number of cations on the basis of 32 oxygen atoms								
Si	0,28	0,36	0,55	0,23	0,18	1,15	0,14	0,00
Ti	2,19	0,31	0,11	1,55	1,51	0,00	2,59	2,73
Al	1,42	0,00	0,30	2,87	2,90	0,13	0,84	0,97
Cr	4,93	0,00	0,00	0,00	0,00	0,00	0,00	0,10
V	0,62	0,00	0,00	0,15	0,00	0,00	0,00	0,00
Fe3+	4,10	14,66	14,38	9,42	9,72	13,56	9,71	9,47
Fe2+	9,69	8,50	8,51	8,67	8,46	8,87	10,16	9,60
Mn	0,78	0,00	0,00	0,13	0,21	0,00	0,14	0,00
Mg	0,00	0,17	0,15	0,98	1,02	0,00	0,43	1,13
Ca	0,00	0,00	0,00	0,00	0,00	0,28	0,00	0,00
Zn	0,00	0,00	0,00	0,00	0,00	0,00	0,00	0,00
Total	24,00	24,00	24,00	24,00	24,00	24,00	24,00	24,00

Oxides in weight percentages. Analysis 1 enclosed by opaque pseudomorph,
2 enclosed by talc pseudomorph, 3 anhedral opaque, 4 and 5 core of opaque, 6 netlike opaque,
7 opaque, 8 opaque in contact with phlogopite

Table 7 talc analyses

	1	2
	K3O1	K3O5
Sample	(R1_18)	(R5_1)
SiO2	64,25	64,99
TiO2	0,00	0,00
Al2O3	0,00	0,00
Cr2O3	0,00	0,00
FeOT	7,95	6,82
MnO	0,00	0,00
MgO	27,80	27,90
CaO	0,00	0,29
Total	100,00	100,00

APPENDIX 3

Table 1 The xenoliths: mode

	P-3	P-4	P-6	P-7	P-8	Xe-1	Xe-4	Xe-10	Xe-11.1	Xe-11.2	Xe-15.1	Xe-15.2A	Xe-16
Amf	0,8	0	0	0	0	0	0	0	0	0	0	0	0
Apat	0,5	0,3	0,4	1,3	1,7	1,2	0,8	0	0,3	0	1,5	0,9	3,6
Ba	0	0	0	0	0	0	0	0	0	0	1,3	0	0
Bi	82,3	10,2	5,1	0	0	0	0	0	2,7	0	2,2	9,3	0
Carb	5,5	1,3	0	1,5	4,5	2,8	4,4	0	0,7	0,5	52,1	52,3	1
Chl	0	0	0	1,1	0	1,2	3,1	0	0	0	0	0	0,6
Cpx	4,7	55,7	23,8	15	43	0	0	18,3	47,8	34,6	0	23,7	38
Grt	0	0	0	17,2	9,9	0	0	0	0	0	25,5	7,9	22
Hbl	0	24,6	0	10,4	0	0	0	0	38,2	46,4	0	0	0,1
Kfs	3,2	0	0	0	0	0	0	0	0	0	17,3	0	0
Opq	0	6,3	4,1	3,2	15	3,5	3,5	3,3	10,3	0,6	0	5,9	7,6
Pl	0		48,8	50,3	26	60	57	64,8	0	17,9	0	0	27
Psm	0	1,6	17,8	0	0	1,8	0	0	0	0	0	0	0
Q	2,1	0	0	0	0	29	32	13,6	0	0	0	0	0
Rut	0,9	0	0	0	0	0	0	0	0	0	0,1	0	0

Abbreviations: Amf, amphibole; apat, apatite; Ba, barite; Bi, biotite; carb, carbonate; chl, chlorite; cpx, clinopyroxene; grt, garnet; hbl, hornblende; kfs, potassium feldspar; opq, opaque minerals; pl plagioclase; psm, pseudomorphs; q, quartz; rut rutile.

Table 2 Dyke 2: mode

	K3O1 marg	K3O 4	K3O1 4
Carb		8,9	9,3
Cpx	3,9	13,2	13
Kfs	10,3	21,5	27,1
Ol psm	17,9	8,8	10,1
Opq		2,5	1,1
Bi		45,1	39,4
Ground mass	67,9		

Abbreviations: Marg, margin of the dyke 2; carb, carbonate; kfs, potassium feldspar; ol psm, pseudomorph after olivine; opq, opaque minerals; bi, biotite.

Table 3 The xenoliths: whole-rock chemistry

Sample	SiO_2	TiO_2	Al_2O_3	Cr_2O_3	FeO	MnO	MgO	CaO	Na_2O	K_2O	P_2O_5	V_2O_5	F	BaO	ZrO_2
P-3	42,1	9,6	9,3	0,0	9,4	0,0	14,5	4,7	0,0	10,2	0,2	0,0	0,0	0,0	0,0
P-4	45,7	1,4	7,2	0,1	13,4	0,1	12,1	17,7	1,4	0,6	0,1	0,0	0,0	0,0	0,0
P-6	55,3	0,8	13,6	0,0	8,7	0,0	7,7	10,7	1,9	1,3	0,2	0,1	0,0	0,0	0,0
P-7	53,2	1,3	18,9	0,0	7,1	0,0	4,0	7,8	5,0	2,0	0,5	0,0	0,1	0,0	0,0
P-8	43,6	5,6	11,1	0,0	17,7	1,5	5,3	13,2	1,0	0,2	0,7	0,0	0,0	0,0	0,0
Xe-1	67,5	0,3	14,6	0,0	4,1	0,0	0,8	6,9	4,8	0,5	0,5	0,0	0,0	0,0	0,0
Xe-4	70,2	0,0	12,9	0,0	5,0	0,1	0,8	4,8	5,2	0,6	0,3	0,0	0,6	0,0	0,0
Xe-10	62,8	2,9	16,9	0,0	2,6	0,0	2,3	7,2	4,9	0,5	0,0	0,0	0,0	0,0	0,0
Xe-11.1	41,1	3,3	8,6	0,0	20,8	0,1	7,0	16,8	0,9	1,5	0,2	0,0	0,0	0,0	0,0
Xe-11.2	48,0	2,2	13,7	0,0	11,6	0,0	6,6	13,8	2,5	1,6	0,0	0,0	0,0	0,0	0,0
Xe-15	20,7	2,6	4,5	0,0	5,7	0,0	0,8	61,7	0,0	3,1	0,6	0,0	0,0	0,1	0,2
Xe-15.2A	18,7	2,5	1,5	0,0	10,4	0,1	4,1	60,9	0,2	0,9	0,4	0,0	0,0	0,2	0,0
Xe-16	46,8	4,1	13,5	0,0	11,6	0,1	6,2	12,5	3,0	0,5	1,5	0,0	0,0	0,0	0,0

Table 4 Dyke 2: whole rock chemistry

Sample	SiO_2	TiO_2	Al_2O_3	Cr_2O_3	FeO	MnO	MgO	CaO	Na_2O	K_2O	P_2O_5	BaO	V_2O_5
K3O4	45,2	3,1	9,8	0,1	10,2	0,1	14,7	8,4	0,2	7,9	0,0	0,1	0,0
K3O14	47,2	2,6	10,1	0,0	8,6	0,1	14,0	8,6	0,2	8,2	0,0	0,1	0,0